Development of Methods to Identify Thermophysical Properties of Complex Media

Elissa El Rassy

THESE

Pour l'obtention du Grade de

DOCTEUR DE L'ECOLE NATIONALE SUPERIEURE DE MECANIQUE ET D'AEROTECHNIQUE

(Diplôme National - Arrêté du 25 mai 2016)

Ecole Doctorale: Sciences et Ingénierie en Matériaux, Mécanique, Énergétique

Secteur de Recherche: Mécanique des solides, des Matériaux, des Structures et des Surfaces

Présentée par:

Elissa EL RASSY

****

Development of methods to identify thermophysical properties of complex media

****

Directeur de thèse: Didier Saury

Co-encadrant: Yann Billaud

****

Soutenue le 24 Octobre 2019

devant la Commission d'Examen

****

JURY

Président:

QUEMENER Olivier, Professeur, Université d'Evry

Rapporteurs:

PEREZ Laëtitia, Maître de Conférences, Université d'Angers

LACHI Mohammed, Professeur, Université de Reims

Membres du jury:

BILLAUD Yann, Maître de Conférences, Université de Poitiers

LEMONNIER Denis, Directeur de Recherche, CNRS

RIGOLLET Fabrice, Maître de Conférences, Aix-Marseille

SAURY Didier, Professeur, ENSMA

SOLOVJOV Vladimir, Maître de Conférences, Brigham Young University

Acknowlegments

Numerous personalities, directly and indirectly, have extended their support and co-operation in order to successfully accomplish this thesis. I'm truly indebted to them and hereby acknowledgment their contributions.

First of all, I would like to express my sincere gratitude to my intelligent thesis director Prof. Didier SAURY for his patience, special guidance, motivation, and immense knowledge. I could not imagine having a better advisor and mentor for my Ph.D study which couldn't have been successfully completed without his splendid guidance and support.

I wish to express my deep-set gratitude and heartfelt appreciation to my co-supervisor, Dr Yann BILLAUD, for the continuous support of my thesis work and related research. He was the person which incented me to widen my research from various perspectives.

Working with both of you (Prof.Didier SAURY and Dr.Yann BILLAUD) has improved me a lot as a student, as a researcher and as a person. I appreciate all your contributions of time and ideas to make my PhD experience productive. You have always listened to my ideas, and the discussions with you have frequently led to progress. Your ability to approach research problems and your high scientific standards set an example. I admire your capacity to balance research interests and personal pursuits. I am thankful for the excellent example you have provided me as a successful and an ambitious researcher.

I would like to thank my committee members for finding the time to read my thesis and for their valuable feedbacks.

A very special gratitude goes out to the European Union and the Nouvelle Aquitaine District for their financial support through the CPER/FEDER 2014-2020 program.

I would like also to express my special and sincere thanks to Professor Denis LEMONNIER and Dr. Florian MOREAU for their guidance and invaluable supports during the past 3 years.

In addition, I have been very privileged to get the support from many other great people who became friends over the last several years.

Special Thanks for Misses Jocelyne BARDEAU and Catherine LAVALLADE for their special administrative support.

I am also grateful to my office doctoral students Paul CHORIN and Alexandre WEPPE, and to my fellow Yang LIU, for their support, cooperation, feedback, and of course friendship.

My special acknowledgment to my friends (Samir, Ahmad, Rami, Wafa,...) who have supported me along the way and did not hesitate to encourage me during my work on this project, but one special thanks goes to Dr. Rita ZROUR, for always being there for me during hard times, you made me feel like a member of your family and a little sister, which I appreciate from my

heart.

Last but not the least, I would like to extend my cordial thanks to my parents : Hiam and Kamal and to my brothers for their moral support and encouragement during my entire work on this project. And special Thanks for the special person Nabil, who has provided me through moral and emotional support and endless love.

Last but not least, I have the honor to thank God for His richest grace and mercy for the accomplishment of this thesis.

Everything is theoretically impossible, until it is done

Robert A. Heinlein

Si c'est possible, c'est fait ; si c'est impossible, cela se fera

Charles Alexandre de Calonne

Table of Contents

Nomenclature

Latin Symbols

$\overline{\overline{a}}$	Thermal diffusivity tensor	$m^2 \cdot s^{-1}$
a_x, a_y, a_z	Thermal diffusivities	$m^2 \cdot s^{-1}$
C	Thermal Capacity	$J \cdot kg^{-1} \cdot K^{-1}$
f	Cost function	(-)
$F_{x,y}$	Shape function associated with the laser beam	m^{-2}
$F_{m,n}$	Fourier coefficients of the shape function	(-)
h	Overall heat transfer coefficient	$W \cdot m^{-2} \cdot K^{-1}$
l_x, l_y, l_z	Sample's dimensions	m
M, N	Harmonics maximum indices	(-)
p	Laplace variable	(-)
Q	Amount of energy absorbed by the sample	J
$R_{m,n}$	Excitation factor	J
Rc	Thermal contact resistance	$K \cdot m^2 \cdot W^{-1}$
r	Laser spot radius	m
Sr	Reduced Sensitivity	K
T	Temperature elevation	K
T_{sys}	System temperature	K
T_∞	Environment temperature	K
$u(t)$	Time shape function of the laser beam	s^{-1}
$u(p)$	Laplace transform of the time shape function	(-)
$X_m(x)$	Basis function in the x-plane	(-)
$Y_n(y)$	Basis function in the y-plane	(-)
$Y*$	Observables	K
$Y(\beta)$	Model outputs	K

Greek symbols

α_m, β_n	Harmonic pulsations	$rad \cdot m^{-1}$
β	Parameter vector to be estimated	(-)
$\hat{\beta}$	Optimal parameters vector	(-)
ρ	Density	$kg \cdot m^{-3}$
$\overline{\overline{\lambda}}$	Thermal conductivity tensor	$W \cdot m^{-1} \cdot K^{-1}$
$\lambda_x, \lambda_y, \lambda_z$	Thermal conductivities	$W \cdot m^{-1} \cdot K^{-1}$
σ	Relative error	(-)
τ_{ex}	Excitation pulse time	s
$\xi_{m,n}(t)$	Normalized harmonics in time domain	K
$\xi_{m,n}(p)$	Normalized harmonics in Laplace domain	$K \cdot s$
$\theta_{m,n}(p)$	Harmonics in Laplace domain	$K \cdot m^2 \cdot s$
$\theta_{m,n}(t)$	Harmonics in the time domain	$K \cdot m^2$
Φ_f	Overall heat losses on front face	J
Φ_b	Overall heat losses on back face	J
$\phi^{ex}_{m,n}(p)$	Excitation in the Fourier and Laplace domains	J
$\phi^{ex}_{x,y}(t)$	Excitation in the physical and time domains	$W \cdot m^{-2}$
$\phi_{m,n}$	The flux in the Fourier and Laplace domains	J

Subscripts and Superscripts

bi	Bilayer model
CPU	Central processing unit
est	Estimated
ex	Excitation
exp	Experiment
f,b	Front and back faces
i	Layer number
k	Total number of layers
m,n	Spatial Fourier modes
meas	Measured
mod	Model
mono	Monolayer model
sys	System
T	Transpose symbol
x,y	Cartesian coordinates

Abbreviations

ABC	Artificial Bee Colony algorithm
ACO	Ant Colony Optimization
BC	Boundary conditions
BF	Back face
BFGS	Broyden-Fletcher-Goldfarb-Shanno method
Bi	Bilayer model
CFRP	Carbon fibers reinforced polymer
Config	Configuration
DE	Differential Evolution
DFP	Davidon-Fletcher-Powell method
DSEH	Direct and Simultaneous Estimation using Harmonics
ENH	Estimation using Normalization of Harmonics
ERH	Estimation using Ratio of Harmonics
Est	Simulated data using estimated values
ES	Evolution Strategy
Exp	Experimental data
FF	Front face
GA	Genetic Algorithms
GLS	Generalized least squares
harm	Harmonics
IC	Initial conditions
Inter	Interface
MAP	Maximum a Posteriori Estimator
MLE	Maximum Likelihood Estimator
Mono	Monolayer model
MSEH	Multiple Steps Estimation using Harmonics
OLS	Ordinary Least Square Estimator
PSO	Particle swarm optimization
Rel. diff	Relative difference
Rel. dev	Relative deviation
Res	Absolute residue
6D	6 dimension = 6 thermal diffusivities (bi-layer Material)
4D	4 dimension = 4 thermal diffusivities (bi-layer Material)

General Introduction

***

Introduction

The continuous emergence of new materials with complex structures, i.e. anisotropic, multilayers, porous, and heterogeneous, in various industrial sectors (e.g. automotive, aerospace, chemical, civil, biomedical), appeals their thermal characterization. As a part of this thermal characterization, the identification of thermophysical properties of such materials has taken from many years a significant and increasing concern. In thermal sciences, the knowledge of properties, in particular the diffusivities, allows the evaluation of the manufactured materials quality as well as the control and the modelling of the heat transfers through the processes, and is required when identifying boundary conditions.

The thermal properties identification consists in, as any parameter estimation, resolving an inverse problem that typically relies on three main steps:

- the elaboration of a mathematical model that mimics the studied phenomenon,
- the measurement acquisition of one or more variable thanks to the appropriate experimental test bench,
- the implementation of an optimization procedure based on the minimization of the difference between the experiment and the model prediction.

The main feature of this work is the development of an identification method allowing a direct and simultaneous estimation of the thermal diffusivities of monolayer or multilayers materials using an analytical 3D transient model and a unique and non-intrusive flash based experiment.

Firstly, after validation on an isotropic material, the proposed method is applied and verified on an orthotropic and opaque homogeneous monolayer. Then, the method is generalized into a two-layers or multilayers material, for which it may be a challenging task to directly measure the diffusivities of all the constituting orthotropic or isotropic layers without the need to prepare free-standing samples.

In all the studied cases, the identification method is based on an inverse heat conduction problem that consists in fitting the outputs of an analytical model inspired from the thermal quadrupoles formalism approach [1] which is conducted to predict the temperature evolution

at the front or the rear face of the handled materials. The temperature evolution resulting from a short and localized thermal excitation applied on one of the sample face and generated by a CO2 laser is recorded by IR camera at the exposed face (Front Face), or at the opposite one (Back Face). The developed model, as well as the choice of the observables, are consistent with the flash method, which is the generic class of frequently used radiometric methods, firstly introduced by Parker [2]. One of the distinctive features of our approach, is that the estimation may be successfully achieved without any a priori knowledge about the shape or the intensity of the laser excitation. Adding to that, it estimates, simultaneously with the thermal diffusivities, the total amount of heat absorbed by the material, and predicts the shape of the thermal excitation applied on the surface of the material.

Considering the complexity, the non-linearity of the inverse problem, as well as the large number of parameters to estimate, gradient based methods appear not suitable for the problem under consideration. A global search algorithm is then preferred and the stochastic methods appear to be a good choice for this purpose. Several existing heuristic and evolutionary algorithms are successfully applied in many engineering fields [3–10], to find a global optimum, and can be good candidates in this study. In order to provide a best possible estimation, a hybrid optimization algorithm combining both a stochastic and a deterministic methods (i.e. gradient based), is applied here.

The overall identification technique is applied on different types of samples, in an increasing order/level of complexity (starting from the simplest types of materials to reach the most complex one investigated at the end of this study) :

1. It is firstly applied on homogenous and opaque monolayer material:
    - Starting by a well known isotropic sample of polyamide, for validation,
    - then, it is applied to orthotropic samples of carbon fibers reinforced polymer (CFRP) composite material, with successful results.
2. Furthermore, it is generalized to multilayer materials and experimentally applied to a two-layers material composed of a CFRP layer combined to a polyamide one.
3. At the end, the thermal characterization of a special two-layers material constituted of thin layer of TPT (Thermographic phosphor thermometry) coating deposited on a polymer substrate, is investigated. This application is a part of a collaborative work with a team from IFPEN (Institut Français du Pétrole et Energies Nouvelles).

After a parametric study and an evaluation of the overall identification method accuracy performed using synthetic noisy data, the estimation method is then applied on real monolayers and bi-layered samples with isotropic and orthotropic properties. The proposed method is validated using materials of known properties, and then the experimental results are compared with results obtained when conducting well-established methods or from thermal diffusivities values found in the literature.

The flexPDE numerical tool, based on a finite element code, is investigated in some cases to reproduce the experiment and generate synthetic data. It is used for some validations/checkings and also conducted in the part that represents an experiment design for a better estimation accuracy, where relatively long laser pulses are compared to very short (impulse) ones, for a front and rear face flash methods. It is also handled in some alternative approaches verifying the possibility to simultaneously estimate the thermal diffusivities of materials without any pre-knowledge about the volumetric thermal capacity, or the possibility to estimate this thermal property, at the same time.

The accuracy and the robustness of the proposed identification methods are also investigated for each type of applications. A sensitivity analysis is typically conducted as a preliminary tool that allows the verification of the simultaneous estimation feasibility and the determination of the optimal conditions for a better estimation accuracy. It is also investigated in some cases, as a key element for the experimental design and for the comparative analysis of different possible experimental configurations.

Outlines

The thesis manuscript is structured and organized in four chapters, as follows:

- **Chapter 1:** This chapter will present the literature review of the existing methods dedicated to thermophysical material properties identification. It starts with the context and industrial application of such methods, then it highlights on the importance of such identification, and especially on the thermal diffusivity estimation. After that, a general classification and overview of existing thermal characterization methods is developed. Finally, a state of art on the flash based methods (conventional and unconventional), investigated in the current study, its types, classifications and evolution over years, will be also presented.

- **Chapter 2:** This chapter will concern the identification technique and develop all elements involved in the inverse heat conduction problem that must be resolved in order to get the set of optimal parameters to estimate. For instance, it will detail the experimental procedure, and present the direct/forward modeling of the problem, and the overall estimation method. Adding to that, some generalities about the estimation methods and sensitivity analysis will be firstly developed and then narrowed into the current application case. All potential errors that can take place in this problem are also presented.

- **Chapter 3:** In this chapter, the overall identification method is applied on a monolayer material. The model is developed by the resolution of the heat equation in an orthotropic homogeneous and opaque domain, with respect to the boundary and initial conditions that mimic the 3D flash based method applied in this study. A numerical application of the estimation technique is also conducted in order to verify the feasibility and the accuracy of the current identification method, and to pursue a best parametric combinations

of the optimization tool. After that, the present method is applied on an isotropic material of polyamide for validation. The same identification method is then applied on an orthotropic material of CFRP, and a sensitivity analysis is performed in each case to explain and deduce the estimation feasibility/conditions. Results are shown to be in good agreements with those obtained using other estimation methods already developed in the literature, and which are applied here on the handled materials, for comparison. Furthermore, several improvements ways for the CFRP identification method are investigated, including the improvements in terms of time consumption reduction and/or accuracy enhancement by different possible strategies, and in terms of experimental design (excitation energy and time duration: impulse or pulse, and measurements sides: front or rear face). Finally, other alternative strategies allowing to estimate additional thermophysical properties, are presented.

- **Chapter 4:** This chapter is dedicated to the generalization of the overall identification method in order to be applied on multi-layered materials. In these cases, the proposed method is of great importance, specifically when layers cannot be easily separated or when the layer that should be characterized is not available as a free-standing sample. A direct model will be developed for such type of materials taking into account the heat equation in each layer, the interface continuity equations and the initial and boundary conditions that should reproduce all experimental conditions. After the validation of the direct model, identification method is applied for the characterization of a CFRP layer combined with an isotropic liner, to form a two-layers material commonly used in many industries. A comparative evaluation based on sensitivity analysis is represented for 4 possible experimental configurations, in terms of thermal excitation and measurement faces combinations (front or rear face). After the development of the identification method and all elements that are involved in the current inverse problem, the latter is numerically applied for the most sensitive case using synthetic measurements for feasibility verification, and for accuracy and robustness evaluation. Then, the proposed characterization method is experimentally applied on a real two layer material with two selected experimental configurations, and two identification dimensions (4D when the polyamide material is considered isotropic, and 6D when it is considered orthotropic). Sensitivity study is also conducted in order to test the feasibility of the estimation for both experimental configurations and both strategies and to explain the differences in the estimation results. Results are also compared to previous estimation values of monolayers diffusivities that are already identified and those obtained using other existing estimators. Lastly, a special case consisting of a thermal characterization of a degenerated two-layer material constituted of a thin coating of phosphorous material deposited on a substrate, is also treated. Two experimental configurations are also compared for two identification dimensions (isotropic or orthotropic substrate).

Résumé substantiel de l'introduction générale

L'émergence de nouveaux matériaux "innovants" ayant des structures de plus en plus complexes (i.e anisotropes, multicouches, poreux ou hétérogènes) utilisé dans un grand nombre de secteurs industriels (automobile, aérospatial, chimique, civil et biomédical par exemple), nécessite la connaissance de leurs propriétés thermophysiques. L'identification des propriétés de tels matériaux suscite depuis de nombreuses années une préoccupation importante et croissante. En sciences thermiques, la connaissance des propriétés, en particulier des diffusivités thermiques, permet d'une part l'évaluation de la qualité des matériaux lors de leur fabrication ainsi que le contrôle et la modélisation des transferts de chaleur au cours de leur utilisation. L'objectif principal de ce travail concerne le développement d'une méthode d'identification permettant une estimation directe et simultanée des diffusivités thermiques d'un matériau anisotrope, monocouche ou multicouches. La méthode développée repose sur le couplage d'un modèle transitoire analytique 3D et d'une expérience non intrusive de type "flash" au moyen d'une procédure d'optimisation.

Dans tous les cas traités, la méthode d'identification correspond à un problème inverse de conduction thermique consistant à ajuster les résultats d'un modèle analytique (inspiré de l'approche des quadripôles thermiques [1]) utilisé pour prévoir l'évolution de la température sur les faces avant ou arrière des matériaux étudiés. La méthode étant basée sur une expérience de type "Flash" [2], l'évolution de la température résulte d'une excitation thermique, brève et localisée sur l'une des faces de l'échantillon, générée par un laser CO_2. L'évolution de la température est enregistrée par une caméra infrarouge sur la face exposée ou sur la face arrière, selon les spécificités du matériau. L'une des principales caractéristiques de la présente approche est que l'estimation peut être réalisée sans connaissance préalable de la forme ou de l'intensité de l'excitation. En effet, en plus d'estimer simultanément les diffusivités thermiques du ou des matériaux, la méthode permet d'estimer la quantité de chaleur absorbée ainsi que la forme de l'excitation appliquée à la surface de l'échantillon.

Compte tenu de la complexité, de la non-linéarité du problème inverse ainsi que du grand nombre de paramètres à estimer, les méthodes déterministes d'optimisation (e.g. de type gradient) ne peuvent pas être appliquées directement dans ce cas. C'est pourquoi ce travail repose sur l'utilisation d'une méthode stochastique d'optimisation, utilisée avec succès pour la résolution de problèmes en thermique [3–10]. Afin de fournir la meilleure estimation possible, la recherche d'optimum par un algorithme de type PSO (i.e. méthode stochastique de type évolutionnaire) est combinée à une recherche par une méthode de points intérieurs (i.e. méthode déterministe). Cette méthodologie hybride permet de tirer parti des avantages de chacune des méthodes, à savoir une recherche globale évitant de ce fait de rester piégé dans des minima locaux, puis une recherche efficace et rapide du minima global.

Le présent manuscrit est organisé en 4 chapitres, en plus de l'introduction et de la conclusion:

- **Chapitre 1:** Ce chapitre présente une étude bibliographique sur les méthodes existantes dédiées à l'identification des propriétés thermophysiques des matériaux. Celui-ci com-

mence par le contexte et les applications industrielles de telles méthodes en mettant en avant l'importance de la connaissance de ces propriétés, en particulier celle de la diffusivité thermique. Une classification générale et un panorama des différentes méthodes de caractérisation thermique existantes sont présentés et discutés. Enfin, un état de l'art sur les différentes variantes de la méthode Flash qui est utilisée dans la présente étude, est présenté.

- **Chapitre 2:** Ce chapitre traite la technique d'identification utilisée et développe l'ensemble des éléments impliqués dans la résolution de problèmes inverses en conduction thermique. Ainsi, le chapitre détaille la procédure expérimentale ainsi que le modèle mathématique et sa méthode de résolution utilisés pour prédire le comportement du système étudié. La méthode d'optimisation utilisée pour trouver le jeu de paramètres permettant de minimiser l'écart entre les mesures expérimentales et les prévisions du modèle est également détaillée dans ce chapitre. Ce chapitre présente également le principe de l'analyse de sensibilité, indispensable dans ce genre d'exercice, ainsi qu'une étude des sources d'erreurs de la méthode.

- **Chapitre 3:** Dans ce chapitre, la méthode d'identification est appliquée sur un matériau monocouche. Dans un premier temps le modèle direct, développé pour prédire le comportement thermique d'un matériau orthotrope et opaque soumis à une sollicitation de type Flash, est présenté ainsi que les conditions aux limites et initiales. La méthode d'estimation développée est utilisée sur des données synthétiques afin, d'une part, de vérifier la faisabilité et la précision de la méthode, et d'autre part, de calibrer les paramètres de la méthode. La méthode est ensuite appliquée sur divers matériaux tels que le polyamide qui est isotrope puis sur un polymère renforcé de fibres de carbone (PRFC) qui est quant à lui orthotrope. Une analyse de sensibilités est effectuée dans chaque cas pour vérifier la faisabilité et en déduire les conditions de l'estimation. Les résultats d'identification sont en bon accord avec des résultats de la littérature et des résultats obtenus à l'aide de méthodes de références. Par la suite, plusieurs pistes d'optimisation de la méthode d'identification sont étudiées, notamment en termes de modélisation (e.g. paramétrisation de l'excitation) permettant une réduction du temps de calcul tout en conservant un niveau de précision élevé. Également, une étude portant sur la conception expérimentale, principalement en ce qui concerne les conditions de l'excitation (quantité d'énergie et durée de l'excitation) et des observables (champ de température en face avant ou arrière).

- **Chapitre 4:** Ce chapitre est consacré à la généralisation de la méthode d'identification présenté précédemment afin de l'appliquer à des matériaux multicouches. Dans ce cas, la méthode proposée revêt une grande importance, en particulier lorsque les couches ne peuvent pas être facilement séparées ou lorsque la couche à caractériser n'est pas disponible séparément (i.e. en tant qu'échantillon autonome). Le modèle est adapté pour traiter ce type de matériaux en tenant compte de l'équation de la chaleur dans chaque couche, des équations de continuité à l'interface et les conditions initiales et aux

limites qui doivent reproduire l'ensemble des conditions expérimentales. Après validation du modèle direct, la méthode d'identification est appliquée pour la caractérisation d'une couche de PRFC combinée à un "liner" isotrope, formant ainsi un matériau bicouche couramment utilisé dans de nombreuses applications (e.g. bouteilles de stockage d'hydrogène, entre autres). Une étude comparative basée sur une analyse de sensibilités est présentée pour 4 configurations expérimentales possibles, en termes de combinaisons des faces d'excitation et de mesure (i.e. face avant ou face arrière). La méthode est par la suite appliqué sur des données synthétiques dans le cas le plus favorable (i.e. sensible) afin de vérifier la faisabilité de la méthode d'une part, et évaluer la précision et la robustesse de la méthode. Par la suite, la méthode de caractérisation proposée est appliquée à des données expérimentales sur un matériau constitué de deux couches pour deux des configurations expérimentales possibles et pour deux stratégies d'identification. Une première stratégie consiste à considérer le materiau isotrope comme tel, nommée "estimation 4D" dans le manuscrit, et une seconde stratégie qui consiste à traiter le matériau isotrope comme si ce dernier était anisotrope, c'est à dire à identifier les diffusivités selon les 3 directions principales. Cette dernière stratégie est nommée "estimation 6D" dans le manuscrit. Les résultats de l'estimation sont ensuite analysés via une étude de sensibilités dans le but d'expliquer les résultats obtenus. Ces résultats sont comparés aux valeurs précédemment obtenus et celles obtenues à l'aide d'autres estimateurs existants. Pour finir, le cas particulier d'un matériau bicouche présentant une couche de faible épaisseur relativement à l'autre, est étudié. L'étude expérimentale correspond à un revêtement constitué d'un matériau phosphorescent déposé sur un substrat utilisé comme technique de mesure par phosphorescence. Deux configurations expérimentales sont évaluées pour les deux stratégies étudiées précédemment.

La conclusion générale présente un résumé du travail ainsi que les différentes perspectives.

Chapter 1

Overview of thermal characterization methods

***

Contents

1.1 Introduction

The ultimate goal of this thesis is the development of methods dedicated to thermally characterize complex materials as orthotropic or isotropic mono-layer materials, multi-layered (specifically bi-layered materials) and coating on substrate which corresponds to a special bi-layered material. Whatever the sample studied in this work, the characterization consists in identifying the thermal diffusivities of each of the constitutive layer.

The materials types investigated in this work are increasingly manufactured and frequently involved in many industrial sectors as discussed in section 1.2. The manufacturing, the composition and the structure of these materials depend on their application. In this context, the identification of thermophysical properties has taken, from many years, a significant and increasing concern (see the panorama of characterization methods in section 1.4), and are used in many sectors (see section 1.3).

This chapter starts by a general context presentation. The applications for which those complex materials are used are presented, the significant importance of their thermal characterization are then discussed. Thereafter, an exhaustive literature review about the existing thermal characterization methods is presented.

A general classification of the wide variety of thermophysical parameters estimation methods, is carried out according to numerous different criteria.

Furthermore, a state of the art of the flash method handled in this work, including a definition of the technique, its origin, its classifications and its advantageous, followed by its continuous improvement over the past years, will be extensively developed.

1.2 Context and industrial applications

Advanced materials with complex structures (i.e. composite materials, multilayers, coatings deposited on substrates) are increasingly used in a large extent of engineering applications. For example those materials are increasingly used in energy storage and production, automotive and aerospace sectors (transport sector), as shown in Figure 1.1, where the challenge is to reduce on-board weight and energy consumption while retaining the mechanical properties.

Figure 1.1 – Some industrial applications of the handled complex materials.

Carbon fiber reinforced polymers composite (CFRP)

The carbon fiber reinforced polymers composite materials (CFRP) can be founded in many applications due to their advantages in terms of thermal, mechanical, and physical properties enhancements, in parallel with weight reduction. One of the major applications of such types of materials concerns the aeraunotical domain, as shown in Figure 1.2, where its proportion may exceed 50 % of the manufacturing volume [11].

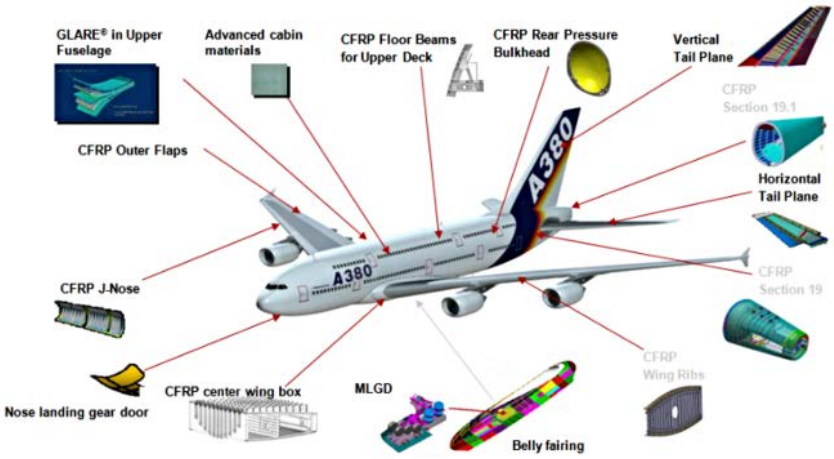

Figure 1.2 – CFRP application in airplanes [11].

This material can be typically used as a monolayer structure or combined to a metallic or polymer liner, or can constitute a layer in a multilayers structure. For instance, in hydrogen

storage and transportation vessels technologies (see Figure 1.3), the CFRP layer is generally deposited on a liner, that could be a metallic (type II and III tank) or a polymer liner (type IV tank) [12], and thus constituting a two-layers material. Such type of materials will be characterized in this work. In many cases, the thermal characterization of some material properties has to be performed while conserving multilayered physical state to avoid any destructive delamination or structure modification of the sample. In such case, a simultaneous estimation of the thermal properties constituting layers is imperative to accurately reproduce the real physical conditions. Therefore, the identification has to be directly conducted on the multilayers sample, which is one of this work aims.

Figure 1.3 – Hydrogen tank type classifications [13].

Coating used for protection or measurement purposes

The increasing use of coatings are dedicated to increase the performance of the treated material, depending on its application. It can play the role of corrosion and oxidation prevention, erosion resistance protection, ablation prevention, electric insulation, emissivity controls, thermal barrier and heat resistance for jet engines and gas turbines, wear and heat shield in gas turbine blades, thermal control system of spacecraft, and many other applications (e.g. arc-shaped magnets in automotive sector, nuclear fuel rods, fuel cells, electrochemical reactors, semi-circular fiber insulated heaters, biomedical industry, power, chemical and civil engineering, building structures, etc...).

It can be also used for temperature measurement techniques, with the two most important techniques: IR thermograhy and phosphorescence thermometry. The latter corresponds to the specific coating application considered in this work. Such type of materials, generally hardly dissociative, is a particular two-layered case frequently found in several disciplines.

The general principle of the phosphorescence thermometry, that motivated a research project in the framework of the thesis, is described. The phosphorescence thermometry consists the radiative emission of a thin layer, designated as TPT coating for "Thermographic Phosphor Thermometry". The thermometry, or temperature measurement via phosphorescence is an optical non intrusive and accurate technique. It relies on some materials phosphorescence

properties for which intensity varies according to its temperature. A large category of materials can be listed for this technique, and they are mainly constituted of inorganic oxides, oxysulfures which is a combination between a component with the oxygen and the sulfur, in addition to other rare metals. This technique offers a lot of advantages for the temperature measurement at the surface of mobile devices such as the piston (see Figures 1.4 or Figure 1.5) or valves (see Figures 1.6) of an internal combustion engine.

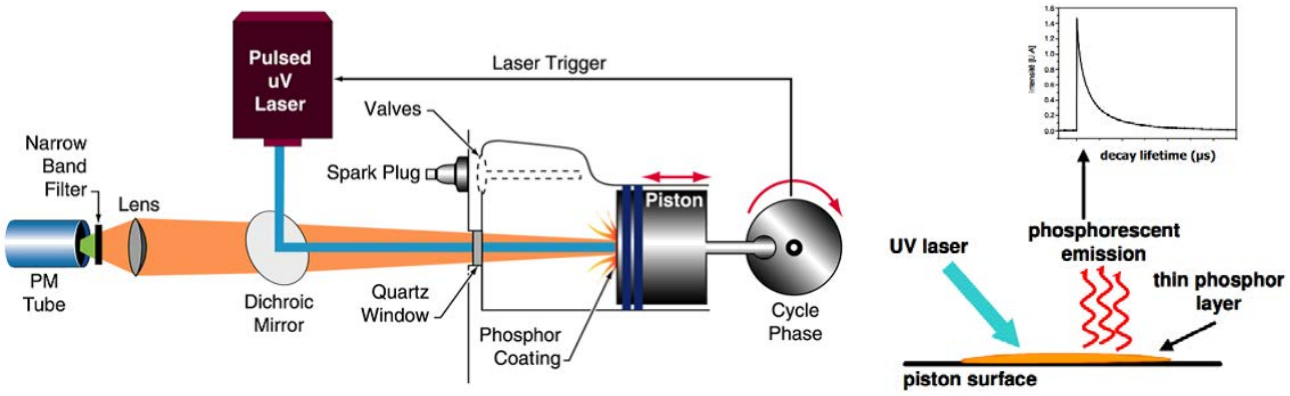

(a) Overview of the application [14]

(b) Measurement principle [15]

Figure 1.4 – Application of the phosphor coating on the surface of the engine piston.

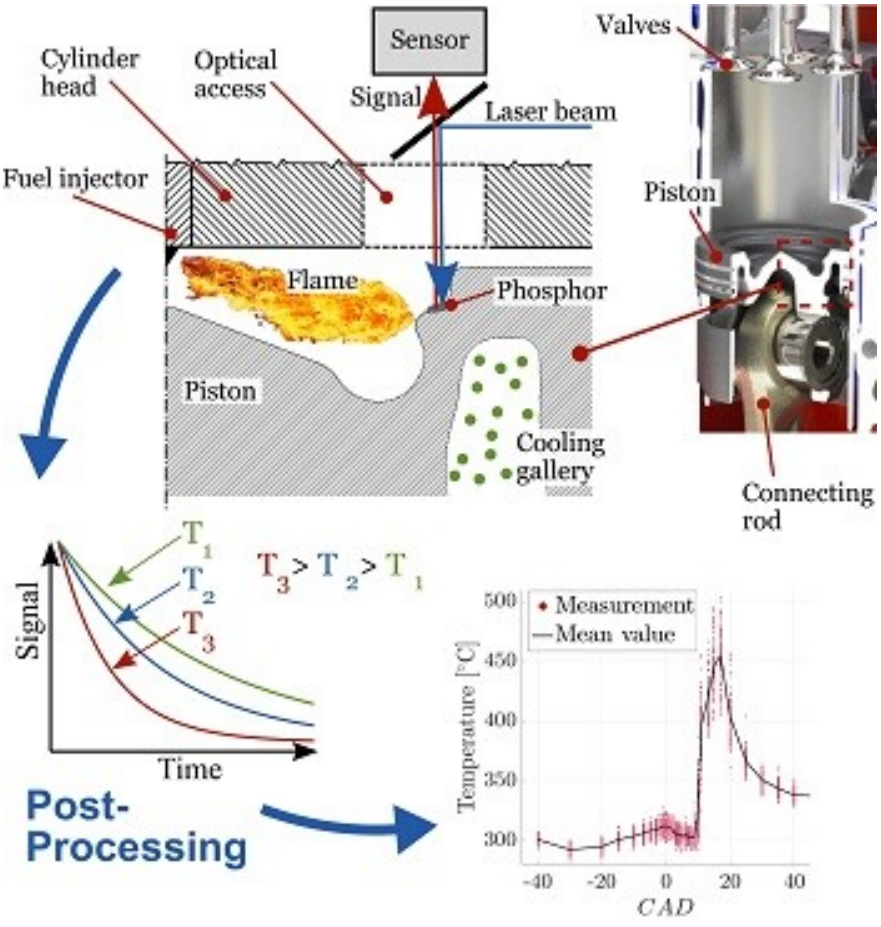

Figure 1.5 – Principle of phosphorescence thermometry at the surface of mobile engine piston [16].

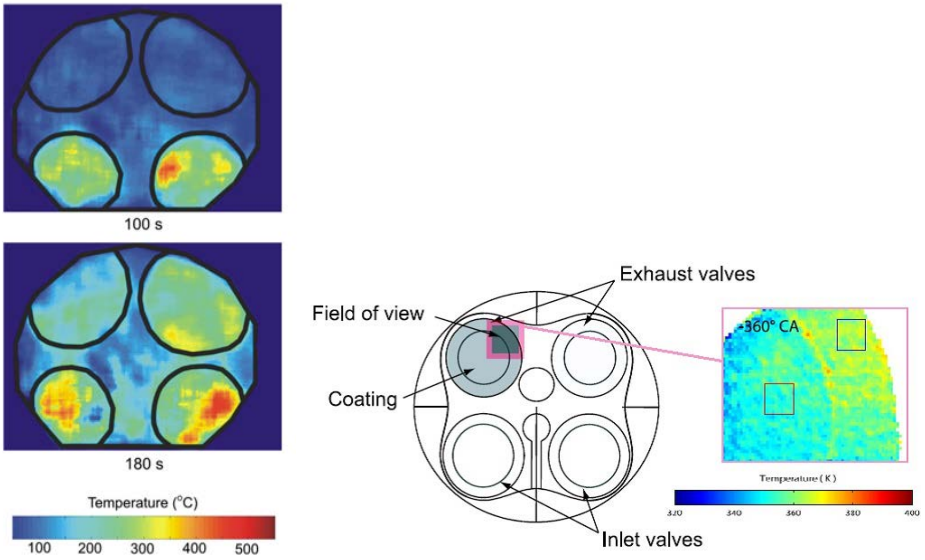

(a) Valves temperatures [17] (b) Zoom-in for more details [18]

Figure 1.6 – Application of the phosphor coating for a 2D temperature measurement at the inlet and exhaust valves surfaces.

1.3 Why thermal characterization?

As previously mentioned, the increasing development in industrial sectors appeals the increasing development of complex materials. Specialists in materials engineering respond to these demand by manufacturing new materials (composites, multilayers, porous, transparent) that can be recognized for beneficial specifications and features required in several domains such as the use at high temperatures, in corrosive medium, at high mechanical constraints and other extreme conditions.

The knowledge of specific thermophysical properties of such materials, as the thermal conductivity, effusivity, diffusivity, or the specific heat, is critical as those data are used in simulation of complex systems (e.g. mutiphysics simulation via CAD). In view of the sensitivities of these properties, it is imperative to thermally characterize them as accurate as possible.

In fact, identifying these properties becomes a crucial issue in the thermal field and retains a significant importance in several applications, for many reasons:

- The measurement of these parameters can be used to accurately test and improve materials
  - for the control and validation of the manufacture processing (i.e. thermal control of the materials thermal behavior during/after manufacturing) ;
  - for the analyses of thermal and/or mechanical stress and shock ;
  - for preventing thermal fracture ;
  - for analyzing fiber placement in production processes to accurately predict temperature profile through a particular composite structure ;
  - for the evaluation of manufactured material quality

- These parameters can serve as inputs for numerical simulations used by engineers to model complex systems in order :
  - to obtain accurate prediction of temperature evolution inside the structure ;
  - to predict the structures behavior to thermal stresses;
  - to modelize the heat transfers;
  - to identify severe boundary conditions;

Why estimating the thermal diffusivities?

The thermal diffusivity quantifies the material heat transfer rate. For a given temperature difference, the larger the diffusivity, the faster is the heat transfer through this material.

The thermal diffusivity parameter appears in the heat equation that describes the heat transfer in solids called conduction. The heat equation is a partial differential equation that simulate the evolution of the temperature or heat over time in a solid medium.

In steady state methods the conductivity λ in $W/(m \cdot k)$ is the only thermal property that may be identified. However, the diffusivity $a[m^2/s]$ or the effusivity $b[J/(m^2 \cdot K \cdot s^{1/2})]$ can only be determined in non-stationary methods.

1.4 Panorama and Classification of thermal characterization methods

There is no universal classification of the different thermophysical parameters estimation methods. Thus several features and criteria can be used to classify those methods:

1. The excitation and measurements method (i.e. with or without contact, see 1.4.1):
   (a) Excitation method: intrusive or non-intrusive, meaning that the excitation/perturbation is performed with a physical contact (electrothermic methods) or without any physical contact (photothermal, photoacoustic methods).
   (b) The measurement method may also be with or without any contact.
2. The measurement spatial extent: local or extended (see 1.4.2).
3. The estimation regime (i.e. stationary or variable including: quasi-stationary for long time, transitional, and periodic states, see 1.4.3).
4. The excitation temporal shape: Dirac (impulse), pulse, step, periodic (modulated), or arbitrary time shape (see 1.4.4).
5. The excitation spatial shape: local, uniform, modulated (in space), pointed, Gaussian, rectangular, parabolic, polynomial cubic spot or random shape (see 1.4.5).

6. The measurement location: localized on or out of the excitation (see 1.4.6).
7. The measured quantities (temperatures, flux, pressures,..., see 1.4.7).
8. The estimated quantities: thermal diffusivity, conductivity, capacity, or effusivity (see 1.4.8).
9. The problem geometry and coordinates that depends on the system geometry (1D, 2D, 3D, nD) and the excitation form: in a Cartesian (rectangular), cylindrical or spherical coordinates system (see 1.4.9).
10. Other minor classifications (see 1.4.10).

A panorama of some existing thermal characterization methods operating in unsteady state regimes, is previously presented by Degiovanni in [19], and then extended by Rodiet in [20], as shown in Figs. 1.7a, 1.7b and 1.8a. A definition of the characterization methods and the corresponding estimated parameters for each of them are tabulated in Table 1.8b.

1.4.1 Contact and non-contact methods

These methods can be also classified as: intrusive and non-intrusive methods, involving the excitation and/or the measurement those can be performed with or without contact with the material specimen.

Contact excitation methods

Methods relying on contact excitation such as the hot plane [21–23], the hot wire [19, 24, 25], the probe method [19], two-rod probe method [22], the hot strip [26, 27] and hot disk methods [22] are easy to implement, have simple instrumentation, and are relatively inexpensive [28]. The major branch of such types of excitation, is the electrothermic methods which manipulates electrical resistance in order to create a temperature gradient in the specimen. It is the oldest and the simplest type to implement, and it gives low-cost solution.

Contact excitation methods are almost always coupled with contact measurements. The measurement (i.e. temperature, fluxes,...) typically required for the identification of the thermophysical properties, are generally performed with contact between the sensors (e.g. thermocouples,...) and the sample. Those methods may face several obstacles that can be overcome when using non-contact methods, citing:

- The determination of contact resistance related to the interface when having non-perfect contact, which is almost always the case in contact methods.
- High temperature handling, which is inaccessible using contact measurement methods, leading to probable destruction of the sensor.
- Sensor thermal capacity determination which is also difficult using contact methods.

Methods in variable states												
Measurements	Perturbations											
				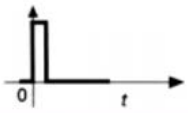			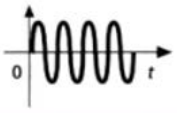					
Geometry	1	2	3	1	2	3	1	2	3	1	2	3
I				A			B					
II		C		D	E, F		G					
III	H						I	J		K	L, M	
IV	N	O	P	Q								

Measurements
I. 1 temperature over the perturbation
II. 1 temperature outside the perturbation
III. 2 temperatures
IV. 1 Flux and 1 temperature

Geometry
1. Plane
2. Cylinder
3. Sphere

(a) Classification of thermal characterization methods

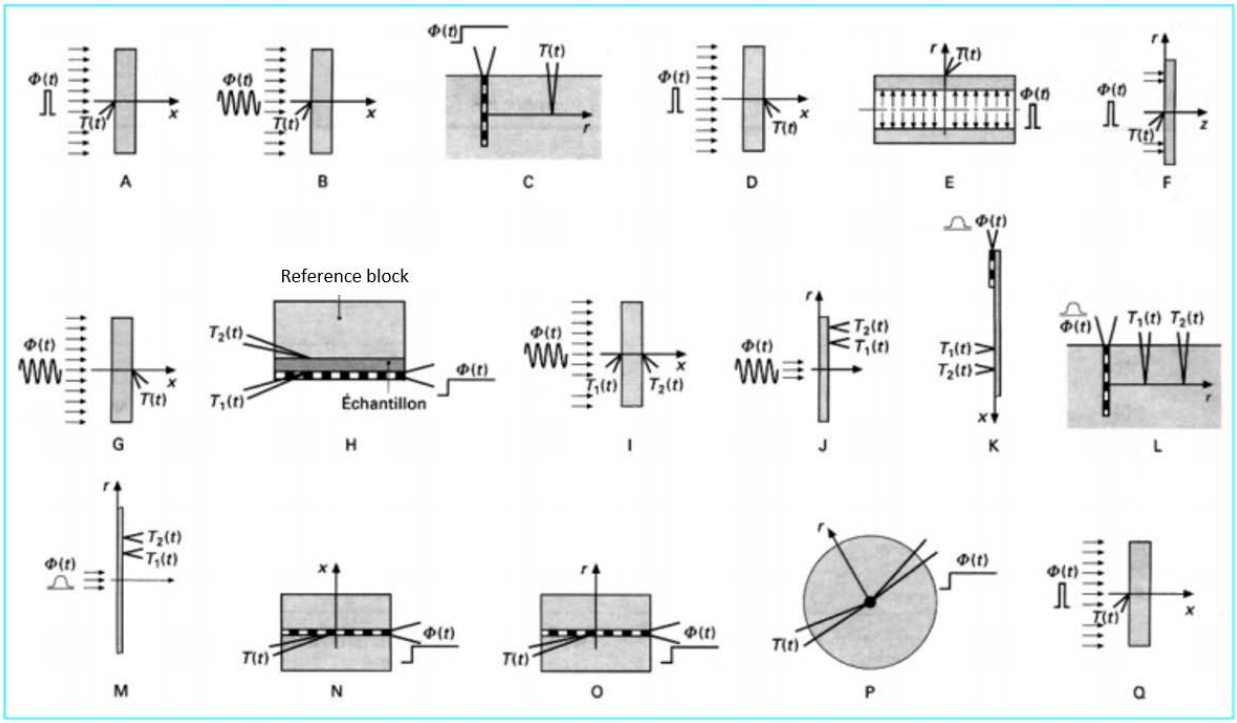

(b) Panorama of the methods

Figure 1.7 – Classification and panorama of thermal characterisation methods in unsteady state, by Degiovanni in [19].

Perturbations / Measurements	Step			Dirac					Periodic			Random			Arbitrary		
I				A					B						R		
II		C		D			E,F		G						S		
III	H								I	J		K,W	L,M,Z				
IV	N,X,Y	O	P	Q													
V				T	U	V						A					
Geometry	1a	2a	3a	1a	1b	1c	2a	3a	1a	2a	3a	1a	2a	3a	1a	2a	3a

Measurements
I. 1 temperature over the perturbation
II. 1 temperature outside the perturbation
III. 2 temperatures
IV. 1 Flux and 1 temperature
V. n temperatures outside the perturbation

Geometry
1. Plane
2. Cylinder
3. Sphere

Perturbation
a. Localized in space
b. Periodic in space
c. Random in space

(a) Classification of thermal characterization methods

Letter	Characterization method	Estimated Parameters
A	Front face flash method	diffusivity a
B	Sinusoidal state at Front face	diffusivity a
C	Two-rode probe method	diffusivity a
D	Flash method	diffusivity a
E	Flash method in cylindrical coordinates	diffusivity a
F	Converging thermal wave technique	diffusivity a
G	Sinusoidal state at Rear face	diffusivity a
H	Calorimetric method	conductivity λ
I	Sinusoidal state at Front and Rear faces	diffusivity
J	Sinusoidal state over a thin film	diffusivity
K	Fins method	diffusivity
L	Three-wire probe method	diffusivity
M	Fins method in radial conduction	diffusivity
N	Hot plane method	effusivity b
O	Hot wire method	conductivity λ
P	Spherical probe method	$\frac{\lambda^3}{\rho C}$
Q	Front face flash method	effusivity b
R	Random perturbation at Front face	diffusivity a
S	Random perturbation at Rear face	diffusivity a
T,U,V	Flash 2D	diffusivity a
W	Three layers method	diffusivity a and volumetric heat capacity ρC
X	Hot disk method	diffusivity a and volumetric heat capacity ρC
Y	Hot strip method	diffusivity a and volumetric heat capacity ρC
Z	Cylindrical Three layers method	diffusivity a and volumetric heat capacity ρC

(b) Methods definitions

Figure 1.8 – Classification of unsteady thermal caracterization methods as given by Degiovanni [19] and Rodiet [20].

- The thermal capacity of each sensor in contact with the material that can disturb the local temperature evolution and interfere with the measurements.

On the other side, it is important to note that non-contact methods are generally more expensive than the contact ones.

A listing of the most common used contact methods as well as their application domain and measurement incertitudes is given by Krapez in [23]. Some complementary information regarding the characteristic times and the measurement scales of these methods are also given by Schick in [29] and Clerjaud in [30].

Non-contact excitation methods

These methods are issued from large developments and successful evolutions of highly sensitive sensors and large bandwidths (MHz) allowing the optical thermal measurements. They have been subjected to successive progresses via the implementation of lasers and multiple opto-electronic and opto-acoustic instruments, and the resulting directional energy sources having a great flexibility of use. Two big classes of these methods could be cited:

- Photoacoustic methods: microphonic, photodeformation, interferometric, or piezoelectrical methods.

- Photothermal methods: photoreflection, radiometric, or mirage effect methods.

Detailed descriptions and comparisons of these methods can be found in [31–34]. The thermal and mechanical phenomena appearing in such classes depend mostly on the nature of the excitation (i.e. uniform, local, impulse, periodic, arbitrary, etc). The general principle of the non-contact thermal methods, i.e. the photoacoustic and the photothermal methods are presented hereafter and some of these methods are also illustrated by Balageas in [35].

Photoacoustic methods

These methods are known to be highly sensitive. This type of method is used as reference method, which is for instance the case of the **microphonic method** [36–38]. The basic principle consists in measuring the pressures variations induced by the heat transfered by natural convection between the specimen and the surrounding gas using a microphone, and where the interpretation is simplified by neglecting the sample motions [37]. This method is sensitive but cannot be used for highly diffused materials, nor for large samples, since it has low bandwidth and resolution related to the microphone cut-off frequency. Concerning the **piezoelectric method** [36, 39, 40], the thermo-elastic strains or waves resulting from the thermal waves and converted into electric signal are measured by piezoelectric transducer attached to the sample surface. It is characterized by a high bandwidth and a complex resolution due to

the coupled thermal-mechanical problem, resulting from the sensor laid on the specimen. The **photodeformation method** [24, 41, 42] exploits the specimen surface deformation induced by a power source. This deformation is detected using a probe beam for which a position sensor is used to measure its reflection. This type of method is characterized by a good spatial resolution and a high bandwidth, however it is difficult to interpret and always requires a well reflective surfaces. It is similar to the effect mirage principle (photothermic method) which is usually preferred due to its simple interpretation. The **interferometric method** is usually applied to measure the thermo-optic and thermal expansion coefficients [43] of materials. It is based on waves that are usually electromagnetic and superimposed, inducing the interference phenomenon that is used to extract information. It is characterized by a high sensitivity, however it experienced a low progression due to its highest complexity (compared to other methods), and its requirement of well reflective surfaces. This method could be also applied for measuring the thermal diffusivity of thin slabs [44].

A synthetic table representing the types of equations to solve, the advantages and the inconvenient of photoacoustic and photothermal non-contact methods, is presented by Remy in [34].

Photothermal methods

Photothermal methods are the consequence of successive developments and continuous technological evolutions. They are the most implemented methods. In this type of methods, the material is subjected to a radiative excitation created via different techniques classified hereafter following a decreasing order of price: CO_2 laser, laser diode (especially at high temperatures), flash lamp, halogen lamp, and radiant panels.

The first types correspond to the **radiometric** methods that are based on the measurement of the thermal emission, generally in the infrared range, emitted as a response to the excitation by the sample surface. A photoelectric collector is used for the monitoring of the temperature evolution during the infrared emissions at the front and/or back face of the material. It is the simplest method, with the largest bandwidth and it can be applied to any sample type. It has some restrictions and inconvenient, such as: i) it requires sometimes the knowledge of the surface emissivity, ii) it cannot be used to characterize semi-transparent materials without coating and iii) has low sensitivity when testing metals. Radiometric methods are characterized by temperature evolution measurements and a possibility to have, using an optical scanning device, a thermal cartography over an extended zone. The infrared thermography is highly implemented in the non-destructive control (NDC) domain.

The flash method is a generic class of frequently used radiometric methods that constitute a significant subset of photothermal methods. This method will be more detailed in the next section 1.5. It consists in subjecting the specimen to a radiative excitation, which generates a heating at the sample surface consequently to the photons absorption. This radiation will increase the front face temperature and give rise to heat fluxes inside the sample due to the generated temperature gradient. Eventually, other phenomena can take place simultaneously,

such as:

- mechanical dilatation phenomenon (**acoustic waves propagation** [29]) ;
- variation of the refracting index of the air located above the tested surface (**mirage effect** [41]) ;
- change in the excitation surface reflection coefficient (**photoreflection methods** [30]).

The **photoreflection method**, particularly adapted for the metals characterization, is based on the measurement of a probe beam intensity variation, when this beam is reflected on the heated sample surface. This method is generally characterized by a simple interpretation, a high spatial resolution and bandwidth. However it requires well reflective surfaces and has a sensitivity that depends on the sample.

The photothermal methods that use **mirage effect** for the deflection measurements, are based on the detection of the air refraction index gradient in the vicinity of the surface, resulting from heating the material by a modulated laser beam. This detection is performed by an optical beam "the probe beam", and lead to in-plane diffusivities estimation. The in-depth diffusivity can be also estimated using two probe beams placed at both sample sides, in addition to an intense pump beam in order to have a unidirectional heat transfer [45]. This estimation technique is characterized by a high sensitivity and simple interpretation, however it has been proved inappropriate for large-width materials [46–50]. Also, it requires several conditions: convex surfaces, good surface condition and it has medium bandwidth and spatial resolution.

All these types of photothermal methods can be conducted using front or rear face measurement, using infrared radiometry or thermocouples (i.e. with or without contact temperature measurement), using periodic or transitory (impulse, pulse) or a any random mode for the excitation, and can lead to the estimation of diffusivity and/or effusivity. This type of methods has the highest sensitivity and can be adopted for opaque as well as semi-transparent materials, with the simple condition of regular surface state.

The strength of photothermal methods lies in their interpretation simplicity; they are based only on the heat equation (1, 2 or 3D according to the excitation type) where the temperature is the only scalar value. In contrast, the photoacoustic methods are hard to interpret, they require a vectorial problem resolution (deformation fields) where the heat equation (thermal part) and the acoustic equation (the mechanic part) are coupled [51].

Contact and non-contact measurement methods

Temperature or heat flux measurements obtained by contact sensors (e.g. thermocouples, some fluxmeter, ...) can be highly noisy. The electrical signal delivered by the sensor is almost always disturbed. These perturbations are then superposed to the measuring signal transmitted in the measurement chain [29] (sensor, transmission line, electronics). On the other hand, non contact temperature measurements, generally conducted by infrared camera, allows to

overcome the problem of exact knowledge about the measures points position. It encourages the parameters estimation optimization in terms of variances reduction, by offering the possibility to have a statistical data treatment due to the significant amount of information given by the camera (e.g spatial resolution about tens of thousands measures in only one experience).

1.4.2 The measurement spatial extent

It could be a subset of the contact and non-contact measurement techniques. Some methods are based on local flux or temperature measurements at specific locations, for instance one temperature measurement such as the original 1D flash technique of Parker, several local temperature measurements at different locations such as the calorimetric method, fins method, three-wire probe method, or flux and temperature measurements such as the hot plane method, hot wire method, spherical probe method, hot disk method, hot strip method.

Or it can be based on extended temperature measurements, such as the 2D and 3D flash methods that can be conducted using several thermocouples or a single IR camera.

1.4.3 The estimation regime

The estimation methods may also be classified in terms of regime of heat transfer.

Steady-state methods

The thermal conductivity λ is the only parameter that could be estimated at steady state regime. This can be achieved by simultaneously measuring the temperature gradient and the constant heat flux passing through the plane sample, following this equation (for a plane slab):

$$\lambda = \frac{S \cdot \Phi}{e(T_1 - T_2)} \tag{1.1}$$

where λ is the thermal conductivity, S the surface crossed by the flux, e the material thickness, Φ the thermal flux, T_i the temperatures. Generally, two global measurement techniques can be mentioned:

- The hot plate method [52–54] and the guarded hot plate method [25, 55]. Those methods are conducted for insulating materials (insulators) and for large size samples where $\lambda < 0.3\ W/(m.K)$.

- The bar method [56–59] that uses the fin model and is applied for conductive materials where $\lambda > 0.3\ W/(m.K)$. This method is not used anymore due to the difficult experimental and theoretical controls [19].

Unsteady-state methods

The variable regime allows the estimation of many thermal properties such as the volumetric thermal capacity $\rho \cdot C$, the conductivity, the diffusivity $a = \frac{\lambda}{\rho \cdot C}$, the effusivity $b = \sqrt{\lambda \cdot \rho \cdot C}$, and other combinations of λ and $\rho \cdot C$. It is important to note that all photothermal methods, including the radiometric method (particularly the flash method), the photoreflection and the methods relying on mirage effects, correspond to variable state methods.

Among the unsteady-state methods, several sub-types methods may be identified.

The quasi-stationary methods

The quasi-stationary methods are characterized by the simultaneous measurement of the generally constant heat flux and the time variable temperature. Based on the model and identification complexity, these methods can estimate one or many thermophysical properties. It is called "quasi-stationary" since the identification often takes place at long times. The corresponding model should take into account the heating element, the medium, and the interface probe-medium. The quasi-totality of such models considers unidirectional heat transfer. Thus, the most adequate modelling tool is the thermal quadrupoles method. Two global measurements techniques could be applied according to the material type: the hot wire method [19, 60] and the probe method [19]. The first method is used for solids and liquids [61] thermal conductivity identification, and can be implemented at high temperatures. The second one is well adapted to porous material thermal conductivity estimation.

The transitional methods

The transitional methods is the generic term for the flash methods. This type on method is characterized by the measurement of the temperature only (sometimes at one point), that quickly change with time. The measurement is simple, which is not the case for the model. The relatively complex identification is generally applied at short time.

Other techniques can be classified as transitional methods, for instance, Scanning thermal microscopy (SThM) technique [29] and 3ω-method [22, 62–64].

The periodic methods

They are usually based on the measurement of one or many temperatures in order to measure the dephasing between two measures or between the measure and the perturbation. The samples corespond to small width disks subjected to a periodic excitation. This type of methods has excatly the same type of applications as the flash methods [19].

1.4.4 Excitation temporal shapes

Flash excitation

This frequently used method, considered as a reference method, is continuously improved but may suffer of some drawbacks due to the relatively high energy level that can lead to the sample

deterioration. The excitation is performed via a flash light or a laser impulse/pulse and generates a thermal response of the sample. The nature of the excitation is of prime importance as it affects the nature of the measured signal. Such type of flash/impulse thermal excitation represented by a Dirac function, is assumed and considered by most of the flash based methods [2, 24, 37, 65–82].

In flash based methods, flash or laser induced excitation are, in most cases, quasi-instantaneous and considered as impulse modeled by a Dirac function, which is almost always the case in this study. However, it can be also modeled by a pulse, which has been the subject of a work in 3.6.3.

Pulse/ crenel excitation:
Such type of excitation is considered in some cylindrical three layers device methods [83], some radiometric methods [36, 84], and in the present study (see 3.6.3).

Step excitation
Several methods relies on a continuous excitation resulting in a step time shape. Among those methods one should quote the two-rod probe method, the calorimetric method, the hot plane method, the hot wire method, the spherical probe method, the hot disk method, the hot strip method, and some radiometric methods such as the Laskar method [85].

Sinusoidal excitation
The sample temperature evolution will be periodic once changing periodically the excitation source (typically a laser) and for one time the steady state. In these cases, it is possible to measure the resulting temperature amplitude and its time delay relative to the excitation signal. This technique was frequently used [86, 87], since it can benefit from the advantages of an excellent signal/noise ratio. However, it is relatively slow and ill-suited for the thick material samples that require high frequencies of excitation. Periodic heat source for the excitation can be used in some hot strip methods for the estimation of very low thermal effusivity [38], or periodic laser based methods [29, 88]. Periodic heat source generating intensity modulated light beam is also used in photoacoustic piezoelectric methods [36, 40], microphonic photoacoustic methods using modulated laser of halogen lamp beam (periodic lighting estimation [36, 38], photopyroelectric method using periodic radiative excitation [89, 90], photodeformation methods using modulated laser beam [24, 41, 42], mirage effect based methods using modulated pump heating laser beam [24, 46, 91] and some radiometric methods [92, 93].

Gaussian excitation
The Guassian time shape excitation is considered in [94].

Random or Arbitrary excitation
This type of excitation treated in [24, 95] is well adapted for photoacoustic control and for NDC, and has been firstly implemented for photoacoustic spectroscopy [96, 97] when PRB (pseudo

random binary) sequence has been used. The benefits of such sequence is the highly abundant frequencies and the low amount of subjected energy. It was also disciplined for photothermal radiometry [98] and implemented in thermal diffusivity measurement [99] and for other applications. Such type of excitation is well more suited for more flexible materials than the pulse type. Its major drawback is its complexity resulting from the requirement of signal processing techniques. For example, one can cite some well-known methods relying on such types of excitation: the fins method [100, 101], the three-wire probe method or the three layers method. Some photothermal radiometry methods consider also such temporal shapes of the excitation, as [20, 24].

Sometime excitation can take arbitrary form, such as three wire probe [19], fins method, three layer method and the case of some laser excitation.

1.4.5 Excitation spatial shapes

The major classes of excitation spatial shapes are: local, uniform, modulated or periodic, pointed, Gaussian, rectangular, parabolic, polynomial cubic spot or random shape excitation. Some methods and references for different types of excitation spatial shapes, can be extracted from literature, citing:

- Localized in space: hot strip method [22], non uniform or uniform fins method, and other flash methods [71, 81].
- Uniform in space: guarded hot plate methods [25, 55, 102], hot wire methods [19, 102], calorimetric methods [19], parker flash model [2, 24, 66, 67], partial times method [24, 103], partial time moments [65, 104, 105].
- Periodic/sinusoidale in space: Krapez periodic grid-like mask technique flash thermography (ENH estimator) [67, 77–79], Bamford flash method with nodal periodic strategies [106], or other spatially periodic flash excitation [67].
- Pointed in space: Dirac function in space and time [107].
- Gaussian in space: [29, 69, 70, 84, 108, 109], or polynomial cubic instead of Gaussian for simplification [110, 111].
- Arbitrary in space: Souhar method for anisotropic materials (MSEH estimator) [37, 74, 75], Remy method for anisotropic materials [76] , Vavilov technique for also anisotropic materials (ENH estimator) [80], and other authors [84, 108]
- Random in space: Batsale flash experiment with random spatial distributionnusing spatially random mask [112], Bidirectional flash method [71].
- Uniformly localized in space: three-wire probe, spherical probe method, modified hot wire technique [19, 22], hot plane method [21, 23], periodic methods [93], radial heat flow methods [113–115].

In this work, some cases considering a parabolic spot with cubic or cosine functions will be treated, see 3.6.1.

1.4.6 Measurement location

Measurement could be performed at different locations, for instance it can be within the perturbation zone or outside this zone as most of the experiments based on flash techniques, three wire probe methods, thermal wave methods [116, 117].

It can be also conducted at the front face (i.e. the face subjected to the excitation) or the rear face of the sample. Front and rear cases will be treated in Chapter 3. Furthermore, when dealing with two-layers or multilayers material, different combinations of excitation and measurements sides (each of these action may be performed on each face) can be considered. This gives rise to four possible experimental configurations that will be detailed in Chapter 4.

For instance, one can cite:

- Front face measurement: a unique temperature measure (generally within the perturbation zone), or several measurements at different locations, both using thermocouples [24, 67], or surface measurement using IR thermography [81, 107, 108, 112, 118–120].
- Rear face: a unique temperature measure at one location or several measures at different locations, both outside the perturbation zone (rear sample side) and using thermocouples [2, 24, 66–68, 71, 103], or a surface temperature evolution measurement using IR thermography [72, 84].
- Front and rear face: where several measures are conducted simultaneously at the front and rear sides, usually using thermocouples [92, 121–123].

1.4.7 Methods classification according to the measured quantities

Sometimes methods can be classified according to the measured quantity that be the temperature at one or several positions, and/or heat flux. A list of these methods is already presented in 1.4.2.

- 1 temperature measurement, such as the original 1D flash technique of Parker, two-rod probe method, some methods performing in sinusoidal state by applying periodic excitation, and other methods.
- 2 temperature measurements such as the calorimetric method, fins method, three-wire probe method, three layers methods, etc.
- Several temperature measurements on both material sides and at different locations, already cited in 1.4.6 [121–123].
- 1 flux and 1 temperature measurements such as the hot plane method, hot wire method, spherical probe method, hot disk method, hot strip method, and others.

The methods can be also classified based on extended temperature measurements, such as the 2D and 3D flash methods, conducted using several thermocouples or IR camera.

1.4.8 Methods classification according to identified quantities

Identification methods based on the study at steady state (e.g. hot plate and guarded hot plate methods, the hot wire method) allows to estimate the thermal conductivity, only.

However, the global well known methods performed in unsteady states, are usually investigated for:

- the estimation of conductivity and/or diffusivity: the flash method, probe methods, fins method, 3ω method, converging thermal wave technique, photoacoustic piezoelectric and photodeformation methods, mirage effect methods,

- the diffusivity and the volumetric heat capacity $\rho \cdot C$ such as the hot strip method, the hot disk method, the three-layers method.

- the estimation of the effusivity b [124] using contact methods [23] such as the hot plane method and non-contact methods [36] such as microphonic photoacoustic methods, and some front face flash method.

- the estimation of thermal capacity with methods known as “calorimetric methods” [125, 126].

- the identification of a set of different parameters, such as the spherical probe method identifying $\frac{\lambda^3}{\rho \cdot C}$.

These identified quantities correspond to those of a monolayer material, which is the case in chapter 3, or of each layer in multilayer or bilayered material, which is the case in chapter 4.

Moreover, when treating multilayers materials (e.g. two-layers or coating on substrate), some authors considered a perfect thermal contact between layers which correspond to neglect interface contact resistance Rc (such as in Chapter 4 and [127–132]) . Others authors estimate the contact resistance at the interface simultaneously with the other required parameters [133–135].

1.4.9 Problem geometry

Thermal identification methods can be dedicated to:

– cartesian plane geometries such as the plane flash methods, the calorimetric method, the hot plane method, the hot disk method, the hot strip method, the fins method, the three layers methods, the hot plate, the guarded hot plate or the bar method.

– cylindrical geometries such as the photoacoustic microscopy by photodeformation, the two-rod probe method, the hot wire method, the cylindrical flash method, the thermal-wave method, the three wire probe method, the fins method in radial conduction or the cylindrical three layer method [83].

– spherical geometries such as the spherical probe method or the SThM technique.

This classification cannot ignore the presence of some methods devoted for plane geometries, but modeled in cylindrical coordinates such as the hot disk methods.

These methods can also be classified according to the "dimension" of the heat transfer. A method can be qualified as one dimensional estimation method (1D) when it can estimate a property in one direction with a one-dimensional heat transfer, e.g. the in-depth thermal diffusivity of one layer. A method can be qualified as two (2D) or three (3D) dimensional when the estimation is extended to properties in two or three different directions. This is particularly important when dealing with orthotropic or anisotropic materials.

– 1D: hot plate and guarded hot plate methods, hot wire methods, hot plane methods, probe methods, hot strip method, cylindrical three layers device method [83], 3ω method [22, 62], microphonic methods, calorimetric methods, 1D flash methods [2, 24, 66, 85, 136–140], etc.

– 2D: Photoacoustic microscopy by photodeformation, photoacoustic-piezoelectric, transient hot wire technique [141], transient hot strip technique [26, 142], 3ω method [63], 2D flash methods [65, 68–70, 72, 73, 81, 105, 112, 119, 120], etc.

– 3D: Spherical probe method [22], transient hot strip method [143], Three-layers method [83, 102], 3ω method [64], 3D flash methods [37, 71, 74–79, 108, 110, 111, 122, 144], etc.

The dimension could be of higher order when considering multilayers materials. The estimation method can be qualified as 6D when estimating the tensors of two orthotropic layers constituting a two-layers material with perfect contact. This last case of estimation will be presented in 4.5.2. In this chapter, 4D estimation, i.e. when one of the layers is supposed isotropic and the other is orthotropic, is also studied.

1.4.10 Other minor classifications

Thermal parameters identification methods can be classified according to other criteria, i.e. criterion related to the model resolution, to the boundary and initial conditions, to the presence of heat generation or thermal contact resistance, and so on.

– Analytical, semi analytical or numerical resolution.

– Methods applied to isotropic, orthotropic or anisotropic (3D) materials.

– Methods applied to monolayers or multilayer materials.

- Methods considering (or not) the non-homogeneous materials properties, their dependencies on the temperature.
- Methods dedicated to multilayer materials and assuming perfect thermal contact or considering a thermal contact resistance between layers.
- Methods taking (or not) into account the heat losses (e.g. convection and radiation losses).
- Methods studying cases where the sample material is placed in vacuum, at atmospheric pressure, at high temperature, or other possible conditions.
- Methods studying heat conduction cases where a homogeneous or heterogeneous heat is (or not) generated inside the sample.
- Methods studying opaque, or semi-transparent materials, porous materials, solids, liquids or gas.
- Methods studying homogeneous or heterogeneous materials.
- Methods classified by the types of their boundary conditions [first (Dirichlet BC), second (Neumann BC) or third kind (Robin BC), or any other non-homogeneous BC].
- Methods whose resolution is based a certain type of minimization algorithm, i.e. deterministic, stochastic, gradient based or gradient free methods, global or local algorithms, and so on.

1.4.11 Concluding remark

A general overview of thermal characterization methods found in the literature and their classifications based on major and minor criteria, was presented. The next sections will focus on the flash method, a generic class of methods, that will be investigated in this work.

1.5 State of art on Flash method and its evolution over past years

The Flash method is known as “the standard technique for measuring solids thermal diffusivity“. Originally developed by Parker in [2], this method is focused on the estimation of the thermal diffusivity of isotropic and homogeneous sample materials. In the past decades, this method experienced successive evolution from various sides (model, experiment, identification strategy), leading to a new class of flash methods using thermal radiative perturbation (usually short laser pulse) has been developed. Nowadays, this method appears to be one of the experimental techniques frequently used in a wide numbers of industries and scientific laboratories.

1.5.1 Flash method origin

Parker [2] proposed the first approach estimating the in-depth (i.e. transverse) thermal diffusivity of homogeneous and isotropic materials. This estimation was performed by means of a one dimensional heat transfer created by a uniform and short energy burst applied at the sample front face. The temperature elevation at the rear face of the sample is recorded using thermocouples (Parker case), or more recently by photodetectors using IR cameras. The transient rear surface temperature is predicted via Fourier series. An estimation strategy is then applied that consists in identifying the temperature limit T_{lim} depending on the amount of energy injected Q, the half rise time $t_{1/2}$ concept and the thermal diffusivity using a graphical method.

This approach has been widely improved over the past 50 years. Some methods were devoted for the estimation of the in-plane and in-depth diffusivities using non-uniform thermal excitation for anisotropic materials [71, 72], or specifically orthotropic materials [145].

1.5.2 Continuous evolution of the flash method

The uniform excitation applied to an isotropic material will often induce a one dimensional (in-depth) heat transfer across the material, which was the case with the classical method of Parker. A method based on a partial surface irradiation of the sample was proposed in 1975 by Donaldson and Taylor [113] for the estimation of in-plane and in-depth diffusivities of anisotropic materials. This method was then exploited by Amazouz [114] in 1987, and then experimentally and theoretically improved in 1991 by Lachi [115]. Fins model was also introduced in transitional regime for the plane heat transfer evaluation when having a homogeneous, opaque and isotropic sample of small width and large extension. The diffusivity is calculated using the ratio of two temperature measured at the same point at two different instants (Harmathy in 1964 [146] and Steere in 1966 [147]. The diffusivity has also been estimated using the ratio of two temperatures measured at the same time at two different points (Katayama in 1969 [148]). This method was then improved, by working in the Laplace domain, in order to eliminate the requirement of the heat flux time shape knowledge (Kavianipour in 1977 [100]), with some exploitations taking into account the lateral losses (Hadisaroyo in 1992 [101]). A method dedicated to the estimation of insulators longitudinal diffusivities was introduced in 2005 by Remy [149] who used the fin model to overcome the knowledge of the boundary conditions as well as a step excitation to have a significant input energy.

Later on, additional techniques have been developed in order to estimate simultaneously the diffusivity in the two principal directions (for orthotropic or anisotropic materials) from transient measurements by creating a bi-dimensional heat transfer using a localized excitation [72, 122, 145]. Furthermore, other improvements have been made concerning the measurements techniques by the development of the IR thermography technologies allowing the excitation spatial abstraction [73, 74, 78], and temporal abstraction [149]. Other attempts have been made to modify the excitation type by replacing laser impulse by laser pulses [85] or by succesives impulsions [140].

Other evolution criteria

The model of parker did not take into account the losses, thus a biased solution was generated. This bias was then reduced by considering the losses by A. Degiovanni who introduced the partial time methods in 1977 where several couples of points and characteristic times are considered in [150, 151] for the diffusivity estimation over a back face thermogram. The same author proposed with M. Laurent in 1986 the partial time moments methods allowing to treat a large amount of information by exploiting all the thermogram points using the weighted sum concept [65, 152]. Other evolution was performed by the measurement of locale and longitudinal thermal diffusivities using IR thermography and non-uniform thermal perturbation conducted via a periodic mask. It was introduced and developed by Krapez in 1999 and 2004 [77–79], by applying Fourrier transformation, after ensuring an increase in the longitudinal thermal gradient. Moreover, one can add the intervention of Batsale [112] in order to identify the bi-dimensional longitudinal diffusivities fields using spatially random mask.

Actually, "flash methods" is a generic term referring to a large methods class broad spectrum of methods that relies on a photothermal excitation, which is usually short in time. As already mentioned, the excitation can be localized and non-uniform in space. The application of this methods class has been largely extended through the past decades: it was applied to thin layers, multilayers, porous, composites [153, 154]), semi-transparent materials [155–157], non-destructive control (NDC) [67, 135, 158, 159] and at high temperatures [37, 75, 138, 139, 160]. In addition to the present method evolution, the estimation procedures have also progressed while taking into account, more and more specifically, the influence of heat losses. The pioneering works were performed without taking into account any heat losses, e.g. the classical method of Parker thas was based on the half-rise time [2], and the slope breaking time method of Hay [103]. Those methods are based on thermogram characteristic points.
Then, the improvements of the measurement techniques, has allowed consideration of heat losses. For example, the "partial time method" [150, 151], improved by the "partial time moments method", uses a weighted sum for the thermogram [65, 152]. The least square method [161] then the "logarithmic transform method" [70], consider the sample cooling with the environment. Improvements, for a better consideration of heat transfers between the sample and the environment, are still in progress.

Focusing on flash methods used to identify the thermal diffusivity(ies) of mono-layered materials, they can roughly be classified according to the dimensions or anistropy of the investigated problem:

1. 1D or one-dimensional identification of the in-depth thermal diffusivity by the original method of Parker et al. [2].

2. 2D or two-dimensional identification of the in-plan thermal diffusivities with a linear estimation:

   (a) ERH: Estimation using Ratio of Harmonics [73, 76, 149],

   (b) ENH: Estimation using Normalization of Harmonics [78, 80, 81].

3. 3D or three-dimensional identification of in-plane and in-depth thermal diffusivities, using 3 steps method known as MSEH or Multiple Steps Estimation using Harmonics [74].

The evolutions of the Parker's method will be presented more in details later in chapter 3.

1.5.3 Non uniformity of the excitation

The increasing use of laser used to generate the thermal excitation allows significant improvements in the thermal diffusivity estimation. Contrary to what was assumed in the first works, the radiative heat flux $q^{''}[W/m^2]$ is non uniform. This assumption was due to a lack of information concerning the excitation spatial distribution and of specific devices for the correction of this non-uniformity [122]. Once the infrared camera was used, the non uniformity of the laser spatial distribution has been revealed and the bias introduced by the excitation problem was regularized for the transversal diffusivity estimation.

In order to estimate the diffusivities through the principal anisotropic axis, a non-uniform excitation is imposed on the anisotropic material surface. This excitation may be localized, periodic or random, therefore a two-dimensional heat conduction takes place in the medium. For the estimation of anisotropic in-plane diffusivities, Philippi [73] proposed in 1994 a method to overcome the spatial form of the thermal perturbation. Later on, Remy developed in 2005 [149] and 2007 [76] a new estimation technique that allows the identification of orthotropic material diffusivities. This work is an extension of the method proposed by Philippi that improved the signal/noise ratio by exploiting all available temporal measurements and overcame the temporal form of the thermal excitation.

The significant contributions of these authors, particularly those performed by Ruffio [110] and Souhar [37], will be detailed afterwards, in the chapter dedicated to the method developed in the framework of this thesis (see 3.5).

How to identify in-plane diffusivities in orthotropic materials?

In order to have access to the longitudinal in-plane diffusivities of an orthotropic or anisotropic material, one of the sample faces should be non-uniformly excited (e.g. local excitation) using:

1. a periodic mask as used in the experimental setup developed by Krapez et al. [77–79].
2. a spatially random mask as used in the experimental setup developed by Batsale et al. [112].
3. a local resistances (in contact methods).
4. a laser emitting a non uniform beam at the surface of the material and an infrared camera to measure the temperatures fields on the front or back face of the sample as used in the experimental setup developed by Gruss et al. [162, 163], and which is the case in this study.

1.5.4 Why using flash method?

The flash method is the most popular method dealing with the solid thermal diffusivities measurement. Despite the fact that numerous methods could be implemented for the estimation of thermophysical properties, flash methods appears to be the most convenient since it is an "non intrusive method". This method, developed for flat surfaces, may also be adapted to slightly curved surfaces. It can also deal with relatively complex materials e.g. anisotropic, nonhomogeneous, porous multilayers materials. It can generate non-uniform heat transfer required for the simultaneous identification of the transversal and longitudinal diffusivities.

Advantages of flash method

The numerous advantages of the flash method, as highlighted by Souhar [37] and Rodiet [20], are listed below:

1. It is a rapid method as the measurement requires only one experiment in the transient regime.

2. It can estimate the thermal diffusivity independently from convective losses.

3. It can be completely non-intrusive as it is possible to conduct excitation and measurement using optical techniques.

4. It necessitates a limited amount of special equipment.

5. Using the same equipment, the heat capacity, thermal diffusivity and conductivity can be estimated.

6. Overall system may be used at low or high temperatures by simply cooling or heating the sample.

7. It does not require neither the temperature calibration (i.e. the signal is normalized and the temperature is slightly raised) nor a standard sample (i.e. direct measurement).

8. This method can overcome many problems encountered with other methods, such as the necessity to have a long time experiment or a large sized sample. It may also overcome difficulties relative to thermal losses (i.e. using small period experiments), or to the contact resistance between the excitations source and the sample (i.e. using a photothermal source) [67].

For those reasons the flash method constitutes a basis for the French standards (according to LNE), American standards (ASTM), Britannic (BS), Japanese (NMIJ) in order to estimate the thermal diffusivities of materials [20].

In practice, the ideal model as described in the classical flash method, can never be reached and several perturbations will definitely affect the calculations. Those perturbations must be taken into account while estimating the material diffusivities.

1.5.5 Uncertainties sources of the flash technique

An exhaustive list of uncertainties have been developed by Hay [103, 152, 164], and Vozar [165, 166]. Focusing on the difficulties encountered while estimating the thermal diffusivity of specific materials (e.g. flat, isotropic, homogeneous, and opaque) the potential uncertainties have been discussed, treated and estimated in various studies and researches [110], Souhar [37], Rodiet [20] and other authors. Some incertitude sources are listed below,

- The influence of non-uniform excitation [104, 119, 166].
- The impulse/pulse form and duration inaccurate pre-knowledge [66, 167–174].
- The influence of thermal external losses (with the environment) and its modelling using one or two heat transfer coefficients [65, 68, 150, 151].
- The non-linearity (temperature dependence) of the thermophysical properties [164, 175].
- The effect of the sensor/sample contact [152, 164, 166, 176], and the consequence of the response time on the temperature measurement [104, 166].
- The influence of the layer of paint applied on the sample exposed to the excitation [101, 173, 177, 178].

1.5.6 Infrared thermography

The infrared thermography is widly used within the framework of themophysical properties characterization and can be considered as a relatively modern technology. The technology evolutions have encouraged the development of this measurement technique by offering more and more affordable infrared cameras having higher acquisition speeds (today it is possible to reach thousands of images per second), multispectral imaging, and higher and highret resolution (in the order of ten micrometers) [67]. This measurement technique is the most adapted for the 3D flash methods, allowing to measure the evolution of temperature fields using appropriate set up.

1.6 Literature review on the orthotropic or isotropic monolayers, two-layers or multilayers characterization

A detailed state of art of the methods dedicated to the thermal characterization of orthotropic monolayer materials, is presented in chapter 3, in order to highlight the originality of the method developed in the present work. An other state of art of the methods dedicated to the

thermal characterization of multilayers (particularly two-layers) materials, i.e. the determination of the thermal diffusivities of the constitutive layers, is presented in chapter 4. The originality of the proposed multilayers identification method will be emphasized. Finally, in the same chapter (see 4.5.3), a literature review of some existing methods dedicated to the characterization of thin layers, also known as coatings, deposited on substrates is also presented to shed the light on the improvements resulting from the development of the present identification technique.

1.7 Summary

To sum up, the general context and industrial applications of the materials that will be thermally characterized in this work, have been presented in this chapter, followed by the importance of their thermophysical properties identifications, in many fields.

An overview of numerous existing thermophysical parameters identification methods found in the literature, was presented. General classifications of these methods, based on several criteria (excitation, measurement, regime, geometry, properties to estimate, etc), are discussed.

The standard flash method, that inspired the method developed and investigated in this work, is described. A literature review of this method and its evolution, in terms of modeling, experiment setup and overall identification strategy, is performed. The advantages of this class of methods are discussed, as well as some probable sources of uncertainties that should be taken into consideration.

In the next chapters, the overall thermal parameters identification strategy conducted in this thesis, and relying on the flash class technique, will be presented in chapter 2. The next chapters corresponds to various applications of the method. The chapter 3 concerns the characterization of monolayer materials. The chapter 4 is dedicated to two-layers material and its potential generalization to multilayers materials.

1.8 Résumé substantiel du chapitre 1

Ce chapitre correspond à un état de l'art des différentes méthodes d'estimation de paramètres thermophysiques. Il commence par une présentation contextuelle générale, suivie d'un aperçu des applications pour lesquelles ce type de matériaux complexes sont utilisés. L'importance de la caractérisation thermique de tels matériaux est mis en avant. Par la suite, une étude bibliographique exhaustive des méthodes de caractérisation thermique existantes est présentée.

Une classification générale de la grande variété de méthodes d'estimation de paramètres thermophysiques est effectuée selon plusieurs critères.

En outre, un état de l'art sur la méthode flash investiguée dans ce travail, comprenant une définition de la technique, son origine et son évolution au cours des années, ses classifications et ses avantages, est présenté.

Ce chapitre, en plus de son introduction et sa conclusion, est composé de 5 parties :

Partie 1. Contexte et applications industrielles

L'utilisation de matériaux présentant des structures complexes (e.g. matériaux composites, multicouches, revêtements déposés sur des substrats) est de plus en plus courant dans de nombreux secteurs industriels et applications d'ingénierie. On les retrouve par exemple dans les domaines du stockage et de la production d'énergie ou encore dans le secteur du transport pour lequel l'enjeu est de réduire le poids embarqué dans l'objectif de réduire la consommation de carburant tout en conservant les propriétés mécaniques.

Les principales applications industrielles des matériaux caractérisés dans ce travail, comme le polymère renforcé de fibres de carbone (PRFC), seul ou constituant une des couches d'un matériau composite, ou encore les revêtements à base de phosphore déposés sur un substrat polymer, sont présentées dans 1.2.

Partie 2. Importance de la caractérisation thermique

Dans cette partie, les principales motivations de ce travail, i.e. la caractérisation thermique de matériaux complexes, sont discutées plus en détail dans 1.3. L'identification de ces propriétés revêt une importance cruciale dans les domaines mettant en jeu la thermique et dans un grand nombre d'applications, pour deux raisons principales:

- Le contrôle non destructif et la validation de procédés de fabrication qui passe par le contrôle thermique d'échantillons pendant/après leurs fabrications. Ces mesures jouent également un rôle essentiel pour l'analyse du vieillissement pour des pièces subissant des contraintes thermiques et/ou mécaniques répétées.

- Ces paramètres peuvent servir de données entrées pour les simulations numériques utilisées en ingénierie pour la modéliser de systèmes complexes. Le dimensionnement de tels systèmes à l'aide d'outils numériques de type CAO (conception assistée par ordinateur) nécessite une connaissance précise des propriétés thermophysiques des matériaux

utilisés et ce afin de prédire convenablement les transferts de chaleur et la dynamique thermique au sein de ces systèmes.

Partie 3. Panorama et classification des méthodes de caractérisations thermiques

Cette partie présente les différentes méthodes existantes de caractérisation thermique, et leurs classifications selon plusieurs critères qui peuvent être:

1. la méthode d'excitation et de mesure (avec ou sans contact, voir 1.4.1):
2. l'extension spatiale de la mesure: locale ou étendue (voir 1.4.2).
3. le régime d'estimation (stationnaire ou variable y compris: quasi-stationnaires, transitoires et périodiques, voir 1.4.3).
4. la forme temporelle de l'excitation: Dirac (impulsion), créneau, échelon, périodique (modulée) ou arbitraire (voir 1.4.4).
5. la forme spatiale de l'excitation: locale, uniforme, modulée (dans l'espace), pointue, gaussienne, rectangulaire, parabolique, polynomiale cubique ou forme aléatoire (voir 1.4.5).
6. l'emplacement de la mesure: localisé ou non sur l'excitation (voir 1.4.6).
7. les quantités mesurées (températures, pressions, flux, etc., voir 1.4.7).
8. les quantités estimées: diffusivités, conductivités, capacités ou effusivités thermiques(voir 1.4.8).
9. la géométrie du problème et ses coordonnées qui dépendent de la géométrie du système (1D, 2D, 3D, nD) et de la forme de l'excitation: dans un système de coordonnées cartésien (rectangulaire), cylindrique ou sphérique (voir 1.4.9).
10. il existe également d'autre critères permettant des classifications moins répandues (voir 1.4.10).

Partie 4. Etat de l'art sur la méthode Flash et son évolution au cours des dernières années

Cette partie est dédiée à la méthode Flash qui est la méthode de référence pour l'estimation des diffusivités thermiques (voir 1.5). Au cours des 50 dernières années, cette classe de méthodes a été améliorée en termes de possibilités d'estimation (méthodes Flash 1D, 2D puis 3D), de prise en compte des pertes radiatives et convectives avec l'environnement, et de techniques de mesure qui n'ont cessé de se développer depuis l'avènement de la thermographie infrarouge. Les avantages de cette méthode sont nombreux, non intrusive elle nécessite un

minimum d'équipement et une unique expérience. Les sources d'incertitudes associées à ce type d'expériences sont également abordées dans cette partie.

Partie 5. Etude bibliographique sur la caractérisation thermique des matériaux monocouches, bicouches ou multicouches, orthotropes ou isotropes

Afin de mettre en avant l'originalité de la méthode développée dans le présent travail, un état de l'art détaillés des différentes méthodes dédiées à la caractérisation thermique de matériaux monocouches isotropes ou orthotropes et de matériaux multicouches (en particulier bicouches, ou couches minces déposées sur des substrats) sont présentés dans les chapitres 3 et 4, respectivement.

Conclusion

Ce chapitre présente le contexte général et les applications industrielles des types de matériaux caractérisés dans le présent travail, ainsi que les enjeux liés à leurs identifications, pour un grand nombre de domaines d'application.

Un aperçu des nombreuses méthodes existantes d'identification présentes dans la littérature est présenté. Les différentes classifications générales de ces méthodes, basées sur plusieurs critères (excitation, mesure, régime, géométrie, propriétés à estimer, etc.) sont discutées.

La méthode Flash standard, de laquelle est inspirée la présente méthode développée et investiguée dans ce travail, est décrite. Un état de l'art de cette méthode ainsi que son évolution au fil des années, en termes de modélisation, de protocole expérimental et de stratégie globale d'identification, est présenté. Les avantages de cette classe de méthodes et les différentes sources d'incertitudes à prendre en compte, sont discutés.

Dans les chapitres suivants, la stratégie globale d'identification des paramètres thermiques menée dans cette thèse, reposant sur la méthode flash, est présentée au chapitre 2. Les chapitres suivants correspondent aux diverses applications de la présente méthode. Le chapitre 3 concerne la caractérisation de matériaux monocouches, et le chapitre 4 est dédié aux matériaux bicouches ainsi qu'à la généralisation de la méthode aux matériaux multicouches.

Chapter 2

Thermal parameters identification principle

***

Contents

2.1 Introduction

The ultimate goal of this thesis is the development of methods dedicated to the thermal characterization of orthotropic and multi-layered materials. The identification of thermophysical properties of such complex materials is generally based on the resolution of an inverse heat conduction problem (IHCP). This chapter presents the general principle of inverse problems and each element involved in the overall procedure. It contains general briefing of each element of the general procedure and its current application in the present method.

For an experimental application, the major sections investigated in the identification technique will be mainly:

- The experiment;
- The direct model;
- The comparison of observable quantities via a cost function;
- The minimization via an identification algorithm;

First of all, an overview of the IHCP problems is presented, followed by the general principle of resolution of such problems. Then, the investigated experiment, based on the well known flash technique, is presented, starting from the procedure, followed by the setup and the device, ending with the post-treatments (calibrations, data acquisitions, post-processing). The third subsection is dedicated to the presentation of the direct model developed to mimic the experimental conditions. The estimation method is detailed in the next section. After an overview of the different categories of minimization techniques, in terms of objective function and algorithms, the currently applied identification technique is developed in details. The sixth section is dedicated to the presentation of the concepts and the different types of sensitivity analysis, in addition to the arguments that motivate our choice. The chapter ended with a discussion on the sources of errors in the estimation.

2.2 Inverse heat conduction problem - IHCP

2.2.1 Context and applications

The IHCP encountered in many branches of sciences and engineering e.g. in aerospace, chemistry, mechanics, statistics, astrophysics and other areas), has been grown in recent years [179, 180]. Such protocols are applied for practical engineering interests, involving the three heat transfer mechanisms (conduction, convection, and radiation). They can be applied as parameters and/or function estimation approaches. According to the researched explanatory variables (i.e. variables to identify), a classification of inverse heat problem (especially heat conduction IHCP) types can be presented as following [181]:

(a) **Inverse problems for the estimation of structural parameters β:** for instance, thermophysical materials properties such as i) Thermal diffusivity, ii) volumetric heat capacity, iii) thermal conductivity, iv) heat exchange coefficient, v) emissivity, vi) thermal resistance, vii) thermal effusivity and others. In addition to the optical or geometrical properties which are typically related to the material structure or the sample shape.

(b) **Inverse problems for the initial condition estimation, e.g.** $T(x, y, z, t = 0)$, also known as "inverse initial state problems". These types of problems are specific for each experiment.

(c) **Inverse problems for the input estimation, known as "inverse entry problems"**. This type of problems is generally recognized in the estimation of the heat sources which may have different forms (point, line, surface, volumetric heat source, etc.). These problems seem to be specific for each realized experiment.

(d) **Reforming problems (inverse shape reconstruction problems)**: In above-presented problems, the domain boundaries are generally pre-defined and fixed. However in some cases, the form and/or the position of one or many boundaries (or a boundary section) may be unknown. Consequently, they will be a part of the system variables that must be estimated.

(e) **Inverse problems for optimum control/design**: This type of problems provides the must relevant measurement devices location, system inputs (flux density, excitation form and/or location, sample dimensions) and so on. They are usually combined with the first type of parameters β estimation, serving in the reduction of estimation errors. It consists in defining the test protocols and designing the experimental device. First of all, the choice of input parameters should be formalized, then a specific criterion relative to the output variables sensitivity to the parameters β, is maximized. In such problems, when finding the optimal inputs, the parameters to be estimated are assumed to be known.

The handled problem is an inverse heat conduction problem (IHCP) whose objective is to retrieve the thermal properties (i.e. type a in the preceding classification), especially the thermal diffusivities, of isotropic or orthotropic, opaque and homogeneous, monolayer or multilayers materials.

Please note that in our case, the inverse problem under consideration corresponds to the parameters estimation or type a, that will be often coupled with the input estimation or type c **"inverse entry problem"**, as the parameters related to the excitation are often unknown (e.g. intensity, shape, time duration).

2.2.2 General principle

The IHCP general principle consists in comparing experimental or synthetic measurements, leading to the "observables" Y^*, with the outputs $Y(\beta)$ resulting from an analytical or numerical model that must, as much as possible, mimic the experiment. Thereby, the model has to provide outputs that must i) be compatible with the measurements Y^* and ii) be dependent

on the parameters to estimate β. This last point is discussed further in the section dedicated to the sensitivity analysis. This comparison is performed by means of a cost function f, also called "objective function". As long as this function does not satisfy a certain criterion, the optimization algorithm adjusts the parameters that will be re-evaluated by the direct model. The process is repeated until the procedure converges to the optimal set of parameters $\hat{\beta}$ with the admissible values, i.e the one that minimizes the difference between the experiment and the model.

The overall estimation strategy concept is illustrated in Fig. 2.1 that presents the connection between the elements involved in the inverse problem resolution. The various steps of the estimation strategy are detailed and discussed in the following sections.

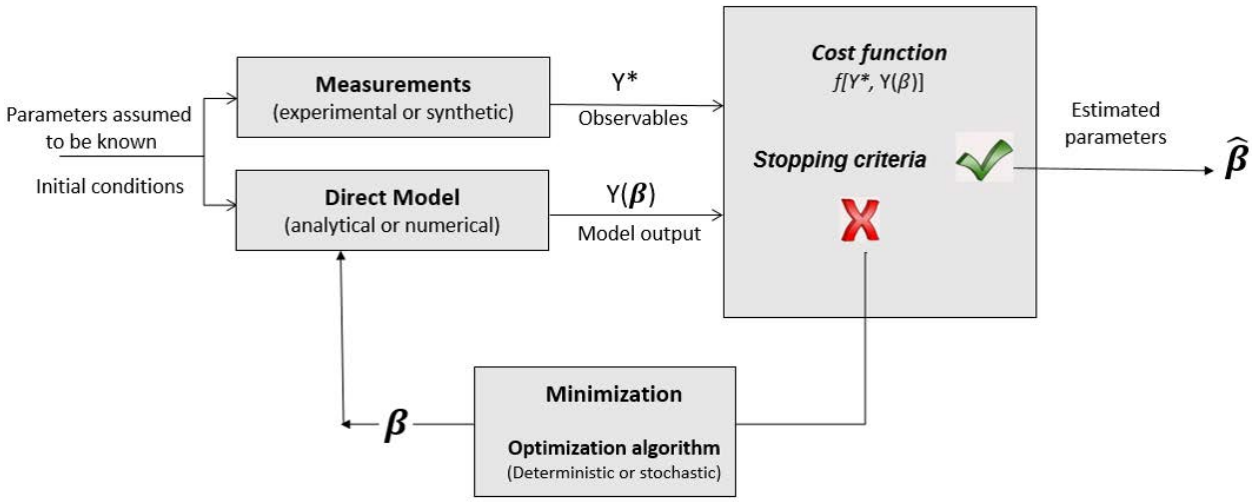

Figure 2.1 – Inverse problem principle and main sections (steps).

Difference between observables and measurements

The measurement is the quantity given by the experimental device, however the “observable” is the quantity appropriately selected to be compatible with the model outputs suitable for estimation, and able to be compared to the model response via the estimation process.

2.2.3 Inverse Crime principle

This type of misguided estimation known as *Inverse Crime* [182] consists in using twice the same theoretical model:

- Firstly, to generate the model outputs from given inputs.
- Secondly, to synthetically generate the observations, with or without adding a certain level of noise into the initial signal.

The overall procedure is shown in Fig. 2.2. This technique is used to evaluate the feasibility of an estimation method, compare different methods or adjust the estimation method parameters. The same model being used twice, it is clear that the success in retrieving the parameter does not ensure the success when applying the method to experimental data. The method does not detect any errors in the model or mismatch between the model and the experiment. However, this strategy may be considered as a preliminary validation of the overall estimation strategy.

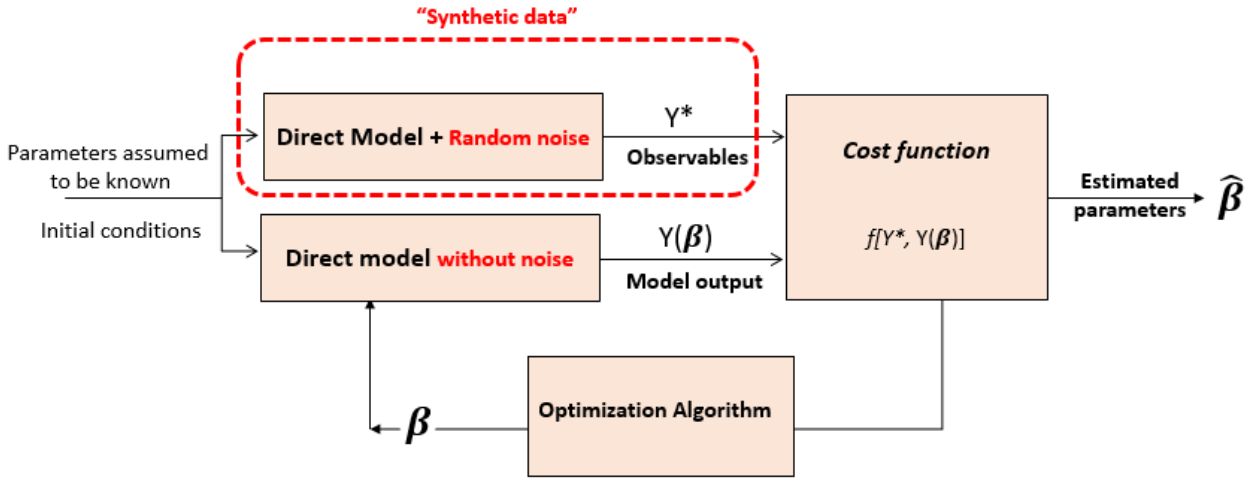

Figure 2.2 – Inverse crime principle.

Once the model is validated, this strategy is used to check the feasibility of the estimation procedure, in terms of parameters correlations, and adequacy of optimization algorithm. In addition, it is used to perform parametric studies in order to define the optimal algorithm parameters for each case under consideration.

2.3 Experimental 3D flash method

In this section, the experiment, in terms of protocol, setup (devices, tools), and data pre- and post-treatments, are presented.

2.3.1 Experimental protocol

The experiment protocol corresponds to an unconventional and 3D flash technique qualified as a non-intrusive method, both in terms of excitation and measurements. In this method, the sample that should be thermally characterized is subjected to a localized and non-uniform thermal excitation using a CO_2 laser. The resulting surface temperature evolution cartography is continuously measured, during the cooling phase. These measurements are performed by an IR camera, at the front or rear faces of the material. Figs. 2.3 represent the experimental setup and the equipment used to generate the experimental data. The specifications of the main devices are detailed hereafter:

- The IR camera is a FLIR SC7000 with a 320×256 pixels resolution at an adjustable frequency up to 200 Hz (full frame).
- The laser is a CO_2 laser DIAMOND GEM-Series by Coherent© that emits at $10,6\mu m$, with adjustable power and duration time, from 5% to 100% of its total capacity of $130W$, and from "10 ms" to many seconds, respectively.

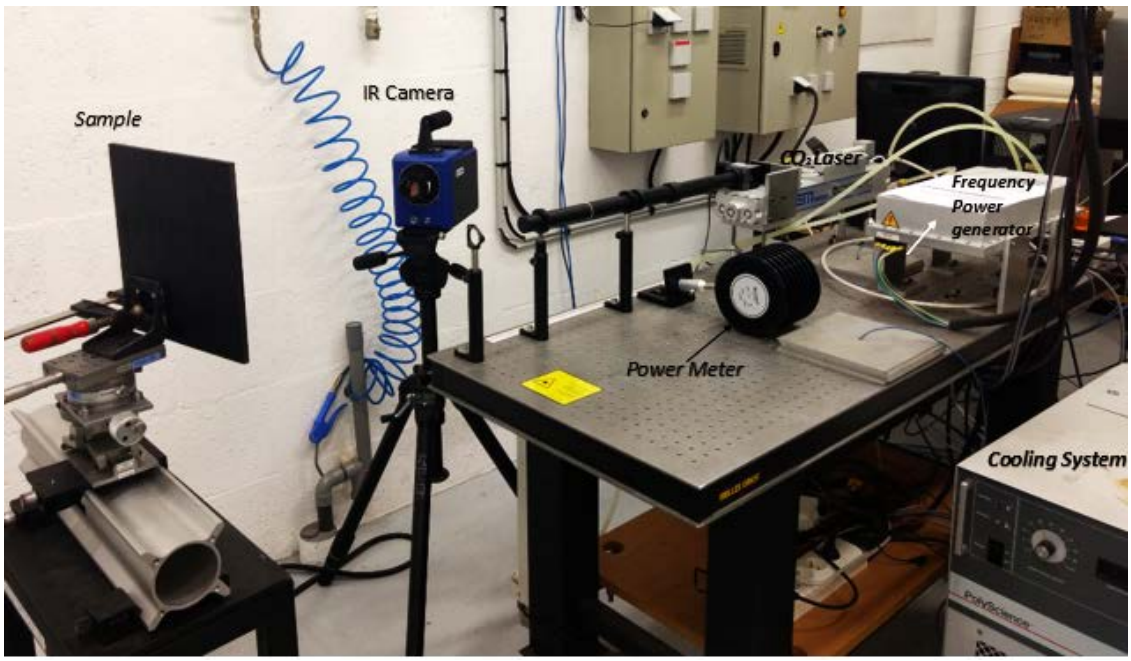

(a)

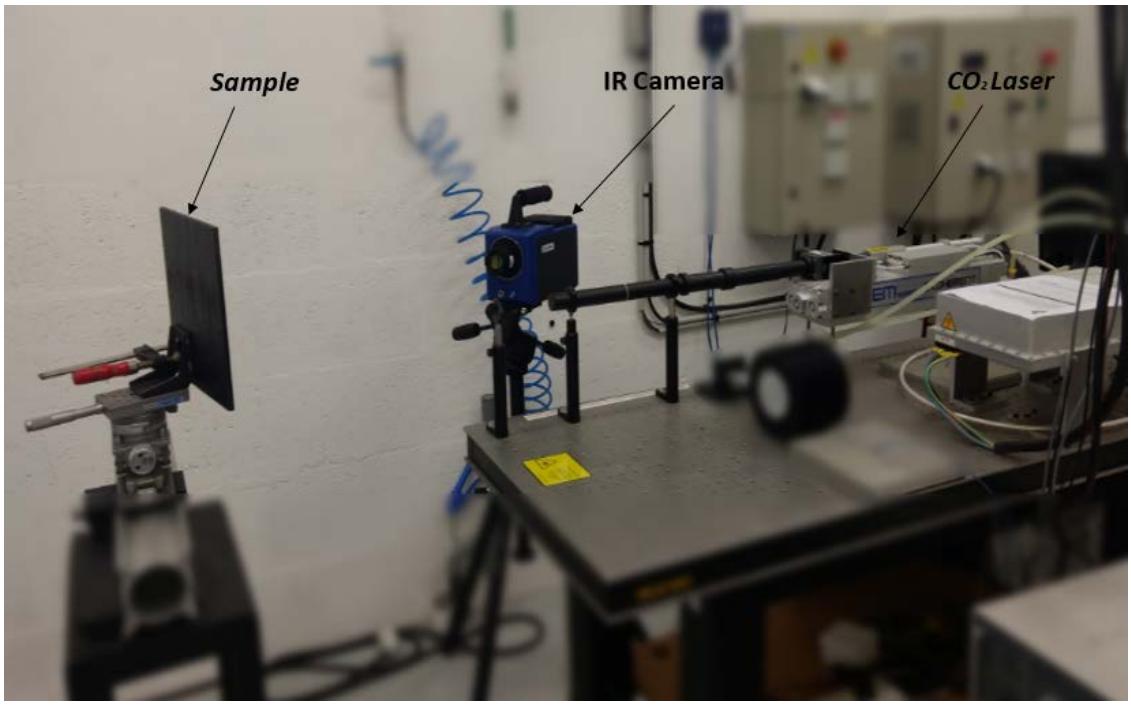

(b)

Figure 2.3 – Experimental setup representing the front face flash method and including the main devices involved in the measurement procedure : the sample, CO_2 laser and IR camera.

2.3.2 Experimental setup

In order to estimate the thermal diffusivity of different materials, an experimental bench based on the flash method developed at the Pprime Institute (Poitiers, France), is used. Fig. 2.3a corresponds to the overall experimental setup. Fig. 2.3b sheds the light on the key elements of the apparatus, i.e. i) The samples material, ii) the thermal excitation source and iii) the infrared camera, which are described thereafter:

Test samples

Fig. 2.4 presents some of the material samples investigated and thermally characterized during this work.

Some of these materials are monolayered such as (a) the polyamide and (b) the carbon fiber reinforced polymer Composite material (CFRP), others are bi-layered materials such as (c) the Composite layer combined to the polyamide liner, and (d) the TPT coating (thermographic Phosphor Thermometry) deposited over a HDPE (high density polyethylene) polymer layer.

(a) PA

(b) CFRP

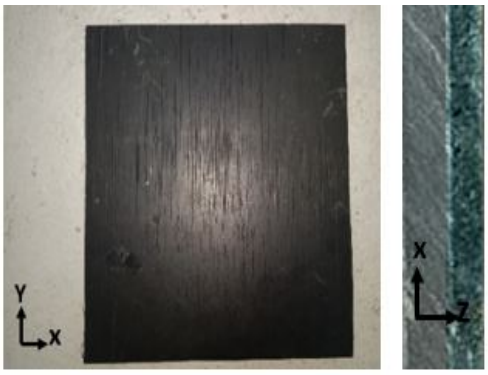

(c) Bilayer CFRP || PA

(d) TPT-coating over HDPE

Figure 2.4 – Samples of tested materials.

Thermal excitation: CO_2 Laser

As mentioned above, the test sample are subjected to a beam emitted by a CO_2 laser (Coherent GEM-100L, see Fig. 2.5).

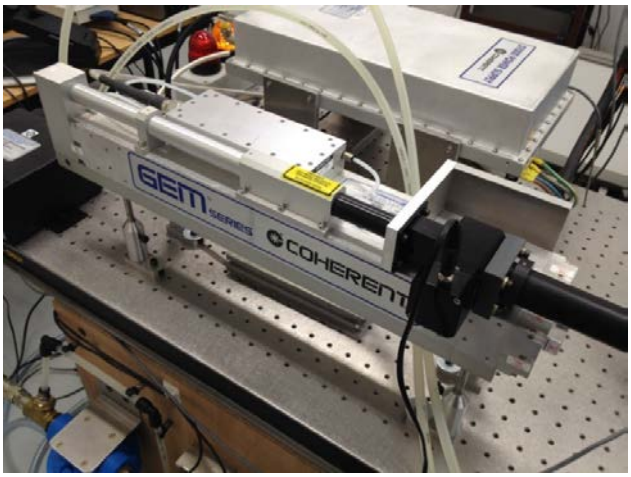

Figure 2.5 – Coherent GEM-100L CO_2 laser.

This type of instruments is considered the most appropriate for multi-purpose testing due to its flexibility in switching configuration settings, in terms of power and duration time control of the beam. It consists of two parts:

- The laser head which contains a mixture of CO_2, He and N_2 in gaseous state. These gaseous components are excited electrically by a radio-frequency (RF) generator.
- The laser body which is linked to the laser head by a single cable transferring the electric signal which will excite the set of gas mixture.

The RF-generator that controls the laser can be set thanks to the controller provided by Coherent (see Fig. 2.6a). There are two operating modes: the first one is manual using the knob rotation, and the second one permits to directly connect the controller to a numerical terminal (i.e. exp. computer). Considering the latter mode, a graphic interface using LabView software (Fig. 2.6b) is developed in order to control the laser emission, on one side, and ensure a synchronization with the IR-camera, on the other side.

Due to the relatively poor efficiency of the laser, a significant amount of energy is lost as heat, which must be evacuated from the laser head and the RF-generator. To do that, a cooling system is set up, as shown in Fig. 2.6c.

The cooling process is provided by a closed loop of glycol water solution. The process itself, is cooled by a temperature control unit (cooling thermostat, see Fig. 2.6d) which is able to extract a power of 2 kW level. The choice of glycol water is based on its properties that allow to cool the fluid that can reach negative temperatures. This solution maintains the water clean without a proliferation of bacteria and it prevents the corrosion phenomenon. As mentioned above, the excitation is provided by a continuous CO_2 laser.

Moreover, in this experimental setup, a laser diode (Fig. 2.6e) and a power meter (Fig. 2.6f) are used for positioning the sample and for the laser shooting test, respectively. This last device is designed to continuously support the shot at a full laser power.

(a) Laser manuel controller

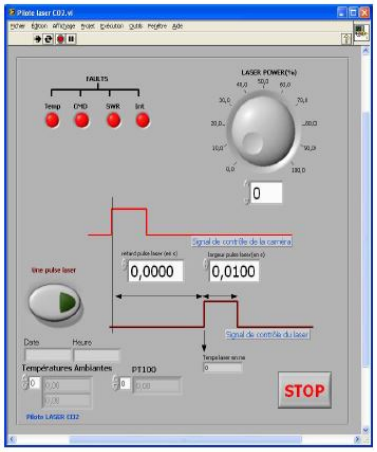

(b) Laser labview

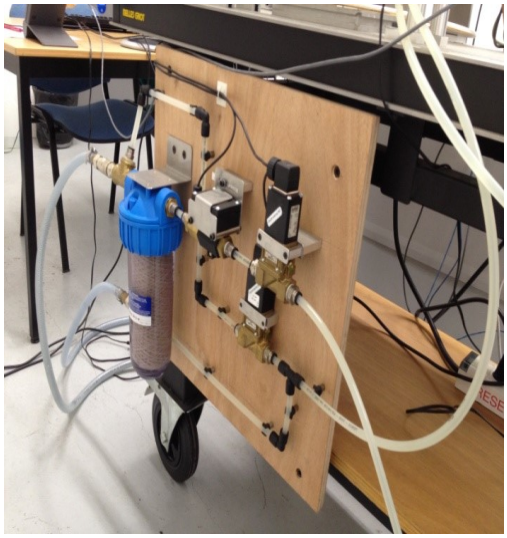

(c) Cooling system

(d) Cooling thermostat

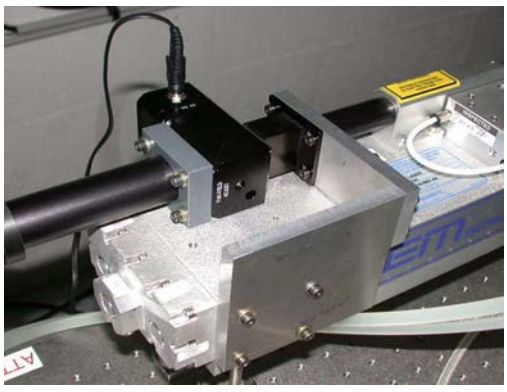

(e) Laser diode

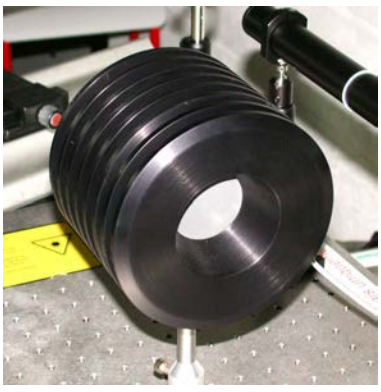

(f) Power meter

Figure 2.6 – Some devices/tools of the experimental setup.

Infrared camera

As previously mentioned, temperature evolution measurements are carried out using an IR-camera or thermographic camera that senses infrared radiation, see Figs. 2.7.

The IR camera is a FLIR SC7000 which is a matrix IR camera with 320×256 pixels resolution and a high sensitivity and noise levels as low as 20 mK. Fullframe acquisition can be carried out at a framerate that could reach up to 200 Hz. For more details about the features of this camera, the reader is invited to consult the FLIR page web [Flir SC7000 IR-camera].

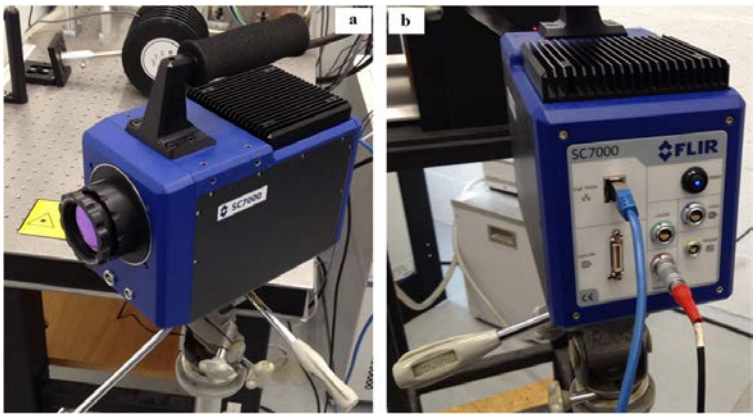

Figure 2.7 – (a) Front and (b) Back infrared camera faces.

All measured signals data provided by IR camera are then processed: raw images are post-treated thanks to a Matlab interface, developed by D. Saury and E. Ruffio [110].

Miscellaneous items

Some experimental devices are also used for the estimation of properties that should be known before the estimation. Those parameter are referred as "parameters a priori known" hereafter.

The volumetric mass density ρ is determined by means of i) a digital micrometer (Fig. 2.8a) to measure the layers thicknesses, and ii) a precision balance with a sensitivity of 0.01 mg to measure the mass of the sample (Fig. 2.8b). The heat capacity is measured by means of a Calvet Calorimeter (C80 by Setaram©).

The thermal conductivity of some sample materials (isotropic and homogeneous ones) are also determined using a TCi when possible. The device was used as a validation tool for the proposed method.

(a) Digital micrometer (b) Precision balance (KERN ABT series)

Figure 2.8 – Miscellaneous items used for the materials densities measurement.

Calvet Calorimeter

The specific heat capacity of some materials investigated in this study was measured by a Calvet Calorimeter . A photography of the device and the internal cells (a.k.a vessels) are given in Figs. 2.9. The cells volume is 12,5 mL. The principle consists roughly in subjecting a regulated heat flux intensity, generated by Joule-effect. The regulation is operated in order to keep constant the temperature elevation, which is predefined by the user [183]. The heat flux required to ensure the regulation setting for the empty cell Φ_{air} is substract from the heat flux required to ensure the regulation setting for the sample cell Φ_{sample}. The difference corresponds to the energy needed to heat up the sample which allows to determine the mass heat capacity $C[kJ.kg^{-1}.K^{-1}]$.

The energy balance in this case could be written as follows:

$$(\Phi_{sample} - \Phi_{air})(t) = mC(t)\frac{dT}{dt} \tag{2.1}$$

Knowing the sample mass, one can deduce the material specific heat capacity C at each instant t. The definition of the temperature-time relation allows to get the evolution of the heat capacity with respect to the temperature T.

In practice, both vessels or measurement cells are not perfectly identical and will consequently not respond to the heating exactly the same way. For this reason, a "system blank test" must be conducted using the same setting with both cells empty (only air). The residual flux (i.e. difference between both cells flux intensities) is then subtracted from the resulting heat flux difference $\Phi_{sample} - \Phi_{air}$.

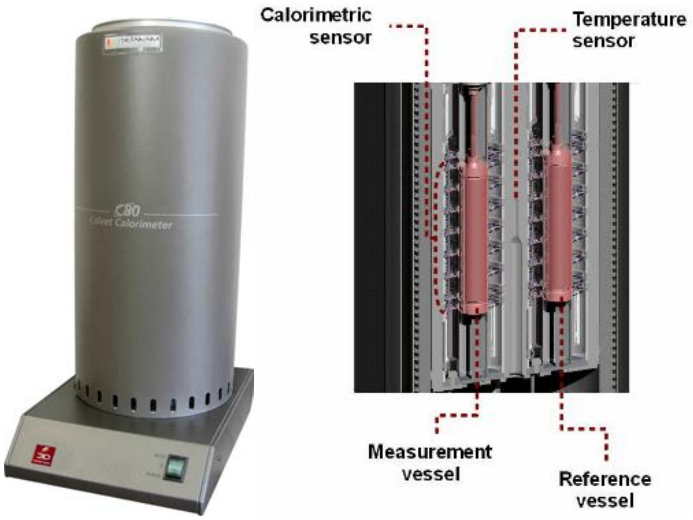

(a) Calorimeter (b) Measurement cells

Figure 2.9 – Calvet Calorimeter(C80 by Setaram©)[183].

TCi Thermal Conductivity Analyzer (C-Therm ®)

A photography of the Thermal Conductivity Analyzer device allowing the measurement of isotropic and homogeneous materials thermal conductivities, is presented in Fig. 2.10. The measurement is based on the *Hot Disk* technique. A wide range of thermal conductivities, from the highly isolating ($\lambda = 0,005$
$W.m^{-1}.K^{-1}$) to the highly conductive ones (λ = 500 $W.m^{-1}.K^{-1}$) can be accurately measured [23].

The sample is positioned over a disk made up of a double spiral, which is the resistive element acting as both: a heating source and a temperature sensor [184]. Thus, in the case of a disk of radius r and assimilated to a set of m concentric coils, the mean temperature T of the disk sandwiched between two blocks considered as semi-infinite walls could be written in the following form [23]:

$$T - T_{ini} = \Delta T_{RC} + \frac{2qr}{\lambda\sqrt{\pi}}\sqrt{\frac{at}{r^2}}\,B\left(\sqrt{\frac{at}{r^2}}\right) \tag{2.2}$$

with T_{ini} is the initial temperature, ΔT_{RC} is a constant thermal bias related to the contact resistance, q is the applied heat flux density and B(x) is given by:

$$B(x) = \frac{1}{x[m(m+1)]^2}\int_0^x \frac{1}{\sigma^2}\sum_{l=1}^{m}\sum_{k=1}^{m} k\ exp\left(-\frac{l^2+k^2}{4m^2\sigma^2}\right) l_0\left(\frac{lk}{2m^2\sigma^2}\right) d\sigma \tag{2.3}$$

with $l_0(x)$ is the Bessel function of order 0. When interpreting the evolution of $T - T_{ini}$ with respect to time, one can interpolate the bias ΔT_{RC}, then proceed to an iterative estimation of the thermal diffusivity a and conductivity λ.

The referred uncertainty of the estimated thermal conductivity is between 2 to 5%, however that of the thermal diffusivity is between 5 to 10%.

Figure 2.10 – TCi Thermal Conductivity Analyzer [184].

2.3.3 Data acquisition and treatments software

In the current study, the IR-camera is connected to a computer by an Ethernet connection and is systematically controlled using its Altair control software (Fig. 2.11a). An export software (Export PTW, Fig. 2.11b) has been also developed by E. Ruffio and D. Saury in order to export the frames generated by Altair from the IR camera measurements. The format in which these frames are exported should be readable by the estimation algorithms involved in this project.

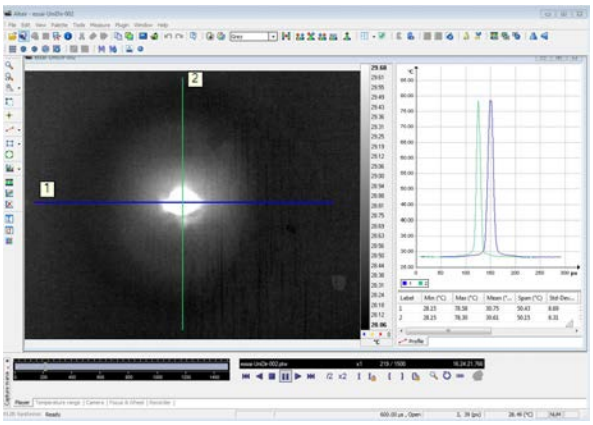

(a) Altair

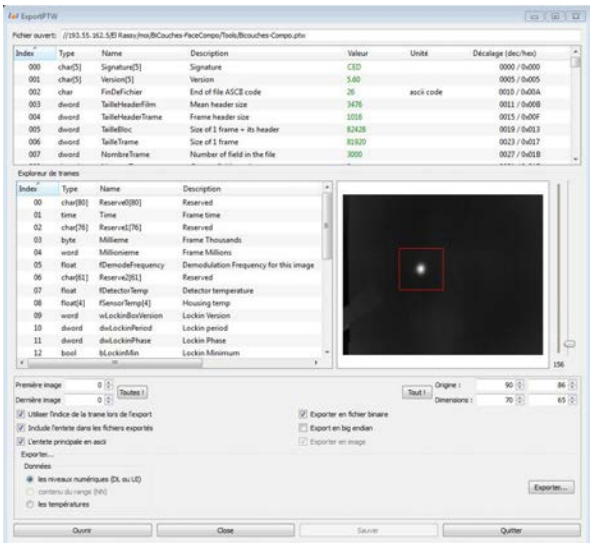

(b) Export PTW

Figure 2.11 – Data acquisition and treatments software.

2.3.4 Images processing and exploitation: Calibrations, scaling, post-treatments

The treatment of the raw data consists in,

1. converting the intensity levels from digital levels (DL) into temperature levels ($°C$),

2. calibrating the data (i.e. definition of the correlation pixel/mm and dimension of the exploitation window l_x and l_y), as shown in Figs. 2.12,

3. centering the resultant frames with regard to the laser spot impact, as shown in Figs. 2.13, for compatibility reason with the mathematical model,

4. identifying the excitation moment and subtracting the bottom signal to manipulate relative temperatures (relative to initial temperature).

5. projecting the data into Fourier-Cosine space,

6. eventually, selecting the data to be exploited.

The choice of the exploitation frames, illustrated by the colored frame in Figs. 2.13, is of prime importance. A compromise is required between a sufficient size to respect the boundary conditions of the direct model (especially the condition of isolated lateral faces) and a surface area restricted to the zone of interest to avoid the degradation of the data (by dilution of the signal in the background signal). This subject will be more detailed in next chapters where practical applications will be presented.

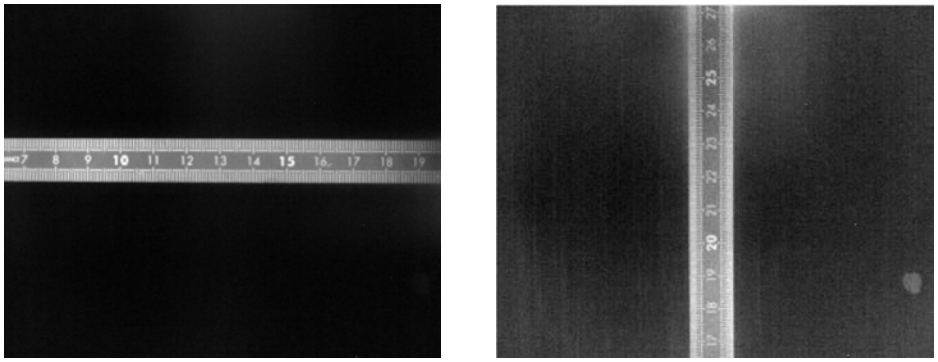

(a) Horizontal thermal picture of the graduated scale used for horizontal calibration

(b) Vertical thermal picture of the graduated scale used for vertical calibration

Figure 2.12 – Calibration of the data (correspondence or correlation pixel/mm) using a graduated scale.

Front and rear face flash experiment

As already mentioned, the experimental setup described in the previous sections is used for the measurement of the temperature evolution as a response to the thermal excitation. The surface subjected to the heat flux (by the laser beam) may be the front or the rear face. In each case, the natural convection-radiation cooling implies both faces. The last case (rear face excitation) will be discussed later as an alternative method (Chapter 3 and Chapter 4). Both strategies, called "front/rear flash methods" are found to be feasible and consistent for the identification purposes and their relative results will be shown in the next chapters.

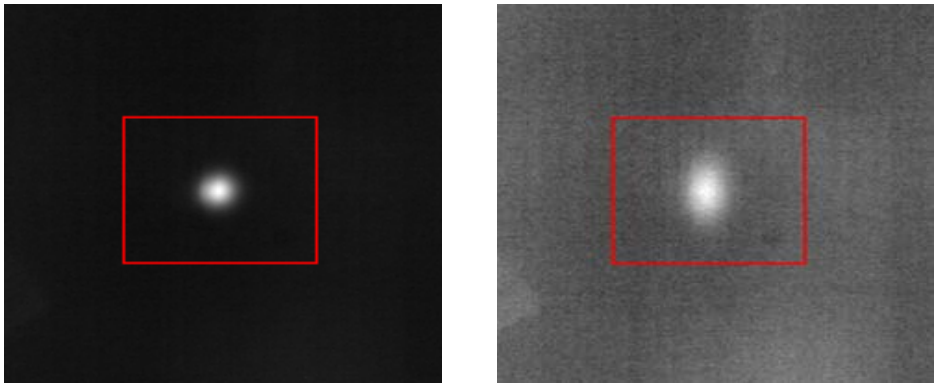

(a) Frame 1 after excitation (b) Frame 50 after excitation

Figure 2.13 – Framing of the measurements exploitation windows (cropping of the pictures or images), the red square bounds the region that will exported for treatments and involved in the identification method.

Unconventional and non-intrusive 3D flash technique

The experiment conducted to generate the required measurements corresponds to an unconventional laser flash technique, since several practical features are different from the original and conventional one, introduced by Parker in [2].

- In this work, the thermal excitation is locally and non-uniformly imposed on one of the sample faces, by a CO_2 laser.
- The excitation duration, in the most of treated cases is $\tau_{ex} = 10ms$, which is considered instantaneous from the simulation point of view. Noting that other cases are treated with pulses of various duration time $\tau_{ex} = [10ms, 0.1s, 1s, 10s, 30s, ...]$;
- In parallel, the temperature response cartography is continuously recorded by an IR camera rather than a local temperature by means of a thermocouple.
- In most characterization cases treated here, the temperature is measured on the excitation face, corresponding to a so-called front-face measurement. This is different than the Parker conventional method where a local temperature evolution is measured at the rear face.

The overall experiment can be qualified as non-intrusive, both in terms of excitation and measurements. The thermal excitation is performed without any contact (heating plate, hot disk,...) with the material that should be characterized. The resulting temperature evolution is measured using the infrared thermography, also without any contact with the material.

It also can be qualified as a 3D flash technique since a local and non-uniform excitation is applied at the surface of the sample, thus generating a non-uniform and three dimensional heat diffusion through the material. Consequently this technique can be consistently conducted for the 3D identification of orthotropic materials, i.e. the identification of three dimensional thermal diffusivity tensor.

It is worth mentioning that, the laser is modulated to obtain a pulse of moderate energy, in order to avoid an overheat of the sample.

2.4 Direct / Forward Model

Regarding the direct modeling of the inverse problem, it must reproduce the same experimental conditions in terms of phenomena involved, initial and boundaries conditions. The resolution of the mathematical formulation derived from the physical model, is based on the resolution of the three-dimensional transient heat equation. Each layer constituting the samples, supposed homogeneous and opaque, may be isotropic or orthotropic.

Semi analytical expression of the front and/or rear face temperature evolution corresponding to a front and/or rear flash experiment, and concerning each case treated in this thesis, (i.e monolayer, bilayer and multilayer material with isotropic or orthotropic thermal structure), will be developed and discussed in the next chapters. All hypotheses considered for each case will be also detailed.

2.4.1 Mathematical formulation/resolution of the direct model

In such inverse problems that require a large number of simulation, it is necessary to develop the fastest possible system resolution. Therefore, an analytical resolution of this system was considered. It is based on integral transformations of Fourier-cosine in space and Laplace domain in time, as shown in Eq. 2.4. These transformations lead to normalized harmonics $\xi_{m,n}$ characterized by the spatial modes m and n corresponding to the direction x and y (in the plane perpendicular to the excitation direction).

$$\xi_{m,n}^{mod}(z,p) = \frac{1}{l_x \cdot l_y} \cdot \int_0^{\infty} \int_0^{l_y} \int_0^{l_x} T^{mod}(x,y,z,t) \cdot X_m(x) \cdot Y_n(y) \cdot e^{-pt}\, dx\, dy\, dt \tag{2.4}$$

The quadrupoles formalism allows to analytically express the temperature evolution taking place at the front or rear face of the sample, in terms of normalized harmonics $\xi_{m,n}$.

Advantages of harmonics

In such type of studies, working with harmonics, instead of physical raw temperatures, is more advantageous, given that the results are less sensitive to the measurement noises, faster and more accurate. Noting that these harmonics have the same amount of data than the individual (single) temperatures present in (x,y) basis [110], and each harmonic is independent to others. Contrarily, the information is not split up in the same way, and it has a more simple extraction than the ordinary basis (x,y) over which each image component or pixel is dependent on all others. Therefore, if any of these pixels is null, and at any moment, it means that it was already and will remain null. This independence characteristic provided by such data transformation, allows us the selection of the harmonics required for the exploitation, and the others that should be dismissed.

In fact, the harmonics of lowest frequencies are the ones providing the major part of information concerning the thermal diffusivities (parameters of interest for the present work). Since information is concentrated at relatively low frequencies, the harmonics investigated in the current identification process are the first M × N even harmonics. The odd harmonics are not taken into account in the estimation. They are practically negligeable, compared to even ones, since the excitation is supposed to be symmetric and the spot is assumed to be centered with respect to the IR images. The re-framing (cropping) of the images should be performed in a way that guarantees these last assumptions.

The outcomes of analytical solution

Unlike “numerical approaches” where the model outputs are calculated for fixed parameters, the analytical solution covers all solutions, and evaluates the outputs variation as a function of input parameters. This type of solutions allows to calculate the sensibility by the derivation of the model, and to overcome the potential numerical resolution errors, even when infinite series are truncated, since the remainder can be easily maximized in that case.

There are also “pseudo-analytical solutions”, also referred as "semi-nalaytical solution", which designate the solutions expressed in particular spaces (“Laplace space”, “Fourier spaces”, etc), and that necessitate an inverse transformation in order to get the physical solutions expression. This inversion is not always possible analytically, and may need numerical methods, such as Laplace inversion currently performed using numerical tools (see 2.4.3) .

2.4.2 Redefinition of the model outputs $Y(\beta)$ and observables Y^*

The previously discussed mathematical formulation of the direct model producing output signals as harmonics in the Laplace and Fourier-Cosine spaces, it is theoretically possible to compare signals (i.e. from models and measurements) in 4 probable domains:

i. the physical domain $T(x,y,z,t)$,

ii. the Laplace domain $T(x,y,z,p)$,

iii. the Fourier Cosine domain $\xi_{m,n}(t)$,

iv. both the Fourier-Cosine and Laplace domains $\xi_{m,n}(p)$.

Extensive trials previously conducted demonstrate that the minimization in the time harmonics space, i.e. domain (iii), is more suitable, both in terms of accuracy (measurement noise filtering by harmonics selection) and identification speed (spatial image compression).

Concerning the latter, identification time will be the time required for the direct calculation of the analyical model discussed in 2.4.1, added to the time required in order to return into the time domain using a Laplace inversion technique, also discussed in 2.4.3.

Solutions obtained into the domain (iii) corresponds to the temporal normalized harmonics resulting from numerical Laplace inversion applied on the analytical solution. This form of the

direct model outputs is qualified as "semi-analytical solution" or "pseudo-analytical solution" $\xi_{m,n}^{mod}(\beta,t)$ and have the same units as the the temperature evolution($^{\circ}C$ or K).

The direct pseudo-analytical model is found to be quasi instantaneous. The resulting calculation time is found to be in the order of $t_{CPU} \sim 10^{-3}s$ using a standard desktop computer, for one normalized harmonic representing the front face temperature evolution at an instant t, and for a monolayer material. This feature is partly due to the information compression by means of the Fourier transform. It also allows to qualify the current model as quasi-instanteous compared to other numerical calculation techniques that will be discussed in the chapter 3. The current system resolution has been pre-tested using other resolution types presented in [110] and discussed in chapter 3.

The model outputs have to be compared to the experiment. Consequently, the experimental signal have to be converted into normalized harmonics. In this case, the cost function that should be minimized, should express the difference between:

- the model ouputs $Y(\beta) = \xi_{m,n}^{mod}(\beta,t)$, achieved by the Laplace inversion applied to the direct analyitcal model outputs $\xi_{m,n}^{mod}(p)$,
- and the experimental observables, $Y^* = \xi_{m,n}^{exp}(t)$ issued from temporal measurement of the front face temperatures, and projected twice in Fourier Cosine space, following the Eq. 2.5.

$$\xi_{m,n}^{exp}(z,t) = \frac{1}{l_x \cdot l_y} \cdot \int_0^{l_y} \int_0^{l_x} T^{exp}(x,y,z,t) \cdot X_m(x) \cdot Y_n(y) \cdot dx\, dy \tag{2.5}$$

Regarding the domain defined in (iv), it requires a process opposite to that in (iii): 1- no transformation for the direct and analytical model outputs $\xi_{m,n}^{mod}(p)$, 2- and the measures should be projected both in Fourier Cosine space (twice) and in the Laplace domain, following the same equation defined in 2.4. That case was not considered since the projection of the experimental measurements into the Laplace domain by applying the integral transformation from zero to infinite, will require measurement/acquisition for a long time.

2.4.3 Laplace inversion technique

The inversion from Laplace to time domain is conducted using different algorithms [185], in order to compare and pursue their convergence (or divergence), their inversion accuracy and time consumption:

- Gaver Stehfest algorithm [186]
- Zakian algorithm [187]
- Classical Fourier transform [1]
- Den Iseger algorithm [188]

- De Hoog transform [189]

These algorithms showed very different performances, depending on the considered function type. The De Hoog transform was found to be the most appropriate inversion technique, applied for the current problem in order to successfully realize the inversion of the model outputs $\xi_{m,n}(p)$ into the required direct model outputs $\xi_{m,n}(t)$. It has given the best compromise between accuracy and time consumption, compared to other cited inversion techniques. Noting that, in some cases that will be discussed later in chap 3 and chap 4, a combination of Stehfest-De Hoog algorithms has been found to be the most convenient technique for the inversion of sensitivities $Sr_{m,n}(p)$ into $Sr_{m,n}(t)$ (in terms of accuracy and time consumption).

2.5 Estimation method

2.5.1 Linear and non-linear concepts

The minimization of the objective function depends on the inverse problem properties and especially its linearity or non-linearity. The main purpose of this section is to define and discern the "linear system" from the "linear direct problem" and "linear inverse problem".

Linear and nonlinear system

A system is a box to which an input is applied in order to give the corresponding output. A thermal system is the layout of an experience. Its input is generally the thermal excitation (energy source), and its outputs are, most of the time, the temperatures measurements. It is also characterized by its initial and boundary conditions.

Such system can be considered linear if its outputs Y (e.g. temperature measurements) is linearly dependent on its inputs X (e.g. thermal excitation), i.e. $Y = A \times X$ [110].

Linearity of direct and inverse problem

The concept of direct problem exists only as an opposition to the inverse problem. It consists in calculating the outputs (temperature field for example) for fixed values of parameters β. The linearity of the inverse problem is independent of the linearity of the direct problem [110].

The inverse problem is linear if the model outputs are linearly dependent of the parameters β via a sensitivity matrix S independent of β: $Y_{mod} = S \cdot \beta$. Here S is the ordinary sensitivity matrix defined and detailed in 2.6.1. If S is not constant, and its coefficients depend on the parameters to estimate, the model is then considered non-linear and is presented by the following equation $Y_{mod} = S(\beta) \cdot \beta$. The dependency of only one of the sensitivity coefficients to one of the parameters, led to a non-linear model. In contrast, if S is constant and none of its coefficients are dependent on any parameters, the corresponding model and inverse problem is defined as linear.

2.5.2 Estimators and Objective function

There are different types of estimators dealing with parameters estimations, and having the same principles that consists in minimizing the difference between the observable Y^* and the model outputs $Y(\beta)$. The strategy in searching for the best set of parameter $\hat{\beta}$ depends on the method, as discussed further in the present chapter. The objective is summarized into the following definition:

$$\hat{\beta} = \beta_{opt} = \text{Arg}\min_{\beta}[f(\beta)] \tag{2.6}$$

Where f is the cost function, also known as objective function, which must be minimized. The definition of the objective function may differ from one method to another.

Most of the time, the objective function is defined as a residue Re, corresponding to the comparison between the experimental and model responses $Re = Y_{exp} - Y_{mod}$. However, due to the discrete nature of the measurements (the time variable in most of the cases), the residue is represented as a vector dependent on the parameter vector β: $Re(\beta) = Y_{exp} - Y_{mod}(\beta)$, and at each vector index j (time index here) $Re_j(\beta) = Y_{j,exp} - Y_{j,mod}(\beta)$.

The cost function, which must be minimized, is the residual norm $|Re|$ that can be defined using L_1, L_2, L_3 ..., or L_x norm [190], where $|Re|_x \equiv (\Sigma_j |Re_j|^x)^{\frac{1}{x}}$, is the norm of dimension x quoted L_x. Another type of norm is the infinity norm L_∞ defined as $|Re|_\infty \equiv \max_j |Re_j|$ for a discrete problem.

In practice, linear estimation problems are conducted according to one of the following strategies:

- Estimating $\hat{\beta}$ by finding the minimum of the norm L_∞, i.e. the minimum of $f_1(\beta) = \max_j |Y_j^* - Y_j(\beta)|$. Noting that $Y^* \equiv Y_{exp}$, are the observales, and $Y(\beta) = Y_{mod}$ are the model outputs.

- Estimating $\hat{\beta}$ by finding the minimum of the norm L_1, i.e. the minimum of $f_2(\beta) = \Sigma_{j=1}^{m}(Y_j^* - Y_j(\beta))$, where m is the measurements number.

- Estimating $\hat{\beta}$ by finding the minimum of the norm L_2, i.e. the minimum of the square deviation $f_3(\beta) = \Sigma_{j=1}^{m}(Y_j^* - Y_j(\beta))^2$, where m is the measurements number. This definition is deeper developed in the following sections since it is the mostly used type of objective function. This quadratic estimator, based on the sum of quadratic deviations, is more efficient compared to the previous estimator, based on sum of deviations, since it prevents the potential compensation between negative and positive deviations [191]. The norms L_1, L_2 and L_∞ are the most used. Norms of higher dimension are not detailed in this work.

- Another frequently used type of objective function is known as "the median of square deviation" [110] with $f_{med}(\beta) = med(Y_j^* - Y_j(\beta))^2 = \dfrac{\max_j \left[Y_j^* - Y_j(\beta)^2\right] + \min_j \left[Y_j^* - Y_j(\beta)^2\right]}{2}$.

To recall, retrieving the optimal set of parameters β to estimate is based on the minimization of the deviation between the output of a mathematical model and experimental measurements.

This fit is achieved by means of an optimization algorithm that minimizes a cost function expressing the discrepancy between both signals. In this work, the latter will be the quadratic deviation between the front face or rear face signal predicted by the direct physical model and the measured signal (e.g. experimental outputs). Thus, the estimator dedicated for the minimization of the cost function, could be written as follows:

$$f = \sqrt{\sum_{m=0}^{M}\sum_{n=0}^{N}[\xi_{m,n}^{mod}(\beta, z=0 \text{ or } l_z, t) - \xi_{m,n}^{exp}(z=0 \text{ or } l_z, t)]^2} \tag{2.7}$$

where m and n are the considered modes for the estimation with maximum values of M and N respectively.

Several monolayers thermal characterization methods using different kind of observables (ERH [73, 76, 149], ENH [78, 80, 81], MSEH [74], DSEH [111] will be represented later on in chapter 3).

Numerous alternative types of objective functions that shall be minimized can be cited. Moreover, some functions may have some conditions/constraints on the optimal solutions, and introduce accordingly the constrained-optimization field (see the following section 2.5.4).

2.5.3 Linear parameters estimation

In general, the methods applied for linear parameters estimation can be classified as following:

1. Least square method (LS)
   (a) Ordinary least square method (OLS)
   (b) Extended least square estimation method (ELS)
   (c) Generalized least squares (GLS)
2. Probability approaches
   (a) Bayesian approach of probability (e.g. MAP (Maximum a Posteriori Estimator))
   (b) Frequentist approach of probability (e.g. MLE (Maximum Likelihood Estimator))

Each class of linear estimation tools cited here, is well detailed in [110].

2.5.4 Nonlinear parameters estimation and Optimization algorithms

Optimization is a term frequently used, at the present time, in several sectors of academic research or industry, where optimization objectives are often required for many potential needs, such as:

- enhancing the manufacturing processing,
- maximizing the efficiencies,

- or minimizing different types of losses.

For any inverse problem, optimization is also an ultimate goal for the reconstruction of hardly measured boundary conditions, the estimation of mechanical or thermophysical properties, etc.

This section consists in an overview of the algorithms commonly used to optimize (maximize or minimize) the estimation function, also known as “goal function”, “objective function”, “ optimal criterion”, “functional criterion”, “discrepancy function” or “cost function”. It focuses on the large scale nonlinear problems for which all above-presented tools (OLS, MAP, and MLE) are not suitable [110].

The task of classifying all the optimization methods is quite complex, due to the diversity of the criteria that can be handled for this classification. All these algorithms are adapted to nonlinear problems, since the minimization in such cases, where sensitivities of the observations to the parameters are dependent on these latter, seems to be impossible with all above-presented tools (OLS, MAP, and MLE) which are generally appropriate for linear models.

The optimization algorithms can be classified through several types of criteria, which are mainly:

- The dimension: One dimensional or n (for $n \geq 1$) dimensional algorithms. Algorithms differ, here, by the type of function that they optimize, and that may involve one variable (1D) or multi-variables (n-D).

- The order: Zero order, first order, or second order algorithms. They need the objective function value for the case of zero-order, the gradient of this function for the first order, and the hessian for the second order.

- The strategy: Gradient free or gradient based algorithms. Gradient free algorithms try to find the minimum of the objective function without calculating the gradient. They are required when the gradient calculation is difficult and time consuming, or when the function has various local minima. Contradictory, the gradient based algorithms find the optimum using the gradient (of order 1, between 1 and 2, or 2) of the objective function.

- The research space area: Local optimal research or global optimal research algorithms. Some algorithms are only able to find the local minimum of the cost function. It has a significant concern if the function contains numerous local optimums. Contrarily, others methods, as Metaheuristics approaches, can randomly find the global minimum.

- The algorithm nature: Stochastic or deterministic algorithms. In a deterministic approach, the output of the identification is fully conditioned by the input values and the initial conditions. In contrary, in a stochastic approach, the output possess some inherent randomness. The same set of input parameter values and initial conditions can lead to a set of different outputs. The stochastic algorithms are found to be more adequate for a global minimum search, especially for the function having multiple local minima where deterministic algorithms may converge to a local minimum.

- The number of set of parameter under consideration: Population or unique individual based algorithms. In population based algorithms (PSO, GA, ES, ...), many candidates are simultaneously evaluated and interact at each iteration. Whereas, individual algorithms manipulate a single solution and enhance it in an iterative manner.

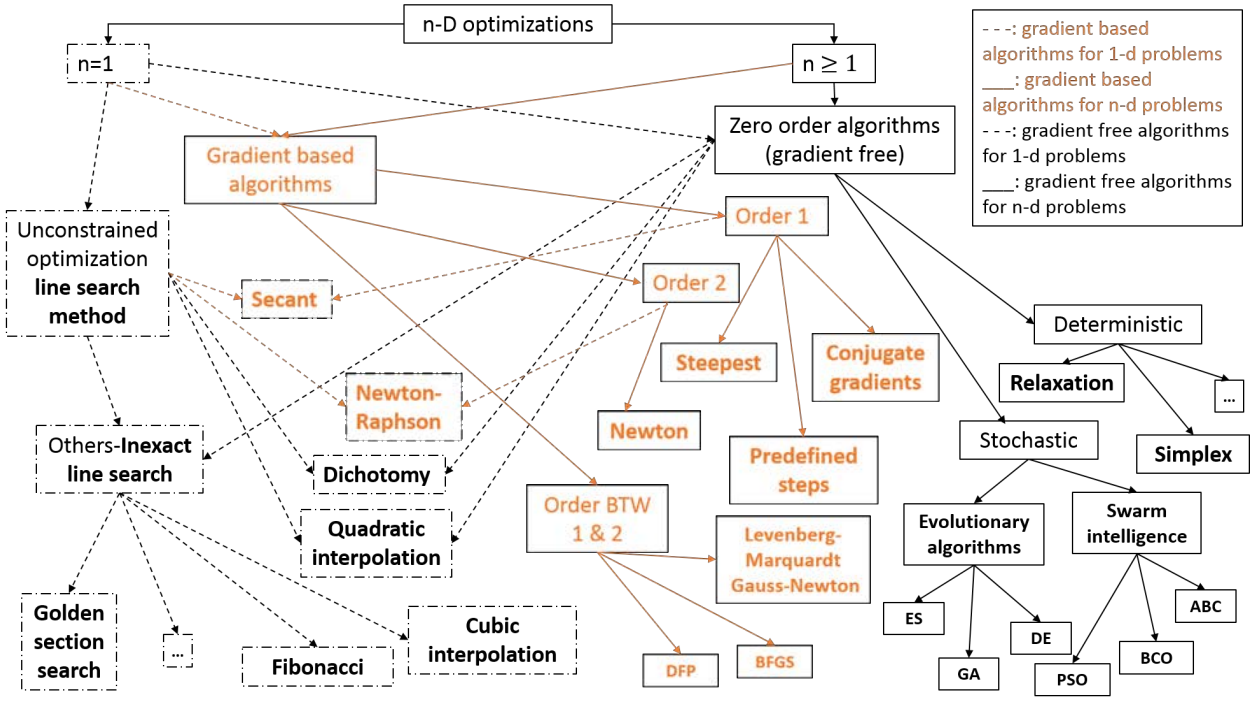

Figure 2.14 – The global classifications of commonly-used optimization methods.

2.5.4.1 Brief description of some commonly used algorithms

One dimensional unconstrained optimization algorithms

This category includes all algorithms able to find the optimum of an unimodal function. These algorithms, also called “line search methods”, are used to solve problems with higher dimensions, in which the iterative method solves at each iteration, a single variable optimization problem. It includes several algorithms. Some of them are gradient based methods, such as the Newton-Raphson method [192], the Secant method [193]. Others are gradient-free methods such as the Dichotomy method [194], the Quadratic interpolation [195], in addition to other inexact line search methods such as the Golden section search method [196], the Fibonacci methods [197] or the Cubic interpolation method [198].

***n* dimensional algorithms (n-D with $n \geq 1$)**

As "one dimensional algorithms", the present class includes gradient and free gradient (a.k.a zero order) algorithms able to find the optimum of a multimodal function.

- The gradient type algorithms include multiple gradient orders types:

  - First order algorithms [199], such as the Predefined steps gradient method, the Steepest descent method or the Conjugate gradient method.
  - Second order algorithms [199], especially the Newton method.
  - Quasi-Newton (between first and second order) methods [196, 200], including the Gauss-Newton method, the Davidon-Fletcher-Powell (DFP) method, the Broyden-Fletcher-Goldfarb-Shanno (BFGS) method, the Levenberg -Marquardt method, etc.

- Gradient free algorithms, including:

  - Deterministic algorithms, such as the Simplex [199] and the Relaxation algorithms [201].
  - Stochastic algorithms, such as Genetic Algorithms (GA) [202], the Evolution Strategy (ES) [203], the Differential Evolution (DE) [204], the Particle Swarm Optimization (PSO) [205], the Ant Colony Optimization (ACO) [206] and the Artificial Bee Colony algorithm (ABC) [207].

Please note that, adding to the deterministic gradient-free type algorithms, all gradient based algorithms are qualified also as deterministic since they give at all executions the same results.

Metaheuristics

Metaheuristics are heuristic methods used to solve complex problems by combining the "exploration" of the entire search space or the "exploitation" of the most promising candidates. Adding to the principles of "exploration" and "exploitation", metaheuristics include the principle of "memory" while using older and current candidates for the search guidance [208]. This class of method have given rise to various benchmarks and test functions used to evaluate their performance (detailed afterwards). This class involves methods having the common following features: they are approximate, zero-order, stochastic, global, single objective, parallel processing, iterative, population based algorithms and inspired from natural mechanisms [202]. Heuristic methods are used for optimization purpose to solve problems without any guarantee to find the exact solution. Those methods are dedicated to the research of satisfying solutions, through the application of experiences and intuitions [209]. The main metaheuristics methods implemented to solver optimization problems are of stochastic type (PSO, GA, ES...).

Test functions

The evaluation of optimization algorithms efficiency and robustness may be performed via functions presenting multiple local minimums. In the litterature, there is numerous type of functions used to test the performance of optimization algorithm with various degree of difficulty [210–212] such as:

- Single-objective unconstrained functions including the Rastrigin function, the Rosenbrock function, the Ackley function, the Three-hump camel function, the Hölder table function, the Eggholder function, the Styblinski–Tang function and tens others.
- Constrained functions including the Bird function, the Simionescu function or the constrained Rosenbrock function .
- Multiple-objective functions including the Zitzler–Deb–Thiele function, the Chakong and Haimes function, the Binh and Korn function, the Viennet function and others .

The Rosenbrock and Rastrigin functions, shown in Figs. 2.15, commonly used as "benchmarks", have been investigated here in order to compare and evaluate the performance of the currently used optimization algorithm.

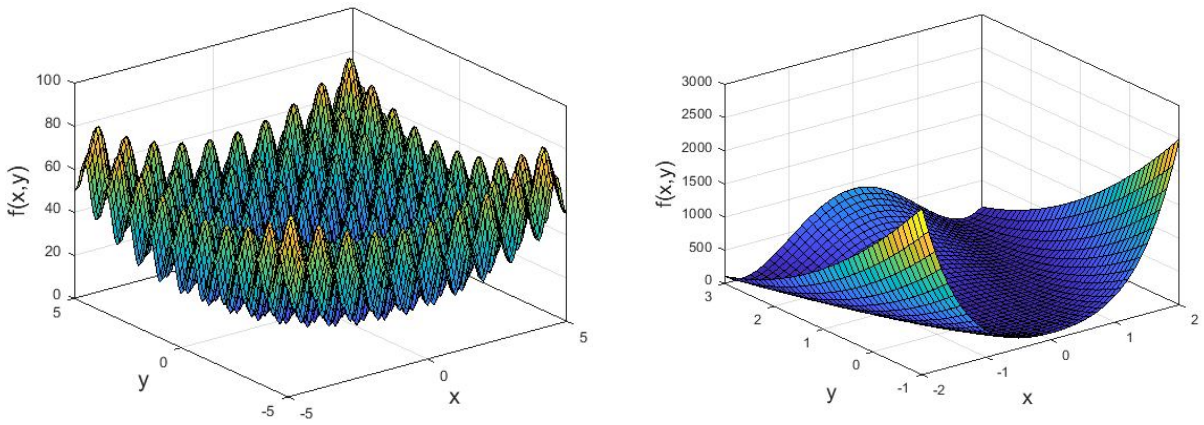

(a) Ratrigin function (b) Rosenbrock function

Figure 2.15 – 3D test functions applied for the optimization algorithms.

2.5.4.2 Stopping criteria for iterative methods

In general, the iterative problems. The resolution shall be stopped using a criterion. The most commonly used stopping criteria are shown here [179]:

- $|\nabla f(\beta^k)| \leq \varepsilon$ applied on the gradient of the cost function.
- $|f(\beta^k) - f(\beta^{k-1})| \leq \varepsilon$ applied on the value of the cost function.
- $|\beta^k - \beta^{k-1}| \leq \varepsilon$ applied on the value of the parameter.
- $f(\beta^k) \leq \varepsilon$ applied on the value of the cost function. This criterion is known as the “maximum discrepancy principle”.

Where k is the iteration index, f the cost function, β the parameters vector, and ε the value chosen for each stopping criterion. The first three criteria are generally used in optimal control and optimization problems. The last one is commonly found in inverse problems whose critical objective functions values are set to the measurements errors variances.

2.5.4.3 Hybrid optimization algorithm applied in the current study

Regarding the relatively large number of parameters to identify β as well as the non-linear nature of the phenomenon studied in the framework of this thesis, the use of a global search algorithm is required. This search is achieved by means of a stochastic approach in order to avoid getting stuck into a local minimum. After many test, the Particule Swarm Optimisation (PSO) has been chosen for its efficiency and its relative accesibility. However in order to ensure a convergence to the optimal value, which is a local minimum located in the global minimum region, the previous stochastic optimization algorithm has been coupled with a deterministic gradient based algorithm.

Thus, identification of the optimum parameters vector $\hat{\beta}$ that minimizes the objective function
$\sum_{m=0}^{M}\sum_{n=0}^{N}[\xi_{m,n}^{mod}(\beta, z=0,t)-\xi_{m,n}^{exp}(z=0,t)]^2$, is achieved by an hybrid optimization procedure combining both a stochastic and a deterministic methods.

Particule Swarm Optimization

Among the existing stochastic methods, the so-called Particle Swarm Optimization (PSO) algorithm is chosen for its capability to deal with such complex problem, its relative ease of understanding and implementation as well as its relatively low number of parameters to set. The efficiency of this algorithm has been proved in many different engineering fields [213–220] , especially when applied to heat transfer problems [3–5, 221–224]. This metaheuristic technique also known as "evolutionary population based method", is a nature inspired and zero order algorithm. It exploits the swarm intelligence that consists in the independent evolution and the interaction of agents in a biological type system.

The swarm is modeled by a swarm of particle or "candidate solution", whose position and velocity are randomly set at the initial time. Those particles, representing a potential solution of the minimization problem, evolves in a collaborative way inside the domain [225–227]. The particles move in the domain field, predefined by a upper and a lower bounds, searching for the optimal solution i.e. for the lowest value of the cost function. Each particle can remember its best position and share it with others, so that all particles will iteratively adjust their velocity based on its personal experience and the information collected from neighbors.

For more detailed explanation, a potential solution of the minimization problem is represented by a particle position P_i. This position will iteratively evolve according to the criterion expressed by the terms on the right hand side of Eq. 2.8.

$$v_i^{k+1} = w\cdot v_i^k + c_1\cdot r_1(i,k)\cdot[\hat{N}_i^k - P_i^k] + c_2\cdot r_2(i,k)\cdot[\hat{P}_i^k - P_i^k] \tag{2.8}$$

The first term, $w\cdot v_i^k$, is related to the particle inertia that linearly depends on the previous velocity and an inertial coefficient w. This coefficient is initially set in order to promote the exploration in the early stage of the search process to $w = 1.1$. The inertial coefficient w is then updated at each iteration considering the number of iteration without any changes of the best

objective function value. For any improvement that occurs after 2 or less previous iterations, the value of w is multiplied by a factor 2. On the contrary, for 5 or more successive iterations without improvement, the value of w is divided by a factor 2. Moreover, a test is implemented to ensure that the value of w is kept into the range $[0.1 - 1.1]$. Higher values of w encourage exploring the search domain, lower values of w speed up the convergence.

The second term, $c_1 \cdot r_1(i,k) \cdot [\hat{N}_i^k - P_i^k]$, represents the social behavior, in which the particle direction is influenced by the experience (i.e. best f) shown among the neighborhood of the particle.

The third term, $c_2 \cdot r_2(i,k) \cdot [\hat{P}_i^k - P_i^k]$, represents the cognitive behavior, in which the particle direction is influenced by its own experience. These two latter terms are weighted by empirical coefficients c_1 and c_2. In order to avoid the algorithm being trapped into a local minima, these terms are completed with coefficients r_1 and r_2 whose values, ranging from 0 to 1, are randomly set at each PSO iteration k and for each particle i.

Once getting the velocity for each component (i.e. parameter to identify, non-indexed for readability reasons), v_i^{k+1}, the new position of the particle in the search domain, P_i^{k+1}, is computed as following:

$$P_i^{k+1} = P_i^k + v_i^{k+1} \tag{2.9}$$

The parameters driving the behavior of PSO particles and used in the set of Eqs. 2.8 are commented in Table 2.1.

PSO parameters	**Values**	**Description**
w	$[0.1 - 1.1]$	inertia (adaptive) of particles
c_1, c_2	1.49	acceleration coefficients
$\hat{N}_i^k$	-	best experience among the neighbors of the particle i
$\hat{P}_i^k$	-	best experience of the particle i
$r_1(i,k), r_2(i,k)$	$U(0;1)$	uniform random vector for each particle i at each iteration k

Table 2.1 – Parameters and values used in the PSO algorithm.

The other PSO algorithm parameters set in this work are listed below:

- Bounds of the parameters values that should be estimated
- Number of PSO particles
- Maximum number of iterations
- Maximum stall iterations, which means the number of consecutive iterations with unchanged objective function value
- Maximum running or calculation time

- Maximum stall time, which means the time over which the PSO particles are blogged in the same solution
- Minimum objective value, $f(\beta^k) \leq \varepsilon$
- Tolerance value, $|f(\beta^k) - f(\beta^{k-1})| \leq \varepsilon$

The result obtained from the PSO search step, is then used as initial condition to a gradient based algorithm, namely the interior point method whose mathematical implementation into computer calculation is described in [228]. The method relies on the idea of a barrier function that handled the constraints linked to the search space domain of each unknown parameter. The resulting approximate problem is solved via the well-known Newton method. When the problem is not locally convex near the current iterate, the problem is solved via a conjugate gradient method. Those deterministic gradient based algorithms, included in the interior point method, are best suited for a local convergence of the solution as detailed below.

Newton method

The Newton method is a second order gradient and descent type algorithm. The first condition to apply this method, is that the objective function must be twice differentiable. The gradient of this function is approximated by a Taylor development, then the new parameter $\beta_k + 1$ is obtained by equaling the approximated gradient to zero:

$$\beta_{k+1} = \beta_k - \frac{\nabla f(\beta_k)}{\nabla^2 f(\beta_k)} \tag{2.10}$$

∇f and $\nabla^2 f$ are the first and the second derivative (or the hessian) of the objective function, respectively. The method should also respect the concept of the descent method, with a descent direction:

$$d_k = -[\nabla^2 f(\beta_k)]^{-1} \cdot \nabla f(\beta_k) \tag{2.11}$$

The step size δ is commonly controlled through an iterative 1D minimization problem with the following calculation :

$$\min_{\delta}[g(\delta) = f(\beta_k + d_k \cdot \delta)] \tag{2.12}$$

followed by the actualization step $\beta_{k+1} = \beta_k + d_k \cdot \delta_k$ [199] . It is important to note that the algorithm risks to diverge if the Hessian is not a positive definite matrix, and when the direction is not a descent one. The Hessian of the objective function f is calculated following this matrix:

$$H(f) = \nabla^2 f = f''(\beta) = \begin{pmatrix} \frac{\partial^2 f}{\partial \beta_1^2} & \cdots & \frac{\partial^2 f}{\partial \beta_1 \partial \beta_{n_\beta}} \\ \vdots & \ddots & \vdots \\ \frac{\partial^2 f}{\partial \beta_{n_\beta} \partial \beta_1} & \cdots & \frac{\partial^2 f}{\partial \beta_{n_\beta}^2} \end{pmatrix} \tag{2.13}$$

However, the above equation can only be applied when the Hessian of the cost function exists, and when it is reversible. Contrarily, if this Hessian is not reversible, the descent direction can be calculated by resolving this equation:

$$[\nabla^2 f(\beta_k)] \cdot d = -\nabla f(\beta_k) \tag{2.14}$$

Conjugate gradient method

The Conjugate gradient method is a first order gradient type algorithm. It is a descent method with an optimal step size able to minimize a quadratic and non-quadratic functions.

For quadratic functions

The first fundamental concept of this method consists in calculating $\delta_k = \min_{\delta}[f(\beta_k - \delta \cdot \nabla f(\beta_k)]$ and like any type of descent methods $\beta_{k+1} = \beta_k + d_k \cdot \delta_k$ [199]. The gradient of the quadratic function is written as $\nabla f(\beta) = (A\beta - b)^T$ and the Hessian $\nabla^2 f(\beta) = A$, where A is defined as a positive symmetric matrix. Each descent direction is chosen to be conjugated to the previous one, with respect to A.

The second step is applied to find the direction d_k, at the iteration k and using a linear combination between the previous direction d_{k-1} and the steepest descent direction $-\nabla f(\beta_k)$: $d_k = s_k \cdot d_{k-1} - \nabla f(\beta_k)$. The value of s_k is calculated to have successive conjugate directions with respect to A. Adding to that, $d_{k-1}^T \cdot A \cdot d_k = 0$. And s_k can be calculated by the Fletcher-Reeves formulation [229]:

$$s_k = \frac{\|\nabla f(\beta_k)\|^2}{\|\nabla f(\beta_{k-1})\|^2} = \frac{\nabla f(\beta_k) \cdot \nabla f(\beta_k)}{\nabla f(\beta_{k-1}) \cdot \nabla f(\beta_{k-1})} \tag{2.15}$$

Or using Polak and Ribiere method [229]:

$$s_k = \frac{\nabla f(\beta_k) \cdot \nabla f(\beta_k) - \nabla f(\beta_{k-1})}{\nabla f(\beta_{k-1}) \cdot \nabla f(\beta_{k-1})} \tag{2.16}$$

Therefore the new descent direction is calculated by this recurrence equation:

$$-d_k = -\nabla f(\beta_k) + \frac{\|\nabla f(\beta_k)\|^2}{\|\nabla f(\beta_{k-1})\|^2} \cdot d_{k-1} \tag{2.17}$$

For arbitrary functions

When considering the reasonable hypothesis assuming that near the solution $\hat{\beta}$, the objective function will not be significantly different from the quadratic function, the same method applied in the previous section can be applied here. In contrast, if the function is significantly far from the quadratic one (even near the solution), the conjugation concept has no significance. In that case, it is wisely recommended to regularly reinitialize the current direction d with the steepest gradient direction $-\nabla f(\beta_k)$ [199].

Conclusion on the Hybrid optimization strategy

Finally, the overall strategy takes advantages of both methods, i.e. the capability of the PSO method to search for the global minimum region and the capability of the interior point method to find the local optimum of the objective function in the global minimum region previously found.

2.6 Sensitivity analysis concept

The sensitivity analysis is a key element, frequently used in inverse problem theory to i) verify the feasibility of the estimation, ii) diagnose the corresponding best conditions required to perform an identification, and iii) ensure the non-correlated nature of the parameters. This tool has to be applied in order to evaluates the influence of parameters to be estimated or known a priori on the direct model outputs, in this work the harmonics $\xi_{m,n}(t, z=0)$, and which of these parameters could be accurately estimated. This evaluation method comes in addition to other possible methods such as the probabilistic methods, variance-covariance matrices and others.

The sensitivity analysis check the feasibility to simultaneously identify several parameters, in the present case, the simultaneous estimation of the material thermal diffusivities (along the three main directions).

It is important to note that, when any correlation between two or more parameters is noticed, their simultaneous estimation is impossible. These correlations could be observed from their sensitivity analysis variation (e.g. time evolution in this work). Finally, several types of sensitivity analysis could be used: ordinary, reduced, normalized or dimensionless sensitivity analysis.

2.6.1 Ordinary sensitivity analysis

It illustrates the effect of a small parameter variation $\partial\beta_j$ on the model outputs $\partial Y(\beta, t)$ which are the front or rear face normalized harmonics, $\partial\xi_{m,n}(\beta, t)$, while keeping all other parameters constant. The derivative (i.e. ratio of variation) is calculated for all modes (m, n) and as a function of time t, as shown in the following equation:

$$S_{m,n}(\beta_j, t) = \frac{\partial Y(\beta, t)}{\partial \beta_j}\Big|_{\beta_{k\neq j}} = \frac{\partial \xi_{m,n}(\beta, t)}{\partial \beta_j}\Big|_{\beta_{k\neq j}} \tag{2.18}$$

The general definition of this matrix is as following:

$$S_{i,j} = \frac{\partial Y_i}{\partial \beta_j}\Big|_{\beta_{k\neq j}} \tag{2.19a}$$

$$S = \begin{pmatrix} \frac{\partial Y_1}{\partial \beta_1} & \cdots & \frac{\partial Y_1}{\partial \beta_{n_\beta}} \\ \vdots & \ddots & \vdots \\ \frac{\partial Y_m}{\partial \beta_1} & \cdots & \frac{\partial Y_m}{\partial \beta_{n_\beta}} \end{pmatrix} \tag{2.19b}$$

2.6.2 Reduced sensitivity analysis

To ensure a more detailed analysis, the sensitivity coefficients must have similar untits (and so similar scale values) in order to properly compare the impact of the different parameters [230, 231].

$$S^*_{m,n}(\beta_j, t) = Sr_{m,n}(\beta_j, t) = \frac{\partial Y(\beta, t)}{\partial \beta_j} \times \beta_j \Big|_{\beta_{k\neq j}} \tag{2.20}$$

In this case, the sensitivity matrix can be written as following

$$Sr = \begin{pmatrix} \frac{\partial Y_1}{\partial \beta_1}\beta_1 & \cdots & \frac{\partial Y_1}{\partial \beta_{n_\beta}}\beta_{n_\beta} \\ \vdots & \ddots & \vdots \\ \frac{\partial Y_m}{\partial \beta_1}\beta_1 & \cdots & \frac{\partial Y_m}{\partial \beta_{n_\beta}}\beta_{n_\beta} \end{pmatrix} \tag{2.21}$$

Similar sensitivities evolution is the indicator of correlation between parameters, i.e. the variation of the model outputs, or observables, may be attributed to any of those parameters. In other words, it exists an infinity of combination of those parameters which are equivalent regarding the system response. In this case, the simultaneous estimation of these parameters is impossible and the procedure has to be modified.

The parameters correlation may also be a consequence of ill-posed problem which can be solved by means of a regularization technique [232], or by finding the exact relation between the parameters. For example if two parameters are correlated and their exact relation is well-known, the estimation of one of them can be successfully performed. The other parameter is then deduced from the correlation itself. The curves of the reduced sensitivities have to be analysed in order to evaluate any correlation. Figs. 2.16 show some examples for well-posed problems, where the reduced sensitivity coefficients are linearly independent and the simultaneous estimation of parameters is possible.

The other figures 2.17 correspond to sensitivites evolution of ill-posed problems, for which the reduced sensitivity coefficients are linearly dependent and the estimation of all parameters is impossible.

In this work, the reduced sensitivity analysis is considered to appropriately compare the influence of parameters on the model outputs and to detect any parameters correlations. The reduced sensitivity was to be found to be the most relevant type of sensitivities, allowing unit homogenization (i.e. $^\circ C$) as well as the order of magnitude, and then facilitating the comparison

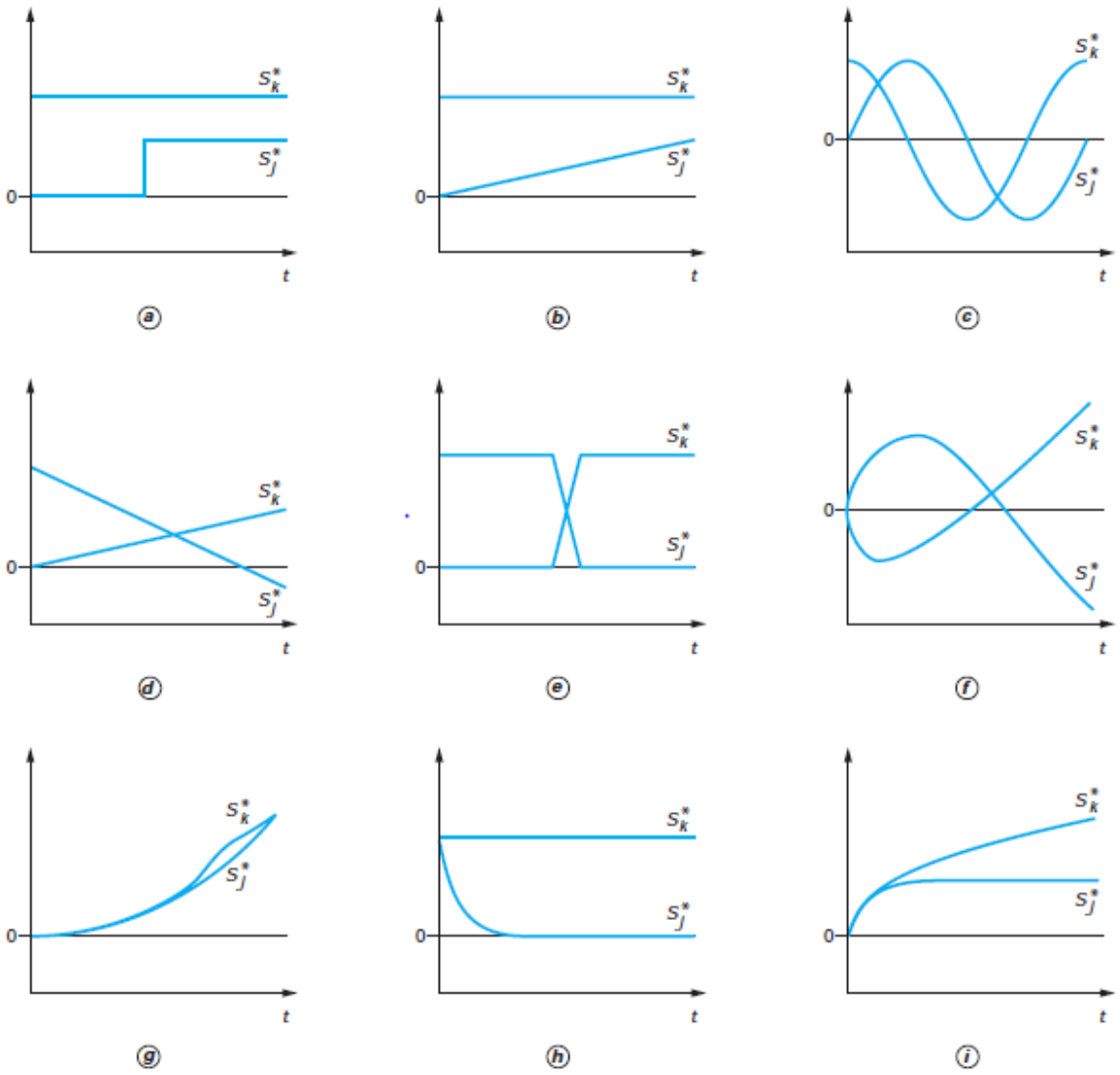

Figure 2.16 – Sensitivities evolution of linearly independent parameters problems (i.e. well-posed problems))[231].

between the parameters.

2.6.3 Dimensionless sensitivity analysis

This type of sensitivity is also known as "relative reduced sensitivity" or "normalized sensitivity". In some cases, where the observables are vitiated by an error having a non-uniform (i.e. dependent on time) standard deviation and noted $\sigma_Y(t)$, a reduced relative sensitivity is conveniently investigated. It is defined by :

$$S^{**}_{m,n}(\beta_j, t) = \frac{\partial Y(\beta, t)}{\partial \beta_j} \cdot \frac{\beta_j}{\sigma_Y(t)}\Big|_{\beta_{k\neq j}} \tag{2.22}$$

This type of sensitivities, although useful, may generate a misunderstanding while treating highly noisy signals. As shown in Eq. 2.22 a high level of standard deviation σ_Y will artificially decrease the sensitivity level.

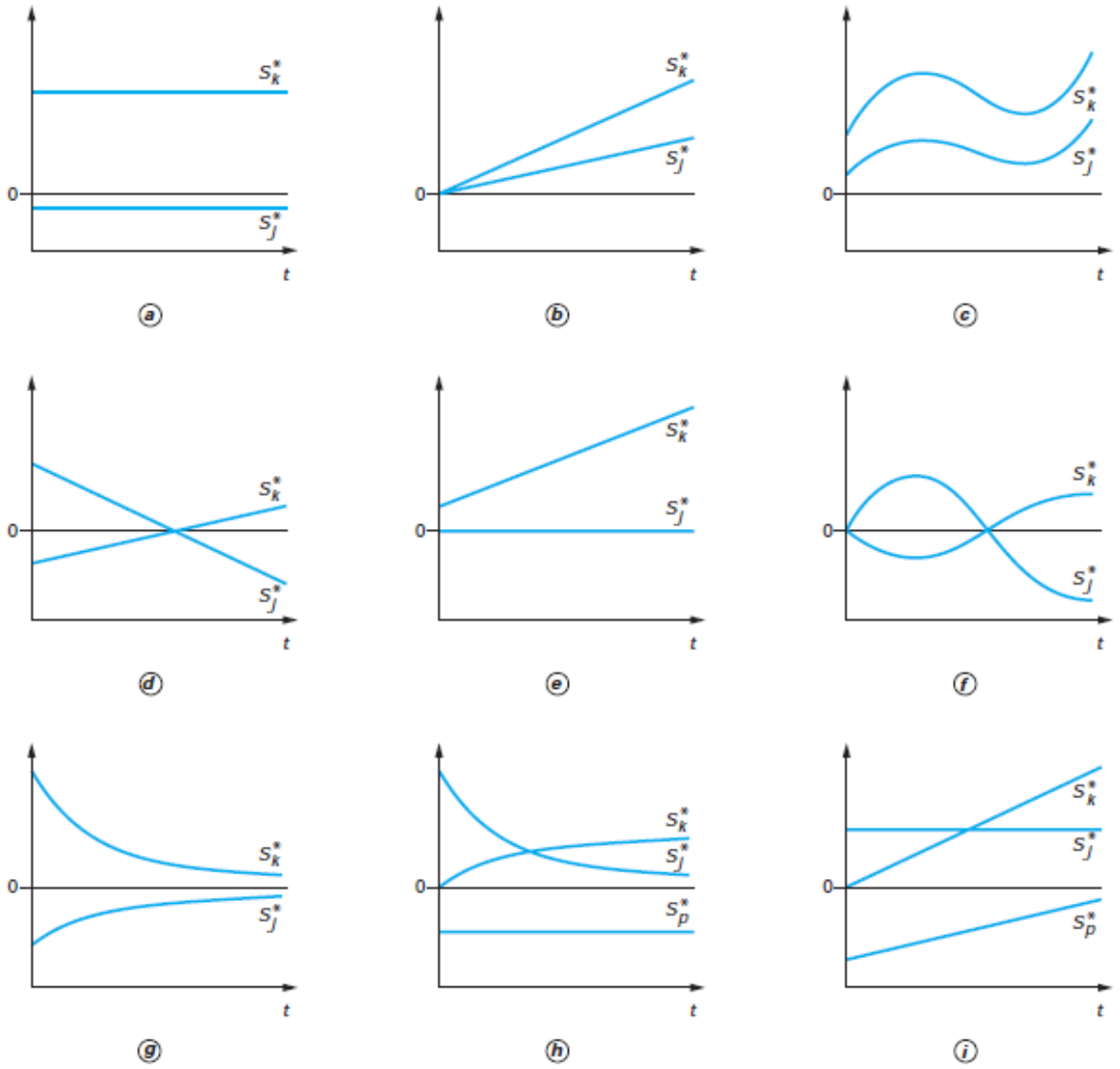

Figure 2.17 – Sensitivities evolution of linearly dependent parameters problems (i.e. ill-posed problems) [231].

Well posed and ill-posed problems

Mathematical models that describe a physical phenomena, and more specifically thermal phenomena, may be rather well-posed or ill-posed.

1. The standard "well-posed problems" satisfy at the same time, according to Hadamard, the following conditions [232–234]:

   (a) The solution must exist: each solution in the observations space should have in parallel a solution in the parameters space.

   (b) The solution must be unique (the same vector Y cannot be the result of two different β values).

(c) The solution must be continuous and stable after being subjected to small inputs variations [233].

2. The so called “Ill-posed problems”, that violates at least one of the above conditions.

Regularization techniques

Different regularization techniques [232] have been developed in order to fix ill-posed problems, that are especially encountered when estimating continuous functions by parametrisation (e.g. boundary condition estimation, type c in 2.2.1), some of these techniques are cited thereafter:

- Regularization using the Tikhonov penalization method
- Regularization using the “future time steps”
- Regularization using SVD technique
- Iterative regularization

Other techniques should be conducted for the regularization of parameters estimations ill conditioned problems. In such cases, the ill conditioning character may appear when some parameters correlations lead to important combinations between the sensitivity matrix columns. It can be explained by the fact that the experiment or synthetic observations are unable to give information regarding these parameters separately [110].

To overcome this issue, several actions may be considered:

- Changing the observations: this strategy consists in changing the observables by modifying the measurements or modifying the experiments in order to enrich the information used by the estimator. This modification is the central point of the design of experiment that tries to get the optimal observations for the parameters estimation problems.
- Modifying the set of parameters to estimate, by using some combinations that guarantee a possible estimation.
- Reducing the parameters number: this method is frequently used in the estimation of boundary conditions.

2.7 Uncertainties and errors or bias sources

2.7.1 General concept

In order to evaluate the validity, the accuracy and the robustness of an inverse problem resolution, it is important to highlight all types of possible uncertainties that can arise in such excercie [235] and take into account all potential sources of errors.

Those uncertainties and errors may appear during the three major phases of the resolution of an inverse problem and implied:

1. The experimental device: in this work the IR camera, i.e. the measured temperature is expressed in terms of an electrical voltage.

2. The conversion: the measured voltages is converted through a calibration law into a physical quantity. The subsequent physical value is treated and transformed in order to get the appropriate observables Y^*, consistent with the model outputs $Y(\beta)$.

3. The estimation process as discussed previsously.

2.7.2 Brief description of errors or uncertainties sources

Errors on the parameter known a priori

Some parameters or properties (thermophysical, geometrical,...) are sometimes predefined, measured or assumed to be known. While these parameters are not to be estimated, they can affect the identification process. In most cases treated in this thesis the specific heat C, the density ρ and the geometrical dimensions are measured, the excitation instant t_0 is estimated, and the heat convection coefficient h is assumed to be known. Therefore, any error on these parameters values may lead to a consequent error on the estimated solution when applying the identification procedure [179].

Errors due to assumptions

This type of error is the most difficult to compensate. It includes the errors due to the hypotheses (e.g. phenomena to take into account, boundary conditions, ...) assumed in the development of the physical model.

Numerical errors

The resolution of the model can introduce errors. It is not a question of accuracy due to numerical scheme, since in this work the direct simulation is performed using an analytical model. However, it designates the errors due to the numerical inverse Laplace transform or infinite series truncation (M, N).

Adding to that, the stochastic minimization of the cost function using the PSO algorithm can also be a source of numerical errors.

Calibration noises

The raw measurements must be converted into experimental quantities having the same physical units as the model outputs. In this work the correspondence between the measured digial levels have to be converted into levels of temperatures via a calibration procedure. Similarly, the images captured by the IR camera in pixels, have to be converted in geometrical dimension along Ox et Oy. Those conversion may introduce errors caused by an incorrect calibration of the IR camera, or a low acquisition frequency which may introduce error concerning the intial time t_0 [200].

Measurement noises

There are two kinds of measurement noises:

- Internal noises (through the measurement system) such as the perturbations induced by electronic measures, and the fluctuations caused by a non-continuous (at the appropriate scale of observation) physical quantity, for instance: pressure, temperature, and luminance.

- External noises also called perturbations which can be generated by the system environment (the electrostatic effects, the variation in the supply voltage, the interactions between electromagnetic fields taking place on the components and circuits which are not shielded) [236]. The influence of the measurement noise is well detailed in [110].

Errors due to ill-posed problem

The errors due to ill-posed problem corresponds to the errors induced by parameterizing a part of the problem (e.g. boundary conditions) in some inverse problems. In that case the problem is modified as the estimation is performed on the parameters of the function rather than the entire values.

The same type of errors can be encountered when modifiying the set of parameters β in inverse problems dedicated to the estimation of structural parameters, taking into consideration the parametric degree of freedom [231].

Cumulative errors due to indirect estimation methods

Thermopysical properties could be directly or indirectly determined. For instance, the flash technique is a direct method for the thermal diffusivity estimation, but indirect for the determination of the thermal conductivity via the general formula: $\lambda = a \cdot (\rho \cdot C)$. Therefore, any error in the thermal diffusivity estimation a, or in the measurement of the volumetric heat capacity $\rho \cdot C$ will lead to errors in the identification of thermal conductivity λ.

Measurement uncertainties

After a deep analysis of the overall measurement process, the determination of the diffusivity or any other parameter uncertainties can be based on the The 5 Ms method (Measurement/medium, Material, Man/mind, Machine, Method) which relies on Ishikawa causes/effects diagrams [103].

Eventually, other sources of errors could be induced during the different phases of the present study. For example, when trying to center the frames according to the laser spot (see 2.3.4). This procedure is applied in order to neglect the odd harmonics (where the modes m and/or n are odd) compared to the even ones.

Variance-Covariance Matrix

The Variance-Covariance Matrix is frequently used as a testing tool for characterizing the solutions dispersion, and is considered as one of the most important estimator properties. Typically, this matrix quantifies the estimations dispersion among the expected value. The best and the most accurate estimator is the one having the lowest variance, in such a way the estimations $\hat{\beta}$ slightly vary when switching the input data. The deepest is the information extraction from observables Y^*, the lowest are the standard deviations/variances of the estimations β.

The estimation variance-covariane matrix, noticed $cov(\hat{\beta})$, of dimension $n_\beta \times n_\beta$, and consistent with the ordinary least square (OLS), is defined by:

$$cov(\hat{\beta}) = E\left[(\hat{\beta} - E[\hat{\beta}]) \cdot (\hat{\beta} - E[\hat{\beta}])^T\right] = \begin{pmatrix} var(\hat{\beta}_1) & cov(\hat{\beta}_1, \hat{\beta}_2) & \dots & cov(\hat{\beta}_1, \hat{\beta_{n_\beta}}) \\ & var(\hat{\beta}_2) & \dots & cov(\hat{\beta}_2, \hat{\beta_{n_\beta}}) \\ & & \ddots & \vdots \\ sym & & & var(\hat{\beta_{n_\beta}}) \end{pmatrix} \tag{2.23}$$

The diagonal coefficients of the Variance-Covariance matrix corresponds to the variance of each parameter β_i constituting the parameters set vector β, however the off-diagonal coefficients represent the covariances. The covariance is the quantification of the interdependence level existing between two random variables. Thus, when the absolute value of the covariance is high, this means that both variables often have same variation (that could be also opposite) with respect to their respective mean value. Contrarily, when the covariance absolute value is small, this means that the variations of both variables are completely decoupled and that these variables could be considered as non-correlated.

When assuming that the measurement noise is non-correlated with a standard deviation of σ_{noise}, and that variances are similar for all observations Y^* (homoscedasticity hypothesis), therefore one can apply the following correlation, given in [110]:

$$cov(\hat{\beta}) = \sigma^2_{noise}[S^T S]^{-1} \tag{2.24}$$

Where S is the sensitivity matrix defined in 2.19.

In this study the measurement noise is assumed Gaussian, additive and constant in time, and it can be qualified by i.i.d (independent and identically distributed). Based on the calculations developed by Ruffio in [82], when working with normalized harmonics $\xi_{m,n}$ (current observables), the diagonal coefficients of the variance covariance matrix are the variances $\sigma^2_{m,n}$ of harmonics and are given by:

$$\sigma^2_{m,n} = \frac{\sigma^2_m}{4 \cdot (N_x \times N_y)} (1+\delta_m) \cdot (1+\delta_n) \tag{2.25}$$

$$\delta_m = \begin{cases} 1 \text{ if } m = 0, \\ 0 \text{ otherwise} \end{cases} \tag{2.26}$$

and

$$\delta_n = \begin{cases} 1 \text{ if } n = 0, \\ 0 \text{ otherwise} \end{cases} \tag{2.27}$$

$\sigma_{m,n}$ here is the standard deviation corresponding to each harmonic and obtained by an IR camera having $N_x \times N_y$ pixels (depending on the exploitation window size at each treated case). The standard deviation of each pixel is $\sigma_m = 0.1^\circ C$.

Therefore we have $\frac{\sigma^2_m}{4 \cdot (N_x \times N_y)} \leq \sigma^2_{m,n} \leq \frac{\sigma^2_m}{(N_x \times N_y)}$

We consider here the same standard deviation of all harmonics, equal to that corresponding to the mean field (the worst case scenario) with:

$$\sigma^2_{m,n} = \sigma^2_{0,0} = \frac{\sigma^2_m}{(N_x \times N_y)} = \frac{0.1^2}{(N_x \times N_y)} \tag{2.28}$$

Thus, in this study

$$cov(\hat{\beta}) = \sigma^2_{m,n} [S^T S]^{-1} = \frac{0.1^2}{(N_x \times N_y)} [S^T S]^{-1} \tag{2.29}$$

2.8 Summary

In this chapter, the principle of thermal properties estimation, based on the resolution of an inverse heat conduction problem (IHCP), is presented, and each step of the overall identification strategy is developed.

In this chapter, the following points have been discussed:

- The experimental devices required to measure the properties known a priori are described.
- The principle of the problem direct modeling that should reproduce the experiment is explained. Then, the mathematical formulation of the present physical model, that was

used to performed the simulations using the quadruples formalism is well detailed. Such type of resolution allowed to analytically express the forward direct model.

- After an exhaustive description of the linear and non-linear estimation methods, the hybrid optimization algorithm coupling a stochastic minimization tool of PSO type followed by a deterministic optimization method of gradient type, is detailed.
- A general description of all sensitivity analysis types is presented, then the most convenient type (reduced sensitivities analysis) for such studies is argued.
- Ultimately, and in order to refine the evaluation of such problems accuracy and robustness, all possible uncertainties types that can arise from this overall identification technique are finally cited.

2.9 Résumé substantiel du chapitre 2

Introduction

Ce chapitre présente le principe général des problèmes thermiques inverses et décrit l'ensemble des éléments impliqués dans la procédure globale. Pour une application d'identification expérimentale de propriétés thermophysiques, les grandes étapes investiguées seront principalement:

- L'expérience,
- Le modèle direct,
- La comparaison entre les observables et les sorties du modèle via une fonction coût,
- La minimisation à l'aide d'un algorithme d'identification.

En plus de l'introduction et de la conclusion, ce chapitre comporte 6 parties, présentées brièvement ci-dessous.

Partie 1. Problème inverse en conduction thermique

Tout d'abord, un aperçu des problèmes inverses en conduction, IHCP pour "inverse heat conduction problem" dans la littérature anglo-saxonne, est présentée (voir 2.2). Le principe général de résolution de ce type de problème repose sur la comparaison de mesures expérimentales (ou de données synthétiques) avec les sorties d'un modèle analytique ou numérique décrivant le plus fidèlement possible l'expérience. Cette comparaison est effectuée au moyen d'une fonction coût, également appelée "fonction objectif". Tant que cette fonction ne satisfait pas un certain critère, l'algorithme d'optimisation ajuste les paramètres à identifier jusqu'à ce que la procédure converge vers l'ensemble optimal de paramètres $\hat{\beta}$ donnant le meilleur accord entre les données expérimentales et les données simulées. La figure 2.18 montre le principe général et les différentes étapes associés aux méthodes classiques d'identification de paramètres.

Les différentes étapes relatives à la stratégie d'estimation développée dans le cadre de cette thèse sont détaillées et discutées dans les sections suivantes.

Partie 2. Expérience "flash 3D"

L'expérience mise en oeuvre dans ce travail, basée sur la méthode "Flash", est présentée en détail dans 2.3, en commençant par la procédure générale, suivie par une description de la configuration expérimental et des systèmes de mesure, pour finir par les post-traitements nécessaires. Le principe général de la technique flash 3D développée peut être qualifié de non conventionnel car assez éloigné de la technique originale. Dans cette variante, la surface de l'échantillon à caractériser est sujette à une excitation thermique localisée non uniforme à l'aide d'un laser CO_2. L'évolution de la température résultante de cette excitation, sur la face avant ou arrière, est

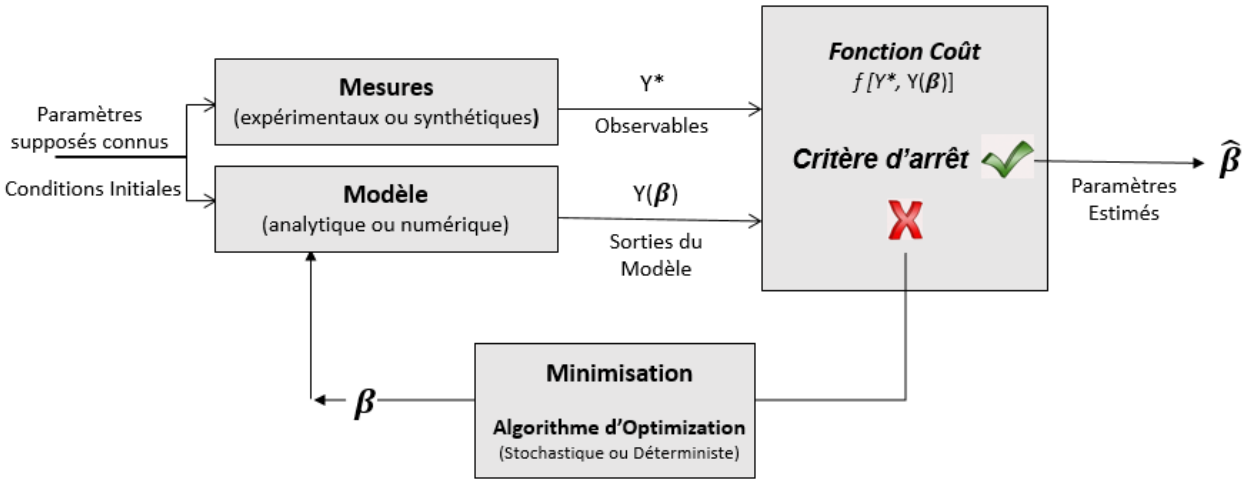

Figure 2.18 – Principe du problème inverse et description des étapes.

mesurée en continu à l'aide d'une caméra infrarouge. De ce fait cette méthode peu être qualifié de non intrusive, à la fois en termes d'excitation et de mesures. La figure 2.3a représente la configuration expérimentale et l'équipement utilisé pour générer les données expérimentales.

Partie 3. Modélisation directe du problème

La modélisation directe du problème inverse doit reproduire le plus fidèlement possible les conditions expérimentales en termes de phénomènes impliqués, de conditions initiales et de conditions aux limites. La formulation mathématique dérivée du modèle physique est basée sur la résolution de l'équation de la chaleur instationnaire et tridimensionnelle dans chaque couche constituant l'échantillon, supposée homogène et opaque et pouvant être isotrope ou orthotrope.

La résolution de ce type de problèmes inverses nécessitant un grand nombre de simulations, il est nécessaire de mettre en oeuvre des méthodes de résolution du système le plus rapide possible. Une résolution analytique a ainsi été envisagée, celle-ci est basée sur des transformations intégrales de type Fourier cosinus en espace et de Laplace en temps. Ces transformations conduisent à des harmoniques normalisées $\xi_{m,n}$ caractérisées par les modes spatiaux m et n correspondants aux direction x et y (dans le plan perpendiculaire à l'excitation).

Des essais précédemment réalisés montrent que l'analyse dans l'espace des harmoniques temporels est plus appropriée, à la fois en termes de précision (filtrage du bruit de mesure par sélection d'harmoniques) et de vitesse d'identification (compression spatiale d'images). Les solutions obtenues dans ce domaine correspondent aux harmoniques temporelles normalisées résultant d'une inversion numérique de Laplace appliquée à la solution analytique. Cette forme de sortie du modèle direct est qualifiée de "solution semi-analytique".

L'expression semi-analytique de l'évolution de la température en face avant et/ou arrière correspondant à l'expérience Flash et concernant chaque cas traité dans cette thèse (matériaux monocouches ou bicouches, à propriétés thermiques isotropes ou orthotropes) est développée et discutée dans les chapitres suivants. L'ensemble des hypothèses considérées pour chaque

cas sont également discuté dans 2.4.

Partie 4. Méthode d'estimation des paramètres

Après un aperçu des différentes techniques de minimisation, la technique utilisé dans ce travail est détaillée dans 2.5. Compte tenu de la nature des conditions aux limites, du nombre important de paramètres à estimer, ainsi que de la nature non linéaire du problème étudié, l'utilisation d'un algorithme de recherche globale est nécessaire. Les algorithmes déterministes (e.g. descente de gradient) se sont révélés moins adaptés que les algorithmes stochastiques. La minimisation de la fonction coût est réalisée au moyen d'une méthode stochastique plus adaptée à la recherche de minima globaux. Après plusieurs tests, l'optimisation par essaims particulaires (PSO) a été choisie pour son efficacité et sa relative accessibilité en terme de mise en oeuvre. Cependant, afin d'assurer une convergence vers la valeur optimale, correspondant au minimum local situé dans la région où se trouve le minimum global, l'algorithme PSO est été couplé à un algorithme déterministe de type gradient. Cette approche hybride permet de tirer partie des avantages que procure chacune de ces méthodes.

Partie 5. Analyse de sensibilités

L'analyse de sensibilité est un outil essentiel fréquemment utilisé dans la résolution de problèmes inverses pour i) s'assurer de la faisabilité de l'estimation, ii) déterminer les meilleures conditions pour effectuer l'identification, et iii) garantir le caractère non corrélé des paramètres. Cet outil doit être appliqué afin d'évaluer l'influence des paramètres à estimer ou connus a priori sur les sorties directes du modèle.

L'analyse des sensibilités vérifie également la faisabilité d'identifier simultanément plusieurs paramètres, dans le cas présent l'estimation simultanée des diffusivités thermiques du matériau (dans les trois directions principales). Plusieurs types de sensibilités peuvent être utilisés: ordinaires, réduites, normalisées ou adimensionnées, voir 2.6. Dans se travail le choix s'est porté sur les sensibilités réduites afin de comparer de manière appropriée l'influence des paramètres sur les sorties du modèle en homogénéisation à la fois les unités et les ordres de grandeur.

Partie 6. Sources d'erreurs et d'incertitudes

Cette section présente un aperçu de l'ensemble des erreurs pouvant affecter l'estimation, pour plus de détails se référer à 2.7. Les causes principales d'incertitudes et d'erreurs en fonction de l'étape de résolution du problème sont listés ci-dessous:

1. les incertitudes et erreurs liés au dispositif expérimental sont principalement due à la caméra infrarouge et concerne la mesure de température ainsi que la synchrionisation de la mesure avec l'excitation.

2. les erreurs de conversion entre les tensions mesurées qui sont converties en température par une loi d'étalonnage.

3. les erreurs liées au processus d'estimation telles que discutées précédemment.

Conlusion

Dans ce chapitre, le principe de l'estimation des propriétés thermiques est présenté, ainsi que chacune des étapes choisies. Ces étapes concernent:

- le dispositif expérimental nécessaire pour mesurer les propriétés connues a priori;
- la formulation mathématique du modèle physique, ainsi que sa résolution grâce au formalisme des quadripôles thermiques. La formulation du problème et sa résolution permet d'exprimer de manière analytique l'observable.
- l'algorithme d'optimisation hybride développé couplant un outil de minimisation stochastique de type PSO suivi d'une méthode déterministe de type gradient.
- les outils d'analyse, notamment l'analyse de sensibilités réduites.
- l'ensemble des sources d'erreurs liés au choix énoncés précédemment.

Chapter 3

Monolayer thermal characterization

***

Contents

3.1 Introduction

In this chapter, a direct and simultaneous estimation method of the main three dimensional thermal diffusivity tensor (a_x, a_y, a_z) of isotropic or orthotropic opaque materials, is presented. This method consists in coupling the non-intrusive and unique 3D flash experiment, presented in 2.3 within a transient nonlinear inverse heat transfer technique, presented in 2.2. A short and non-uniform excitation is applied on the surface of the sample using a CO_2 laser, while the front face temperature cartography is measured over time by an IR camera. The present work focuses on the development of a pseudo-analytical model, based on the thermal quadrupole approach [1], developed to predict the front (sometimes rear) face temperature evolution of orthotropic materials exposed to a Dirac type imposed flux and subject to natural cooling.

The inverse problem investigated in the present study is based on the minimization of the least-squares criterion between the outputs of a 3D model and experimental measurements. In order to properly estimate the thermal diffusivities, parameters related to the thermal excitation, in terms of shape and intensity, should also be estimated. Considering the large number of parameters to estimate, as well as the non-linear nature of the problem, a hybrid optimization algorithm combining both a stochastic and a deterministic method is applied 2.5.4.3. The identification method proposed in this work, named DSEH (Direct and Simultaneous Estimation using Harmonics), is validated using an isotropic opaque polyamide material of known properties. Finally, the method is used on an orthotropic carbon fiber reinforced polymer composite material (CFRP), commonly used in industries thanks to its thermal and mechanical characteristics (see 1.2). Moreover, the identification results are compared with results from well-established methods as ENH [78, 81] and MSEH [74], which are described in this chapter. The parameters identification is completed by a sensitivity analysis in order to demonstrate the feasibility of the simultaneous estimation, and evaluate the method in terms of robustness and accuracy.

The second part of this chapter is dedicated to the improvement of the identification method in terms of time reduction, accuracy improvement, and experiment design optimization (e.g. excitation face, pulse duration). The diffusivities identification of a reference CFRP sample, already experimentally characterized in a previous section 3.4.2, is performed with the direct model by means of a parametric excitation whose shape is defined thanks to actual experimental data.

Then, the direct model is independently solved using a finite element code, FlexPDE. This numerical resolution is compared with the analytical resolution used in the identification procedure, in terms of precision and calculation time. The present numerical tool is found to be a good candidate to generate pseudo measurements and compare the different experimental set up strategies. The validated overall identification method is then numerically applied on a fictitious orthotropic CFRP sample, for a range of experimental set up corresponding to the combination of different energy intensity and time duration of the excitation. The estimation

results as well as the sensitivities are studied for both measurement face strategies. A set of most realistic experimental set up is selected for investigation to find the best compromise between i) a signal intensity level that should be high enough to be measured and ii) a moderate temperature elevation in order to keep the thermophysical parameters relatively constant.

Finally, alternative strategies allowing the additional estimation of the specific heat capacity or the thermal diffusivities identification without any a priori knowledge about the specific heat capacity, are presented.

3.2 Literature review on monolayers thermal characterization

Among the methods dedicated to the thermal characterization of monolayer materials, the flash method, proposed by Parker [2], is now one of the standard techniques for measuring solid thermal properties.

This transient approach was originally based on a homogeneous short duration light pulse with a local measurement of the temperature at the back face of the sample. The in-depth thermal diffusivity is determined by means of a one dimensional conductive heat transfer model. This technique has been widely improved over the past 50 years. Those improvements are discussed hereafter, according to the geometry of the problem.

The extension of this 1D approach into 2D, was first motivated to take into account non uniform excitation [113], then it was improved by Amazouz [114] and applied by Degiovanni [71], Maillet [237] and Lachi [115] in order to estimate the in-plane diffusivity of anisotropic solid materials. This technique has also been applied to the estimation of both in-plane and in-depth diffusivities of anisotropic materials, or specifically orthotropic materials [145], i.e. having principle diffusivities directions aligned with the orthogonal Cartesian coordinate system. The flash method is then used in cylindrical coordinates to separately estimate radial and axial diffusivities [72, 122].

Furthermore, the extension of some contact and non-contact methods into 3D identification methods leads to some achievements, notably the compatibility between the model and the experimental conditions, which is usually a difficult task. The pioneer works conducted by Sawaf [238] are an illustration of this constraint. The attempt to estimate each of the three main diffusivities of a sample by subjecting a constant heat flux on one face, while keeping other faces insulated, is difficult to achieve experimentally. The compromise between the experimental accuracy and the capability of the model has to be consistent. The consideration of new boundary conditions, with the aim of a better environmental conditions control of the experiments, combined with the increase in the calculation capacity, led to the emergence of new estimation methods based on numerical simulations. Several methods that solve the 3D heat conduction problem using the finite difference or finite volume methods [239, 240] the finite element method [118, 241, 242] the boundary element method [243, 244] and the singular boundary method [245], have proven to be highly time consuming.

In this context, the development of estimation methods, whether in 2 or 3-D coordinates, based on the analytical resolution of heat transfer problem is still relevant. Flash based meth-

ods, such as the Estimation using Ratio of harmonics (ERH) proposed by Philippi [73] then developed by Remy [76, 149], in addition to the Estimation using Normalization of harmonics (ENH) [78, 80, 81], has been developed and successfully used for the identification of the in-plane diffusivities (i.e. a_x and a_y). Another method based on the resolution of the conductive heat transfer by means of Fourier transform is known as the Multiple Steps Estimation using harmonics (MSEH) [74]. This technique conducts a step by step estimation starting by the estimation of the in-depth diffusivity from the average field, which is the most sensitive parameter to environmental noise. The estimated in-depth diffusivity is then used to identify the transverse diffusivities (a_x and a_y). Although giving relevant results, this method may experience a low accuracy due to its sequential nature. The multi-step identification strategy is also used by other authors to estimate the orthotropic material diffusivity tensor, for instance Rodiet [246] who uses the average temperatures in the in-plane directions or Perez [247] using different phase lags at different or same periodic excitation frequencies. The above discussion has been conducted from the direct model point of view and its exploitation via the identification procedure. One should notice that some works are purely theoretical, others are based on experiments that rely on intrusive measurements (e.g. thermocouples) [122, 241, 248], and/or intrusive heating source [63, 239–241, 248]. Also, the experimental protocol may be sophisticated, some authors have developed methods based on two experiments (e.g. sample rotation) or on the duplication of the set of devices (e.g. two series of laser and IR camera [118, 242].

The main feature of this work relies on the combination of the direct and simultaneous estimation of the 3 principle components of the diffusivity tensor of orthotropic material using an analytical 3D transient model and a unique and non-intrusive experiment in terms of both excitation and measurements. The direct model, relying on the Fourier transform that allows the exploitation of a large amount of spatial data, is the key element of the estimation method referred in this work as “Direct and Simultaneous Estimation using Harmonics” (DSEH) [111, 249]. The importance of direct identification method was first mentioned by Ruffio in a comparative study [82].

3.3 Resolution of the inverse heat conduction problem - Thermal identification problem

In this section, the various stages involved in the inverse problem resolution as part of the overall identification strategy, whose principles are introduced in previous chapter 2.2, are detailed and discussed hereafter.

3.3.1 Physical configuration and mathematical model

The main objective being the determination of the 3 thermal diffusivity components of orthotropic materials, the configuration to handle has to be tridimensional. As already mentioned, the model must be consistent with the flash experiment investigated in this problem (see 2.3) and must reproduce all experimental conditions meet the experimental requirements.

To recall, the procedure consists in exposing samples of such material to an impulse type excitation, produced by a CO_2 laser, and localized on the front face ($z = 0$). This non uniform thermal excitation generates a local temperature elevation that diffuses into the sample. The elevation must be moderate in order to keep the thermophysical properties as constant as possible, and independent on the temperature. The resultant temporal and spatial evolution of the temperature inside the opaque and homogeneous material is described by a partial differential equation, completed by equations describing the initial and boundaries conditions. The front and rear faces are exposed to convection and radiation losses, described by a linearized global heat exchange coefficients h_f at the front side and h_b at the back side. Nonetheless, the four other lateral faces are assumed to be thermally insulated, this condition is discussed later on. The set of differential partial Eqs. 3.1 describing the system is given hereafter as well as in Fig. 3.1.

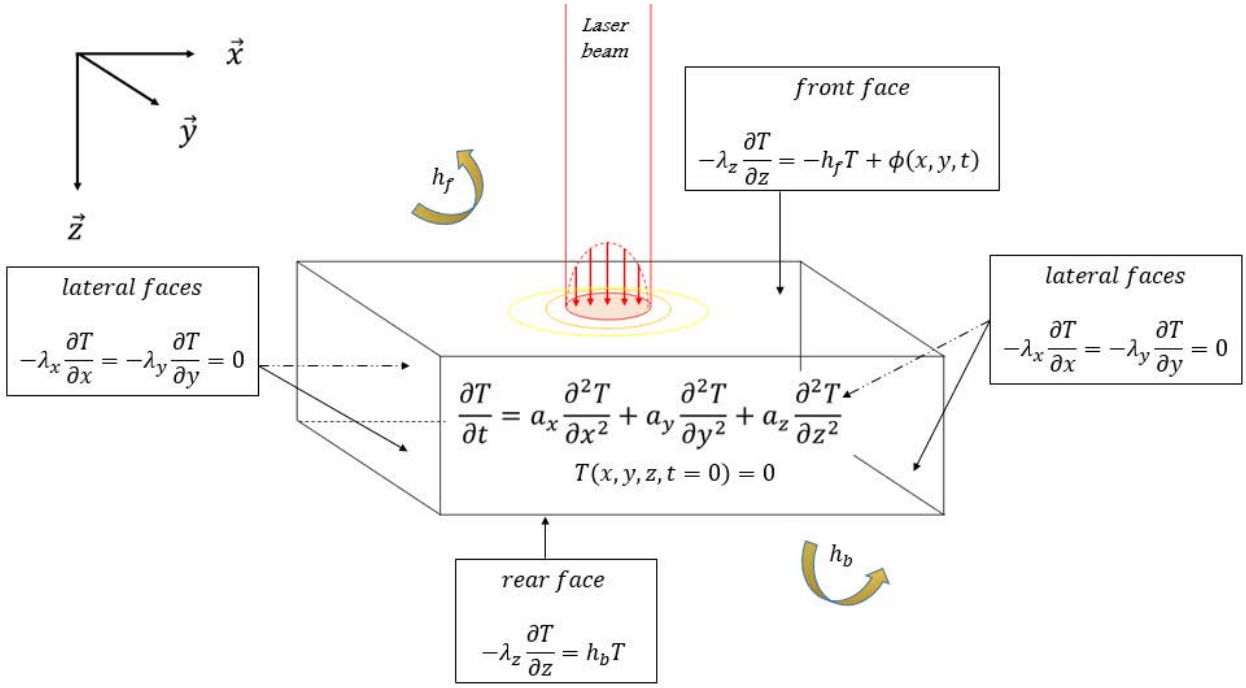

Figure 3.1 – Physical configuration, mathematical modelling and boundary conditions in the real domain.

Please notice that the system of Eqs. 3.1 depends on the relative temperature T, i.e. the difference between the local temperature and the initial temperature $T(t = 0)$. Before each experiment, the sample is supposed to be at thermal equilibrium with the environment, i.e. the initial temperature is considered to be equal to the temperature of the surrounding environment.

$$\begin{cases} \dfrac{\partial T}{\partial t} & = a_x \cdot \dfrac{\partial^2 T}{\partial x^2} + a_y \cdot \dfrac{\partial^2 T}{\partial y^2} + a_z \cdot \dfrac{\partial^2 T}{\partial z^2} \text{ for } z \in [0, l_z],\ t > 0 \\ -\lambda_x \cdot \dfrac{\partial T}{\partial x} & = 0 \text{ for } x = 0 \text{ and } x = l_x,\ t > 0 \\ -\lambda_y \cdot \dfrac{\partial T}{\partial y} & = 0 \text{ for } y = 0 \text{ and } y = l_y,\ t > 0 \\ -\lambda_z \cdot \dfrac{\partial T}{\partial z} & = -h_f \cdot T + \phi^{ex}_{x,y}(t) \text{ for } z = 0,\ t > 0 \\ -\lambda_z \cdot \dfrac{\partial T}{\partial z} & = h_b \cdot T \text{ for } z = l_z,\ t > 0 \\ T(x,y,z) & = 0 \text{ for } t = 0 \end{cases} \tag{3.1}$$

The parameters identification relies on the post-treatment of the temperature evolution at the sample front or rear face. This treatment consists in an integral transformation, applied to both experimental measurements and direct model outputs, in Fourier cosine spaces. Fourier transformations result in the appearance of harmonics, $\theta_{m,n}$, whose main advantages are a fast treatment of the direct simulation and a capacity of noise filtering by selection of the relevant harmonics, see 2.4.1. Given that the harmonics of low spatial frequencies hold the largest quantity of information related to diffusivities, the exploited harmonics in this study will be the first $M \times N \leq 6$, even modes. These harmonics (Fourier-Laplace domain) are defined as:

$$\theta_{m,n}(z,p) = \int_0^{\infty} \int_0^{l_y} \int_0^{l_x} T(x,y,z,t) \cdot X_m(x) \cdot Y_n(y) \cdot e^{-pt} \cdot dx \cdot dy \cdot dt \tag{3.2}$$

where $X_m(x) = cos(m \cdot \pi \cdot \dfrac{x}{l_x})$ and $Y_n(y) = cos(n \cdot \pi \cdot \dfrac{y}{l_y})$ are the basis function defining the Fourier-Cosine space, with l_x and l_y referring to the exploitation window (frame) size. Those functions have been chosen according to the boundary conditions considered in this study.

As mentioned in 2.4.1, the odd harmonics (i.e. where m or n are odd), are not taken into account since they are quasi-null (three order of magnitude lower than the even harmonics values) due to the symmetric characteristic of the excitation. Thus, the information is concentrated only on even harmonics which are then considered for the identification procedure. Following the formalism of the thermal quadrupoles method applied on the system, the relative front-face or rear-face temperature evolution, is given by solving the system of equations shown in Fig. 3.2.

The value of this overall coefficient is assumed to be equal on both sides, $h_f = h_b = h$ and represented by the constant and uniform coefficient h. As a first guess, this value is taken to be $h = 10\ W \cdot m^{-2} \cdot K^{-1}$, which is a common value for such environmental conditions (this value will be discussed later on through the sensitivity analysis).

The system of equations in Fig. 3.2 lead to:

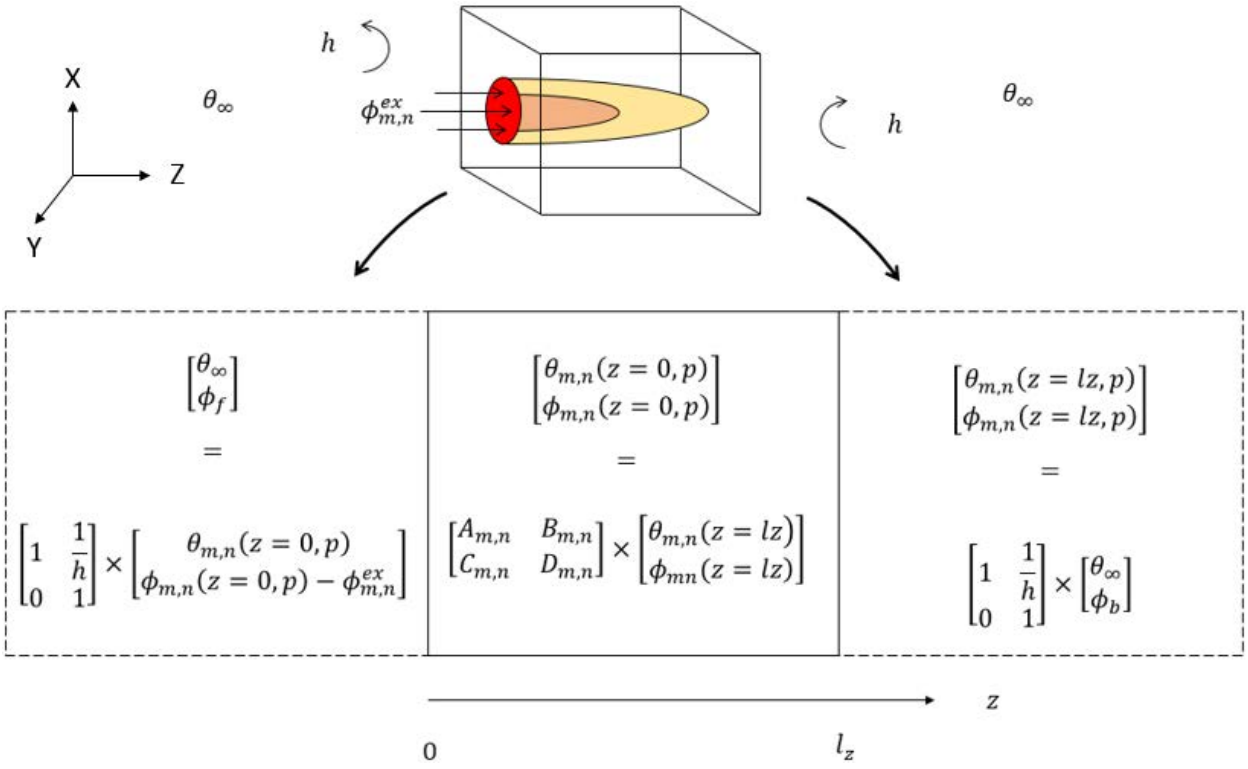

Figure 3.2 – Physical configuration, mathematical modelling and boundary conditions in the xy-Fourier and t-Laplace domains.

$$\begin{pmatrix}\theta_{m,n}(z=0,p)\\ \phi^{ex}_{m,n}(p)-h\cdot\theta_{m,n}(z=0,p)\end{pmatrix}=\begin{pmatrix}A_{m,n}(p) & B_{m,n}(p)\\ C_{m,n}(p) & D_{m,n}(p)\end{pmatrix}\times\begin{pmatrix}\theta_{m,n}(z=l_z,p)\\ h\cdot\theta_{m,n}(z=l_z,p)\end{pmatrix} \tag{3.3}$$

The temperature of the environment being the same on both sides of the sample, the relative temperature in the Fourier-Laplace domain is $\theta_\infty = 0$. The conductive heat behavior is driven by the quadrupole terms defined as [1] :

$$\begin{pmatrix}A_{m,n}(p) & B_{m,n}(p)\\ C_{m,n}(p) & D_{m,n}(p)\end{pmatrix}=\begin{pmatrix}\cosh(l_z\cdot K_{m,n}(p)) & \frac{\sinh(l_z\cdot K_{m,n}(p))}{\rho\cdot C\cdot a_z\cdot K_{m,n}(p)}\\ \rho\cdot C\cdot a_z\cdot K_{m,n}(p)\cdot\sinh(l_z\cdot K_{m,n}(p)) & \cosh(l_z\cdot K_{m,n}(p))\end{pmatrix} \tag{3.4}$$

where $K_{mn,i}(p)=\sqrt{\frac{p}{a_z}+\alpha_m^2\cdot\frac{a_x}{a_z}+\beta_n^2\cdot\frac{a_y}{a_z}}$, $\alpha_m=\frac{m\cdot\pi}{l_x}$ and $\beta_n=\frac{n\cdot\pi}{l_y}$

ϕ^{ex} designates the excitation that can be decomposed into the product of its magnitude Q and two functions: a function $F(x,y)$ representing the space shape and a function $u(t)$ characterizing the time evolution. Thus, $\phi^{ex}_{x,y}(t)=Q\cdot F(x,y)\cdot u(t)$.

This expression projected into the Laplace and Fourier domains gives: $\phi^{ex}_{m,n}(p)=Q\cdot F_{m,n}\cdot u(p)$ with $F_{m,n}=\int_0^{ly}\int_0^{lx}F(x,y)\cdot X_m(x)\cdot Y_n(y)\ \cdot dx\cdot dy$ and $u(p)=1$ for an impulse of Dirac

type. The dimensionless parameters $F_{m,n}$ and $u(p)$ represents the shape and the time factors, respectively.

In order to get comparable quantities having the unit of Kelvin (K), the model outputs and measurements signals are both normalized by $l_x \cdot l_y$:

$$\xi_{m,n}(z=0,t) = \frac{\theta_{m,n}(z=0,t)}{l_x \cdot l_y} \tag{3.5}$$

Following Eqs. 3.3 and 3.4, the rear face normalized harmonics $\xi_{m,n}(z=l_z,p)$ is calculated as following:

$$\xi_{m,n}(z=l_z,p) = \frac{\dfrac{Q \cdot F_{m,n} \cdot u(p))}{l_x \cdot l_y}}{\lambda_z \cdot K_{m,n} \cdot \sinh(l_z \cdot K_{m,n}) + 2 \cdot \cosh(l_z \cdot K_{m,n}) \cdot h + \dfrac{\sinh(l_z \cdot K_{m,n})}{\lambda_z \cdot K_{m,n}} \cdot h^2} \tag{3.6}$$

Front face harmonics in the Laplace domain yields to:

$$\xi_{m,n}(z=0,p) = \xi_{m,n}(z=l_z,p) \cdot (A_{m,n}(p) + B_{m,n}(p) \cdot h) = \frac{\dfrac{Q \cdot F_{m,n} \cdot u(p))}{l_x \times l_y} \times (\cosh(l_z \cdot K_{m,n}) + \dfrac{\sinh(l_z \cdot K_{m,n})}{\lambda_z \cdot K_{m,n}} \cdot h)}{\lambda_z \cdot K_{m,n} \cdot \sinh(l_z \cdot K_{m,n}) + 2 \cdot \cosh(l_z \cdot K_{m,n}) \cdot h + \dfrac{\sinh(l_z \cdot K_{m,n})}{\lambda_z \cdot K_{m,n}} \cdot h^2} \tag{3.7}$$

Calculation time obtained for one harmonic for a p vector size of 1200 (i.e. about $24s$ of physical time in the present work) is less than $10^{-3}s$. The approximate number of harmonics used for identification is 16, which make the typical direct calculation time used for the identification about $t_{CPU} \sim 10^{-2}s$. The overall computational time is compatible with a stochastic identification approach.

As already discussed in 2.4.2, identification is performed in the transformed space (i.e. using harmonics) instead of the physical space. The benefits of such strategy in such complex estimation problem has already been argued previously. For those reasons, the experimental front face temperature evolution is also transformed using a Fourier-Fourier space projection.

One should notice that the comparison between the model and the experimental outputs is performed in the real time domain. Thus, a Laplace inversion is applied to the model output, leading to a "pseudo-analytical" model. A fast De-Hoog inversion technique [189], found to be well adapted for this application compared to others (see 2.4.3), is applied to the model outputs. This procedure converts $\xi_{m,n}(z=0,p)$ into $\xi^{mod}_{m,n}(z=0,t)$, directly comparable to the experimental harmonics $\xi^{exp}_{m,n}(z=0,t)$.

Despite this numerical inversion, the direct pseudo-analytical model is still quasi instantaneous ($t_{CPU} \sim 10^{-2}s$, for one harmonic). The calculation time is many order of magnitude lower than those found in the literature whose estimations are based on numerical simulations.

Linearization of the heat losses coefficient (overall heat transfer coefficient)

In practice, the heat lost by natural convection with the environment, taking place at the sample front or rear face, can be simply expressed by $\varphi_{conv} = h_{conv} \cdot (T - T_\infty)$. Radiation losses can be also linearized until the temperature evolution is kept moderate. The radiation losses are then represented by a radiation heat transfer coefficient h_{rad}. The heat losses by radiation is then linearized as follows: $\varphi_{rad} = \varepsilon \cdot \sigma \cdot (T^4 - T_\infty^4) = \varepsilon \cdot \sigma \cdot (T^2 + T_\infty^2) \cdot (T + T_\infty) \cdot (T - T_\infty) = h_{rad} \cdot (T - T_\infty)$. In this work the sample emissivity $\varepsilon = 1$ is considered constant, since the material is coated with a high temperature black paint. Therefore the overall heat losses with the environment can be linearized as following: $\varphi_{loss} = \varphi_{conv} + \varphi_{rad} = h \cdot (T - T_\infty)$ with $h = h_{conv} + h_{rad}$. The value of this overall coefficient is assumed to be equal on both sides. As a first guess, this value is taken to be $h = 10\ W \cdot m^{-2} \cdot K^{-1}$, which is commonly admit value for such environmental conditions.

Validation with another solution form

For the same system configuration, another form of pseudo-analytical model, in which harmonics are already in the time domain, can be also found in literature [110].

$$\xi(\alpha_m, \beta_n, z, t) = \xi_{m,n}(z, t) = \frac{Q \cdot F_{m,n}}{\rho \cdot C \cdot l_x \cdot l_y \cdot l_z} \left[2 \sum_{k=1}^{\infty} \frac{u_k \cdot Z_k(z)}{u_k^2 + H^2 + 2H} e^{-\tau_z u_k^2 t} \right] e^{-\left(\tau_x (m\pi)^2 + \tau_y (n\pi)^2 \right) t} \tag{3.8}$$

with $\tau_x = \frac{a_x}{l_x^2}$, $\tau_y = \frac{a_y}{l_y^2}$ and $\tau_z = \frac{a_z}{l_z^2}$. Adding to that $H = \frac{h \cdot L_z}{\lambda_z}$ is the Biot number, and $Z_k(z) = u_k \cdot cos(u_k \cdot \frac{z}{l_z}) + H \cdot sin(u_k \cdot \frac{z}{l_z})$.

$F_{m,n}$ are the excitation shape coefficients, u_k are the positive solutions of the transcendent equation $[2H \cdot u \cdot cos(u) = sin(u) \cdot (u^2 - H^2)]$. Therefore, the front or rear face harmonics evolutions are calculated as following:

$$\xi_{m,n}(z = 0 \text{ or } z = l_z, t) = \frac{Q \cdot F_{m,n}}{\rho \cdot C \cdot l_x \cdot l_y \cdot l_z} \left[2 \sum_{k=1}^{\infty} \frac{u_k \cdot Z_k(z = 0 \text{ or } z = l_z)}{u_k^2 + H^2 + 2H} e^{-\tau_z u_k^2 t} \right] e^{-\left(\tau_x (m\pi)^2 + \tau_y (n\pi)^2 \right) t} \tag{3.9}$$

For same input parameters, i.e. same thermophysical properties $(a_x, a_y, a_z, \rho \cdot C)$ and geometrical dimensions, the analytical model outputs are compared to the results obtained with the three-dimensional quadrupoles semi-analytical model.

For brevity and illustrative reasons, only the front and rear face normalized harmonic with $m = n = 2$ are plotted in Fig. 3.3b. This spatial mode is generally considered as the reference [82] due to its low frequency and its sensitivity to non-uniform fluctuations that could occur simultaneously along both X and Y directions.

The great coincidence between the model presented in 3.9 and referred by "model" in Figs. 3.3, and the quadrupoles model (Eqs. 3.7 and 3.6) investigated in this work and referred by

"quad" in the same figure validates the consistency between both models. Both models are evaluated for the same set of input parameters: having an orthotropic material with following thermal properties and geometrical dimensions: $[a_x, a_y, a_z] = [0.75, 7, 0.6]\ mm^2 \cdot s^{-1}, \rho C = 2 \times 10^6\ J \cdot K^{-1} \cdot m^{-3}, l_x = l_y = 45\ mm, l_z = 7\ mm, h = 10\ W \cdot m^{-2} \cdot K^{-1}$. The amount of energy absorbed at the surface of the material is assumed to be Q= 0.4J, coherent with following experimental applications. Regarding the model represented in the Eq. 3.9, the sum is truncated at 1000 with k = [1 1000].

The mean fields normalized harmonics $\xi_{0,0}$ and the harmonics $\xi_{2,2}(t)$ are plotted in Figs. 3.3 for both models, and the obvious agreements verify the consistency between these models.

However, the three-dimensional quadrupoles formalism was proved, using simulated measurements to be more adequate and convenient for the direct estimation, by giving a better convergence with a lower calculation time, compared to the other one described in Eq. 3.9.

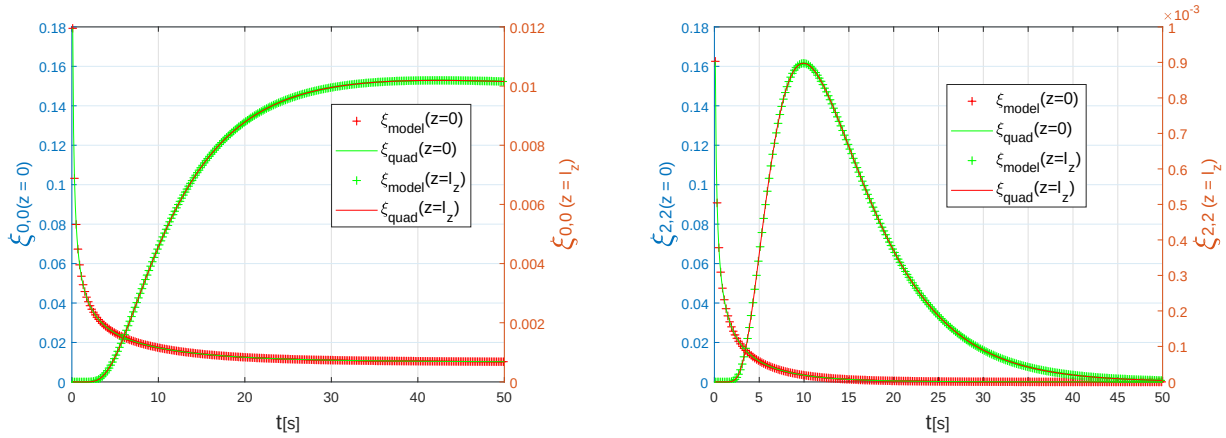

(a) m=0, n=0

(b) m=2, n=2

Figure 3.3 – Front and rear face normalized harmonics for both models: "model" representing the direct correlation found in the literature and presented in 3.9, and "quad" representing the one developed using quadrupoles formalism (Eqs. 3.7 and 3.6).

3.3.2 Identification strategy

In this part, the inverse strategy and the estimation procedure leading to the parameters identification are detailed. It involves three main elements constituting the concept of an inverse problem: i) the vector of parameters to identify, ii) the cost function and iii) the optimization algorithm. The buildup method is validated using synthetic data. This strategy, literally known as "Inverse crime", allows to validate the consistency of the optimization method by retrieving the parameters used to generate the data. This strategy can by no means validate the consistency of the direct model used in the overall estimation procedure. The results of this theoretical exercise also allows to set the PSO algorithm.

3.3.2.1 Parameters vector

The inverse problem treated here is rather complex because, besides the estimation of the thermal diffusivities tensor, the parameters related to the excitation has to be estimated due to their influence on the system response. The parameters vector to identify is then $\beta = [a_x, a_y, a_z, R_{0,0}, R_{0,2}, \cdots, R_{m,n}, \cdots, R_{M,N}]$ with $R_{m,n} = Q \cdot F_{m,n}$ corresponding to the heat flux distribution in the Fourier modes space. In this way, the size of the parameters vector that should be estimated depends on the number of modes chosen to describe the excitation. The number of even modes depends on both, the shape of the laser beam and the minimum number of modes required to ensure a proper direct simulation. For symmetrical reason, M and N should be chosen equal. The number of parameters to be estimated is then equal to $3 + (\frac{M}{2} + 1)^2$ when considering only even modes, which is the case here.

3.3.2.2 Cost function

The cost function, also known as objective function, and previously defined and presented in 2.5.2, is the quadratic deviation between the measured signal and the signal predicted by the direct physical model. Thus, the estimator dedicated for the minimization of the cost function, is written as follows:

$$\hat{\beta} = \min_{\beta} \sqrt{\sum_{m=0}^{M} \sum_{n=0}^{N} [\xi_{m,n}^{mod}(\beta, t) - \xi_{m,n}^{exp}(t)]^2} \tag{3.10}$$

In this method, the considered harmonics are equally weighted. The first term of Eq. 3.10, $\xi_{m,n}(\beta, t)$, corresponds to the temporal normalized harmonics, achieved by the Laplace inversion which is applied to the direct model outputs (Eqs. 3.6 and 3.7), $\xi_{m,n}(p)$. The second term, $\xi_{m,n}^{exp}(t)$, represents the observables issued from front face temperature evolution measurement, projected in Fourier Cosine space.

3.3.2.3 Optimization algorithm

In addition to the general parameters presented in the algorithm section in previous chapter 2.5.4.3, the PSO specifications and stopping criteria selected for the estimation procedure are represented in Table 3.1. The stopping criterion is a combination of several conditions. The iterative minimization will be stopped if the maximum number of iterations is achieved, or if the number of stall iterations without any significant change and with a best value of the cost function less than the tolerance value, exceeds the maximum stall iterations.

The evolution of the PSO particles and their convergence into the global minimum region during the estimation process, especially in the first part of the cost function minimization using the stochastic search, are illustrated for the CFRP identification case in Figs 3.4.

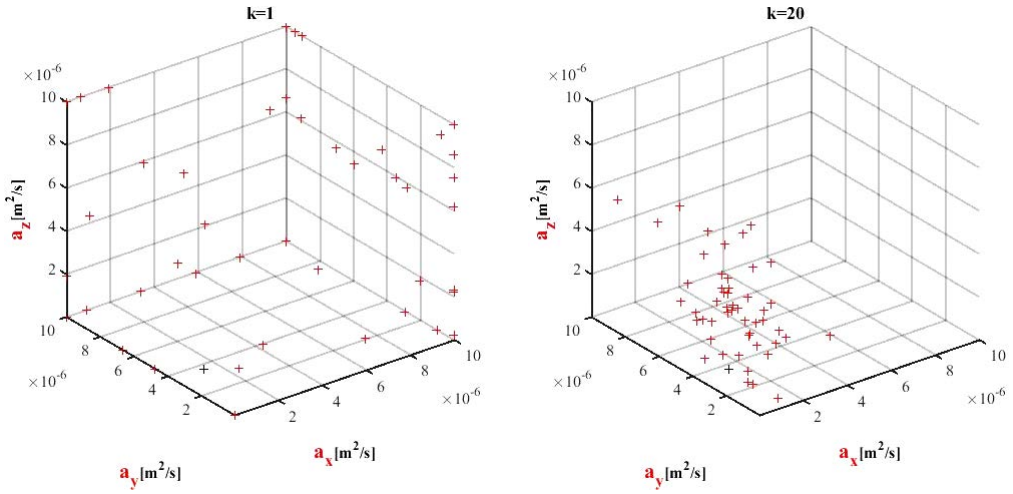

(a) 1^{st} iteration (b) 20^{th} iteration

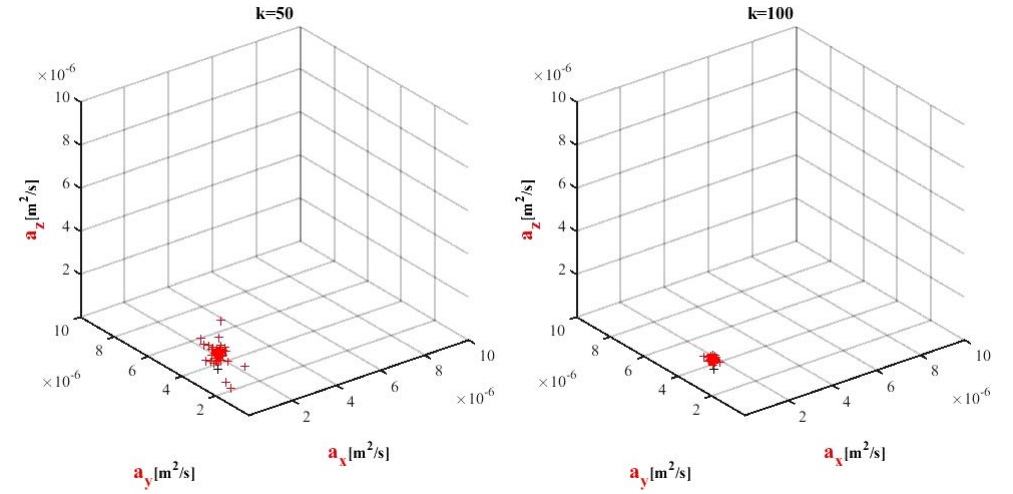

(c) 50^{th} iteration (d) 100^{th} iteration

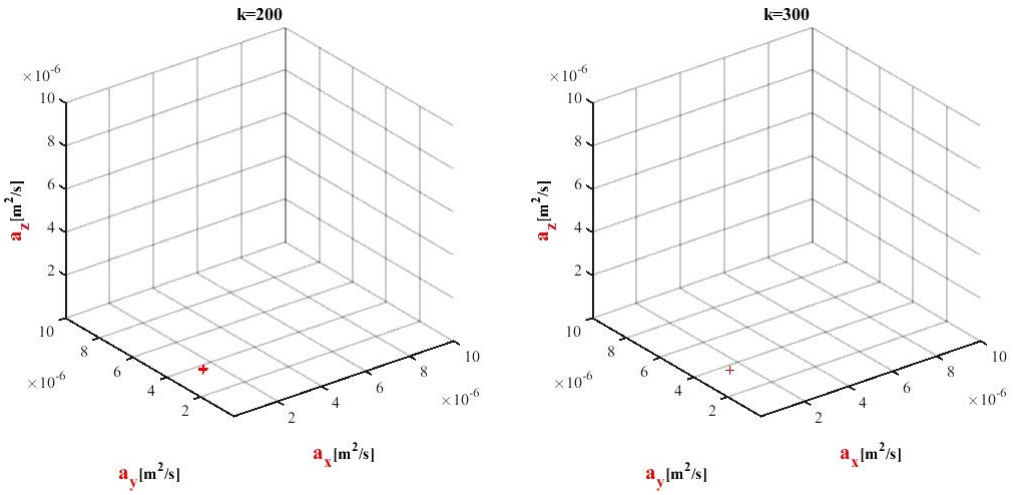

(e) 200^{th} iteration (f) 300^{th} iteration

Figure 3.4 – PSO particles evolution during the optimization process, applied for the characterization of the CFRP material.

Conditions	Values
Bounds of $\overline{\overline{a}}$	$[10^{-9};10^{-4}]\ m^2 \cdot s^{-1}$
Bounds of $R_{m,n}$	$[-100;+100]\ J$
Number of PSO particles	20
Maximum iterations	500× size of β
Maximum stop (stall) iterations	20
Tolerance value	10^{-8}
Maximum time	$+\infty$
Maximum stall time	$+\infty$
Minimum objective value	$-\infty$

Table 3.1 – PSO specifications, and stopping criteria selected for the estimation procedure.

3.3.3 Experimental procedure

The investigated experiment in this work relies on a front face flash method. The corresponding experimental setup, composed of a CO_2 laser that generates the localized thermal excitation and an IR camera used to record the temperature evolution on the exposed face (front face), is already detailed in terms of procedure and tools, in 2.3.1. Figs. 2.3 (p. 47) represent the experimental setup and the equipment investigated to generate the experimental data.

To recall, the present experiment corresponds to an unconventional laser flash technique, since several practical features are different from the original one [2]. In this work, the thermal excitation is locally and non-uniformly imposed on one of the sample face by a CO_2 laser. The excitation duration is $10ms$, which is considered instantaneous from the simulation point of view. The thermal response of the sample is recorded at the front face of the sample during $\approx 30s$ by an IR camera at a frequency of 60 Hz.

Some experimental devices are also used for the estimation of properties that should be known a priori, i.e. before the estimation. A digital micrometer is used to measure the layers thicknesses, an analytical balance sensitive to 0.01 mg is used to estimate the density, and a Calvet Calorimeter (C80 by Setaram©) is used to estimate the heat capacity of the samples.

3.3.4 Images processing and exploitation

Regarding the principles of raw data treatments and IR images exploitation, some generalities are already discussed in 2.3.4. The developed procedure lead to the experimental data $\xi_{m,n}^{exp}(t)$

used in Eq. 3.10 to perform the estimation.

As shown in Figs. 3.5, the choice of the exploitation frame, illustrated by the colored frame, is of prime importance. A compromise is required between a domain large enough to respect the lateral boundary conditions related to the direct model and a surface area restricted to the zone of interest to avoid the degradation of the data by dilution of the signal into the background signal.

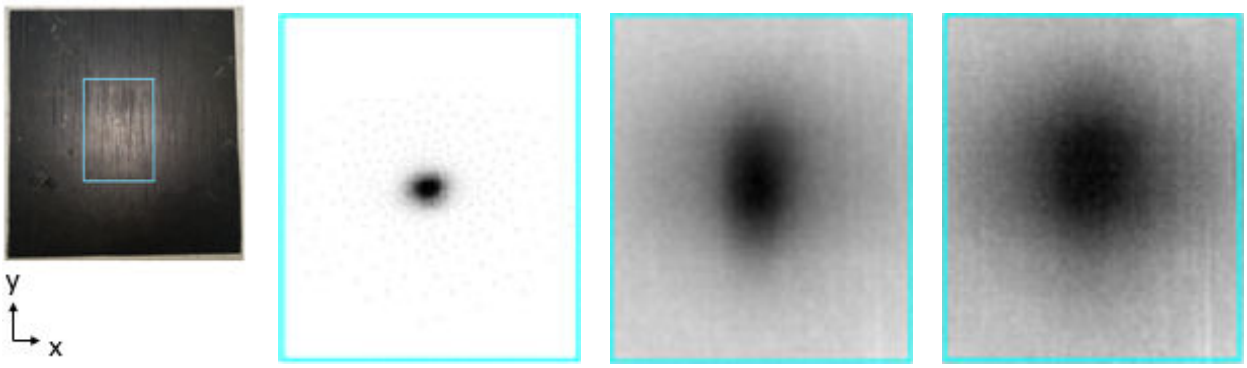

(a) Carbon fiber composite sample (b) $t = t_0 + 0.08s$ (c) $t = t_0 + 8s$ (d) $t = t_{end}$

Figure 3.5 – Raw pictures cropping ($l_x \times l_y = 39.0 \times 45.0\ mm$) at different time after the laser beam impact at t_0, on the surface of CFRP sample

Regarding the boundary conditions, Fig. 3.6 shows the experimental temperature elevation on a composite front surface, just after the excitation and at the time t_{end}, corresponding to the exploitation limit of experimental data.

An image processing technique as well as a raw data treatment are performed in order to obtain the exploitable experimental measurements $\xi^{exp}_{m,n}(z = 0, t)$ dedicated to the identification section.

The thermal exploitation area, or size of the frames ($l_x \cdot l_y$) is chosen in such a way that:

- The heat does not reach the edges of the frame in order to respect the isolated lateral boundary condition ;
- The frame size should not be too large, in order to have significant harmonics magnitudes for the estimation. Increasing the size of the frame will reduce the weight of the signal at the center of the frame and dilute the information within the noise of the IR camera;
- The frame should be centered regarding the laser axis. Thus, the excitation will be symetric and most of the information will be carried by the even harmonics (m and n even). In turn, odd harmonics will contain negligible information.

Adding to that, the size of the measured signals that will be involved in the estimation process, is defined by the camera acquisition frequency and the size of the time vector t over which the temperature evolution at the surface of the material is measured. Those settings dictate the number of images to process, and so the estimation duration time.

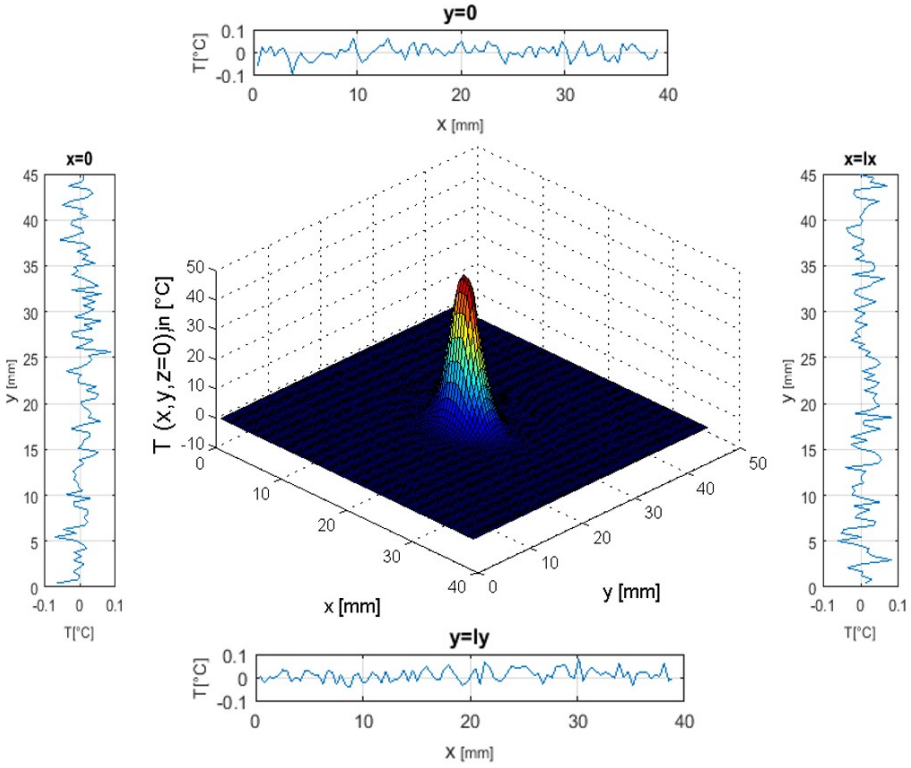

(a) $t = t_0$

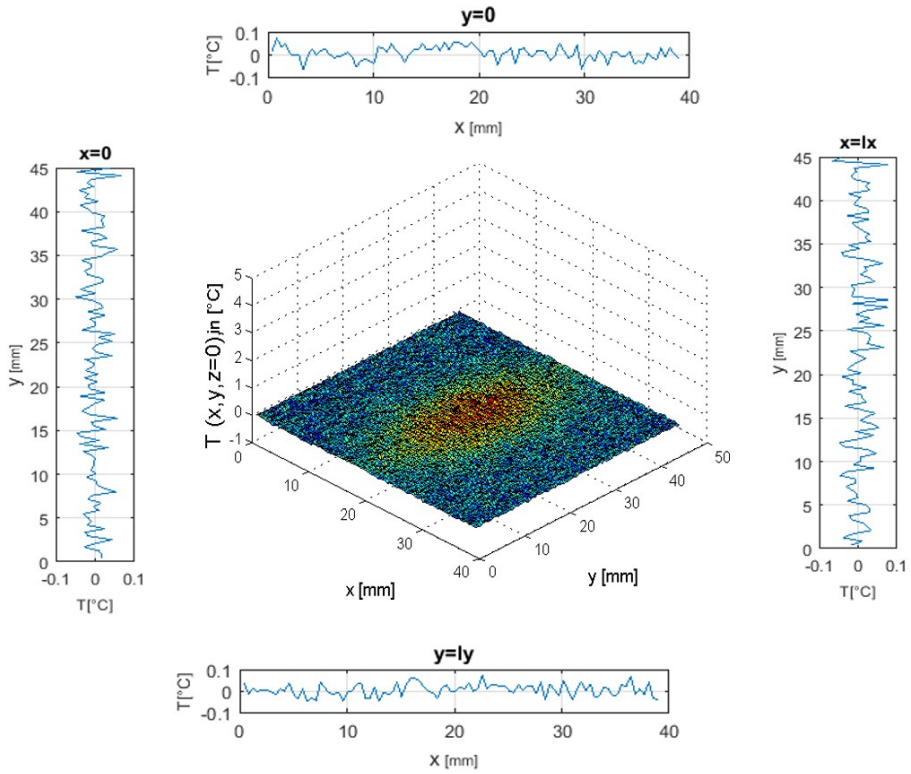

(b) t_{end}

Figure 3.6 – Experimental temperature fields on the exposed surface ($z = 0$), and temperature profiles at the boundaries ($x = 0$, $x = l_x$, $y = 0$ and $y = l_y$), just after the excitation and at the exploitation limit, for the orthotropic CFRP studied material.

The choice of these parameters should also respect the compromise between some experimental hypothesis and limitations:

- As already mentioned, the signal should not reach the frame edges over the time t .
- The measurements should be sensitive to the parameters to estimate during the overall acquisition time.
- The signal measured over the time t must have sufficient intensity, in such a way to have an acceptable range of signal/noise ratio (≥ 10).
- The acquisition frequency is limited by the maximum attainable frequency of the IR camera used in this work.

For those reasons, the acquisition time is limited. Adding to that, the laser is controlled to impose a pulse of moderate energy in order to avoid an overheat of the sample. The latter can deteriorate the sample surface or contradict the assumption that considers the properties (e.g. a_x, a_y, a_z but also ρ or C) constant during the measurement duration time and independent on the temperature evolution.

3.4 Experimental applications and estimation results

In this section, the overall proposed identification method is experimentally validated on a reference isotropic polyamide sample (PA) whose properties are well-known, and then applied on an orthotropic sample of carbon fibers composite (CFRP). The photos of these samples are shown in Fig. 3.7.

(a) PA (b) CFRP

Figure 3.7 – Samples of tested materials.

3.4.1 Isotropic material

Due to the difficulty of assessing the performance of the method on a reference orthotropic material of perfectly known properties, the validation is conducted on an isotropic polymer

Unknown values	DSEH (present study)	ENH	Rel. diff	MSEH	Rel. diff
a_x [mm^2.s^{-1}]	0.163 ($\sigma = 5.4 \cdot 10^{-4}$, 0.340%)	0.165 ($\sigma = 3.91 \cdot 10^{-3}$, 2.37%)	1%	-	-
a_y [mm^2.s^{-1}]	0.165 ($\sigma = 3.6 \cdot 10^{-4}$, 0.220%)	0.166 ($\sigma = 5.75 \cdot 10^{-3}$, 3.46%)	< 1%	-	-
a_z [mm^2.s^{-1}]	0.150 ($\sigma = 3.61 \cdot 10^{-5}$, 0.022%)	-	-	0.147	2%
Q [J]	0.54 ($\sigma = 5.13 \cdot 10^{-4}$, 0.095%)	-	-	0.52	3.7%

Table 3.2 – Comparison of the diffusivity values estimated by the Direct and Simultaneous Estimation using Harmonics (DSEH), with the values obtained by the Estimation using the Normalization of Harmonics method (ENH) and the Multiple Steps Estimation using Harmonics (MSEH).

sample whose thermal properties has been already identified by various method. The experimental procedure previously described, is conducted on a polyamide sample of thickness $l_z = 2.4 \pm 0.05\ mm$ measured by a digital micrometer, of heat capacity $C = 1670 \pm 50\ J \cdot kg^{-1} \cdot K^{-1}$ measured by a Calvet calorimeter and a density of $\rho = 1140 \pm 17\ kg \cdot m^{-3}$ deduced from the weight and volume measurements of the sample.

As presented in Table 3.1, the predefined search space domain of the unknown diffusivities is $[10^{-9}; 10^{-4}\ m^2 \cdot s^{-1}]$ and the search space domain of the $R_{m,n}$ terms that describe the thermal excitation is $[-10^{-2}; 10^{3}]$. The largest even harmonics modes used for the estimation are $M = N = 6$, so the corresponding modes are $m, n \in \{0,2,4,6\} \bigotimes \{0,2,4,6\}$, and the number of parameters to estimate is 19. The dimension of the exploitation window are $l_x = 28,0 \pm 0.05\ mm$ and $l_y = 26,1 \pm 0.05\ mm$, centered on the laser impact.

Results achieved using various estimator are shown in Table 3.2. The diffusivity values retrieved by the present estimation method (DSEH) shows a relatively low dispersion around the mean value (0.159), 2.5%, 3.8% and -5.5% for the x, y and z components, respectively. Considering the investigated material that has to be isotropic, the dispersion of the directional diffusivities is consistent, and verify the isotropic nature of this latter, considering $a_x \approx a_y \approx a_z$.

The estimated values are also consistent with the value found by Santos [136] which gives for the Polyamide $a = 0,147 \times 10^{-6}\ m^2.s^{-1}$. The diffusivities results of the present method, along the x and y axis, are compared in Table 3.2 to those obtained from a 2D reference estimation method known as ENH [78, 81], which has been numerically implemented for the exercise purpose. The relative difference between the 2 methods are small as it does not exceed 2%. Finally, the estimated z-component value is compared to the one retrieved using the MSEH principle [74] based on the mean harmonic (0,0) only, and that can estimate also the total amount of the absorbed energy Q. Once again, the agreement is quite convincing as the relative difference is below 1%. These results confirm the perspective made by Ruffio in [82], where the potential of the DSEH method has been evoked from a theoretical point of view, without any implementation.

Fig. 3.8 shows the normalized front face harmonics evolution as a function of time, resulting

from both, the experiment, $\xi^{exp}_{m,n}(t)$, and the simulation performed with the optimized parameters $\hat{\beta}$, $\xi_{m,n}(\hat{\beta},t)$. The comparison of the evolution shows a very close agreement between the signals. The relative error (in %) $\%err$ between the experimental and the estimated signals are calculated separately for each harmonics following the matrix 3.11, and are presented at the top of sub-figures in Fig. 3.8 for both characterized materials, the polyamide material being referred as index 1, and the composite material as index 2. Based on Eq. 2.29, the variance covariance matrix of the estimated parameters are calculated and the standard deviations of the results are presented in brackets in Table 3.2.

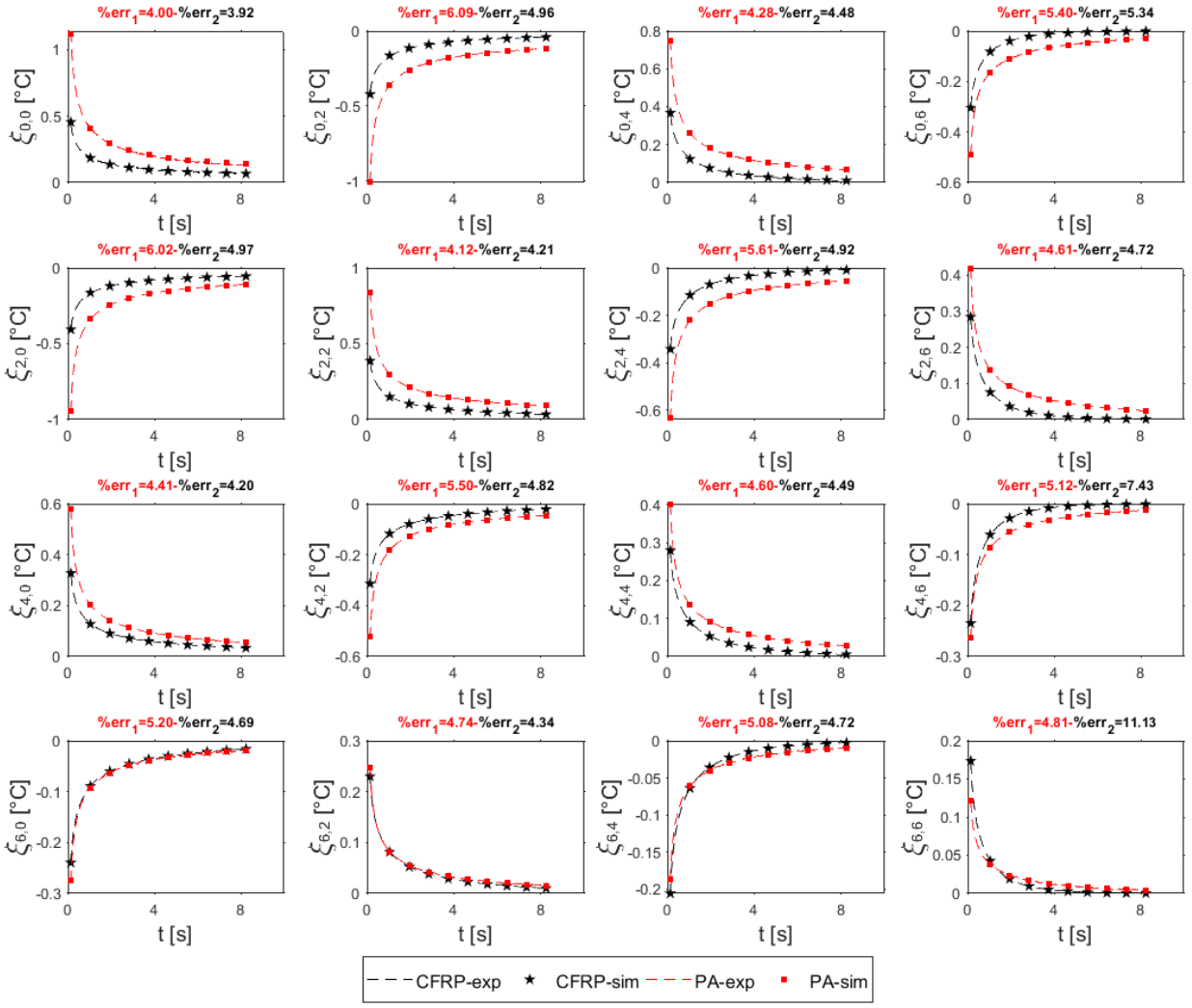

Figure 3.8 – Normalized harmonics temporal evolution for experimental (dotted or normal lines) and inversely estimated data (symbols), applied for the polyamide -PA (red; square) - and the composite -CFRP (black; pentagram) -samples.

It is worth mentioning that $R_{0,0} = Q \cdot F_{0,0}$. Thus, the energy Q may be indirectly estimated since $F_{0,0} = 1$ is the mean shape function in the Fourier basis (Fourier transform at frequency 0). In addition to the diffusivities estimation, the present method allows the estimation of the total amount of energy Q absorbed at the surface of the studied material sample. For the polyamide sample, the total amount of energy imposed on the material surface is $Q = R_{0,0} = 0.54\ J$, in $\Delta t = 10\ ms$. This estimation corresponds to 41.5% of the maximum laser capacity, which is

consistent with the experimental settings.

$$\%err = \begin{pmatrix} \frac{1}{N_t}\sqrt{\sum_{t_i=t_0}^{t_{end}}\left[\frac{\xi_{0,0}^{exp}(t_i)-\xi_{0,0}^{est}(t_i)}{\xi_{0,0}^{exp}(t_i)}\right]^2} & \cdots & \frac{1}{N_t}\sqrt{\sum_{t_i=t_0}^{t_{end}}\left[\frac{\xi_{0,N}^{exp}(t_i)-\xi_{0,N}^{est}(t_i)}{\xi_{0,N}^{exp}(t_i)}\right]^2} \\ \vdots & \ddots & \vdots \\ \frac{1}{N_t}\sqrt{\sum_{t_i=t_0}^{t_{end}}\left[\frac{\xi_{M,0}^{exp}(t_i)-\xi_{M,0}^{est}(t_i)}{\xi_{M,0}^{exp}(t_i)}\right]^2} & \cdots & \frac{1}{N_t}\sqrt{\sum_{t_i=t_0}^{t_{end}}\left[\frac{\xi_{M,N}^{exp}(t_i)-\xi_{M,N}^{est}(t_i)}{\xi_{M,N}^{exp}(t_i)}\right]^2} \end{pmatrix} \tag{3.11}$$

3.4.2 Orthotropic material

The orthotropic material studied in this section is a single embedded fiber composite, constituted of carbon fibers in an epoxy matrix, and known as carbon fibers reinforced polymer composite material (CFRP). The orientation of the carbon fibers is the same along the material plane. The same experimental procedure as used in the validation section is conducted on a sample of thickness $l_z = 8.16 \pm 0.05\ mm$, of heat capacity $C = 1001 \pm 30\ J \cdot kg^{-1} \cdot K^{-1}$ and of density $\rho = 1286 \pm 18\ kg \cdot m^{-3}$. The exploiting window is defined by $l_x = 39,0 \pm 0.05\ mm$ and $l_y = 45,0 \pm 0.05\ mm$, perfectly centered at the laser impact. Once again, Fig. 3.8 shows the excellent agreement between the experimental normalized harmonics, $\xi_{m,n}^{exp}(t)$, and the simulated harmonics obtained with the optimized parameters $\hat{\beta}$, $\xi_{m,n}(\hat{\beta}, t)$.

A comparison between values retrieved by the present method with values obtained from various estimator are shown in Table 3.3. The relative deviation between the present estimator and the ENH estimator, reveals a relative difference of about 2.5%. for a_x and 1.5% for a_y. For a_z, the comparison is conducted with MSEH and shows a relative difference of 4.5%. Considering the carbon fibers being oriented along the y-axis, the ranking of the diffusivity components is consistent, $a_y > a_x$ and a_z.

Unknown values	**DSEH (present study)**	**ENH**	**Rel. diff**	**MSEH**	**Rel. diff**
a_x [mm^2.s^{-1}]	0.40 ($\sigma = 1.04 \cdot 10^{-3}$, 0.260%)	0.39 ($\sigma = 6.71 \cdot 10^{-3}$, 1.72%)	2.5%	-	-
a_y [mm^2.s^{-1}]	2.59 ($\sigma = 2.41 \cdot 10^{-3}$, 0.093%)	2.63 ($\sigma = 0.062$, 2.36%)	1.5%	-	-
a_z [mm^2.s^{-1}]	0.84 ($\sigma = 2.5 \cdot 10^{-4}$, 0.029%)	-	-	0.88	4.5%
Q [J]	0.71 ($\sigma = 7.01 \cdot 10^{-4}$, 0.098%)	-	-	0.73	2.7%

Table 3.3 – Comparison of the diffusivity and energy Q (J) values estimated by the Direct and Simultaneous Estimation using Harmonics (DSEH), with the values obtained by the Estimation using Normalization of Harmonics method (ENH) and the Multiple Steps Estimation using Harmonics (MSEH).

The reproducibility of the algorithm is verified by running the code several times. The deviation of the reached solutions does not exceed 5%, whatever the parameter and despite the

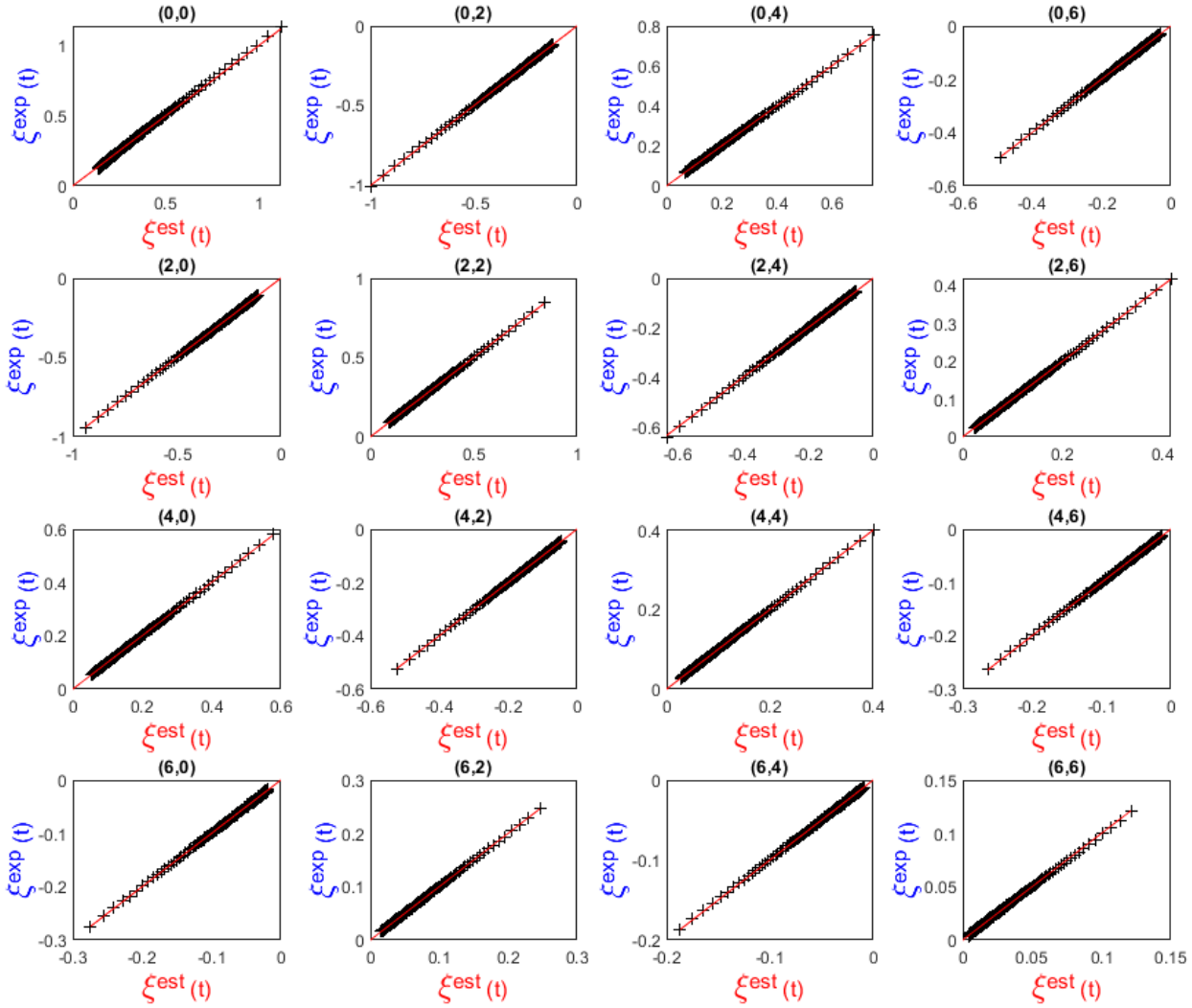

Figure 3.9 – Parity plots for the Composite material (experimental and estimated data)

stochastic nature of the first stage of estimation method. Results are more accurately compared using parity plots as shown in Figs. 3.9 and 3.10.

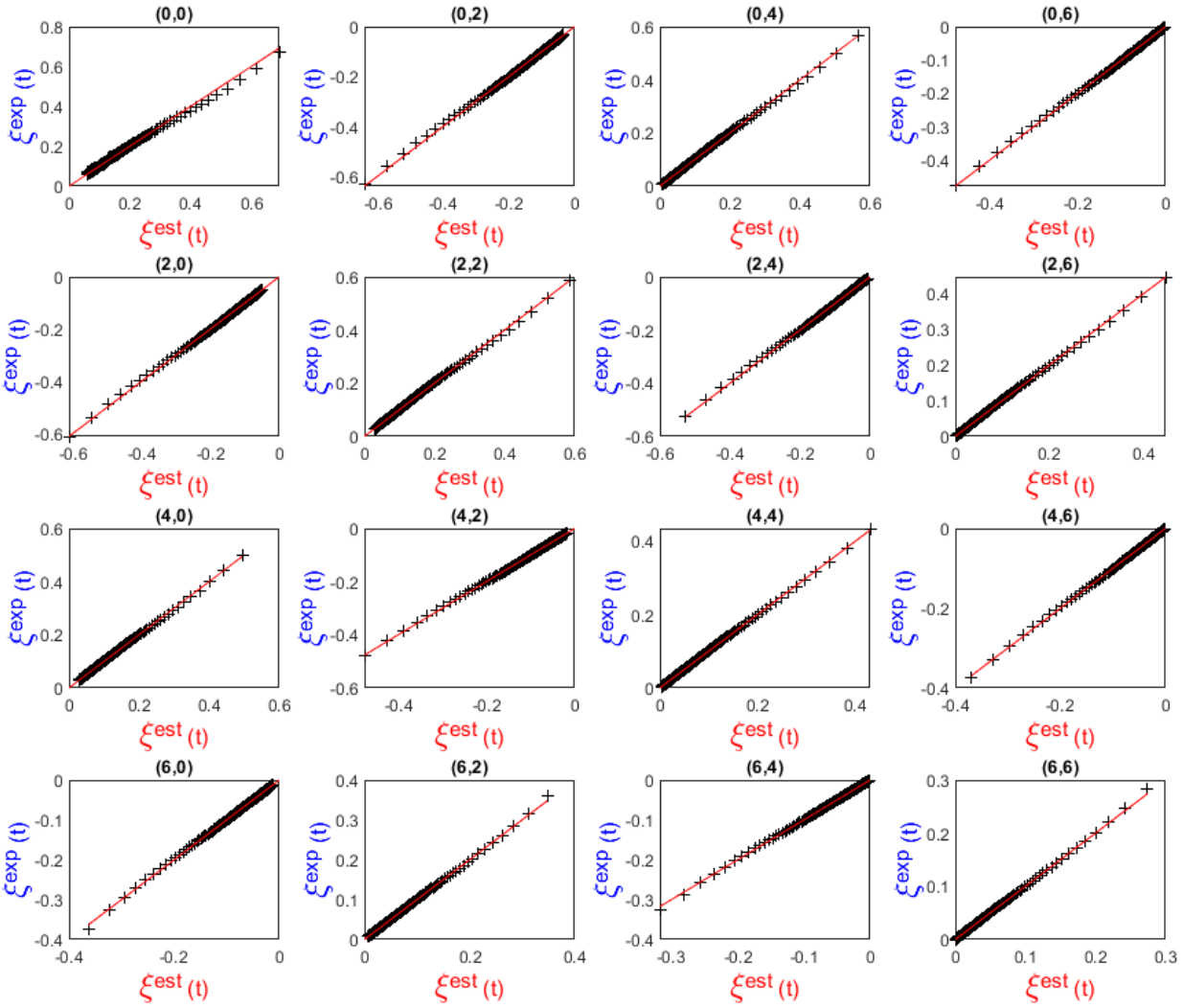

Figure 3.10 – Parity plots for the polyamide material (experimental and estimated data).

3.4.3 Discussion based on sensitivity analysis

In this section, the credibility of the previous estimation is verified by means of a sensitivity study. In the present case, this tool is used to ensure the feasibility of the simultaneous estimation of the diffusivities.

Thus, the variation of the front face normalized harmonics, $\partial\xi(\beta,t)$, caused by a relatively small variation in each parameter, $\partial\beta_j$, is evaluated, while keeping all other parameters constant, with $\beta = [\beta_1, \beta_2, \cdots, \beta_n]$ and n is the number of parameters to be estimated. In this work, reduced sensitivities are considered, as discussed previously in the section 2.6.

One should notice that the sensibility analysis requires the values of the parameters to estimate. A sensitivity study performed before the estimation step is then a qualitative evaluation rather than quantitative. A preliminary sensitivity study, conducted using a supposed set of parameters in probable ranges of values, was used to set the optimization algorithm, particularly the time interval and the harmonics to exploit.

$$Sr_{m,n}(\beta_j, t) = \frac{\partial \xi_{m,n}(\beta, t)}{\partial \beta_j} \times \beta_j \Big|_{\beta_{k\neq j}} \tag{3.12}$$

3.4.3.1 Sensitivity to thermal diffusivities

A sensitivity study is now performed using the previously identified values. Fig. 3.11 and Fig. 3.12 show the reduced sensitivity of the harmonics, during the overall exploitation time, used for the estimation of the diffusivities. For example, the reduced sensitivity of harmonic (0,0) to the diffusivity along the x-axis is done using $Sr_{0,0}(a_x, t) = \frac{\partial \xi_{0,0}(\beta, t)}{\partial a_x} \cdot a_x \Big|_{\beta_k \neq a_x}$. To evaluate the sensitivities, time dependent harmonics gradients with respect to the unknown parameters, has to be treated. A large number of tests performed on various Laplace inversion techniques, shows that a coupled inversion technique was found to be the most appropriate for this exercise. It involves a Gaver-Stehfest method ([186]), more stable at short time, and a Hoog inversion ([189]) in the remaining time. The reduced sensitivity of the harmonics to the polyamide and to the composite diffusivities are plotted in Fig. 3.11 and Fig. 3.12, respectively. The reduced sensitivities analysis reveals the importance of each harmonics:

- $\xi_{0,0}$ carries information about a_z only. This harmonic, corresponding to the mean temperature field, contains most of the energy transferred.
- $\xi_{m,0}$ with $[0 < m \leq 6, n = 0]$, are only sensitive to a_x and a_z without any correlation.
- $\xi_{0,n}$ with $[m = 0, 0 < n \leq 6]$, are only sensitive to a_y and a_z without any correlation.
- $\xi_{m,n}$ with $[0 < m \leq 6, 0 < n \leq 6]$ are sensitive to all diffusivities, but a_x and a_y exhibit a correlation, as revealed by the proportionality between the sensitivity signals. Thus, those harmonics does not carry any useful information for the estimation of these parameters. However, those harmonics are kept because it gives additional information to estimate a_z properly.

Other sensitivity study was conducted in order to verify that the acquisition time range is well chosen in order to avoid any correlation between the in-depth thermal diffusivity a_z and the total amount of heat absorbed at the surface of the sample Q, for both samples as illustrated in Figs. 3.13. The sensitivities to a_z and Q of the mean field $S_{0,0}$, which is the most sensitive harmonic to these parameters, are represented as well as their ratio in order to catch their non-linearity starting time. For the polyamide sample in Fig. 3.13a, the decorrelation of the signals is ensured at $t \geq 4.5$ s). For the composite sample in Fig. 3.13b, it is ensured at $t \geq 11$ s).

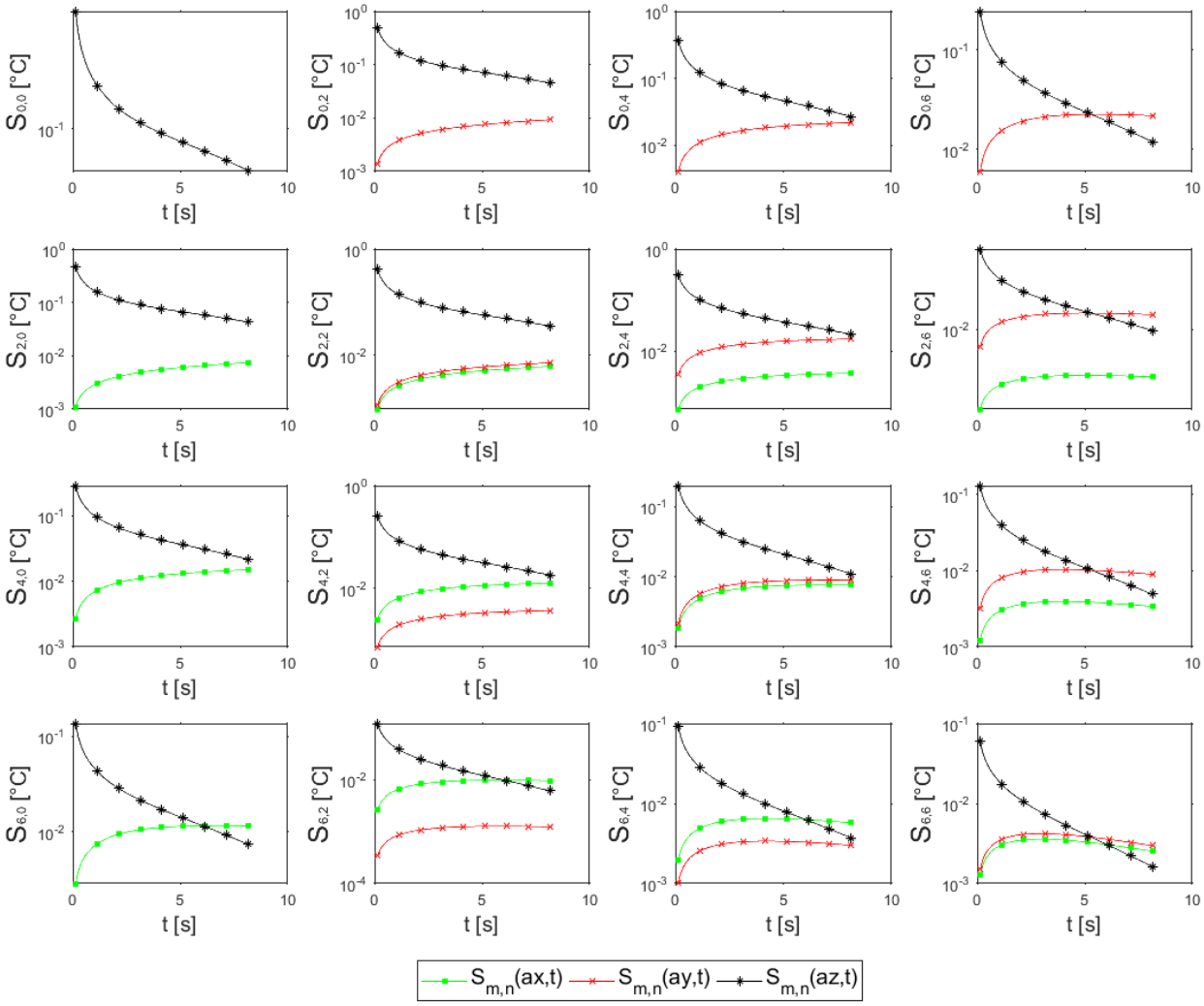

Figure 3.11 – Sensitivities of the entire harmonics modes used for identification of the polyamide three main thermal diffusivities.

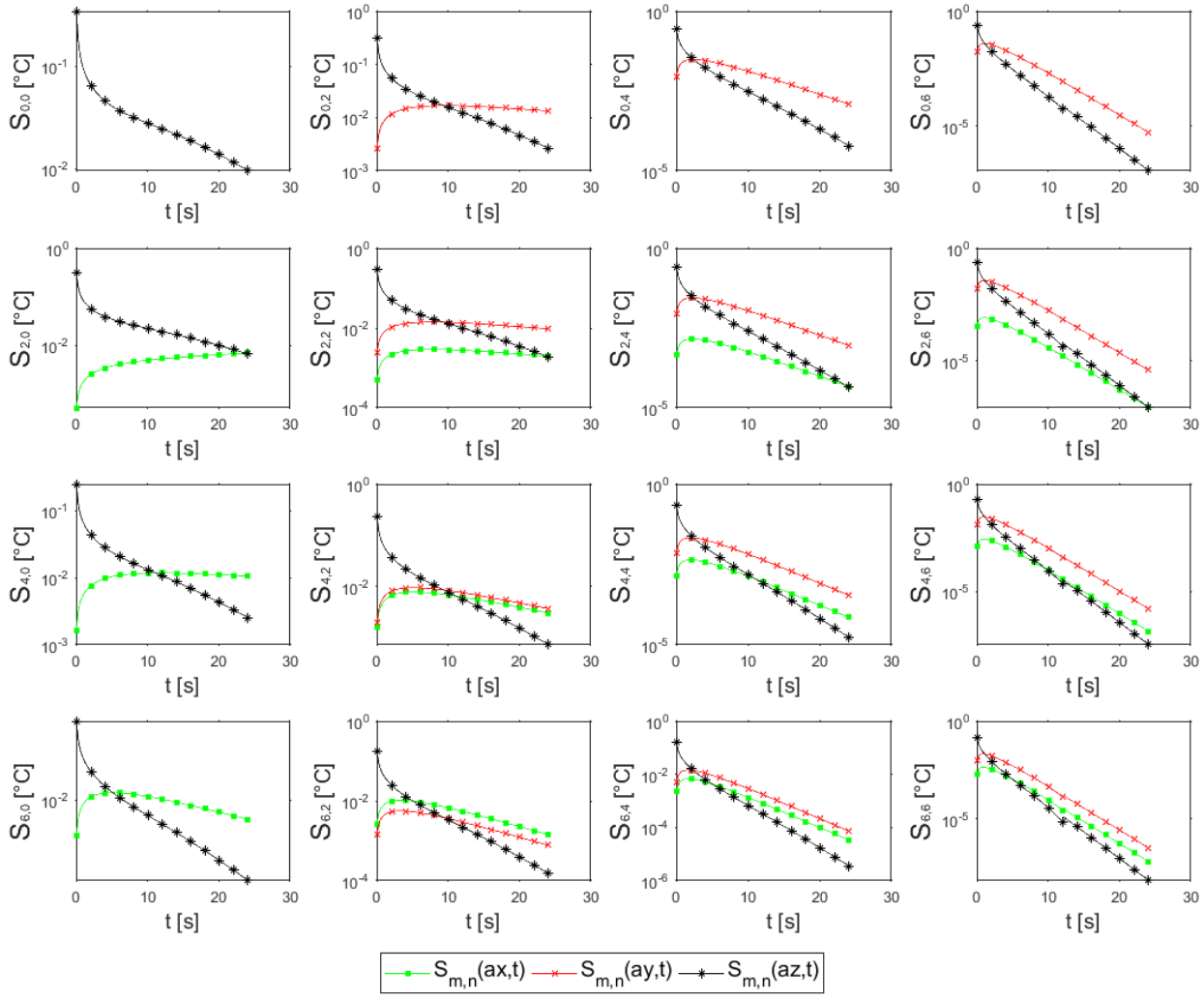

Figure 3.12 – Sensitivities of the entire harmonics modes used for identification of the composite three main thermal diffusivities.

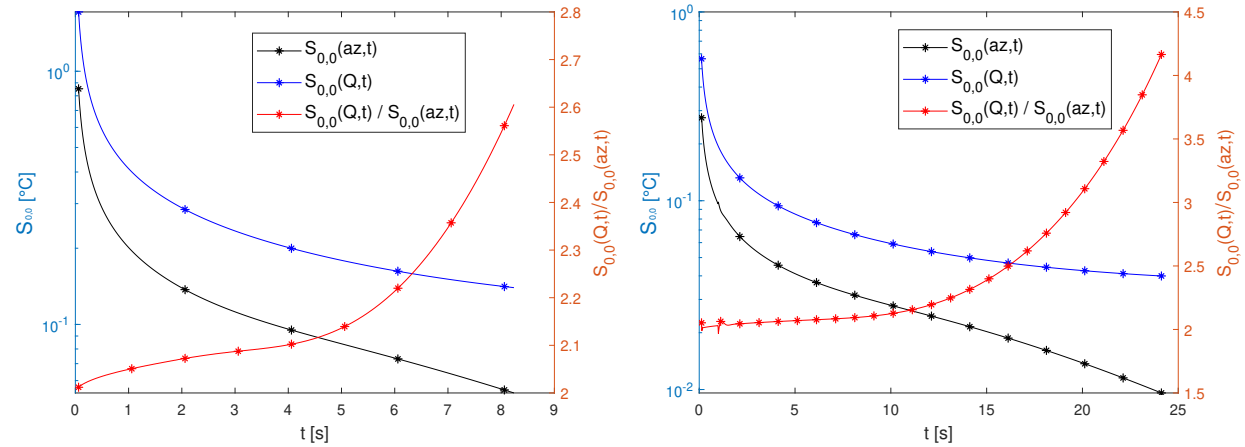

(a) PA material

(b) Composite material

Figure 3.13 – Sensitivities of the front face first harmonics representing the mean fields $\xi_{0,0}$, to the in-depth diffusivies a_z and the total amount of heat Q absorbed at the surface of both samples, with their ratio in order to detect the decorrelation between both parameters.

3.4.3.2 Sensitivity to the overall heat transfer coefficient

The heat exchange, involving radiation and convection modes, between the environments and the materials is considered to take place at the front (i.e.exposed) and rear faces of the samples, only. To highlight the negligible influence of the overall heat transfer coefficient on the front face temperature, the front face signal issued form the analytical model, has been plotted for different extended values of $h \in \{0,5,10,15,20\}$ $W \cdot m^{-2} \cdot K^{-1}$ in Fig. 3.14 using parameters consistent with experimental conditions. As shown in this figure, the value of the overall coefficient has negligible effect on the first 4 harmonics during the considered time of exploitation ($t < 25$ s).

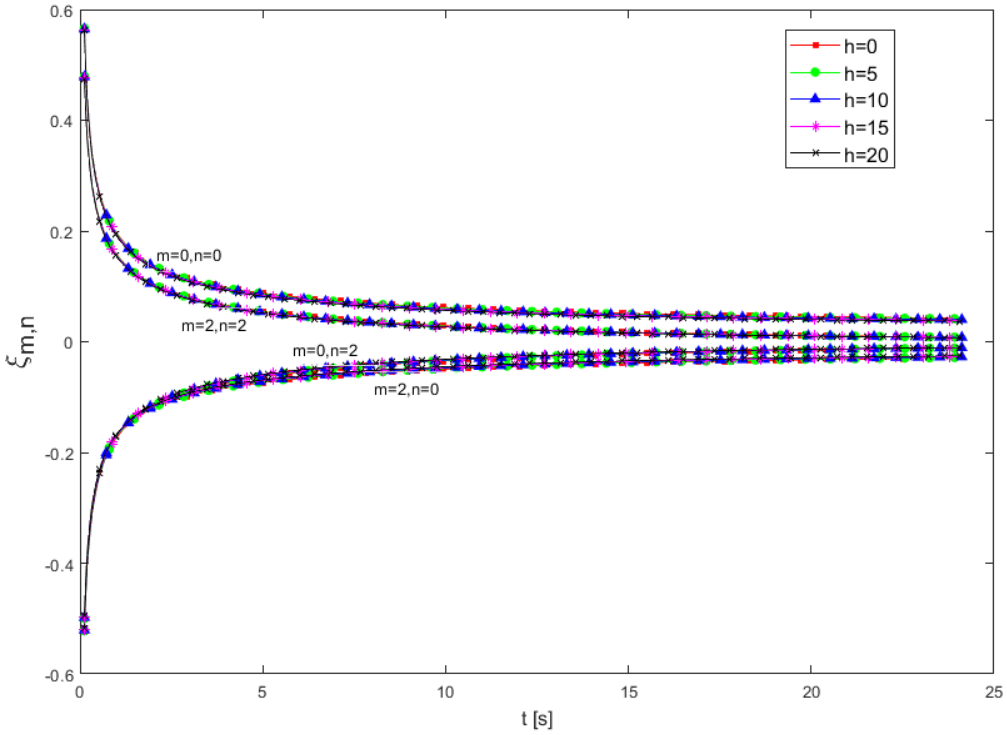

Figure 3.14 – Evolution of the first 4 harmonics, according to the value of the overall heat coefficient h.

A second plot in Fig. 3.15 representing the time evolution of the relative absolute deviation or error (in %) between the front face normalized harmonics obtained with an overall heat transfer $h = 10$ $W \cdot m^{-2} \cdot K^{-1}$ and those obtained without heat losses $h = 0$ $W \cdot m^{-2} \cdot K^{-1}$, verify also the negligible effect of this assumption, with a relative deviation < 7% for (t < 25 s).

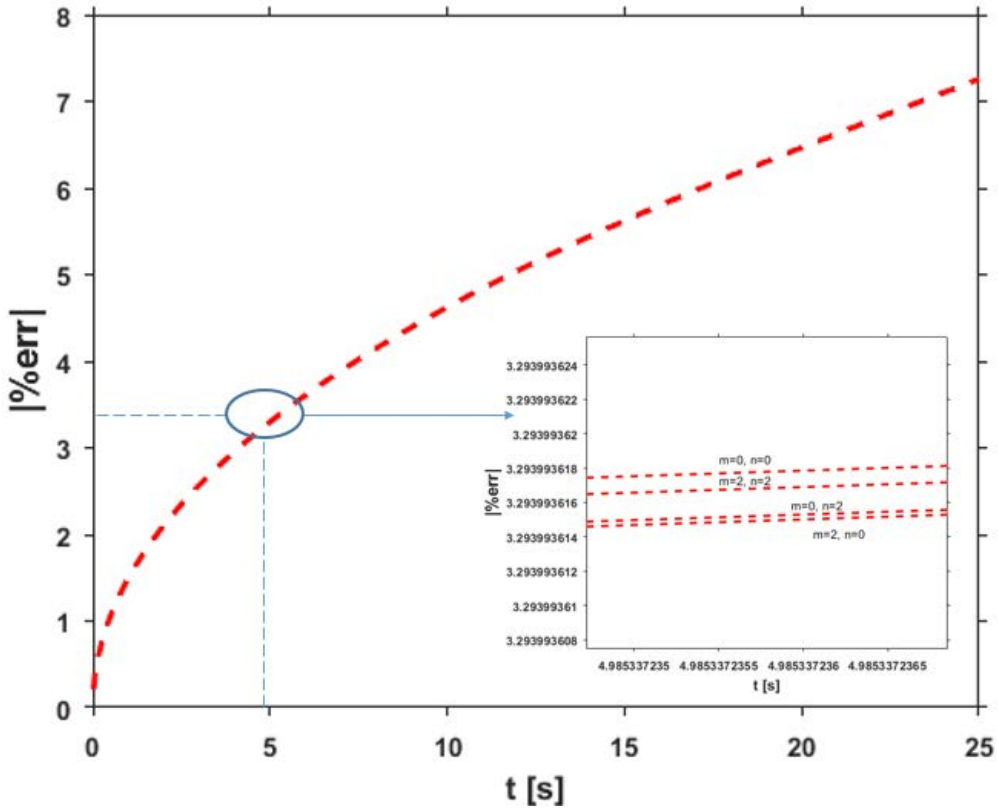

Figure 3.15 – Time evolution of the relative absolute deviation (error in %) between the front face normalized harmonics with an overall heat transfer $h = 0\ W \cdot m^{-2} \cdot K^{-1}$ and those with $h = 10\ W \cdot m^{-2} \cdot K^{-1}$.

3.4.4 Reconstruction in the physical real space domain

In order to return to the physical real space, the Fourier space field is projected in the normalized basis of X_m and Y_n. Since X_m and Y_n are orthogonal, real and physical space temperature profiles can be eventually achieved using the following correlations:

$$T(x,y,z,t) = \sum_{m=0}^{\infty}\sum_{n=0}^{\infty} \theta(\alpha_m,\beta_n,z,t)\cdot\frac{X_m(x)}{\|X_m\|^2}\cdot\frac{Y_m(x)}{\|Y_m\|^2} \tag{3.13}$$

$$T(x,y,z=0,t) = \sum_{m=0}^{\infty}\sum_{n=0}^{\infty} \xi(\alpha_m,\beta_n,z=0,t)\cdot l_x\cdot l_y\cdot\frac{X_m(x)}{\|X_m\|^2}\cdot\frac{Y_m(x)}{\|Y_m\|^2} \tag{3.14}$$

with

$$\|X_m\|^2 = \begin{cases} l_x \text{ if } m=0, \\ l_x/2 \text{ if } m>0 \end{cases} \tag{3.15}$$

and

$$\|Y_n\|^2 = \begin{cases} l_y \text{ if } n=0, \\ l_y/2 \text{ if } n>0 \end{cases} \tag{3.16}$$

The number of harmonic needed to perform a successful estimation has been carefully studied. In this work, only 6 harmonics $M = N = 6$ are found to be sufficient to ensure an optimum estimation. The same number of harmonics is used for the reconstruction of the physical temperature fields evaluated using the estimated parameters. In Fig. 3.16, the reconstructed signal using the estimated parameters is compared to the signal representing the physical experimental evolution of the front face temperature, both for the polyamide sample.

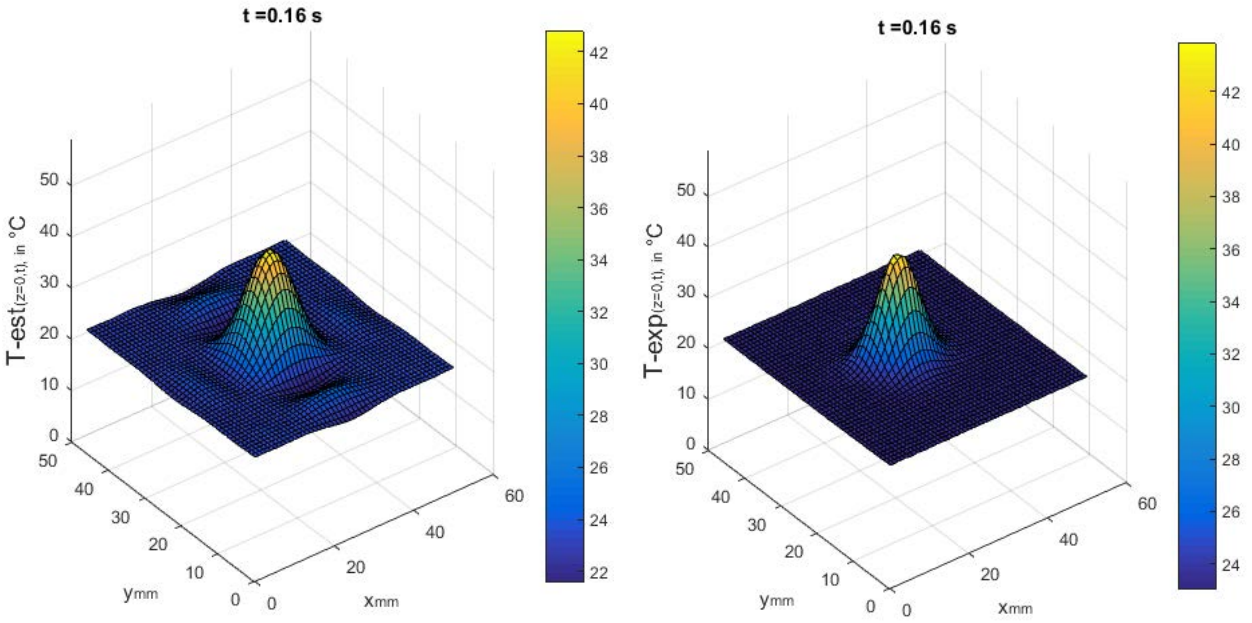

(a) Reconstructed signal

(b) Experimental signal

Figure 3.16 – T(x,y,z=0,t) at the surface of polyamide sample, reconstructed from estimated parameters (left figure), and experimentally measured (right figure).

As shown in Fig. 3.16, the number of harmonics used for the identification was not sufficient for the best reconstruction of the physical signal. Much more spatial modes are needed to achieve this purpose, thus necessitating a higher time consumption. This point can also argue the implementation in this work, of the pseudo-analytical model in the Fourier domain coordinates instead of the physical domain coordinates, for a faster identification of the required thermal properties.

3.5 DSEH compared to other existing identification methods (ERH, ENH, MSEH)

This section presents some estimation methods developed in the literature that investigate harmonics in order to estimate only in-plane diffusivities such as ERH and ENH estimators or in-plane and in-depth diffusivities of orthotropic or anisotropic material, such as MSEH estimator.

In this section Y designates the observables, and θ the harmonics. In addition, $H = \frac{h \cdot L_z}{\lambda_z}$, $\tau_x = \frac{a_x}{l_x^2}$, $\tau_y = \frac{a_y}{l_y^2}$, $T_{lim} = \frac{Q}{\rho \cdot C \cdot l_x \cdot l_y \cdot l_z}$, and $E_{m,n} = T_{lim} \cdot F_{m,n}$ also called "harmonic signature".

3.5.1 ERH: Estimation using Ratio of Harmonics

The ERH estimator was proposed by Philippi in 1995 [73], for thin aluminum plates, then upgraded and improved by Remy [76, 149]. This method allows the estimation of a_x and a_y. The estimation of these in-plane diffusivities is based on the resolution of the following equations:

$$a_x = \frac{1}{m^2(t_2 - t_1)} \left[ln \left| \frac{\theta_{0,0}(z,t_2)}{\theta_{0,0}(z,t_1)} \right| - ln \left| \frac{\theta_{m,0}(z,t_2)}{\theta_{m,0}(z,t_1)} \right| \right] \tag{3.17}$$

$$a_y = \frac{1}{n^2(t_2 - t_1)} \left[ln \left| \frac{\theta_{0,0}(z,t_2)}{\theta_{0,0}(z,t_1)} \right| - ln \left| \frac{\theta_{0,n}(z,t_2)}{\theta_{0,n}(z,t_1)} \right| \right] \tag{3.18}$$

This method is then improved by Ruffio [82], who has proposed to estimate a_x and a_y in one step using all harmonics simultaneously, instead of using only $\theta_{m,0}$ and $\theta_{0,n}$ once at a time.

3.5.2 ENH: Estimation using Normalization of Harmonics

The ENH estimator is quite similar to the ERH estimator but instead of dividing the same harmonic at two different times, harmonics are normalized by the average temperature field $\theta_{0,0}$. Thus, the observables take the following form:

$$Y_{m,n}(z,t_k) = ln \left| \frac{\theta_{m,n}(z,t_k)}{\theta_{0,0}(z,t_k)} \right| = ln \left| \frac{E_{m,n}}{E_{0,0}} \right| - (\tau_x m^2 + \tau_y n^2)\pi^2 t_k \tag{3.19}$$

Based on this equation, this estimator can simultaneously identify a_x and a_y.

Harmonics can also be normalized by a reference signal other that the average temperature

field $\theta_{0,0}$.

$$Y_{m,n}(z,t_k) = ln\left|\frac{\theta_{m,n}(z,t_k)}{\theta^{ref}_{p,q}(z,t_k)}\right| = C_{m,n} + \tau_x(p^2-m^2) + \tau_y(q^2-n^2)\pi^2 t_k \tag{3.20}$$

with

$$C_{m,n} = ln\left|\frac{E_{m,n}}{E^{ref}_{p,q}}\right| = ln\left|\frac{F_{m,n}}{F^{ref}_{p,q}}\right| \tag{3.21}$$

The parameters vector will take this form $\beta = [\tau_x, \tau_y, C_{0,0}, C_{2,0}, C_{0,2}]$

Noting that, there is a nonlinear relationship between the harmonics and thermal diffusivities, however when implementing ENH or ERH estimators, the application of logarithmic transform converts the problem into a linear estimation one.

Considering that $\theta_{0,0}$ is more sensitive to environemental perturbations than other frequencies, this method has been improved by Ruffio [82] using $\theta_{2,2}$ as a reference harmonic, since it is the lowest frequency having sensitivity to only non-uniform fluctuations that occur simultaneously along x and y axis.

3.5.3 MSEH: Multiple Steps Estimation using Harmonics

The MSEH estimator is a multiple step estimation developed by Souhar in [74]. This estimation strategy requires only "gross harmonics" without any harmonics transformation. Here, the estimation problem is non-linear (with respect to β) and the estimator relies directly on the model outputs. The unknown parameters vector $\beta = [\tau_x, \tau_y, \tau_z, H, E_{0,0}, E_{m,n}, \dots]$ is estimated using 3 consecutive steps:

1. H, τ_z and $E_{0,0}$ (see Eq. 3.8) are firstly estimated based on the average temperature field $\theta_{0,0}$.

2. After being considered as perfectly known, H and τ_z are then used in the estimation of τ_x using $\theta_{m,0}(t)$.

3. The same for the estimation of τ_y using $\theta_{0,n}(t)$.

This method relies only on the frequencies having the spatial modes $(0,n)$ and $(m,0)$.

In brief, as a first step estimation of H ,τ_z and $E_{0,0}$ was based only on the $\theta_{0,0}$. In the next two steps, these estimated values are used for the identification of τ_x and τ_y, and consequently a_x and a_y .

It is important to realize that the use of $\theta_{0,0}$ for the estimation of H and τ_z seems to be insufficient since all other harmonics can give additional information regarding that estimation. Moreover, the errors made on the estimation of these parameters will definitively propagate through the method until the estimation of τ_x and τ_y. Adding to that, $\theta_{0,0}$ being the most sensitive to the environmental conditions, i.e. to any change that could occur in the surroundings, any estimation relying on this harmonic might be inaccurate.

3.5.4 Originality of the current DSEH: Direct and Simultaneous Estimation using Harmonics

The identification method developed in this work (DSEH) does not require any post-treatment of the harmonics (e.g. logarithmic transformation, normalization as ENH or ERH, etc) as it exploits directly the "gross normalized harmonics" without any additional transformation.

It allows, in an unique step, a direct and simultaneous estimation of the three dimensional thermal diffusivity tensor for an orthotropic material.

Adding to that, it requires a unique experiment with both non-intrusive excitation and temperature evolution measurements.

Furthermore, the pseudo-analytical expression of the temperature evolution occurring at the front or rear face of the sample allows a fast treatment of the direct model, thus a faster estimation technique.

Finally, this method does not require any a priori knowledge about the excitation characteristics (i.e. intensity, spatial distribution shape), which can be simultaneously estimated.

3.6 Improvements of Identification Method

In the next section, experimental data are sometimes replaced by synthetic noisy data, generated by the direct model itself or by a finite element code. The purpose is to validate the estimation method and by no mean the physical direct model.

3.6.1 In terms of time reduction

As previously shown, the time consumed to perform this estimation, which relies on an analytical model, is quite moderate, compared to numerical methods. Nevertheless, an improvement may be achieved, while conserving a certain level of accuracy. Regarding that time consumption sources, the PSO minimization section has proved to be the more consuming. The main objective of this section is to reduce the consumption time, by means of many strategies.

- Filtering the images required for the identification, this strategy does not reduce significantly the computational time.
- Reducing the number of PSO particles will decrease the CPU time but makes it vulnerable to local convergence and some authors prescribed the optimal number of particle to be set as 10 times the number of parameter to identify.
- Decreasing the number of exploited harmonics. For example, changing from a number of harmonics $M = N = 6$ to $M = N = 4$, reduces the number of parameter to estimate from 19 to 12. This still conduct to precise results but also does not reduce the calculation time significantly.
- Using more restricted bounds, or applying more moderate stopping criteria (e.g. smaller number of maximum iterations, higher tolerance value for the objective function, lower

value of maximum stall iteration, etc). However, these strategies can reduce the performance of the global search that could be achieved by the PSO algorithm.

- Imposing the shape of the excitation that, in turn, may significantly reduce the number of parameters to identify. Currently, the identification of the 3 thermal diffusivities requires the estimation of 16 parameters related to the form of the excitation. Thus, the reduction of the number of parameters needed to mimic the excitation is investigated in this part. One strategy consists in considering the excitation with an a priori knowledge of its shape. In this case, the number of parameters is reduced to the number of parameters of the analytical function describing the prescribed flux distribution. Several laser excitation forms, is considered in literature [82]: Gaussian, parabolic, triangular, uniform, pointed, etc.

Many of these strategies have been tested, the results of two of them: a predefined shape of excitation and a smaller number of exploited harmonics ($M = N = 4$ instead of 6), and their influences on the calculation time and estimation accuracy, is presented hereafter (see Table 3.4).

Spatial shape of the excitation

In this work, according to IR camera images at the excitation time, two excitation spatial shapes seem to be physically consistent. The shape function associated with the laser beam, $F_{x,y}$, is assumed to follow a cosine function or a polynomial cubic form. Fig. 3.17 represents the temperature evolution when having these two possible shapes of laser beam.

Cosine function as shape function

The shape of the excitation is described, along the x-axis, by the function

$$f(x) = \frac{1}{r} \cdot \begin{cases} \frac{1}{2} \cdot \left(1 + cos(\frac{\pi \cdot x}{r})\right) & \text{for } -r < x < r \\ 0 & \text{otherwise} \end{cases} \tag{3.22}$$

with r the radius of the laser spot. The Fourier transform of the previous function is

$$f_m = \int_0^{l_x} f(x - \frac{lx}{2}) \cdot cos(\frac{m\pi x}{l_x}) dx = \frac{1}{r} \cdot \frac{l_x^3 \cdot cos(\frac{m \cdot \pi}{2}) \cdot sin(\alpha_m \cdot r)}{l_x^2 \cdot m \cdot \pi - r^2 \cdot m^3 \cdot \pi} \tag{3.23}$$

The same function is used for $f(y)$. Then, the shape function associated with the laser beam, $F_{x,y} = f(x) \cdot f(y)$, in the Fourier domain, leads to the dimensionless shape factor:

$$F_{m,n} = \frac{1}{r^2 \cdot \pi} \cdot \left(\frac{l_x^3 \cdot l_y^3 \cdot cos(\frac{m \cdot \pi}{2}) \cdot cos(\frac{n \cdot \pi}{2}) \cdot sin(\alpha_m \cdot r) \cdot sin(\beta_n \cdot r)}{(l_x^2 \cdot m - m^3 \cdot r^2) \cdot (l_y^2 \cdot n - n^3 \cdot r^2)} \right) \tag{3.24}$$

Polynomial cubic as shape function

The shape of the excitation is described, along the x-axis,

$$f(x) = \frac{1}{r} \times \begin{cases} 1 - 3 \cdot (\frac{x}{r})^2 - 2(\frac{x}{r})^3 & \text{for } -r \leq x < 0 \\ 1 - 3 \cdot (\frac{x}{r})^2 + 2(\frac{x}{r})^3 & \text{for } 0 \leq x < r \\ 0 & \text{otherwise} \end{cases} \tag{3.25}$$

The Fourier transform of the previous function is

$$f_m = \int_0^{l_x} f(x - \frac{l_x}{2}) \times cos(\frac{m \cdot \pi \cdot x}{l_x}) dx = \frac{-24\Big(cos(\frac{m \cdot \pi}{2}) \cdot \big(cos(\alpha_m \cdot r) - 1 + \frac{\alpha_m \cdot r}{2} \cdot sin(\alpha_m \cdot r)\big)\Big)}{r^4 \cdot \alpha_m^4} \tag{3.26}$$

The same function is used for $f(y)$. Consequently, the shape function associated with the laser beam, $F_{x,y} = f(x) \cdot f(y))$, in the Fourier domain, leads to the dimensionless shape factor:

$$F_{m,n} = \frac{24^2}{r^8 \cdot \alpha_m^4 \cdot \beta_n^4} \cdot \Bigg[\Big(cos(\frac{m \cdot \pi}{2}) \cdot \big(cos(\alpha_m \cdot r) - 1 + \frac{\alpha_m \cdot r}{2} \cdot sin(\alpha_m \cdot r)\big)\Big) \cdot \Big(cos(\frac{n \cdot \pi}{2}) \cdot \big(cos(\beta_n \cdot r) - 1 + \frac{\beta_n \cdot r}{2} \cdot sin(\beta_n \cdot r)\big)\Big)\Bigg] \tag{3.27}$$

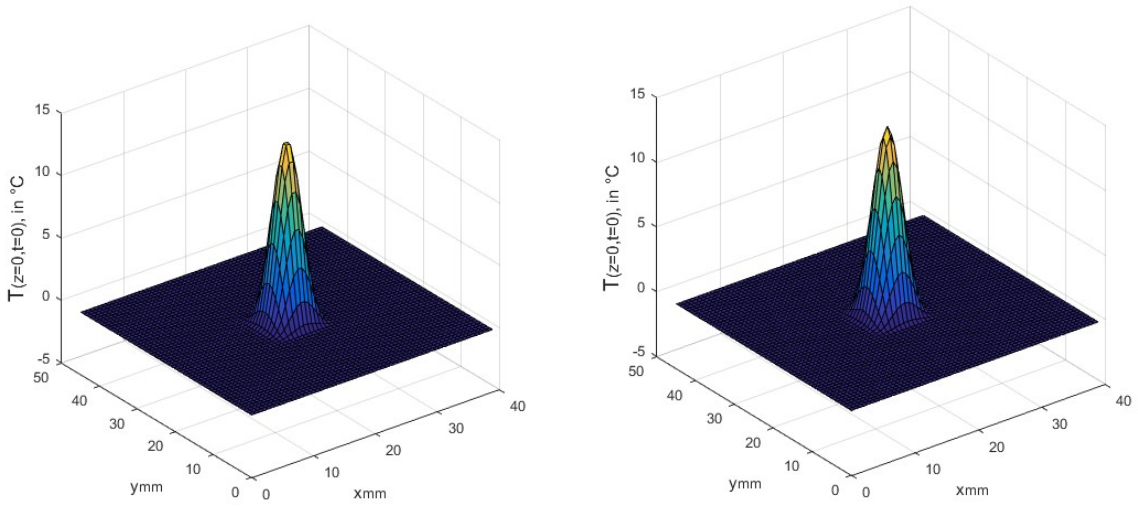

(a) cosine shape

(b) cubic polynomial shap

Figure 3.17 – Temperature elevation fields at $t = t_0$ for the cosine and cubic polynomial predefined shapes.

Considering any of the 2 predefined shapes, defined in Eqs. 3.24 and 3.27, the only unknown

parameter is the laser radius r. The excitation distribution, described by $\phi^{ex}_{m,n}(p) = Q \cdot F_{m,n} \cdot u(p)$, that appears in Eq. 3.7, implies the knowledge of the excitation intensity Q, which is also identified in the present version of the method. Therefore, the parameters vector is now reduced to $\beta = [a_x, a_y, a_z, Q, r]$.

To recall, the current DSEH estimation strategy without predefined excitation shape, allows an indirect estimation of the total amount of absorbed heat Q, by estimating the parameter $R_{0,0} = Q \cdot F_{0,0} = Q$.

The identification exercise is performed on the previously studied orthotropic material, for different hypotheses regarding the nature of the predefined shape of the excitation and the number of investigated harmonics. For comparative purposes, the estimations are conducted using the same PSO parameters.

Unknown values	**Non-predefined shape (6 harm)**	**Non-predefined shape (4 harm)**	**Cubic (6 harm)**	**Cosine (6 harm)**	**Cubic (4 harm)**	**Cosine (4 harm)**
a_x [mm^2.s^{-1}]	0.401	0.411	0.504	0.500	0.485	0.485
a_y [mm^2.s^{-1}]	2.590	2.610	2.370	2.370	2.470	2.470
a_z [mm^2.s^{-1}]	0.839	0.828	0.901	0.902	0.856	0.857
Q [J]	0.717	0.714	0.714	0.706	0.712	0.708
t_{CPU} [min]	35	25	3	3	2	2

Table 3.4 – Summary of the diffusivities a_x, a_y, a_z and energy Q estimation results as a function of the excitation spatial form.

As shown in Table 3.4 the results obtained are quite similar whatever the presupposed shape. The calculation time is one order of magnitude lower than the original estimation.

Concerning the estimated values, the level of accuracy is acceptable as the relative error of the global estimation (i.e. the summation of the independent relative error) does not exceed 8 %. The present strategy, could be conducted as a first guess approach, whose results may be used to initialize and ranging the unknown parameters of the original method in a closer search domain.

Besides the estimation of the diffusivities, this version of the method can also identify the amount of energy absorbed by the sample Q, and the laser spot radius r. In both cases (cubic or cosine shapes), the identified values are close, with $Q \approx 0.71\ J$ and $r = 5.6\ mm$. The value of Q corresponds to 55% of the maximum laser capacity (130W) which is coherent with the laser settings. The value of r corresponds roughly to the observation on the first IR images, illustrated in Fig. 3.5. Those results, $\beta = [a_x, a_y, a_z, Q, r]$, may be used as is, when the constraints may require a fast estimation (i.e. quality control in manufacturing), or as a preliminary guess in order to restrict the search domains.

For this purpose a two-steps method was conducted. It consists in estimating $\beta' =$

$[a'_x, a'_y, a'_z, Q, r]$ by applying a predefined shape (cosine or cubic). Then, the search space domain of the original method (with a non-predefined shape), is re-initialized with a more-restricted area, using the previous resulting vector β'. Having $F_{m,n}$ always between -1 and 1, $R_{m,n}$ is comprised between –Q and Q. The new search space domain for $[a_x, a_y, a_z, R_{m,n}]$ will have a lower bound of $[a'_x/2, a_y/2', a_z/2', -2Q]$ and an upper bound of $[2 \cdot a'_x, 2 \cdot a'_y, 2 \cdot a'_z, 2Q]$. The results of this two-steps method are represented in Table 3.5, and compared to the results obtained via the one-step method with non-predefined shape of the laser beam.

Unknown values	**Non-predefined shape (6 harm)**	**Two-steps method (6 harm)**
a_x [mm^2.s^{-1}]	0.401	0.400
a_y [mm^2.s^{-1}]	2.590	2.590
a_z [mm^2.s^{-1}]	0.839	0.840
Q [J]	0.717	0.718
t_{CPU} [min]	35	18

Table 3.5 – Comparison of the results between the one-step (non-predefined) and two-step methods.

3.6.2 In terms of accuracy

An other improvement point concerns the effect of the number of harmonics (e.g. $M = N = 8$ instead of 6) on the accuracy. Also, the strategy that consists in taking into account the odd harmonics in the estimation and adding them into the cost function: $m, n \in \{0, 1, 2, ..., M\} \bigotimes \{0, 1, 2, ..., N\}$ is evaluated. The estimation results of these alternative improvement strategies, and their corresponding time consumption, are tabulated in Table 3.6. One can observe that the resulting time consumption increase without any significant change in the estimation results, compared to those of the original current estimation.

In addition to the previous strategies, others are tested in order to evaluate the influence of some harmonics selection on the estimation accuracy. The first case excludes $\xi_{0,0}$. The results retrieved without taking into account the mean temperature field, are approximately the same, as shown in Table 3.7. This may be useful when try to limit the surroundings influence. The robustness of the method is then maintained. The other case considers only the $\xi_{m,0}$ and $\xi_{0,n}$ with $0 \leq m, n \leq 6$, that are found, based on sensitivity analysis 3.4.3.1, sufficient in terms of decorrelation to simultaneously estimate the three thermal diffusivities.

The corresponding results tabulated in Table 3.7 prove that whatever the selection of harmonics investigated, it slightly reduce the consumption time without any significant change in the results.

Diffusivities	**DSEH (current)**	**DSEH (M=N=8)**	**DSEH (with odd harm)**
a_x [mm^2.s^{-1}]	0.401	0.399	0.412
a_y [mm^2.s^{-1}]	2.590	2.583	2.582
a_z [mm^2.s^{-1}]	0.839	0.809	0.825
t_{CPU} [min]	35	60	74

Table 3.6 – Comparison of estimation results between other more accurate alternative strategies, and those of the current method.

Diffusivities	**DSEH (current)**	**DSEH (without $\xi_{0,0}$)**	**DSEH ($\xi_{0,n}$ & $\xi_{m,0}$)**
a_x [mm^2.s^{-1}]	0.401	0.402	0.400
a_y [mm^2.s^{-1}]	2.590	2.582	2.597
a_z [mm^2.s^{-1}]	0.839	0.825	0.793
t_{CPU} [min]	35	30	25

Table 3.7 – Comparison of estimation results between other tested cases, and those of the current method.

3.6.3 Optimization of flash experiment design in terms of time shape duration (Pulse, Impulse) and measurement face

In this section, an experiment design of the flash method, dedicated to orthotropic materials thermal characterization, is treated. The present study relies on a comparative evaluation of the laser excitation duration time and intensity level effects, with respect to the measurement face on the estimation accuracy of anisotropic materials thermal diffusivities. Both the direct pseudo-analytical model and the estimation strategy are validated using an experimental test bench conducted on a CFRP (Carbon fibers reinforced polymer composite) sample. The evaluation of various experiment designs, corresponding to different combinations of laser spot intensity and duration time, is conducted according to the face of the observation. A sensitivity analysis is conducted to complete the search of the optimal configuration. This numerical work, corresponding to a comparative evaluation of different possible setup combination, allows to find the optimal parametrization of the actual flash experiment, and thus, can be qualified as a design of experiment exercise.

A study of the estimation performance for such material according to i) the measurement

face, ii) the energy and iii) the duration time of the excitation, will be presented.

3.6.3.1 Literature review on flash based methods: excitation time shape and temperature measurement face

"Flash methods" is a generic term referring to a large class of methods that relies on photothermal excitation. Usually the excitation is of short duration, but not necessary an impulse type excitation. Among those methods, some rely on the measurement of the front face temperatures evolution and are classified as "front face flash method". Other methods rely on the measurement of the rear face temperatures evolution and are classified as "rear face flash method". The "rear face flash method" have taken an increasing interest in many researches [2, 66, 70, 73–75, 105, 106, 113, 114, 144, 177, 246, 250, 251] because it can be applied in cases where the front face strategy does not work. This is the case of highly conductive material that does not allows to capture temperature evolution at short time, unless at high acquisition frequencies which is not always possible with frequently used IR camera.

Regarding rear face flash methods, instantaneous thermal disturbances (impulse or very short heat pulse) is applied in most cases [2, 66, 70, 73–75, 105, 106, 113, 114, 144, 250, 251], some others used short pulse with finite time correction [177], or short rectangular pulse (< 0.5 s) [246]. Other attempts have been made to modify the type of excitation by replacing the impulse by a continuous (or step) excitation [85] or by a succession of impulsion [140]. Regarding the front face flash methods, most of the works consider the case where an impulse is applied on the surface of the materials [81, 107, 108, 111, 112, 119, 120, 249]. Otherwise, some authors investigated both rear and front face flash methods [78, 79, 82, 122], as do the present work.

3.6.3.2 Problem description

The experiment under consideration, relies on the flash method whose parameters related to the excitation are investigated in terms of estimation capability. Among those parameters, the influence of the excitation/measurement face as well as the intensity and duration time of the pulse, will be studied.

The experimental setup, whatever the two possible measurements sides, is illustrated in Fig. 3.18.

3.6.3.2.1 Physical and Mathematical Formulation of the Model

To recall, the direct calculation of the rear and front face normalized harmonics $\xi_{m,n}(z = 0, p)$ and $\xi_{m,n}(z = l_z, p)$ is already presented in Eqs. 3.6 and 3.7.

3.6.3.2.2 Spatial shape of the thermal excitation: $F_{x,y}, F_{m,n}$

Regarding the spatial shape of the excitation, and for simplification reason, a previously tested distribution described by a polynomial cubic function and presented in 3.6.1 is considered in this case.

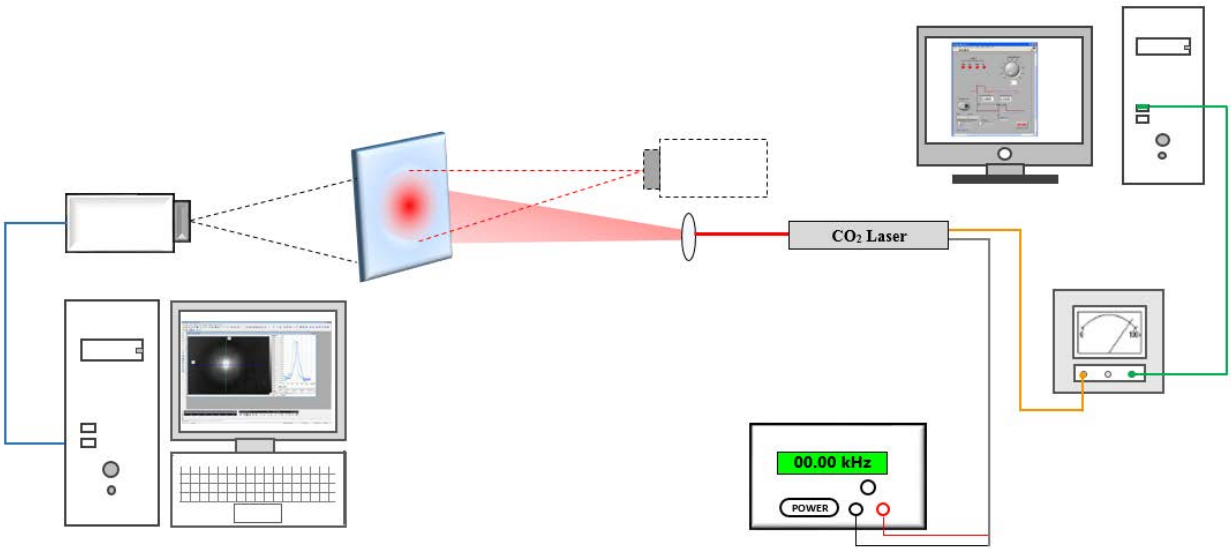

Figure 3.18 – Experimental setup overview.

3.6.3.2.3 Time shape of the thermal excitation: $u(t)$, $u(p)$

It is worth mentioning that the thermal excitation intensity should be carefully controlled, since it should generate a moderate temperature elevation through the overall system in order to consider the thermophysical properties (ρ, C) constant anywhere in the domain, at any time. Any important increase of the temperature could generate thermal dependence of these properties and the considered model will not be able to accurately describe the thermal behavior. On the other hand, the temperature elevation should be high enough to be accurately detected by the IR camera, especially when observing the rear face. The ratio signal over noise have to be checked in order to ensure a sufficient quality of measurements.

In this work, two time distributions, i.e. an ideal impulse (Dirac function) and a pulse (with duration time τ_{ex}), are considered to describe the laser beam thermal excitation dynamic 3.19.

The ideal impulse is considered using the Dirac function defined as:

$$u(t) = \delta(t) = \begin{cases} +\infty \text{ for } t = t_0 \\ 0 \text{ for } t \neq t_0 \end{cases} \tag{3.28}$$

In the Laplace domain, the impulse will give

$$u(p) = \int_0^\infty u(t) \cdot e^{-pt}\, dt = \int_0^\infty \delta(t) \cdot e^{-pt}\, dt = 1 \tag{3.29}$$

However the pulse will be expressed as

$$u(t) = \begin{cases} A \text{ for } t_0 \leq t \leq t_0 + \tau_{ex} \\ 0 \text{ elsewhere} \end{cases} \tag{3.30}$$

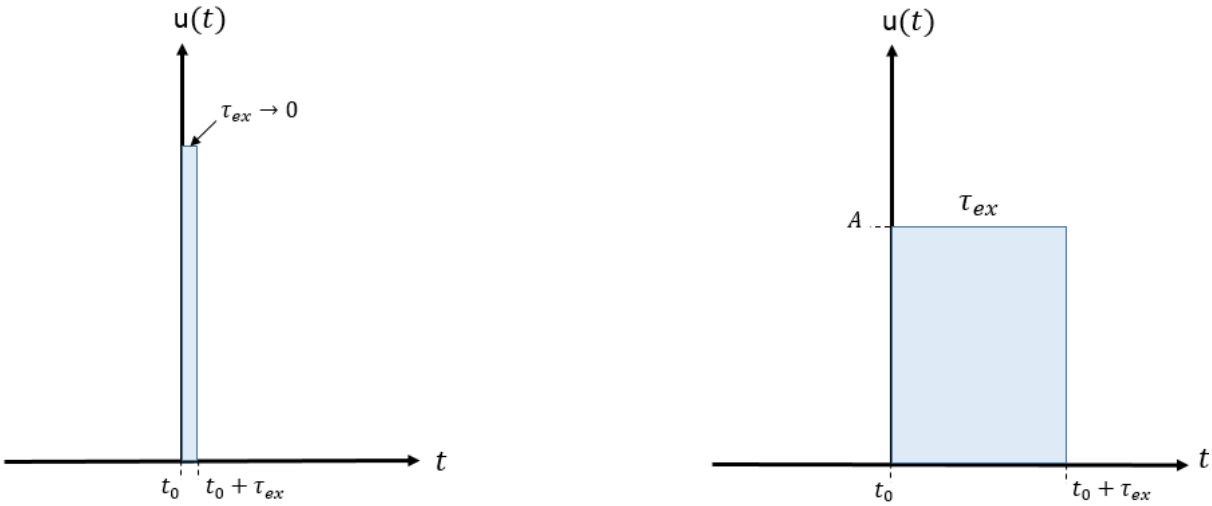

(a) Ideal impulse (dirac)

(b) Pulse of time duration τ_{ex}

Figure 3.19 – Thermal excitation time distribution.

leading in this case to

$$u(p) = \int_0^{\infty} u(t) \cdot e^{-pt}\, dt = A \cdot \left(\frac{1}{p} - \frac{e^{-p\tau_{ex}}}{p}\right) \cdot e^{-pt_0} \tag{3.31}$$

Where A is the amplitude of the signal, τ_{ex} is the duration of the CO_2 laser pulse and t_0 the initial excitation instant (set to zero here).

3.6.3.2.4 Resolution of the IHCP

The same strategy of resolution of inverse problem than used in section 3.3 is conducted here. It involves the same definition of the cost function as well as the same hybrid optimization algorithm. The set of parameters to estimate is represented by $\beta = [a_x, a_y, a_z, Q, r]$, since a predefined shape of the thermal excitation, parameterized by the amount of absorbed heat Q and the spot radius r, is assumed for simplification in this section.

3.6.3.3 Experimental & Numerical Results

3.6.3.3.1 Finite pulse time correction for experimental identification

As a first verification exercise, previous experimental measurements conducted on the front face of a sample subjected to a 10 ms pulse are used to estimate the thermal diffusivities of 2 distinct samples made of polyamide and Carbon Fiber Reinforced Polymer Composite (CFRP), respectively. The thermal characterizations, already conducted and validated in the previous section 3.4 where considering an impulse (Dirac function), are now repeated considering a finite pulse time correction with $\tau_{ex} = 10\ ms$. The comparison between the previous estimations and the present ones (with their relative deviations in brackets) are performed in Table 3.8.

The relative difference between both estimation does not exceed 5%. The most significant

Material	**polyamide**		**CFRP**	
Excitation type	Pulse $\tau_{ex} = 0.01s$	Impulse	Pulse $\tau_{ex} = 0.01s$	Impulse
a_x [mm^2.s^{-1}]	0.160 (−1.8%)	0.163	0.393 (−2.0%)	0.401
a_y [mm^2.s^{-1}]	0.163 (−1.2%)	0.165	2.535 (−2.1%)	2.590
a_z [mm^2.s^{-1}]	0.153 (2.0%)	0.150	0.875 (4.1%)	0.839

Table 3.8 – Values of the identified thermal diffusivities for the polyamide and CFRP using two possible shapes of thermal excitation.

difference occurs for the in-depth diffusivity estimation for the CFRP, with relative difference of 4.3%. The estimation performed while considering the impulse tends to underestimate the in-depth diffusivities, probably due to the underestimation of the excitation time duration. This underestimation may also be compensated in the other directions as the results clearly show an overestimation of the in-plane diffusivities. Both experimental and identified normalized harmonics evolution on the front face of the sample are compared for the 2 materials in Fig. 3.20 and Fig. 3.21, respectively.

Whatever the case, i.e. impulse or pulse excitation, the estimated normalized harmonics are close to the experimental ones as the parity plot illustrates. The two signals can hardly be distinguished from each other. For both cases, the worst fitting between experimental and estimated signals is observed in the mean field $\xi_{0,0}(t)$. As already discussed, this harmonic is known to be highly influenced by environmental factors. Previous test presented in Table 3.7, proved the possibility not to take into account this mean harmonic through the estimation, thus it could be excluded from the estimation procedure.

Regarding the consistency between the estimations, the implementation of the time correction in the estimation procedure may be considered as validated. This upgrade enable the possibility to use more realistic time evolution of the excitation, especially when measuring the rear face temperature evolution, as it will be discussed in the following sections.

Moreover, in order to have signals of the same order of magnitudes at the rear face (i.e. that could be detected by IR camera), and involve these information in the identification procedure, a severe increase in the front face temperature would be observed at short time when applying a similar duration of the very short thermal excitation. This increase in the temperature is not recommended because it may deteriorate the front face surface or it can lead to a thermal dependence of thermal properties.

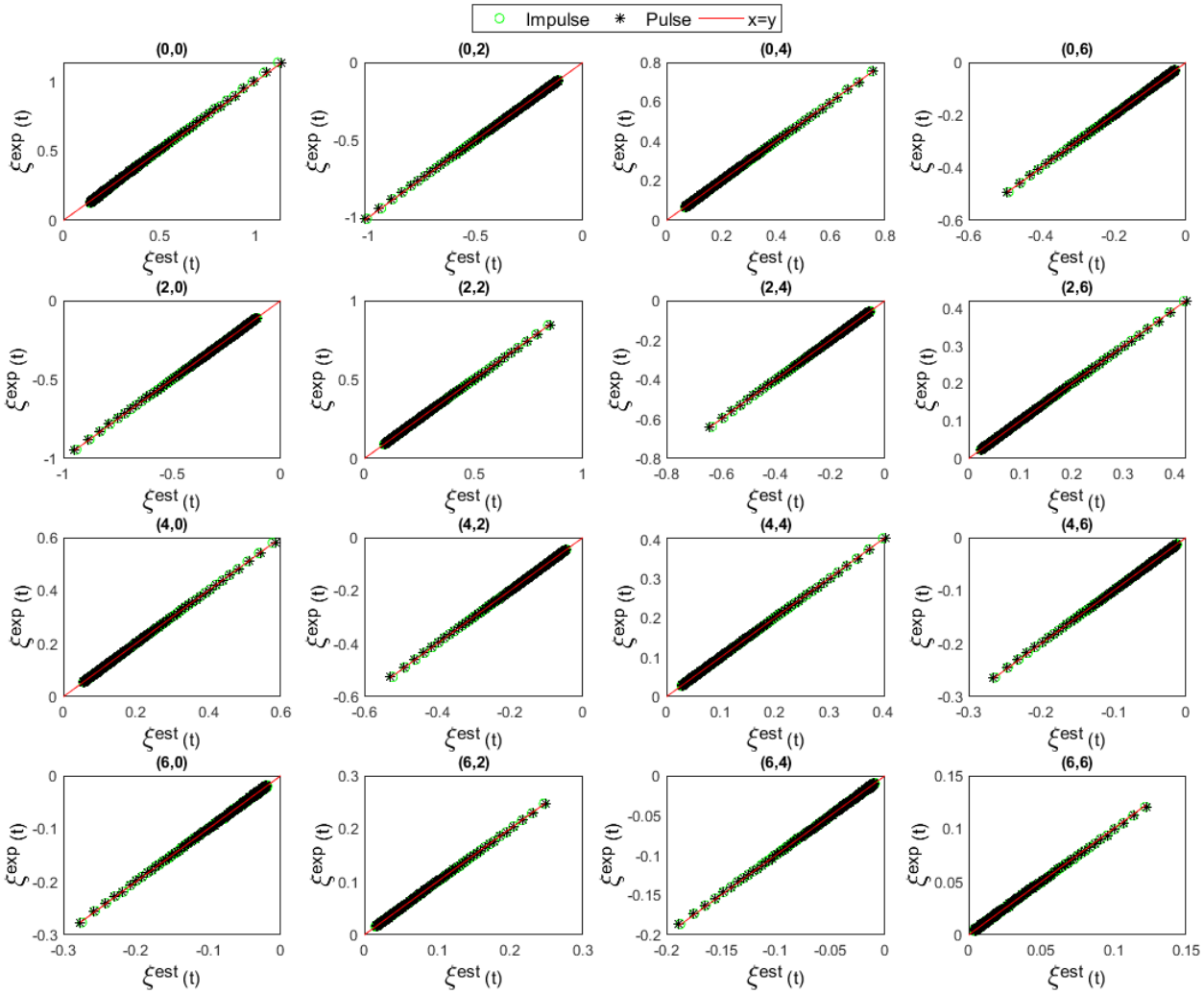

Figure 3.20 – Comparison between experimental and estimated normalized harmonics evolution using impulse (circle) and pulse (star) type excitation for the polyamide material.

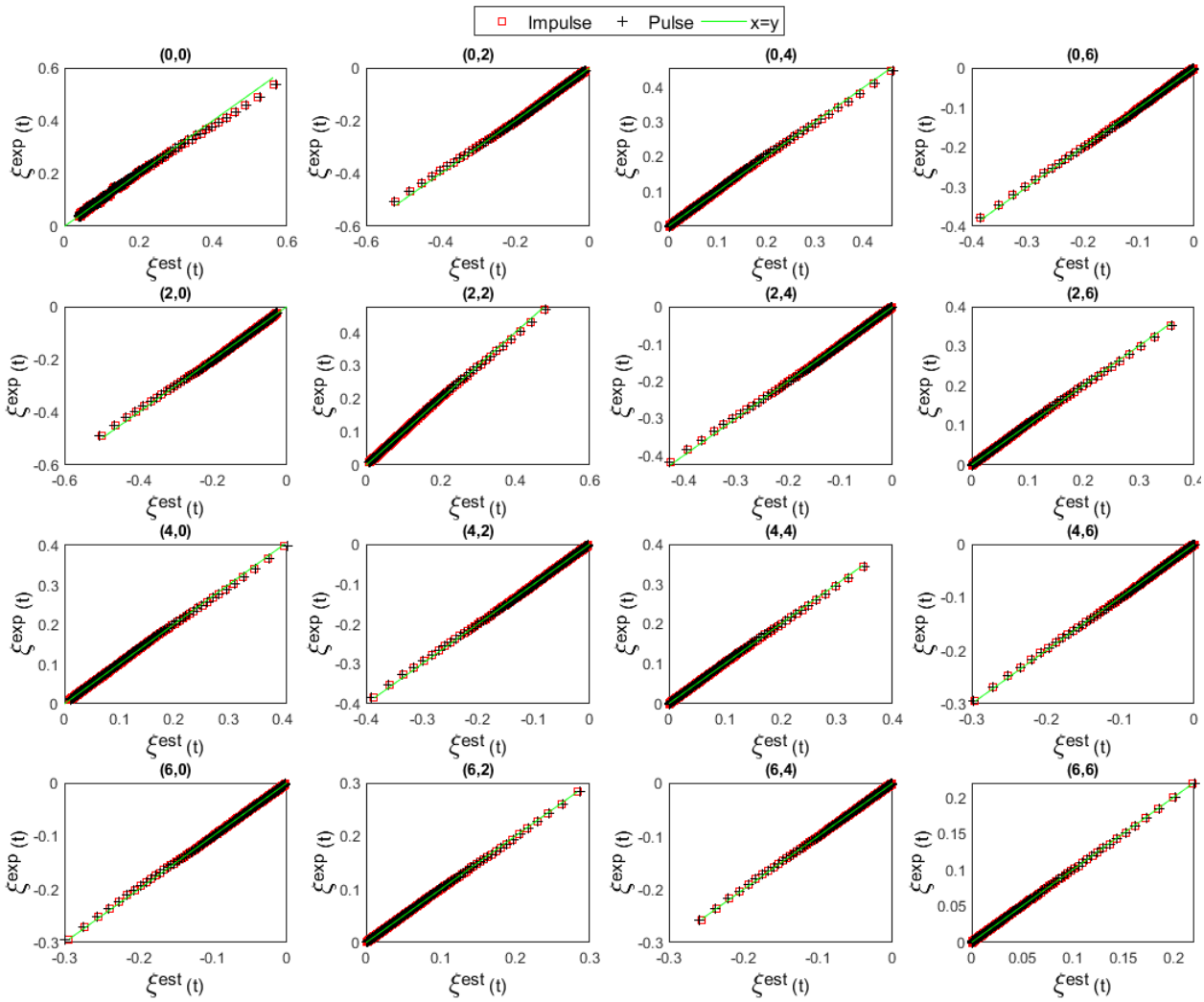

Figure 3.21 – Comparison between experimental and estimated normalized harmonics evolution using impulse (circle) and pulse (star) type excitation for the CFRP material.

3.6.3.3.2 Numerical experiment

This section is devoted to the design of an experiment that is based on the flash method, especially to set the optimal excitation time shape and duration, according to the examined measurement face. For this numerical exercise, the finite element code FlexPDE is used to mimic the experiment. In addition to the semi analytical approach, the same physical model is solved by means of finite element code. In order to compare accuracy and calculation time, a first set of calculation is performed as a function of the excitation duration time τ_{ex}, from 10^{-2} to 30 s. The evolution, regarding the excitation time duration τ_{ex}, of the semi analytical and numerical simulations calculation time, are plotted in Fig. 3.22. As the estimation is performed in the Fourier domains, i.e. in which the observables are $\xi_{m,n}(t)$, the present test is performed in the same space which requires the projection of the FlexPDE data into the Fourier space, following this equation:

$$\xi_{m,n}(t) = \frac{1}{l_x \cdot l_y} \int_0^{l_y} \int_0^{l_x} T^{exp}(x,y,z,t) \cdot cos(m \cdot \pi \frac{x}{l_x}) \cdot cos(m \cdot \pi \frac{y}{l_y}) \cdot dx \cdot dy \tag{3.32}$$

While the above step is quasi-instantaneous, the calculation time associated with FlexPDE simulations, i.e. to get $T^{exp}(x,y,z,t)$, is $2 \cdot 10^2 < t_{cpu} < 5 \cdot 10^2$ s. On the other hand, the calculation time associated with quasi analytical simulations is $t_{cpu} \approx 10^{-1}$ s (for 16 normalized harmonics), whatever the value of the excitation duration time. This first observation, as already discussed in 3.3.1, justifies the implementation, in the inverse problem resolution, of the direct analytical model instead of numerical codes less appropriate for experimental identification. Moreover, the deviation in $°C$ between both signals, defined as $\overline{err} = \frac{1}{(\frac{M}{2}+1)\cdot(\frac{N}{2}+1)} \cdot \sqrt{\sum_{m=0:2}^{6} \sum_{n=0:2}^{6} \sum_{t_i=t_0}^{t_{end}} [\xi_{m,n}^{exp}(t_i) - \xi_{m,n}^{est}(t_i)]^2}$ where $M = N = 6$ in our case, shows that numerical simulations introduce significant errors as the excitation duration time tends to small values. Analytical simulations are shown to be highly faster and more accurate than FlexPDE simulations. It is worth mentioning that other possible ways to express the observable, as the most intuitive physical form $T(x,y,z,t)$, is not investigated due to the highly time consuming-nature of the inverse Fourier transform that should be applied to the pseudo-analytical model data.

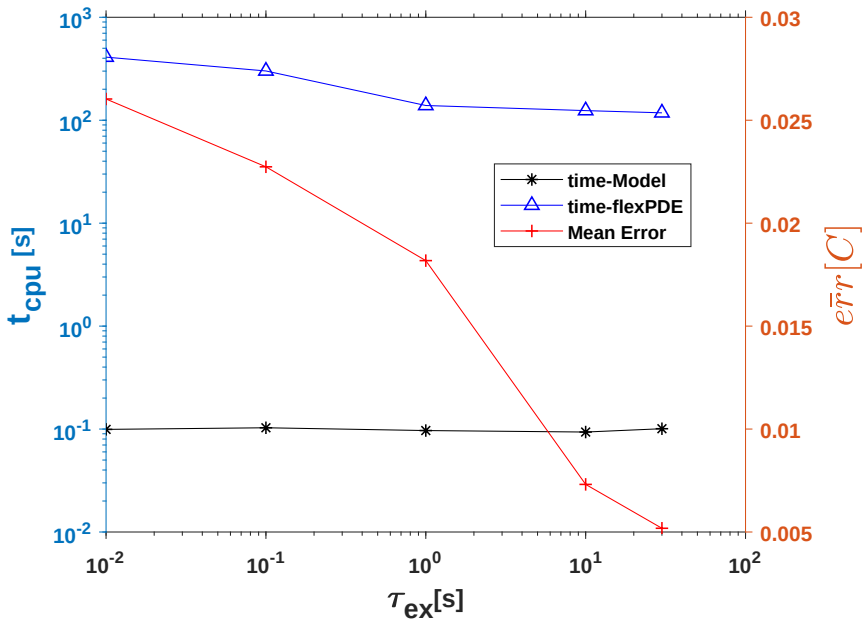

Figure 3.22 – Calculation time relative to both the pseudo-analytical and numerical simulations according to the excitation duration time τ_{ex}, with the average quadratic error between the two signals.

When experimentally applying a very short excitation, a high measurement acquisition frequency is required due to the extreme dynamic evolution of the temperature at very short time, i.e. during the excitation time plus the first instants of the cooling phase. For this reason, cases where $\tau_{ex} \leq 0.01$ s are not investigated here.

The following section is dedicated to the study of the influence of both the duration time

and energy delivered during the excitation, on the estimation efficiency.

3.6.3.3.3 Design of experiment

The present experiment, may be set in order to optimize its estimation capability. In this section, the parameters related to the excitation are studied to show the influence of the excitation and measurement faces as well as the intensity and duration time of the pulse. The analysis is conducted while keeping in mind the main ideas behind flash methods:

1. Temperature elevations should be moderate in order to keep the thermophysical properties (i.e. a, ρ, C) constant in time and space. Moreover, very high temperature may deteriorate the surface of the material which would harm the estimation consistency. An elevation of about $20°C$ is considered reasonable.

2. The maximum temperatures reached at the measurement face should be high enough so that the signal over noise ratio is sufficient for such exercise. From previous experimental observation noise level is considered within this range $[-0.1°C; +0.1°C]$. Therefore the signal, i.e. the relative temperature evolution, should be $|\Delta T| \geq 1°C$ in order to have a ratio ≥10.

In this section, the result of simulations performed using different excitation duration times τ_{ex} and different amount of energy absorbed by the sample Q, are compared in terms of maximum temperature reached on the front and rear faces. The values of the fixed parameters of the present study are presented in Table 3.9. Those parameters are set thanks to measured or identified values through previous experimental identification performed on CFRP composite materials, and presented in 3.4.2.

Parameters	**Values**
$[a_x, a_y, a_z]$	$[0.4; 2.6; 0.8]\ mm^2 \cdot s^{-1}$
l_z	$8.16\ mm$
l_x	$39\ mm$
l_y	$45\ mm$
C	$1001\ J \cdot kg^{-1} \cdot K^{-1}$
ρ	$1286\ kg \cdot m^{-3}$
r	$\frac{l_x}{7}\ mm$

Table 3.9 – Values of the parameters required for the numerical and analytical simulations and the sensitivity analysis.

Table 3.10 shows both the front and rear maximum central temperature, i.e. at $x = \frac{l_x}{2}$, $y = \frac{l_y}{2}$, $z = 0$ or l_z respectively, for different laser pulse durations $0.1 \leq \tau_{ex} \leq 30$ s and different amount of enegy $0.1 < Q < 100$ J.

Measurement face	**Front face flash method**				**Rear face flash method**			
$\tau_{ex}[s]$ / Q[J]	$0.1s$	$1s$	$10s$	$30s$	$0.1s$	$1s$	$10s$	$30s$
0.1	9.28	2.71	0.516	0.20	0.0264	0.0264	0.0257	0.0220
1	92.7	27.1	5.16	2	0.264	0.264	0.257	0.220
10	941	271	51.6	20	2.64	2.64	2.57	2.20
100	9301	2710	516	200	26.4	26.4	25.7	22.0

Table 3.10 – Front and rear maximum temperature evolution (in ° C) at the center of the material, for different laser pulse durations τ_{ex} and amount of the heat subjected on the surface of the material Q (J).

The shaded cells correspond to the cases that respect both conditions (1 and 2) mentioned above. One can deduce from Table 3.10, that for a fixed amount of energy Q, the rear face temperature elevation will be substantially the same whatever the excitation pulse duration time. Whereas an increase of the excitation pulse duration time will significantly decrease the temperature elevation at the front face, mainly due to convective and diffusion effects. An increase in the amount of excitation energy will proportionally increase the temperature elevation on both faces. When submitting the sample to a brief excitation, whose limiting case is the impulse excitation i.e. $\tau_{ex} \to 0$, is found to be inappropriate for rear face estimation. In such case, measuring a non-negligible temperature elevation implies a relatively large amount of heat Q (e.g. 10 J) leading to a very high temperature elevation at the front face (e.g. 941°C). On the other side, a low amount of heat leads to a low level of rear face temperature elevation which may be difficult to differentiate from the measurement noise. Among all investigated cases, only two can be considered as suitable ($Q = 10$ J, $\tau_{ex} \geq 10$ s) in terms of measurement accuracy at the rear face and temperature elevation level at the front face. Those points will be discussed in more details in the following sections. The next sections is dedicated to the analysis of the optimum cases i.e. whose excitation intensity is $Q = 10$ J. An evaluation of several strategies to inject this amount of energy in the system is conducted.

Temperature evolution as a function of pulse duration time τ_{ex}

A comparison of temperature evolution in responses to laser pulses of different duration times has been conducted in order to deduce the most convenient setup for an identifica-

tion purpose. This comparison is performed in both physical (i.e. by means of $T(x,y,z,t)$), and transformed (i.e. by means of $\xi_{m,n}(t)$) domains as shown in Fig. 3.23. According to real physical temperature elevation behaviors, at the center of the material front or rear face $T(\frac{l_x}{2},\frac{l_y}{2},z=0 \text{ or } l_z,t)$, shown in Fig. 3.23a, the signal can be experimentally detected at the rear face as its magnitude is about $2.5°C$, whatever the pulse duration time τ_{ex}. However, for pulse duration time τ_{ex} below 10 s significant front face temperature elevations are observed which is a sensitive point regarding the thermal dependence of the material properties. Thus, one should realize that when measuring the temperature evolution at the rear face, imposing a thermal disturbance with a pulse duration time $\tau_{ex} \geq 10$ s (in this particular case), instead of an impulse or short pulses is better suited for a successful parameter estimation. In that case, an equivalent temperature elevation occurs at the rear face associated with a moderate temperature elevation at the front face, allowing to keep the constant thermophysical properties hypothesis valid.

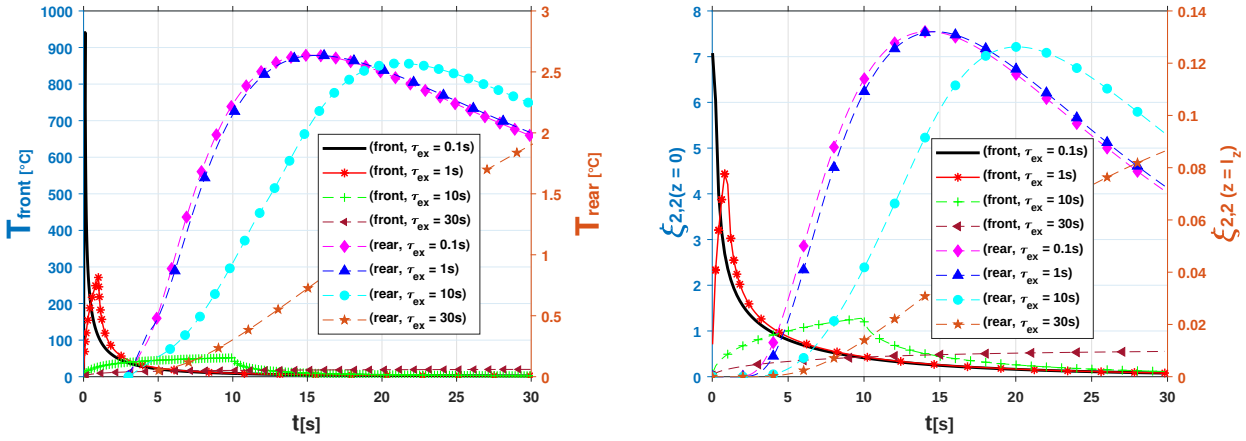

(a) Temperatures evoltuions

(b) Normalized harmonics evolutions

Figure 3.23 – Temperatures and normalized harmonics (m=n=2) evolution at the front and rear for different pulse durations when applying an amount of energy Q= 10J.

For brevity and illustrative reasons, only the harmonic $m=n=2$ (reference mode) is plotted in Fig. 3.23b. The same observations, as discussed in the physical domain, can be made which confirms the setting for a proper identification. The next section is dedicated to the analysis of sensitivities of both front and rear face temperature evolutions to thermal diffusivity parameters for the different excitation duration time under investigation, $0.1 \leq \tau_{ex} \leq 30$ s.

Measurement faces comparison based on sensitivity analysis

A sensitivity analysis of the front (Fig. 3.24) and rear (Fig. 3.25) faces temperature evolution to the thermal diffusivities is performed. The present analysis is restricted to the thermal diffusivity tensor and conducted for different pulses duration time and for a fixed value of heat absorbed by the material $Q = 10$ J. For brevity and illustrative reasons, only the first even harmonics $(M,N \leq 0,2)$, and the pulses of $\tau_{ex} = [0.1, 10, 30$ $s]$ are plotted in Figs. 3.24 and 3.25

thereafter.

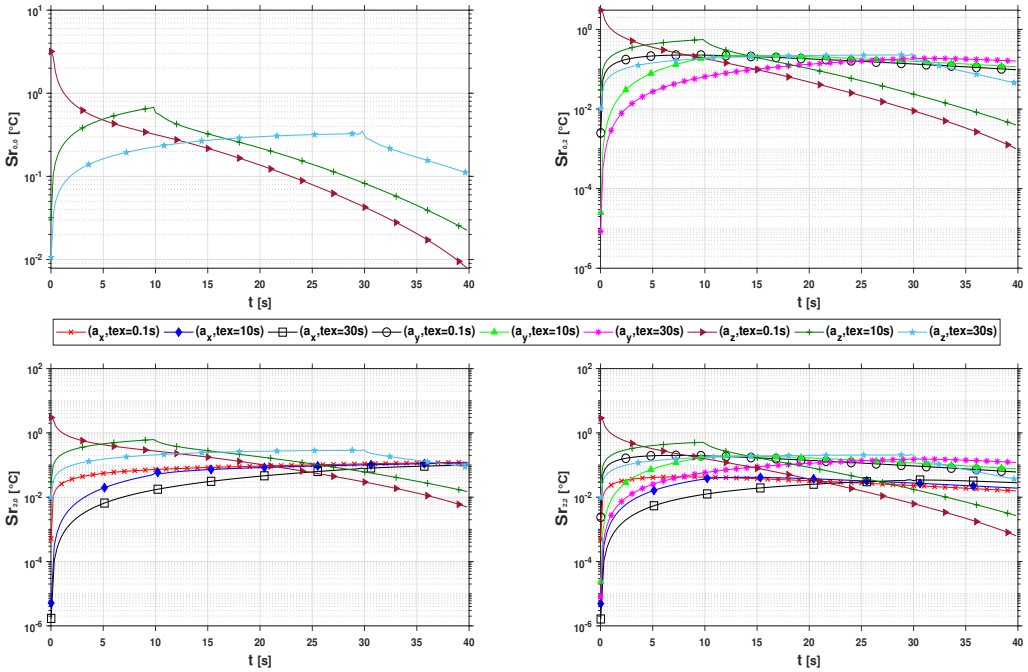

Figure 3.24 – Reduced sensitivities of the front first four even normalized harmonics to the composite diffusivities (a_x, a_y, a_z), as a function of the laser pulse duration time (0.1, 10 and 30 s).

Due to the very wide temperature range implied on the sample front face, depending on the excitation duration time, a logarithmic scale is used (Fig. 3.24). For this case, the sensitivities of the three diffusivity components appear to be relatively correlated, whatever the excitation duration time and the harmonic under consideration. This observation suggest estimation difficulties as the three components act in a similar way on the temperature response on the front face. When considering the rear face, the sensitivity of the harmonics to any parameter (a_x, a_y, a_z), are slightly affected, in terms of amplitude of the temperature response, by the duration of the excitation (Fig. 3.24). Moreover, the longer the excitation is, the less the signal are correlated. For those reasons, the rear face is more convenient for the simultaneous estimation, due to the stronger decorrelation between sensitivities. This is especially observed for the in-depth diffusivity a_z, whose decorrelation with in-plane diffusivities (a_x, a_y) increase with the excitation duration time. The present sensitivity analysis highlights:

– The benefits of a rear face estimation strategy, which decorrelates the sensitivities, especially the in-depth with the in-plane diffusivities.

– The importance of significant pulse durations, typically $\tau_{ex} \geq 10\ s$, when measuring the rear face temperature evolution. This ensures an optimum signal decorrelation for a correct simultaneous estimation.

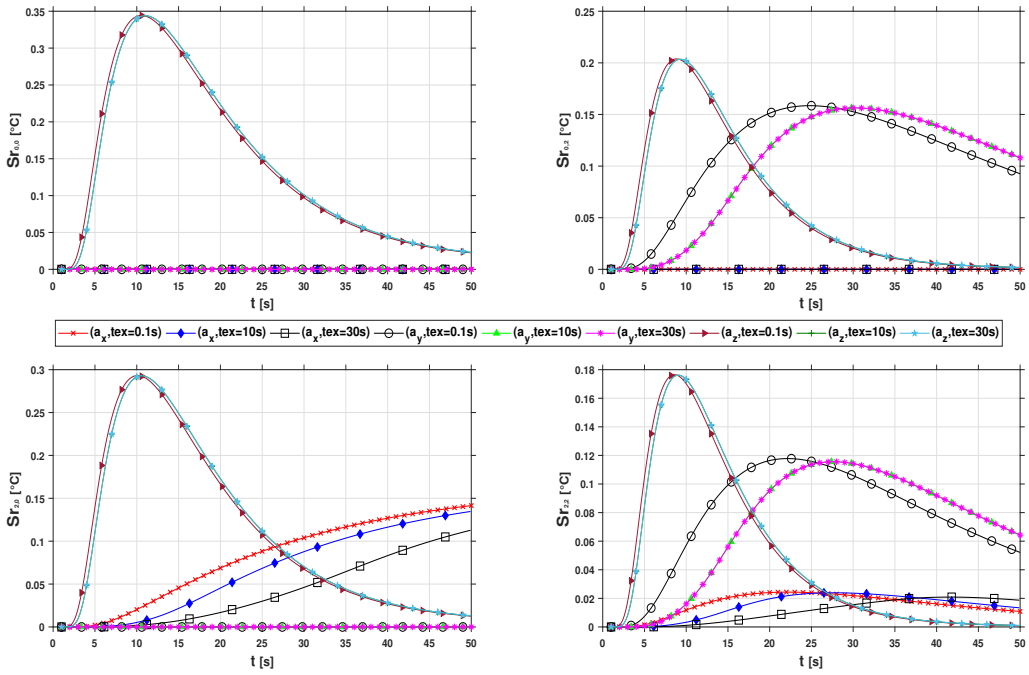

Figure 3.25 – Reduced sensitivities of the rear first four even normalized harmonics to the composite diffusivities (a_x, a_y, a_z), as a function of the laser pulse duration time (0.1, 10 and 30 s).

3.6.3.3.4 Application to noisy data

The numerical identification of the required parameters using the direct model and synthetic data generated by the finite element code FlexPDE follows the procedure presented in Fig. 3.26.

The general procedure is constructed in order to minimize the difference between the signal reached by the direct model $\xi^{mod}_{m,n}(z=0,t)$ or $\xi^{mod}_{m,n}(z=l_z,t)$ and that obtained by the numerical finite element code (FlexPDE) $\xi^{exp}_{m,n}(z=0,t)$ or $\xi^{exp}_{m,n}(z=l_z,t)$. The present analysis, consisting in estimating parameters following the proposed procedure, is performed on the same basis as previously, i.e. i) the input parameters are set following the values presented in Table 3.9, ii) the thermal excitation is fixed in terms of amount of heat absorbed by the material, $Q = 10\ J$, iii) the duration time of the pulse varies $0.1 \leq \tau_{ex} \leq 30\ s$. Pseudo experimental data are generated by means of FlexPDE for which an additional noise is added to the initial signal in order to reproduce more or less severe experimental conditions. The noise intensity is derived from a statistical analysis performed on front temperature measurements that are achieved through experimental protocol close to the present configuration. The original signal, corresponding to the temperature elevation evolution at the central point of the exposed face, is processed using the least-squares smoothing filter Savitsky-Golay algorithm [252]. The parameter of the algorithm has been set on a polynomial basis of degree 3. The difference between the original signal and the smoothed signal allows to display the noise, see Fig. 3.27. The plot of the noise intensity level distribution reveals a Gaussian like distribution, see Fig. 3.28. In this case, the evaluation

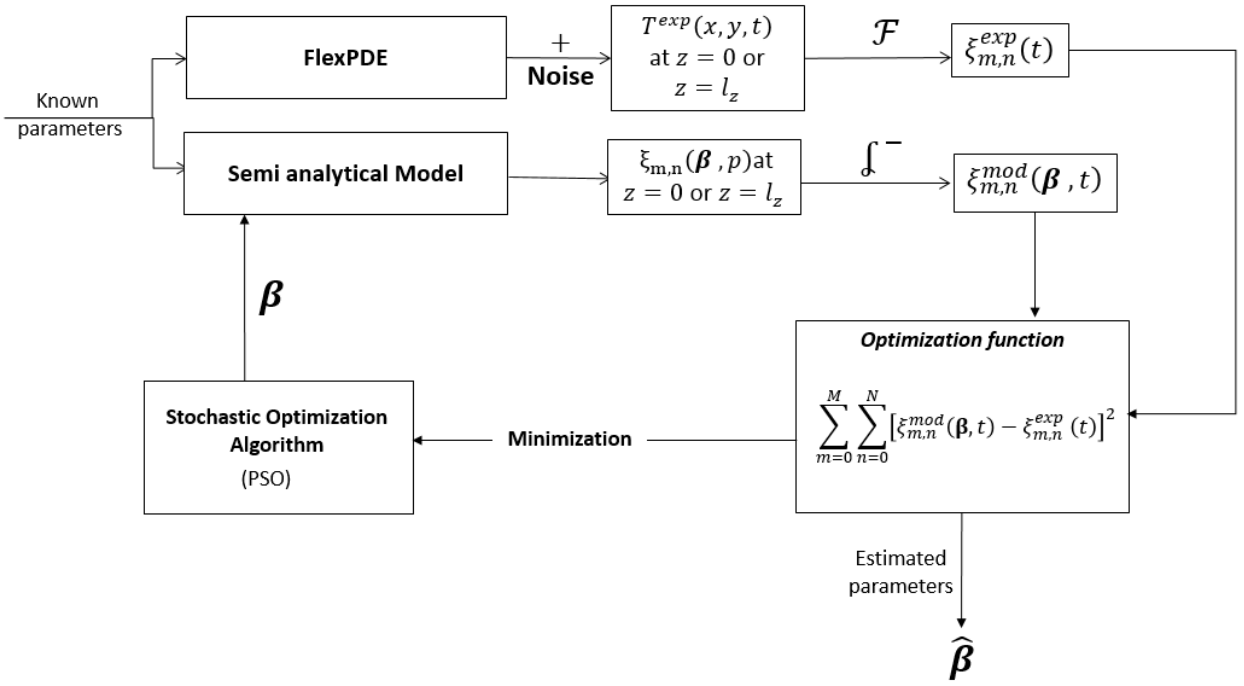

Figure 3.26 – General principle of the identification procedure consisting in finding the set of parameter β minimizing the differences between the synthetic projected data ξ^{exp} and the inverse projected model output ξ^{mod}.

of the standard deviation and mean value gives: $\mu = 4.4479 \cdot 10^{-4}\ °C$ and $\sigma = 0.0223\ °C$, respectively. Those values, deduced from experimental observations, are used hereafter to mimic actual data.

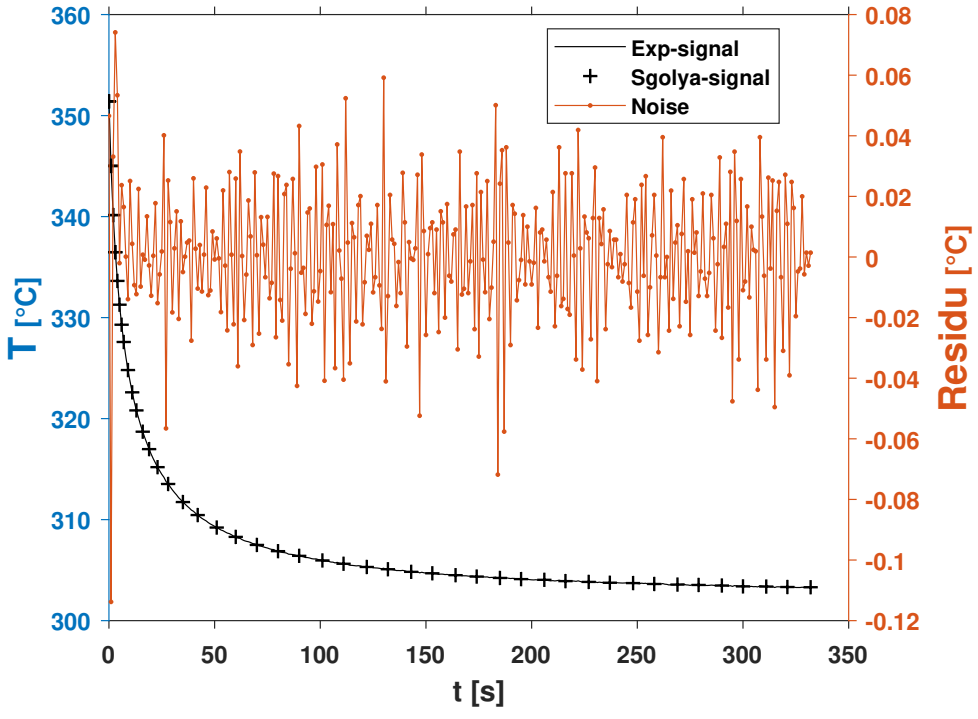

Figure 3.27 – Raw and filtered experimental signals revealing the noise level.

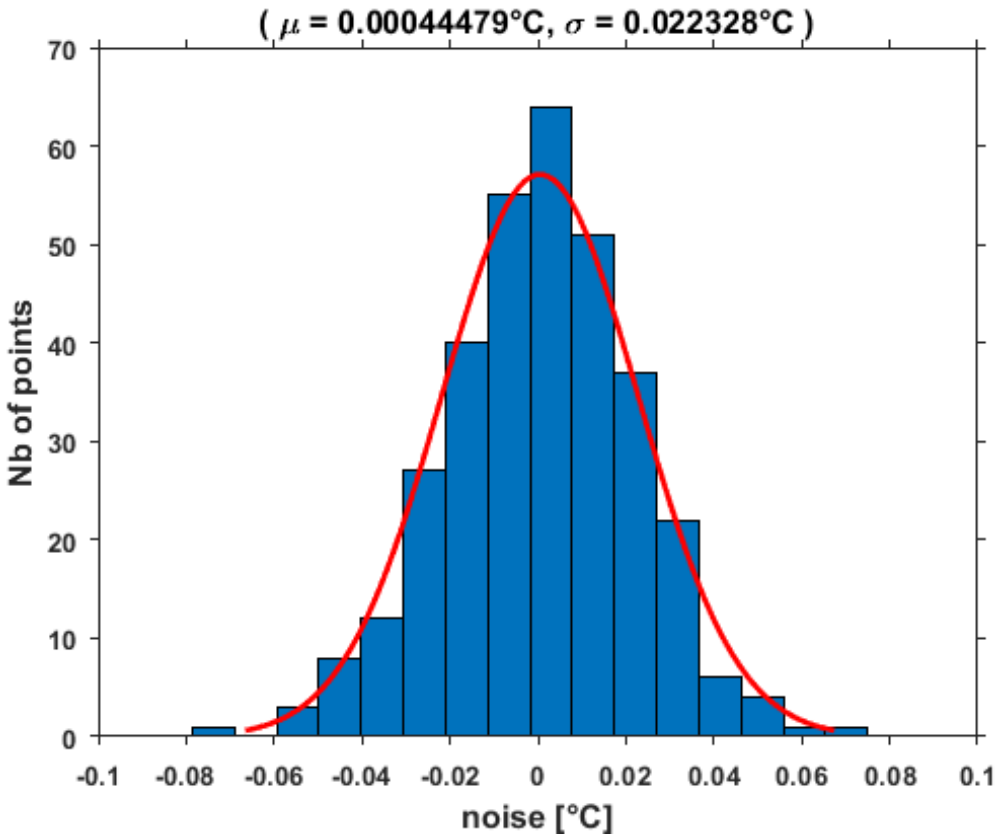

Figure 3.28 – Distribution of the noise intensity level.

A noisy signal is generated using random number generator following a Gaussian distribution that is parametrized thanks to the previously discussed result. The noise is then added to the simulation results achieved using FlexPDE, for both strategies (front face and rear face flash method) and various excitation durations (see Table 3.11).

Measurement face	**Front face flash method**				**Rear face flash method**			
$\tau_{ex}[s]$ / Relative deviation	$0.1s$	$1s$	$10s$	$30s$	$0.1s$	$1s$	$10s$	$30s$
$\frac{\lvert\Delta a_x\rvert}{a_x}$	6.7%	3.4%	3.7%	1.3%	1.3%	1.1%	2.8%	1.1%
$\frac{\lvert\Delta a_y\rvert}{a_y}$	7.0%	4.5%	3.2%	1.4%	0.9%	0.9%	0.8%	0.1%
$\frac{\lvert\Delta a_z\rvert}{a_z}$	11.9%	6.7%	1.1%	5.9%	1.9%	1.7%	0.7%	1.1%

Table 3.11 – Relative deviation between estimated and actual values of the CFRP diffusivities $\overline{\overline{a}} = [0.4; 2.6; 0.8]\ mm^2 \cdot s^{-1}$, for the front and rear face flash methods.

As shown in Table 3.11, the shortest excitation case ($\tau_{ex} = 0.1$ s) corresponds to the highest estimation errors, disregarding the direction (in-depth or in-plane). This observation is con-

sistent with previous observations (see Fig. 3.22 for instance), mainly due to the numerical approach that produces noisy signal at short time which is a kind of numerical approaches limitations. The low relative deviation values between the actual and the estimated parameters confirm the validity of the method and proves its robustness to experimental noise. The method is, as previously observed, more efficient in its rear face version, as the relative deviation values are significantly lower than those obtained within the front face strategy. This assessment is valid whatever the pulse duration time and confirms the previous discussion on the sensitivity analysis. To complete this analysis, the front and rear face normalized harmonics are plotted in the following Figs. 3.29 and 3.30, considering the case where $\tau_{ex} = 10\ s$. This case was found to be one of the most appropriate cases, in terms of experimental feasibility, moderate temperature elevations at the front face and measurable temperature change at the rear face. The front and rear faces normalized harmonics evolution generated by means of FlexPDE simulations, with some added noise, are compared with the reconstructed signals thanks to the estimated parameters in Figs. 3.29 and 3.30.

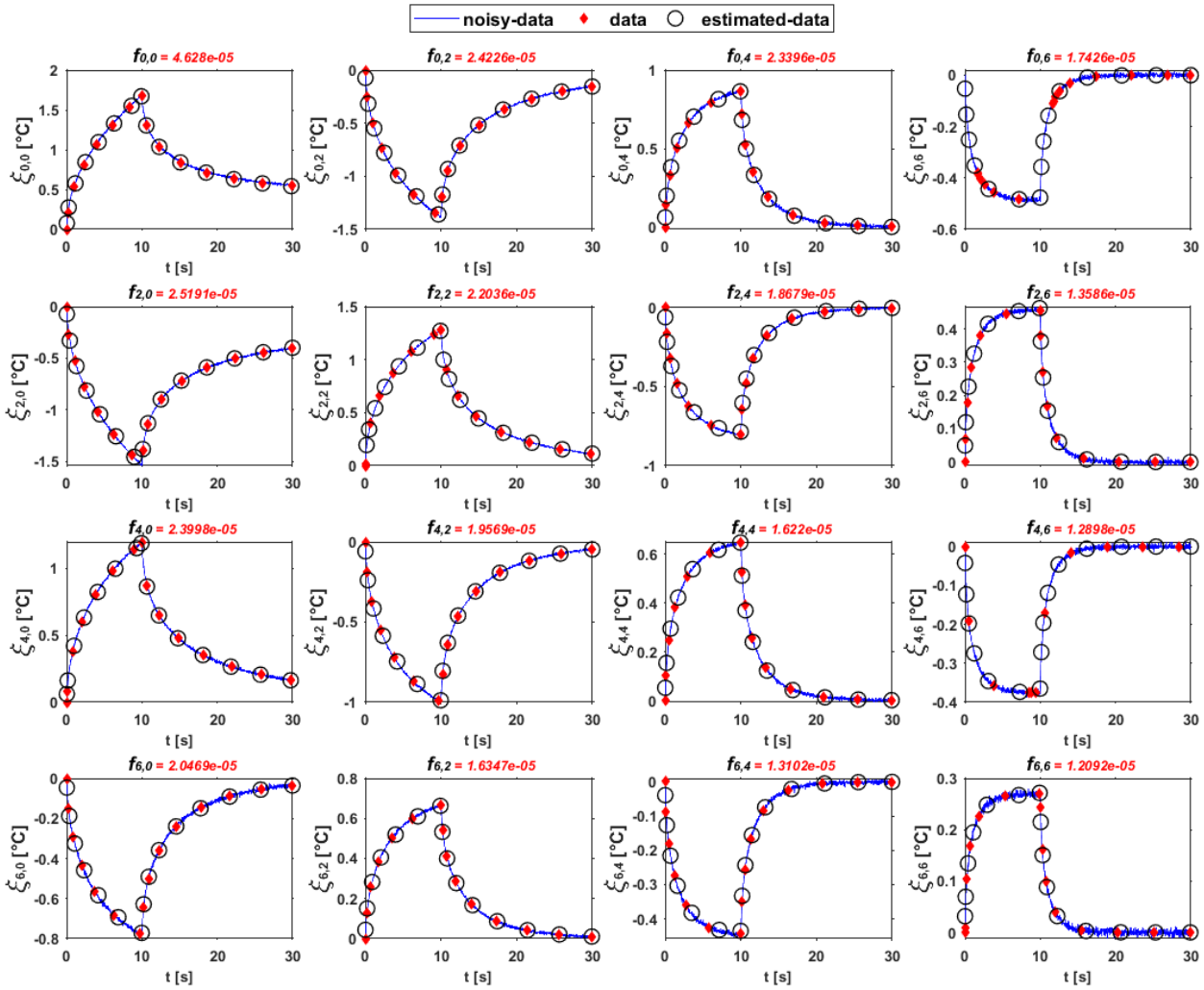

Figure 3.29 – Front face normalized harmonics evolution related to synthetic experimental data (raw data and noisy data simulated by FlexPDE) and reconstructed data by means of estimated parameters, for Q=10J and $\tau_{ex} = 10$ s.

In addition to these signals, the deviation matrix representing the cost function is calculated

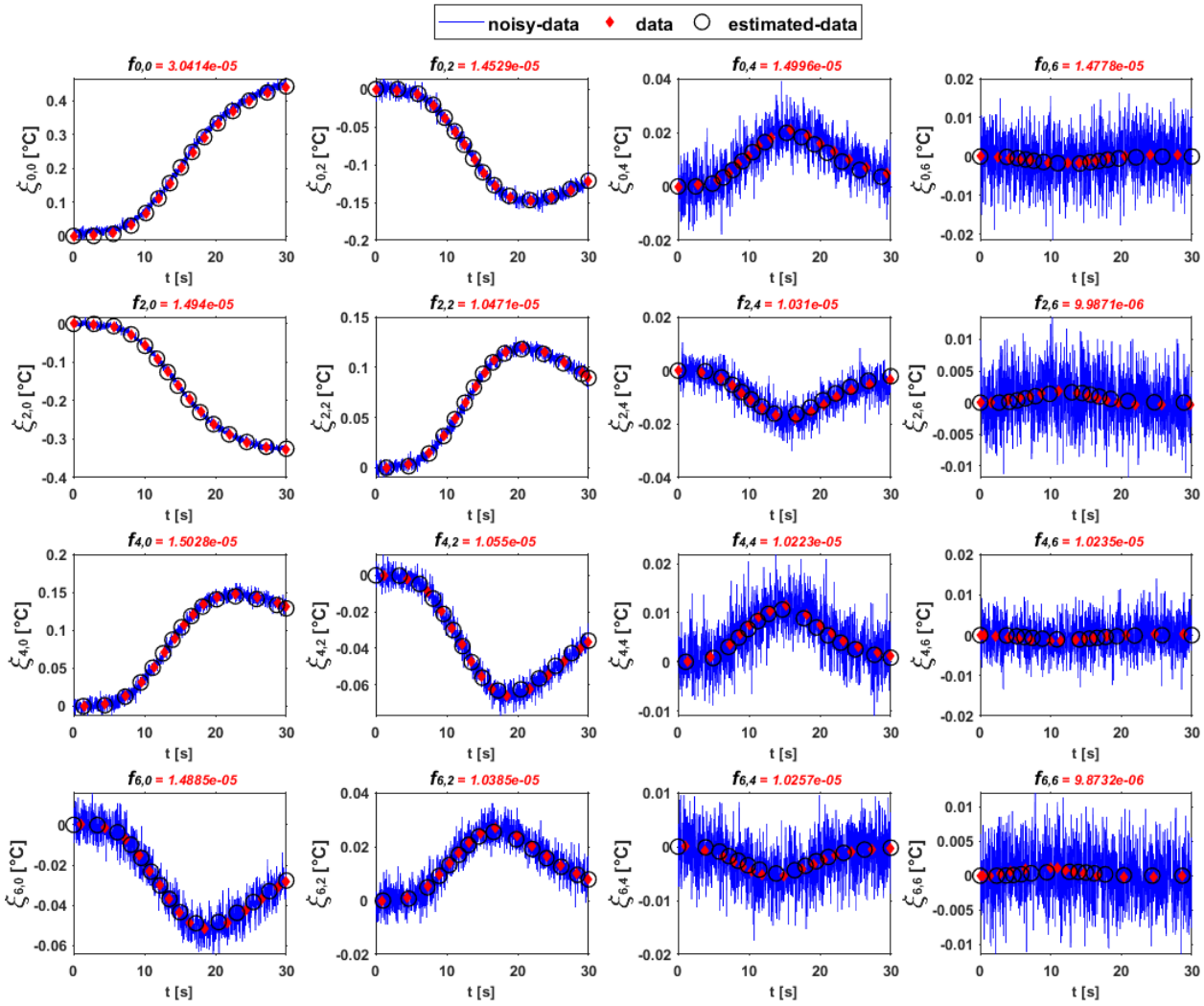

Figure 3.30 – Rear face normalized harmonics evolution related to synthetic experimental data (raw data and noisy data simulated by FlexPDE) and reconstructed data by means of estimated parameters, for Q=10J and τ_{ex} = 10 s.

for each harmonics, as following $f_{m,n} = \frac{1}{N_t}\sqrt{\sum_{t_i=t_0}^{t_{end}}[\xi_{m,n}^{exp}(t_i) - \xi_{m,n}^{est}(t_i)]^2}$ in $^\circ C$, where N_t is the size of the time vector. The agreement between the experimental and the estimated data, while better in the front face case, is still very good for the rear face case, even with the relatively large noise level. The increasingly observed noise with the harmonics index at the rear face does not affect much the identification as the relative error values are comparable with those obtained at the front face.

The overall identification method is verified, in terms of estimation feasibility and optimization algorithm accuracy. One can conclude that the proposed method succeeds in retrieving the original data parameters even for the rear face when having relatively high additional noise level, compared to the low initial signal at this face.

3.7 Other approaches to estimate additional thermophysical properties

In this section, some alternative estimation strategies are investigated and their feasibility tested, using numerical validation by means of noisy synthetic measurements generated by the model or by the finite element code (flexPDE). An experimental application has been conducted in order to verify the feasibility, and accuracy of the estimation strategies. These strategies consist in identifying, simultaneously and in addition to thermal diffusivities, the product $\rho \cdot C$ when knowing the energy Q, or estimating the thermal diffusivity tensor without knowing the value of the product $\rho \cdot C$ of the material.

Those studies have been conducted on the CFRP monolayer material, previously characterized in 3.4.2, and using the thermophysical properties previously measured or identified.

The stages of the verification are presented below:

1. Synthetic noisy data (Inverse crime) with a random noise of Gaussian distribution (σ = 0.25°C), and an intensity level of 5 % of the initial signal.

2. FlexPDE finite element code, with a noise coherent with experimental observation (as presented in 3.6.3.3) that is added to the original signal before minimization procedure.

3. Reconduction of previous experimental measurements, already conducted for the CFRP estimation in 3.4.2.

3.7.1 Simultaneous identification of $\beta = [a_x, a_y, a_z, \rho \cdot C, r]$, knowing Q for a predefined shape

Some excitation techniques can control the amount of heat subjected to the material. Moreover, a perfect knowledge of the radiative surface properties, allows to quantify the energy absorbed by the sample. In such case, the shape of the excitation can be predefined and estimating $\rho \cdot C$ and r is found to be quite easy to achieve.

The results obtained by means of numerical simulation (to mimic measurements) are tabulated in Table 3.12. Those obtained by means of FlexPDE are presented in Table 3.13, and the experimental results with their relative deviations from the previous estimation results conducted with a predefined cosine shape in Table 3.4, are in Table 3.14.

In all these cases: $Q = 0.71$ J is the value already obtained in previous experimental identifications, and the predefined shape considered here is parameterized using the cosine function (see 3.6.1).

The small deviations between the CFRP estimated thermal properties (thermal diffusivities and the volumetric heat capacity) and and the previous value presented in 3.4.2, 3.6 and Table 3.4 in the three cases, prove the feasibility and the accuracy of the proposed estimation strategy.

Relative deviation	$\frac{\lvert\Delta \mathbf{a_x}\rvert}{\mathbf{a_x}}$	$\frac{\lvert\Delta \mathbf{a_y}\rvert}{\mathbf{a_y}}$	$\frac{\lvert\Delta \mathbf{a_z}\rvert}{\mathbf{a_z}}$	$\frac{\lvert\Delta \rho\cdot \mathbf{C}\rvert}{\rho\cdot \mathbf{C}}$
Impulse (front face)	$5.6\cdot10^{-3}$%	$3.3\cdot10^{-3}$%	$2.7\cdot10^{-3}$%	$1.0\cdot10^{-4}$%
Impulse (rear face)	$1.2\cdot10^{-2}$%	$7.7\cdot10^{-3}$%	$2.65\cdot10^{-3}$%	$4.7\cdot10^{-2}$%
Pulse ($\tau_{ex}=3s$, front face)	$1.7\cdot10^{-1}$%	$1.7\cdot10^{-1}$%	$4.79\cdot10^{-2}$%	$3.28\cdot10^{-1}$%
Pulse ($\tau_{ex}=3s$, rear face)	$7.67\cdot10^{-3}$%	$1.13\cdot10^{-3}$%	$1.89\cdot10^{-3}$%	$2.91\cdot10^{-2}$%

Table 3.12 – Estimation results using synthetic measurements where Q is already known ($Q=0.71\ J$), and excitation shape is predefined, CFRP properties: $\overline{\overline{a}}=[0.4;2.6;0.8]\ mm^2\cdot s^{-1}$ and $\rho\cdot C=1287\ KJ\cdot m^{-3}\cdot K^{-1}$.

Relative deviation	$\frac{\lvert\Delta \mathbf{a_x}\rvert}{\mathbf{a_x}}$	$\frac{\lvert\Delta \mathbf{a_y}\rvert}{\mathbf{a_y}}$	$\frac{\lvert\Delta \mathbf{a_z}\rvert}{\mathbf{a_z}}$	$\frac{\lvert\Delta \rho\cdot \mathbf{C}\rvert}{\rho\cdot \mathbf{C}}$
Pulse ($\tau_{ex}=1s$, front face)	4.55%	4.90%	5.42%	2.24%
Pulse ($\tau_{ex}=1s$, rear face)	0.37%	0.78%	1.91%	3.41%
Pulse ($\tau_{ex}=10s$, front face)	1.98%	2.69%	6.81%	1.47%
Pulse ($\tau_{ex}=10s$, rear face)	3.73%	0.94%	0.35%	9.69%

Table 3.13 – Estimation results by means of flexPDE measurements where Q is already known ($Q=0.71\ J$), and excitation shape is predefined, CFRP properties: $\overline{\overline{a}}=[0.4;2.6;0.8]\ mm^2\cdot s^{-1}$ and $\rho\cdot C=1287\ KJ\cdot m^{-3}\cdot K^{-1}$.

Unknown values	**Flash experiment (τ_{ex} = 10 ms, front face)**	**Previous values from Table 3.4**
a_x [mm^2.s^{-1}]	0.493 (−1.40%)	0.500
a_y [mm^2.s^{-1}]	2.409 (+1.65%)	2.370
a_z [mm^2.s^{-1}]	0.893 (−1.00%)	0.902
ρC [$KJ\cdot m^{-3}\cdot K^{-1}$]	1377 (+6.99%)	1287 (measured)

Table 3.14 – Estimation results using previous experimental data, where Q is already known ($Q=0.71\ J$), and excitation shape is predefined, compared to the estimation results with a predefined cosine shape presented in Table 3.4.

3.7.2 Simultaneous identification of $\beta = [a_x, a_y, a_z, \frac{Q}{\rho \cdot C}]$ for a predefined shape at short time or under vacuum

At short time, the influence of the overall heat transfer coefficient h is quasi-negligible as already proved in 3.4.3.2, thus this coefficient can be assumed null $h = 0\ W \cdot m^{-2} \cdot K^{-1}$). This condition correspond to an experiment performed under vacuum with a limitation of radiation effects (low temperature elevation). When neglecting the heat losses by natural convection and radiation with the environment, the model can be degenerated. Front and rear face normalized harmonics can be expressed as following:

$$\xi_{m,n}(z=0,p) = \frac{Q \cdot F_{m,n} \cdot u(p) \cdot \cosh(l_z \cdot K_{m,n})}{l_x \cdot l_y \cdot \rho \cdot C \cdot a_z \cdot K_{m,n} \cdot \sinh(l_z \cdot K_{m,n})} \tag{3.33}$$

$$\xi_{m,n}(z=l_z,p) = \frac{Q \cdot F_{m,n} \cdot u(p)}{l_x \cdot l_y \cdot \rho \cdot C \cdot a_z \cdot K_{m,n} \cdot \sinh(l_z \cdot K_{m,n})} \tag{3.34}$$

Except under vacuum condition with negligible radiation effects, the assumption of neglected overall heat transfer coefficient is only valid at short time. Thus, this method is only valid for the front face measurement, which is not sensitive to the heat transfer coefficient. When working under vacuum, with particular radiative condition, such coefficient can be neglected for front and rear face measurements.

Moreover, in the case where the excitation shape is predefined, the additional parameter that can be estimated is $\frac{Q}{\rho \cdot C}$. Results obtained using simulated results are tabulated in Table 3.15, those obtained using flexPDE are tabulated in Table 3.16. Experimental results and their relative deviations from the previous estimation results conducted with a predefined cosine shape in Table 3.4, are presented in Table 3.17.

The very good agreements between estimated values and the original one prove the accuracy and the feasibility of the proposed estimation method.

Relative deviation	$\frac{\lvert\Delta \mathbf{a_x}\rvert}{\mathbf{a_x}}$	$\frac{\lvert\Delta \mathbf{a_y}\rvert}{\mathbf{a_y}}$	$\frac{\lvert\Delta \mathbf{a_z}\rvert}{\mathbf{a_z}}$	$\frac{\lvert\Delta(\mathbf{Q}/\rho \cdot \mathbf{C})\rvert}{\mathbf{Q}/\rho \cdot \mathbf{C}}$
Impulse excitation (front face)	0.25%	0.08%	0.12%	0.49%
Pulse ($\tau_{ex} = 1s$, front face)	0.40%	3.5×10^{-3}%	0.11%	0.45%

Table 3.15 – Estimation results using synthetic measurements, with a predefined excitation shape, CFRP properties: $\overline{\overline{a}} = [0.4; 2.6; 0.8]\ mm^2 \cdot s^{-1}$ and $\frac{Q}{\rho \cdot C} = 5.515 \cdot 10^{-7}\ m^3 \cdot K$, $h = 0\ W \cdot m^{-2} \cdot K^{-1}$.

Another strategy, consists in generating using FlexPDE, front face temperature evolution with an overall heat transfer coefficient $h = 10\ W \cdot m^{-2} \cdot K^{-1}$, while estimating the required

Relative deviation	$\frac{\lvert\Delta \mathbf{a_x}\rvert}{\mathbf{a_x}}$	$\frac{\lvert\Delta \mathbf{a_y}\rvert}{\mathbf{a_y}}$	$\frac{\lvert\Delta \mathbf{a_z}\rvert}{\mathbf{a_z}}$	$\frac{\lvert\Delta(\mathbf{Q}/\rho\cdot\mathbf{C})\rvert}{\mathbf{Q}/\rho\cdot\mathbf{C}}$
Pulse ($\tau_{ex}=1s$, front face)	5.41%	4.74%	1.03%	4.86%
Pulse ($\tau_{ex}=1s$, rear face)	2.06%	1.12%	1.71%	1.51%
Pulse ($\tau_{ex}=10s$, front face)	2.27%	2.27%	5.88%	1.59%
Pulse ($\tau_{ex}=10s$, rear face)	3.91%	1.13%	0.48%	5.73%

Table 3.16 – Estimation results by means of flexPDE measurements, with a predefined excitation shape, CFRP properties: $\overline{\overline{a}}=[0.4;2.6;0.8]\ mm^2\cdot s^{-1}$ and $\frac{Q}{\rho\cdot C}=5.515\cdot10^{-7}\ m^3\cdot K$, $h=0\ W\cdot m^{-2}\cdot K^{-1}$.

Unknown values	**Flash experiment (τ_{ex} = 10 ms, front face)**	**Previous values from Table 3.4**
a_x [mm^2.s^{-1}]	0.515 (+3.00%)	0.500
a_y [mm^2.s^{-1}]	2.443 (+3.08%)	2.370
a_z [mm^2.s^{-1}]	0.869 (−5.66%)	0.902
$\frac{Q}{\rho C}$ $[m^3\cdot K]$	5.112×10^{-7} (−6.80%)	5.485×10^{-7}

Table 3.17 – Estimation results by means of previous experimental data, with a predefined excitation shape, and $h=0\ W\cdot m^{-2}\cdot K^{-1}$, compared to the estimation results with a predefined cosine shape presented in Table 3.4.

parameters $\beta=[ax,ay,az,\frac{Q}{\rho C}]$ by considering the degenerated model 3.33 obtained for $h=0\ W\cdot m^{-2}\cdot K^{-1}$. The results of such approach are tabulated in Table 3.18 and prove also its consistency.

3.7.3 Simultaneous identification of $\beta=[a_x,a_y,a_z,\frac{QF_{mn}}{\rho\cdot C},r]$ for a non-predefined shape at short time or under vacuum

As discussed in 3.7.2, it is a kind of model degeneration where $h=0\ W\cdot m^{-2}\cdot K^{-1}$, that leads to new formulations of front and rear face normalized harmonics as expressed in Eqs. 3.33 and 3.34.

In the case considering non-predefined excitation shape, one should estimate the new parameter $\frac{Q\cdot F_{mn}}{\rho\cdot C}$, instead of estimating $\frac{Q}{\rho\cdot C}$ as in 3.7.2.

Results obtained when repeating the estimation procedure using previous experimental data, are tabulated in Table 3.19. Estimated results in this case, very close to the previous val-

Relative deviation	$\frac{\lvert\Delta \mathbf{a_x}\rvert}{\mathbf{a_x}}$	$\frac{\lvert\Delta \mathbf{a_y}\rvert}{\mathbf{a_y}}$	$\frac{\lvert\Delta \mathbf{a_z}\rvert}{\mathbf{a_z}}$	$\frac{\lvert\Delta(\mathbf{Q}/\rho\mathbf{C})\rvert}{\mathbf{Q}/\rho\mathbf{C}}$
Pulse ($\tau_{ex} = 1s$, front face)	4.72%	4.99%	6.40%	1.18%
Pulse ($\tau_{ex} = 10s$, front face)	0.46%	2.76%	5.19%	1.34%

Table 3.18 – Estimation results by means of flexPDE measurements (generated with $h = 10\ W \cdot m^{-2} \cdot K^{-1}$), with a predefined excitation shape, CFRP properties: $\overline{\overline{a}} = [0.4; 2.6; 0.8]\ mm^2 \cdot s^{-1}$ and $\frac{Q}{\rho C} = 5.515 \times 10^{-7}\ m^3 \cdot K$, $h = 0\ W \cdot m^{-2} \cdot K^{-1}$.

ues deduced from 3.4.2 and Table 3.4 for a non-predefined shape of the excitation (with small relative deviation), prove the feasibility of this last approach, and the possibility to consider a neglected overall heat transfer coefficient in such experimental exercise, for short time front face temperature acquisition.

Unknown values	**Flash experiment (τ_{ex} = 10 ms, front face)**	**Previous values from Table 3.4**
a_x [mm^2.s^{-1}]	0.425 (+5.98%)	0.401
a_y [mm^2.s^{-1}]	2.665 (+2.89%)	2.590
a_z [mm^2.s^{-1}]	0.834 (−0.59%)	0.839
$\frac{Q \cdot F_{0,0}}{\rho C}$ $[m^3 \cdot K]$	5.206×10^{-7} (−6.55%)	5.571×10^{-7}

Table 3.19 – Estimation results using previous experimental data, with a non-predefined excitation shape and $h = 0\ W \cdot m^{-2} \cdot K^{-1}$, compared to the estimation results with a non-predefined cosine shape presented in Table 3.4.

3.8 Conclusion

In this work, an identification method devoted to the thermal characterization of orthotropic materials, is presented. The originality of this method lies in its ability to directly and simultaneously estimate, i.e. in only one calculation step, the three main diffusivities of any orthotropic material. The proposed identification procedure relies on the analytical resolution of the heat transfer equation, and the non-intrusive measurements of the temperature field induced by a local non-intrusive excitation. A unique experiment is required to achieve this goal. Generally, the parameters relative to the excitation are highly dependent on the laser beam heat flux distribution which is particularly difficult to identify. In this context, one of the distinctive features of the current approach, is that the estimation may be successfully achieved without any a pri-

ori knowledge about the shape or the intensity of the excitation. The present method estimates, simultaneously with the thermal diffusivities, the total amount of heat absorbed by the material as well as the distribution of the thermal excitation absorbed at the surface of the material. In addition, the method being based on pseudo-analytical model, it allows the use of a stochastic approach that is imperative considering the non linear nature and the number of unknown parameters of the problem. The corresponding results demonstrate that the hybrid optimization strategy combining a PSO algorithm and a gradient based method is a good candidate for solving such complex and non-linear inverse problem.

After validation with isotropic materials of known properties, the method is applied on an orthotropic fiber composite material. The very good agreement between the results in the present study and results obtained from other estimators (e.g. ENH, MSEH) demonstrated the accuracy of the method. Thanks to estimated parameters, a sensitivity study is then conducted using these values to verify the simulatenous estimation feasibility.

Furthermore, some alternative strategies developed to improve the identification method, in terms of accuracy and time reduction, followed by a study dedicated to the optimization of the flash based experiment for a better estimation accuracy, are presented. This last section is a systematic comparison of possible designs, considering the measurement face, the laser excitation energy and duration time. The overall identification method is then applied on a fictitious CFRP sample (with same properties as that previously characterized), whose temperature response to various excitation settings is calculated using a finite element code (FlexPDE). The comparison, in terms of temperature level, estimation accuracy and calculation time, has enabled to identify the optimum settings, taking into account both the theoretical and experimental point of view. The study is completed by a sensitivity analysis performed on the cases with the highest identification potential. This analysis, in addition to the present numerical study confirmed the pre-established observations, i.e. the rear face estimation strategy is the most convenient for a simultaneous estimation of the three main thermal diffusivities, especially the in-depth diffusivity, thanks to the decorrelation between the in-depth and the in-plane thermal diffusivities. Moreover, for a rear face estimation procedure of a CRFP like medium, a laser excitation pulse duration time in the order of 10 of seconds with an intensity of 10 J has been proven, based on numerical results, to be the most adapted.

Lastly, some approaches consisting in estimating the volumetric heat capacity simultaneously with the thermal diffusivity tensor of an orthotropic material, or allowing this estimation without any previous information about the volumetric heat capacity value, are presented and verified with promising results. These latter are achieved i) numerically by noisy data generated using the model itself or any numerical approach, and ii) experimentally by repeating estimation using previous experimental data.

The work presented in this chapter assumed a perfectly homogeneous orthotropic monolayer material. Based on retrieved results, this method seems to be very promising in order to identify thermophysical properties of more complex multilayers structures, such as two layers or coatings on substrate materials that will be addressed in the following chapter 4.

3.9 Résumé substantiel du chapitre 3

Introduction

Dans ce chapitre, une méthode d'estimation directe et simultanée du tenseur des diffusivités thermiques (a_x, a_y, a_z) de matériaux opaques isotropes ou orthotropes, est présentée. Cette méthode consiste à coupler les résultats issus d'une expérience Flash 3D, présentée dans 2.3, à une méthode de minimisation, présentée dans 2.2. En plus de l'introduction et de la conclusion, ce chapitre comporte 6 parties, résumées ci-dessous.

Partie 1. Etat de l'art des méthodes de caractérisation thermique de matériaux monocouches

Afin de mettre en avant l'originalité de la méthode développée dans le présent travail, un état de l'art des méthodes existantes dédiées à la caractérisation des diffusivités thermiques de matériaux monocouches est présenté dans 3.2.

Parmi ces méthodes, certaines sont monodimentionelles car capables d'identifier la diffusivité thermique uniquement selon l'épaisseur du matériau. D'autres sont bidimentionnelles et peuvent estimer deux composantes du tenseur de diffusivité thermique dans le cas de matériaux orthotropes ou anisotropes.

Parmi les méthodes tridimensionnelles dédiées à l'estimation du tenseur des diffusivités thermiques, certaines sont basées sur des modèles numériques et sont donc longs à résoudre, ou sur une estimation en plusieurs étapes, ou parfois sur une expérience très sophistiquée ou difficile à réaliser. Citant ainsi un grand nombre de méthodes qui se reposent sur des expériences intrusives, en terme d'excitation ou de mesures de températures.

La principale caractéristique de ce travail repose sur la combinaison de l'estimation directe et simultanée des 3 composantes principales du tenseur des diffusivités du matériau orthotrope à l'aide d'un modèle transitoire analytique 3D et d'une expérience unique et non intrusive en termes d'excitation et de mesures. Le modèle direct, résultant d'une transformée de Fourier permettant l'exploitation d'une grande quantité de données spatiales, est l'élément clé de la présente méthode d'estimation nommée dans ce travail «Estimation directe et simultanée à l'aide des harmoniques». L'importance de la méthode d'identification directe a été mentionnée pour la première fois par Ruffio [82] au sein d'une étude comparative.

Partie 2. Résolution du problème inverse en conduction thermique

Dans cette section, les différentes étapes de la résolution du problème inverse dans le cadre de la stratégie globale d'identification, dont les principes ont été introduits dans le chapitre précédent 2.2, sont détaillées et discutées dans 3.3.

Le présent travail porte sur un modèle pseudo-analytique, basé sur l'approche des quadripoles thermiques, développé pour prédire l'évolution de la température de la face avant

(ou arrière) d'un matériau orthotrope exposé à un flux thermique sur l'une de ses faces et sujet au refroidissement naturel.

Le problème inverse résolu dans la présente étude est basé sur la minimisation de l'écart quadratique entre les sorties d'un modèle 3D et les mesures expérimentales. Afin d'estimer correctement les diffusivités thermiques, il convient également d'estimer les paramètres liés à l'excitation thermique, en termes de distribution surfacique de l'intensité. Compte tenu du grand nombre de paramètres à estimer, ainsi que de la nature non linéaire du problème, un algorithme d'optimisation hybride combinant à la fois une méthode stochastique et une méthode déterministe est appliqué 2.5.4.3.

Partie 3. Applications expérimentales et résultats des estimations

Dans cette section, la méthode globale d'identification proposée est validée expérimentalement sur un échantillon isotrope de référence de polyamide dont les propriétés sont bien connues, puis appliquée sur un échantillon orthotrope de composite polymère renforcé de fibres de carbone (PRFC, voir 3.4) et couramment utilisé dans l'industrie en raison de ses propriétés thermiques et mécaniques (voir 1.2). Le très bon accord entre les résultats de la présente identification et ceux obtenus aux moyens d'autres estimateurs déjà établies (e.g. ENH, MSEH) a démontré la précision de la méthode. L'identification des paramètres est complétée par une analyse des sensibilités afin de valider la faisabilité de l'estimation simultanée et d'évaluer la méthode en termes de robustesse et de précision.

Partie 4. Comparaison de la méthode d'identification (DSEH) avec d'autres méthodes existantes (ERH, ENH, MSEH)

Après une brève présentation de méthodes existantes d'identification basées sur les harmoniques comme i) Estimation par rapport des harmoniques (ERH), ii) Estimation par normalisation des harmoniques (ENH) et iii) Estimation en plusieurs étapes par séparation des harmoniques (MSEH), l'originalité de la présente technique d'estimation, l'estimation directe et simultanée au moyen des harmoniques (EDSH) ou DSEH en anglais, est mise en avant (voir 3.5).

La méthode d'identification développée dans ce travail (DSEH) ne nécessite aucun post-traitement des harmoniques (par exemple, transformation logarithmique, normalisation, etc.), car elle exploite directement les "harmoniques brutes normalisées" sans transformation supplémentaire. Elle permet, en une seule étape, une estimation directe et simultanée du tenseur des diffusivité thermiques tridimensionnel correspondant à un matériau orthotrope. En plus, elle nécessite une expérience unique avec à la fois une excitation thermique et des mesures d'évolution de la température, non intrusives. L'expression pseudo-analytique de l'évolution de la température en face avant ou arrière de l'échantillon permet un traitement rapide du modèle direct, donc une technique d'estimation plus rapide. Enfin, cette méthode ne nécessite aucune connaissance préalable des caractéristiques de l'excitation thermique (c'est-à-dire l'intensité, la distribution spatiale), qui sont estimées simultanément.

Partie 5. Améliorations de la méthode d'identification

La deuxième partie de ce chapitre (voir 3.6) est consacrée à l'amélioration du processus d'identification en termes de réduction du temps de calcul, d'amélioration de la précision et d'optimisation de la conception d'expérience. L'identification des diffusivités d'un échantillon de PRFC déjà caractérisé expérimentalement dans une section précédente 3.4.2 est réalisée avec le modèle direct en appliquant une excitation paramétrée dont la forme est prédéfinie à l'aide de données expérimentales réelles.

Dans le but de simuler des données expérimentales, le modèle direct est résolu à l'aide d'un code d'éléments finis, FlexPDE. Dans un premier temps, cette résolution numérique est comparée à la résolution analytique utilisée dans le processus d'identification, en termes de précision et de temps de calcul. L'outil numérique actuel s'avère être un bon candidat pour générer de pseudo-mesures et comparer les différentes configurations expérimentales. La méthode d'identification globale déjà validée est appliquée numériquement sur un échantillon fictif de PRFC orthotrope, pour une gamme de configurations expérimentales correspondantes à la combinaison de différentes intensités énergétiques et durées de l'excitation. Un ensemble de configurations expérimentales réalistes est sélectionné afin de trouver le meilleur compromis entre i) un niveau d'intensité du signal suffisamment élevé pour pouvoir être mesuré et ii) une élévation modérée de la température afin de maintenir les paramètres thermophysiques relativement constants.

L'étude est complétée par une analyse des sensibilités réalisée sur les cas présentant le potentiel d'identification le plus élevé. Cette analyse, en plus de la présente étude numérique, a confirmé les observations préétablies, à savoir que la méthode flash face arrière est la plus adaptée pour une estimation simultanée des trois principales diffusivités thermiques, notamment la diffusivité selon la profondeur, car elle permet de décorréler cette dernière et les diffusivités dans le plan. De plus, pour une estimation avec une mesure en face arrière, une durée d'excitation laser de l'ordre de 10 secondes avec une intensité de 10 J s'est révélée, sur la base des résultats numériques, être la plus adaptée.

Partie 6. Autres approches pour estimer des propriétés thermophysiques supplémentaires

Dans cette section, certaines stratégies alternatives d'estimation sont examinées et leurs faisabilités sont testées i) numériquement par des données synthétiques bruitées générées par le modèle ou par un code tierce basé sur la méthode des éléments finis (flexPDE), et ii) expérimentalement en répétant l'estimation à l'aide de données expérimentales antérieures. Ces stratégies consistent à identifier, simultanément en plus des diffusivités thermiques, la capacité thermique spécifique $\rho \cdot c$ lorsqu'on connaît l'énergie Q, ou à estimer le tenseur des diffusivités thermiques sans aucune connaissance préalable de la valeur de ce produit.

Ces études ont été menées sur le matériau monocouche de PRFC, caractérisé précédemment dans 3.4.2 en utilisant les propriétés thermophysiques mesurées ou identifiées auparavant (voir 3.7).

Conlusion

Dans cette section, une méthode d'identification consacrée à la caractérisation thermique des matériaux orthotropes est présentée. L'originalité de cette méthode réside dans sa capacité à estimer directement et simultanément, i.e. en une seule étape de calcul, les trois principales diffusivités thermiques ainsi que les prpriétés liées à l'excitation. La procédure d'identification proposée repose sur la résolution analytique de l'équation de la chaleur et sur des mesures non intrusives du champ de température induit par une excitation thermique locale également non intrusive. Une expérience unique est nécessaire pour atteindre cet objectif et la formulation pseudo-analytique du modèle permet l'utilisation d'une approche de résolution du problème inverse stochastique. Les résultats obtenus, démontrent que la stratégie d'optimisation hybride combinant un algorithme stochastique (PSO) et une méthode déterministe de type gradient est un bon candidat pour résoudre ce type de problème inverse. Les paramètres relatifs à l'excitation dépendent fortement de la distribution du flux de chaleur induit par le faisceau laser, qui est particulièrement difficile à identifier. Dans ce contexte, l'une des caractéristiques distinctives de cette approche repose sur l'estimation qui peut être réalisée sans connaissance préalable de la forme ou de l'intensité de l'excitation. Ainsi, la méthode développée estime, simultanément aux diffusivités thermiques, la quantité totale de chaleur absorbée ainsi que la répartition spatiale de l'excitation thermique à la surface du matériau.

Les applications présentées dans ce chapitre supposaient un matériau monocouche orthotrope parfaitement homogène. Sur la base des résultats obtenus, cette méthode semble très prometteuse afin d'identifier les propriétés thermophysiques de structures multicouches, telles que les matériaux bicouches ou le cas des revêtements déposés sur des substrats, qui sont abordés dans le chapitre suivant 4.

Chapter 4

Generalization to multilayer materials

***

Contents

4.1 Introduction

This present chapter presents the extension of an experimental identification technique dedicated to the thermal characterization of opaque multilayers materials. Indeed, some orthotropic materials can be only used in association with other materials. In those cases, it may be a challenging task to independently measure the diffusivities of the orthotropic material because of the difficulty in preparing free-standing samples. To avoid any destructive delamination or structure modification during the estimation process, a strong emphasis is placed on the direct and simultaneous nature of the thermal characterization of all constitutive materials. The next section is dedicated to the characterization of an orthotropic carbon fiber reinforced polymer composite material (CFRP) combined with an isotropic liner, which constitute a two-layers material commonly used in many industries.

First, the procedure developed to identify the 3D thermal diffusivity of each layer material is presented. The pseudo-analytical model, relying on the quadrupoles formalism and predicting the transient heat conduction into a multi-layer system in a flash method context, is described. After validation of the direct model using a fictitious sample subdivision and a finite element numerical code, the complete identification method is validated using an isotropic opaque monolayer material already characterized in 3.4.1.

Then, a study is conducted on two two-layers fictitious samples inspired from the hydrogen storage and transportation vessels technologies. The samples are constituted of a CFRP layer combined with an isotropic layer of metal (type III tank) or a polymer liner (type IV tank). Excitation and measurement faces combinations leading to four possible experimental protocol, the main objective is to prioritize, via a sensitivity study, those protocols depending on the liner type (metal or polymer).

The identification method is then performed on an actual two layers sample manufactured for this purpose and constituted with an isotropic polyamide (PA) polymer and an anisotropic carbon fibers reinforced polymer (CFRP) composite. The accuracy and the robustness of the method is discussed depending on the excitation and measurement faces. Two distinct experimental configurations, pre-selected according to the sensitivity of the observables to the CFRP and polyamide diffusivities, are investigated. The a priori isotropic nature of the polymer leads to what we call the 4D identification case. The same experiment is performed by considering the polyamide polymer layer as an orthotropic material, referred to as the 6D identification case. Results are also compared with previous estimation values of monolayers properties already characterized in chapter 3, and using the ENH monolayer and two-dimensional estimator. A strong emphasis is placed on the sensitivity analysis in order to evaluate the feasibility of the estimation for both experimental configurations and both strategies (i.e. 4D and 6D identification).

Finally, the method is applied to estimate the thermal diffusivity of coatings deposited on substrate materials. The application concerns the thermographic phosphor thermometry tech-

nic used in combustion environments to measure wall surface temperatures and heat fluxes. The objectif is to estimate the thermal properties of the thin layer of phosphor deposited on an isotropic or orthotropic liner. This exercise, which constitute a special case of the developed overall method due to the thicknesses ratio of the layers, is discussed in the last section.

4.2 Literature review on two or multi-layers thermal characterization techniques

In the context of two or multi-layers materials thermal characterization, very few research works were focused on the thermal properties identification of each layer constituting these structures. Among those research works, some attempted to reach the one-dimensional thermal diffusivity of one isotropic layer present in two or three layered system composed by isotropic layers [127, 128, 130, 131, 253]. In most of the previously cited works, the identification of the thermal properties of one layer requires the knowledge of its all other thermal properties and the properties of the remaining layer(s). Thus, any error in these properties will be propagated through the model and results in an inaccuracy of the required estimation.

Most authors have been interested in the characterization of 1D thermal diffusivity or conductivity of thin films [254–256] or coatings [132, 134, 135, 257–262] on substrates, or 1D temperature dependent thermal diffusivity (i.e. $a(T)$) of a viscous intumescent coating with a moving boundary system [263]. In those works, a priori knowledge of the substrate properties or a determination of these properties through a previous experiment, is often required [132, 133, 254, 257, 258, 261, 263–266].

In such types of applications, being increasingly used for mechanical and thermal protection or optical properties improvement reasons, one of the distinctive features is the difficulty, or impossibility in most situations, to obtain these coatings separately from their substrates. Others tried to overcome this limitation by identifying the thermal diffusivities of the coating without any knowledge about the substrate properties. However, their method relies on a two-steps identification technique that allows such measurement but only at very short time [81], limiting this method to relatively thick coatings. Any estimation strategy applied for multilayers, or for all layers constituting that multilayers material, and involving more than one step, may cumulate errors throughout the various stages of estimation. For example, one can cite the method of gobbé et al. [267] where the in-plane and in-depth thermal conductivities of a multilayers sample are estimated successively by the hot wire and the hot strip methods, or a strategy developed by Li et al. [268] in order to characterize both layers (i.e. the coating and the substrate), by repeating the experiment/measurements several times.

Among research works that deal with simultaneous estimation of two or more layers in a multilayer structure, only few works have tried to estimate the thermal diffusivity of each isotropic layer. Some authors have attempted to develop methods allowing the simultaneous and direct estimation of 2D thermal properties in cylindrical coordinates, of anisotropic coatings deposited on an isotropic substrate, with limited results [133, 264].

The present study consists in estimating simultaneously, i.e. using one unique step, via a non-intrusive flash experiment, the thermal diffusivities of all constituting layers. The method is then extended to the special case of coatings deposited on a substrate material.

4.3 Resolution of the inverse heat conduction problem - Thermal identification problem

The handled problem consists in an inverse heat conduction problem whose objective is to retrieve the thermal diffusivity tensor based on the minimization of the deviation between the output of a mathematical model and experimental measurements. This fit is achieved by means of an optimization algorithm that minimizes a cost function expressing the discrepancy between the two signals, in this case the quadratic error between the model and the experimental outputs. The overall estimation strategy concept is illustrated in Fig. 2.1 that presents the connection between each elements involved in the inverse problem. The various stages of the estimation strategy are detailed and discussed in the following sections.

4.3.1 Direct model

The objective of this study being to estimate thermal diffusivity tensor of the constituents of a layered material, an appropriate thermal multi-layer model is developed. The choice of the boundary conditions has to be consistent with the experimental setup which corresponds to an unconventional 3D flash technique conducted for the 3D identification purpose.

The direct physical model developed here, which constitute an extension of the thermal mono-layer model developed in 3.3.1, describes the three dimensional heat transfer through a multi-layer material constituted by k layers, as shown in Fig. 4.1. The material is subjected to a local and short thermal excitation on one of its face whose non uniform temperature elevation generates conductive heat transfer in all directions.

The experiment is designed in such a way that the temperature elevation is moderate in order to keep the layers thermophysical properties constant and independent of the temperature during the exploiting time. The lateral sides are assumed to be thermally isolated, while the front and rear faces are exposed to convection and radiation losses, described by linearized and global heat exchange coefficients h_f at the front side and h_b at the back side. The thermal contact resistances Rc_i at the interfaces between layers are assumed to be uniform. The system is assumed to be initially at thermal equilibrium with the environment, and all temperatures considered are relative to the environment temperature $T = T_{sys} - T_\infty$.

Given the above-mentioned assumptions, the thermal behavior of the multi-layer system is described by the set of differential Eqs. 4.1, linked by the conservation of flux at interfaces 4.2. The thermal excitation and the cooling phases are taken into account by means of the boundaries conditions BC1 4.3 and BC2 4.4. The initial conditions IC is described Eq. 4.5.

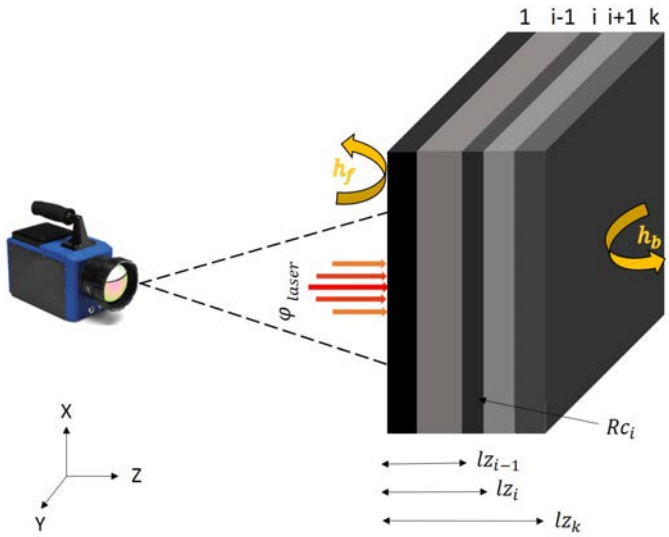

Figure 4.1 – Multi-layer material subjected to a short and non-uniform laser excitation at the front face, with a continuous measurement of the corresponding temperature recording via an IR camera.

$$\text{layer } i: \ \frac{\partial T_i}{\partial t} = a_{x_i}\frac{d^2T_i}{dx^2} + a_{y_i}\frac{d^2T_i}{dy^2} + a_{z_i}\frac{d^2T_i}{dz^2} \ \text{ for } t>0,\ i=[1,...,k] \tag{4.1}$$

$$\text{Interfaces:} \begin{cases} \lambda_{z_i}\dfrac{\partial T_i(z=l_{z_{i-}})}{\partial z} = \\ \qquad\qquad \lambda_{zi+1}\dfrac{\partial T_{i+1}(z=l_{z_{i+}})}{\partial z} \ \text{ for } z=l_{z_i}\ t>0,\ i=[1,...,k-1] \\ Rc_i\lambda_{z_i}\dfrac{\partial T_i(z=l_{z_{i-}})}{\partial z} = \\ \qquad\qquad T_{i+1}(z=l_{z_{i+}}) - T_i(z=l_{z_{i-}}) \ \text{ for } z=l_{z_i}\ t>0,\ i=[1,...,k-1] \end{cases} \tag{4.2}$$

$$\text{Boundary Condition 1}: \begin{cases} -\lambda_{x_1}\dfrac{\partial T_1}{\partial x} = 0 \ \text{ for } x=0 \text{ and } x=l_x,\ t>0 \\ -\lambda_{y_1}\dfrac{\partial T_1}{\partial y} = 0 \ \text{ for } y=0 \text{ and } y=l_y,\ t>0 \\ -\lambda_{z_1}\dfrac{\partial T_1}{\partial z} = -h_f(T_1-T_\infty) + \phi^{ex}_{x,y}(t) \ \text{ for } z=0,\ t>0 \end{cases} \tag{4.3}$$

$$\text{Boundary Condition 2}: \begin{cases} -\lambda_{x_k}\dfrac{\partial T_k}{\partial x} = 0 \ \text{ for } x=0 \text{ and } x=l_x,\ t>0 \\ -\lambda_{y_k}\dfrac{\partial T_k}{\partial y} = 0 \ \text{ for } y=0 \text{ and } y=l_y,\ t>0 \\ -\lambda_{z_k}\dfrac{\partial T_k}{\partial z} = -h_b(T_k-T_\infty) \ \text{ for } z=l_{z_k},\ t>0 \end{cases} \tag{4.4}$$

Initial Condition: $T_i(x,y,z) = 0$ for $t = 0,\ i = [1,...,k]$ (4.5)

It is important to note that all layers have the same dimension in the x-y plane, i.e. $l_{x_1} = l_{x_2} = ... = l_{x_k} = l_x$ and $l_{y_1} = l_{y_2} = ... = l_{y_k} = l_y$, where k stands for the number of layer. On the other side, those layers may have different thicknesses l_{z_i} with $i \in [1,...,k]$.

A direct analytic resolution of such linear problem with some non-linearity in the boundary conditions is performed using three integral transformations. The physical relative temperature $T(x,y,z,t)$ is projected into Fourier space (x and y directions) and also projected into Laplace domain (time). The resulting quantity $\theta_{m,n}(z,p)$ is called harmonics with corresponding Fourier space modes m,n. Based on the boundaries conditions, especially the isolated lateral faces, the projection basis in the Fourier Cosine space is chosen with the following form:

$$X_m(x) = cos(m\pi\frac{x}{l_x}) \text{ and } Y_n(y) = cos(n\pi\frac{y}{l_y}) \tag{4.6}$$

The harmonics obtained by projection of the physical temperature evolution into Fourier space domains (in 4.6) and the Laplace time domain is given by 4.7.

$$\theta_{m,n}(z,p) = \int_0^{\infty}\int_0^{l_y}\int_0^{l_x} T(x,y,z,t)\cdot X_m(x)\cdot Y_n(y)\cdot e^{-pt}\,dx\,dy\,dt \tag{4.7}$$

Using the three dimensional thermal quadrupoles formalism, the system is described by a set of three equations detailed here :

$$\begin{pmatrix}\theta_{in}\\ \\ \Phi_f\end{pmatrix} = \begin{pmatrix}1 & \frac{1}{h_f}\\ \\ 0 & 1\end{pmatrix}\times\begin{pmatrix}\theta_{m,n}(z=0)\\ \\ \phi_{m,n}(z=0)-\phi^{ex}_{m,n}\end{pmatrix} \tag{4.8a}$$

$$\begin{pmatrix}\theta_{m,n}(z=0)\\ \\ \phi_{m,n}(z=0)\end{pmatrix} = \prod_{i=1}^{k-1}\left\{\begin{pmatrix}a_{m,n,i} & b_{m,n,i}\\ \\ c_{m,n,i} & d_{m,n,i}\end{pmatrix}\times\begin{pmatrix}1 & Rc_i\\ \\ 0 & 1\end{pmatrix}\right\} \times\begin{pmatrix}a_{m,n,k} & b_{m,n,k}\\ \\ c_{m,n,k} & d_{m,n,k}\end{pmatrix}\times\begin{pmatrix}\theta_{m,n}(z=l_{z_k})\\ \\ \phi_{m,n}(z=l_{z_k})\end{pmatrix} \tag{4.8b}$$

$$\begin{pmatrix}\theta_{m,n}(z=l_{z_k})\\ \\ \phi_{m,n}(z=l_{z_k})\end{pmatrix} = \begin{pmatrix}1 & \frac{1}{h_b}\\ \\ 0 & 1\end{pmatrix}\times\begin{pmatrix}\theta_{out}\\ \\ \Phi_b\end{pmatrix} \tag{4.8c}$$

In our case, the environmental relative temperature in the considered space is $\theta_{in} = \theta_{out} = 0$. Likewise, Φ_f and Φ_b are obtained by integration of the heat loss fluxes at the front and rear faces, respectively.

The matrix terms of Eq. 4.8 are given by the equations below.

$$a_{mn,i}(p) = d_{m,n,i}(p) = \cosh(l_{z_i} \cdot K_{m,n,i}(p)) \tag{4.9a}$$

$$b_{m,n,i}(p) = \frac{\sinh(l_{z_i} \cdot K_{m,n,i}(p))}{\lambda_{z_i} \cdot K_{m,n,i}(p)} \tag{4.9b}$$

$$c_{mn,i}(p) = \lambda_{z_i} \cdot K_{m,n,i}(p) \cdot \sinh(l_{z_i} \cdot K_{m,n,i}(p))) \tag{4.9c}$$

$$K_{mn,i}(p) = \sqrt{\frac{p}{a_{z_i}} + \alpha_m^2 \frac{a_{x_i}}{a_{z_i}} + \beta_n^2 \frac{a_{y_i}}{a_{z_i}}} \tag{4.9d}$$

$$\alpha_m = \frac{m\pi}{l_x} \tag{4.9e}$$

$$\beta_n = \frac{n\pi}{l_y} \tag{4.9f}$$

The combination of Eqs.4.8 and Eqs.4.9 led to the following equation that relates the temperatures of the front and rear faces.

$$\begin{pmatrix} \theta_{m,n}(z=0,p) \\ \phi^{ex}_{m,n}(p) - h_f \theta_{m,n}(z=0,p) \end{pmatrix} = \begin{pmatrix} A_{m,n}(p) & B_{m,n}(p) \\ C_{m,n}(p) & D_{m,n}(p) \end{pmatrix} \times \begin{pmatrix} \theta_{m,n}(z=l_{z_k},p) \\ h_b \theta_{m,n}(z=l_{z_k},p) \end{pmatrix} \tag{4.10}$$

with

$$\begin{pmatrix} A_{m,n}(p) & B_{m,n}(p) \\ C_{m,n}(p) & D_{m,n}(p) \end{pmatrix} = \prod_{i=1}^{k-1} \left\{ \begin{pmatrix} a_{m,n,i}(p) & b_{m,n,i}(p) \\ c_{m,n,i}(p) & d_{m,n,i}(p) \end{pmatrix} \times \begin{pmatrix} 1 & Rc_i \\ 0 & 1 \end{pmatrix} \right\} \times \begin{pmatrix} a_{m,n,k}(p) & b_{m,n,k}(p) \\ c_{m,n,k}(p) & d_{m,n,k}(p) \end{pmatrix} \tag{4.11}$$

Then, the front face harmonics can be calculated following this equation:

$$\theta_{m,n}(z=0,p)=\theta_{m,n}(z=l_{z_k},p)\cdot(A_{m,n}(p)+B_{m,n}(p)\cdot h_b)=\frac{\phi^{ex}_{m,n}(p\cdot(A_{m,n}(p)+B_{m,n}(p)\cdot h_b)}{C_{m,n}(p)+D_{m,n}(p)\cdot h_b+A_{m,n}(p)\cdot h_f+B_{m,n}(p)\cdot h_f\cdot h_b} \tag{4.12}$$

And the rear face harmonics $\theta_{m,n}(z=l_{z_k},p)$ can be also obtained using the Eq. 4.12:

$$\theta_{m,n}(z=l_{z_k},p)=\frac{\phi^{ex}_{m,n}(p)}{C_{m,n}(p)+D_{m,n}(p)\cdot h_b+A_{m,n}(p)\cdot h_f+B_{m,n}(p)\cdot h_f\cdot h_b} \tag{4.13}$$

Analytical approaches are still of significant importance because they highlight the dependency of the system thermal behavior on thermal properties of each layer and provides a direct insight into the physical processes.

4.3.2 Experiments

The experiment conducted to generate the required measurements corresponds to an unconventional laser flash technique, all details are already presented in 2.3.1 and 3.3.3.

In the present case, the temperature response is continuously recorded by an IR camera, on the same or the opposite face of the excitation, corresponding to a so-called front-face or rear face measurement, respectively. The overall experiment, that could be qualified as a 3D unconventional and non-intrusive front flash method, is previously described in Fig. 2.3b. Also, the same image processing, presented in 2.3.4 and 3.3.4, is used.

4.3.3 Cost function

As already discussed in 2.5.2 and 3.3.2.2, the signals are exploited in the Fourier space. The cost function is then the summation of all the deviation between the measured and predicted output of the considered spatial modes. The odd harmonics (whose values of m and/or n are odd), are three order of magnitude smaller than the even harmonics, due to the symmetrical nature of the excitation. The odd harmonics, found to be quasi-negligible, are not used in the cost function definition.

To recall, the projection into the Fourier space allows the selection of the most energetic modes, which are distributed from low values of m and n to higher values. The harmonics that are exploited for the identification procedure are the even and low frequencies harmonics, $\xi_{m,n}$ where $m\times n$ combination corresponds to $[0,2,...,M]\times[0,2,...,N]$. Thus, the cost function is defined as following:

$$f=\sqrt{\sum_{m=0}^{M}\sum_{n=0}^{N}[\xi^{mod}_{m,n}(\beta,z=0\ or\ l_{z_k},t)-\xi^{exp}_{m,n}(z=0\ or\ l_{z_k},t)]^2}\text{ , where m and n are both even modes} \tag{4.14}$$

Thanks to the optimization algorithm, this comparison criterion is minimized in order to determine the values of the parameters that should be estimated.

4.3.4 Parameters vector β

As already discussed, one of the distinctive features of this approach is its capacity to identify the excitation characteristics by estimating the imposed heat flux distribution in the Fourier space domain $R_{m,n} = Q \cdot F_{m,n}$, and the total amount of heat received by the sample surface Q embedded in the mean excitation factor $R_{0,0} = Q \cdot F_{0,0}$ with $F_{0,0} = 1$. Therefore, this work allows the direct and simultaneous estimation of the required thermal diffusivity tensor without any a priori knowledge of the intensity or the shape of the excitation. As a consequence, the parameters vector contains the diffusivities of the different layers, the intensity Q and the shape factors $R_{m,n}$. Generally the number of modes is chosen in order to capture the shape of the excitation distribution.

$$\beta = [a_{x_1}, a_{y_1}, a_{z_1}, \cdots, a_{x_i}, a_{y_i}, a_{z_i}, \cdots, a_{x_k}, a_{y_k}, a_{z_k}, R_{0,0}, R_{0,2}, \cdots, R_{m,n}, \cdots, R_{M,N}] \tag{4.15}$$

Considering the even modes with a symmetric combinations ($M = N$), the parameters vector has a size of $3k+(\frac{M}{2}+1)^2$, where k stands for the number of layers considered. Other measurable thermophysical properties, such as the layers thicknesses, densities ρ and heat capacities C are previously measured before the estimation process (see 4.3.2).

4.3.5 Optimization algorithm

Hybrid optimization algorithm applied in the current study and detailed in sections 2.5.4.3 and 3.3.2.3, is also used here to minimize the cost function and retrieve the required parameters constituting the optimal vector $\hat{\beta}$. The relatively complex estimation problem and the nonlinear nature of the phenomenon require the use of a stochastic approach in order to avoid getting stuck into a local minimum. Thanks to the present coupled stochastic-deterministic optimization algorithm, a global search of the minimum region is achieved by the PSO algorithm, followed by a local search of the cost function minimum value, carried out by the gradient based method.

4.4 Method Validation

In this section, several validation are presented, starting by the numerical validation of the multilayers direct model using the subdivision principle in 4.4.1. The next validation step consists in a comparison between results of simulations obtained via the present model and those obtained via a finite element code (FlexPDE) in 4.4.2. Then, the overall identification method is evaluated by confrontation with experimental data in 4.4.3. The data used corresponds to previous experimental data obtained on monolayer polyamide material already characterized in

the previous chapter (see 3.4.1).

4.4.1 Numerical validation by subdivision (segmentation) principle

The principle of this first validation exercise consists in considering a monolayer material as a fictitious multi-layer material (Fig. 4.2). It consists in a simple subdivision of the sample thickness into many layer thicknesses. The thermophyscial properties of each fictitious layer are strictly identical to the original monolayer sample properties. The interface thermal resistances are assumed to be null.

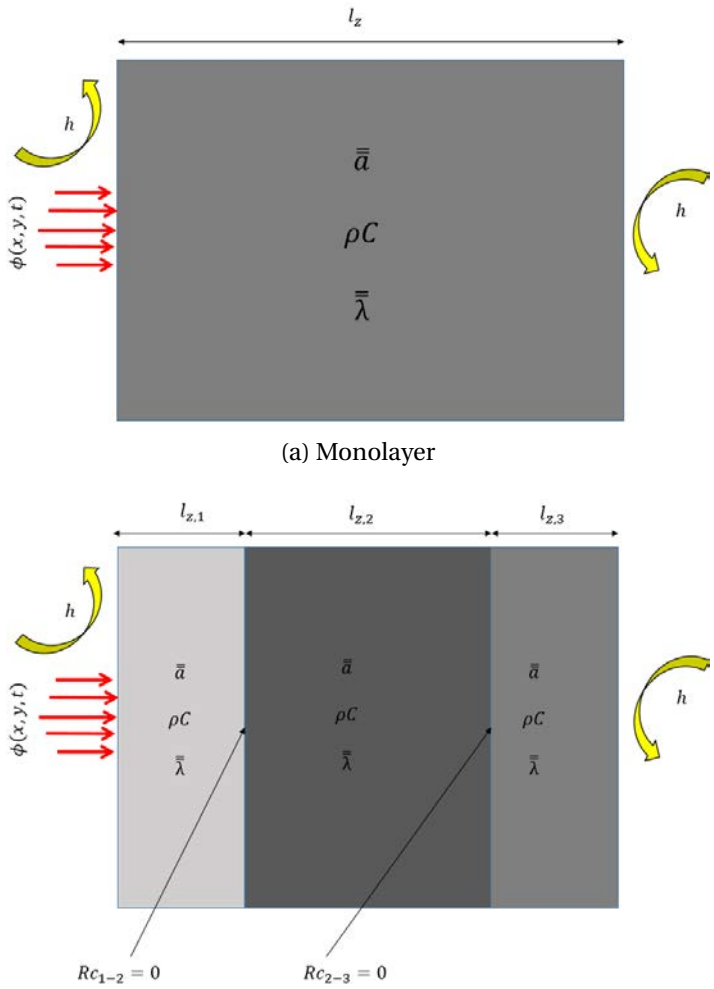

(a) Monolayer

(b) Multilayer

Figure 4.2 – Subdivision principle for the multilayers model validation.

Figs. 4.3 and 4.4 show the front and rear face normalized harmonics using the monolayer model presented in 3.3.1, for the polyamide (PA) and composite (CFRP) materials characterized in chapter 3, and those obtained using the multilayers model presented in 4.3.1, by considering a three-layers material with a subdivision of the sample thickness l_z into three thicknesses $[\frac{l_z}{4}, \frac{l_z}{2}, \frac{l_z}{4}]$. The perfect coincidence between both models signals is quite obvious, whatever the spatial mode (i.e. m=0,n=0 and m=2,n=2).

To recall, the properties of the PA and CFRP monolayers are those previously measured or

identified in 3.4 (for PA $\overline{\overline{a}} = [0.163, 0.165, 0.150]\ mm^2 \cdot s^{-1}, \rho = 1140\ kg \cdot m^{-3}, C = 1670\ J \cdot kg^{-1} \cdot K^{-1}$ and for CFRP $\overline{\overline{a}} = [0.40, 2.59, 0.84]\ mm^2 \cdot s^{-1}, \rho = 1286 kg \cdot m^{-3}, C = 1001 J \cdot kg^{-1} \cdot K^{-1}$).

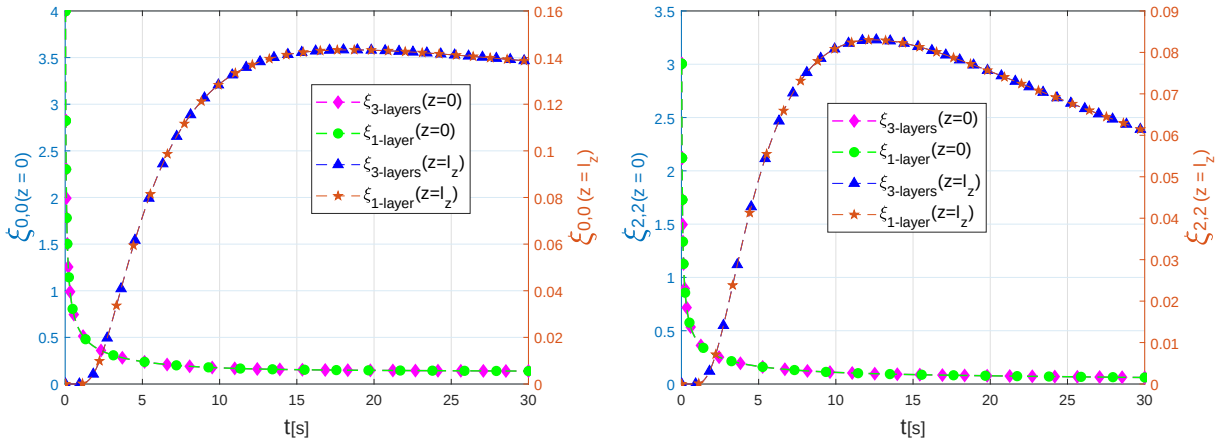

(a) m=0, n=0 (b) m=2,n=2

Figure 4.3 – Front and rear normalized harmonics using the monolayer and three-layers models, applied on the PA monolayer material fictitiously divided into three layers.

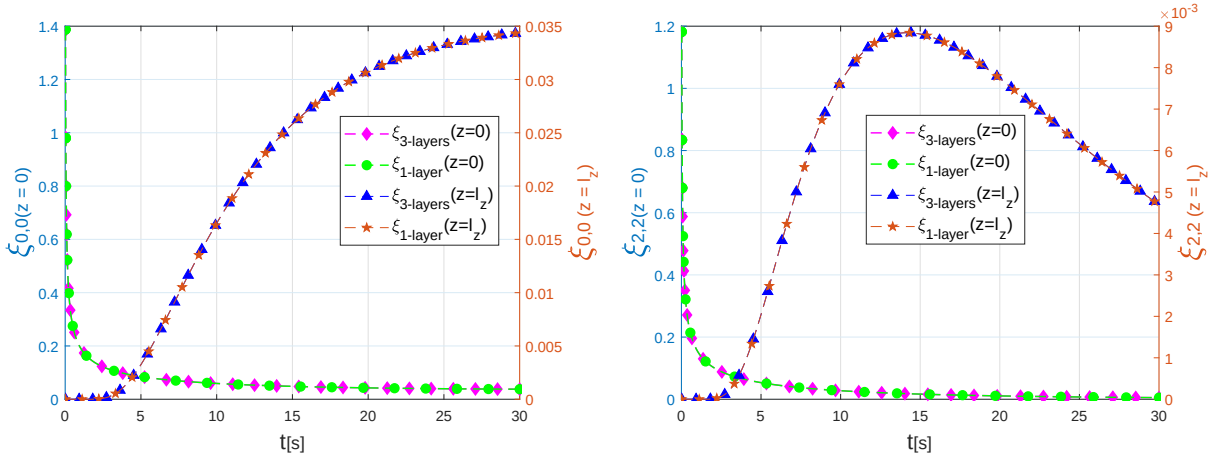

(a) m=0, n=0 (b) m=2,n=2

Figure 4.4 – Front and rear normalized harmonics using the monolayer and three-layers models, applied on the CFRP monolayer material fictitiously divided into three layers.

4.4.2 Numerical validation by FlexPDE

The coincidence between the FlexPDE simulated measurements, projected into the Fourier domain $\xi_{m,n}^{exp}(t)$, and the model outputs $\xi_{m,n}^{mod}(\beta, t)$ is already observed in 3.6.3. A second validation is performed in this section using a fictitious two-layers sample constituted by the composite CFRP and the polyamide materials previously characterized in chapter 3 with the same thermophysical properties (measured and estimated) and same dimensions. FlexPDE is used to simulate temperature evolution measurements at the center of the front face $T^{exp}(lx/2, ly/2, z = 0, t)$ as a response to a step excitation. The signal is compared to the analytical model (two-layers

model) outputs re-inverted into the real domain using inverse tranform algorithm presented in 3.4.4, $T^{mod}(\beta, lx/2, ly/2, z=0, t)$. Simulations are performed for various values of considered mode, from M=N= 4 to 60.

One can see in Fig. 4.5 the good agreement between signals obtained by FlexPDE and by the analytical model with $M = N \geq 6$. In the case where $M = N = 6$, the relative deviation or error is $< 0.9\%$. Thus, arguing the number of modes under consideration and which is set to $M = N = 6$ for the rest of the chapter.

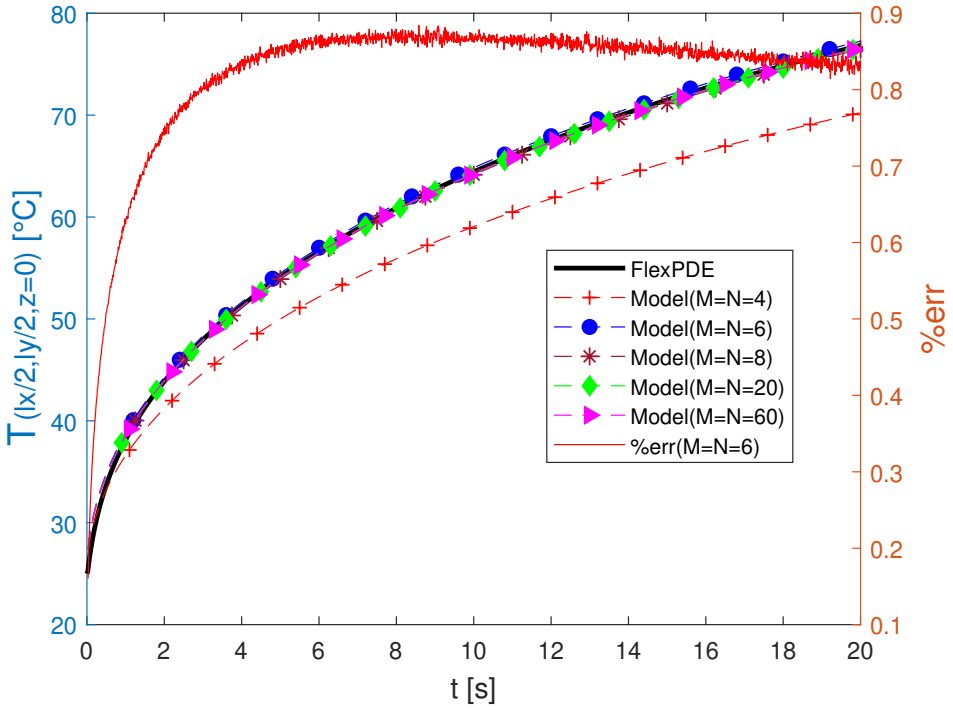

Figure 4.5 – FlexPDE simulated measurements of the temperature evolution at the center of the front face as a response to a step excitation, compared to the model outputs re-inverted into the real domain, for different considered numbers of harmonics.

4.4.3 Experimental validation

This section is dedicated to the application of the proposed identification method on a two-layer material, i.e. a multilayer material with $k = 2$. In this case, the thermal diffusivities of both layers, $\overline{a_1} = [a_{x,1}, a_{y,1}, a_{z,1}]$ and $\overline{a_2} = [a_{x,2}, a_{y,2}, a_{z,2}]$, have to be estimated. Calculation of the front face normalized harmonics can be performed by Eqs. 4.12 and 3.5 with the coefficient given by Eq. 4.16:

Properties	Values
l_z	2.4 mm
l_x	28 mm
l_y	26 mm
C	1670 $J \cdot kg^{-1} \cdot K^{-1}$
ρ	1140 $kg \cdot m^{-3}$
m, n	$\{0,2,4,6\} \otimes \{0,2,4,6\}$
Size of the vector β_{mono}	19
Number of PSO particles	50
Bounds of $\overline{\overline{a}}$	$[10^{-9}; 10^{-4}]$ $m^2 \cdot s^{-1}$

Table 4.1 – Thermophysical properties of the reference sample and specification of the estimation procedure required for the two-layers identification method.

$$\begin{pmatrix} A_{m,n}(p) & B_{m,n}(p) \\ C_{m,n}(p) & D_{m,n}(p) \end{pmatrix} = \begin{pmatrix} a_{m,n,1}(p) & b_{m,n,1}(p) \\ c_{m,n,1}(p) & d_{m,n,1}(p) \end{pmatrix} \times \begin{pmatrix} 1 & Rc \\ 0 & 1 \end{pmatrix} \times \begin{pmatrix} a_{m,n,2}(p) & b_{m,n,2}(p) \\ c_{m,n,2}(p) & d_{m,n,2}(p) \end{pmatrix} \tag{4.16}$$

The present validation relies on an isotropic monolayer for which the thermal diffusivity tensor has been identified using a monolayer 3D characterization method developed in a previous chapter (see 3.4.1) and validated using other estimators and literature values. The material used is a polyamide slab (PA) whose specifications are tabulated, as well as some parameters of the identification procedure, in Table 4.1.

The validation of the two-layers 3D characterization method is performed by subdividing the above mentioned PA monolayer material into two layers of arbitrary thicknesses. The sample is considered as a two-layer material with a perfect thermal contact (i.e. $Rc = 0$ $m^2 \cdot K \cdot W^{-1}$), whose thicknesses are chosen such as $l_{z_1} = \frac{l_z}{3}$ and $l_{z_2} = \frac{2l_z}{3}$. The other properties are the same as in Table 4.1, whatever the layer. This consideration conducts to a larger size of the parameters vector, i.e. from $\dim(\beta_{mono}) = 19$ to $\dim(\beta_{bi}) = 22$ parameters. The identified diffusivity tensors of both layers are represented in Table 4.2.

The present results are in good agreement with those proposed in the previous study presented in 3.4.1 . For comparison purposes, the estimation performed by DSEH was $\overline{\overline{a}} =$

Estimated parameter	**Values** [$\mathbf{mm^2 \cdot s^{-1}}$]
a_{x_1}	0.145 (−8.80%)
a_{y_1}	0.152 (−4.40%)
a_{z_1}	0.149 (−6.29%)
a_{x_2}	0.159 (−0.00%)
a_{y_2}	0.155 (−2.52%)
a_{z_2}	0.160 (+0.63%)

Table 4.2 – Two-layers thermal diffusivities obtained using the bilayer identification method, applied on the PA monolayer material that has $\overline{\overline{a}} = [0.163, 0.165, 0.150]\ mm^2 \cdot s^{-1}$ previously identified in 3.4 and presented in Table 3.2.

$[0.163, 0.165, 0.150]\ mm^2 \cdot s^{-1}$, which was already compared with success to values found by other estimators [75, 78, 82].

Noting that the estimated values, either $\overline{\overline{a}}$ included in $\hat{\beta}_{mono}$ or $\overline{\overline{a_1}}$ and $\overline{\overline{a_2}}$ included in $\hat{\beta}_{bi}$ are consistent with the isotropic nature of the corresponding sample, as the relative deviations presented in brackets in Table 4.2 do not exceed 8.8% from the average value $< a >= 0.159\ mm^2 \cdot s^{-1}$.

To illustrate the consistency of the method, evolution of the first experimental harmonics $\xi^{exp}_{m,n}(z = 0, t)$ are compared with the estimated harmonics $\xi^{mono}_{m,n}(\hat{\beta}_{mono}, z = 0, t)$ and $\xi^{bi}_{m,n}(\hat{\beta}_{bi}, z = 0, t)$ in Fig. 4.6. For the sake of brevity and clarity, only the first four harmonics, instead of the 16 investigated, are represented in this figure. The discrepancy between experimental and estimated data are represented by residual lines that illustrate the great fit between the experimental and the estimated signals. One should notice that the highest deviation is always observed in the mean field normalized harmonic $\xi_{0,0}$ which is highly affected by the environmental changes.

However, and as already argued in 3.6, the mean field $\xi_{0,0}$ can be excluded from the estimation. Previous tests have proven the possibility to exclude the mean harmonic from the estimation process. Without the mean field the parameters vector would have a size of $3k + (\frac{M}{2} + 1)^2 - 1$

$$\beta = [a_{x_1}, a_{y_1}, a_{z_1}, \cdots, a_{x_i}, a_{y_i}, a_{z_i}, \cdots, a_{x_k}, a_{y_k}, a_{z_k}, R_{0,2}, \cdots, R_{m,n}, \cdots, R_{M,N}]$$

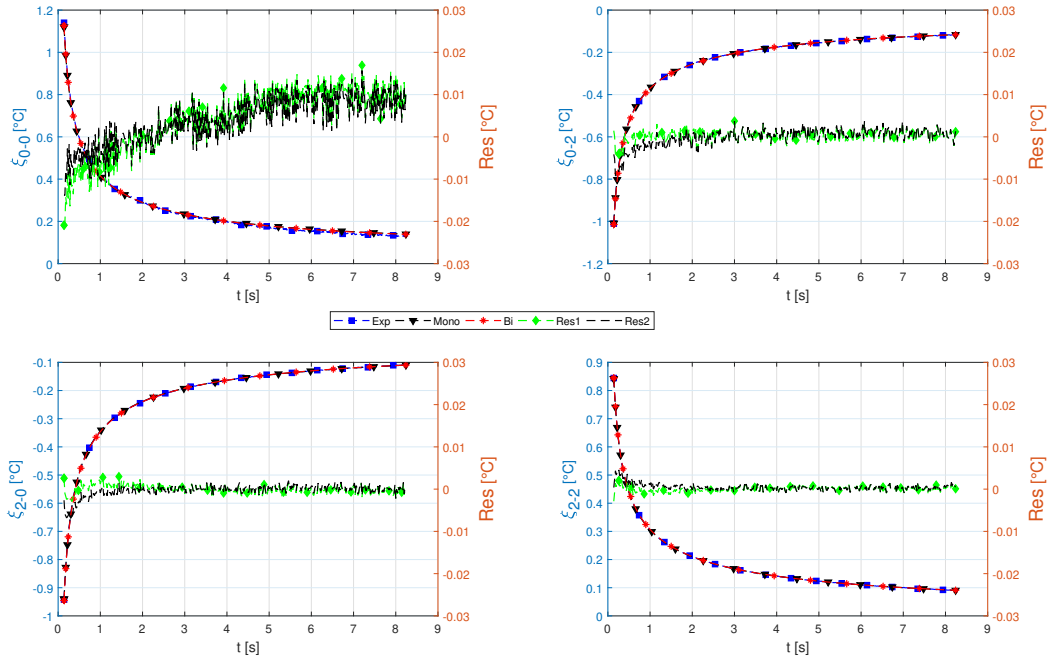

Figure 4.6 – Evolution of the first four normalized harmonics for experimental (Exp.) and simulated data using monolayer (Mono.) and bilayer (Bi.) direct models. The absolute deviation (residue) between the experience and monolayer model (Res1), and bilayer model (Res2) are also plotted.

4.5 Numerical and Experimental applications

In this section, several applications are presented, starting by the thermal characterization of an orthotropic CFRP layer covered by a metallic or polymer liner in 4.5.1, followed by the characterization of CFRP and the polymer liner constituting a two-layer material in 4.5.2. The last application concerns the characterization of a 'special' two-layers material constituted by a thin phosphate coating deposited on a substrate in 4.5.3.

4.5.1 Characterization of one orthotropic CFRP layer covered by a metallic or polymer liner

The main objective of this application is the three dimensional, simultaneous and direct estimation of the orthotropic thermal diffusivity tensor of a composite medium embedded in a two-layers material [269]. Two fictitious two-layers samples, inspired from the hydrogen storage and transportation vessels technologies, are considered. These samples are constituted of a CFRP orthotropic composite material already characterized in 3.4.2 and covered by an isotropic layer of metal (type III tank) or polymer liner (type IV tank), see Fig. 1.3.

The different possible combinations, in terms of excitation and measurement faces lead to four possible experimental protocol. One of the goals is to prioritize these protocols depending on the liner type (metal or polymer). In order to apply the method, two bi-layer samples are considered.

4.5.1.1 Two-layers direct model with perfect contact

The model describing this case is inspired from the multilayers model developed in 4.3.1 and applied for a two layer material, shown in Fig. 4.7.

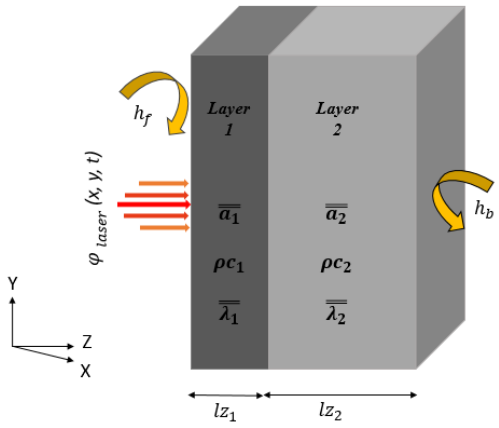

Figure 4.7 – Homogeneous two-layer plane material subjected to non-uniform flash excitation at the front face.

The set of differential partial equations describing the heat transfer inside the medium (layer 1 and 2), the condition at interface, and the initial and boundaries conditions are presented hereafter:

$$\text{layer 1}: \frac{\partial T_1}{\partial t} = a_{x_1}\frac{d^2T_1}{dx^2} + a_{y_1}\frac{d^2T_1}{dy^2} + a_{z_1}\frac{d^2T_1}{dz^2} \text{ for } z \in [0, l_{z_1}],\ t > 0 \tag{4.17}$$

$$\text{layer 2}: \frac{\partial T_2}{\partial t} = a_{x_2}\frac{d^2T_2}{dx^2} + a_{y_2}\frac{d^2T_2}{dy^2} + a_{z_2}\frac{d^2T_2}{dz^2} \text{ for } z \in [l_{z_1}, l_{z_1} + l_{z_2}],\ t > 0 \tag{4.18}$$

$$\text{Interface:} \begin{cases} \lambda_{z_1}\dfrac{\partial T_1(z = l_{z_{1-}})}{\partial z} = \lambda_{z2}\dfrac{\partial T_2(z = l_{z_{1+}})}{\partial z} \text{ for } z = l_{z_1},\ t > 0 \\ T_2(z = l_{z_{1+}}) = T_1(z = l_{z_{1-}}) \text{ for } z = l_{z_1},\ t > 0 \end{cases} \tag{4.19}$$

$$\text{Boundary conditions 1}: \begin{cases} -\lambda_{x_1}\dfrac{\partial T_1}{\partial x} = 0 \text{ for } x = 0 \text{ and } x = l_x,\ t > 0 \\ -\lambda_{y_1}\dfrac{\partial T_1}{\partial y} = 0 \text{ for } y = 0 \text{ and } y = l_y,\ t > 0 \\ -\lambda_{z_1}\dfrac{\partial T_1}{\partial z} = -h_f(T_1 - T_\infty) + \phi^{ex}_{x,y}(t) \text{ for } z = 0,\ t > 0 \end{cases} \tag{4.20}$$

$$\text{Boundary conditions 2 :} \begin{cases} -\lambda_{x_2}\dfrac{\partial T_2}{\partial x} & = 0 \text{ for } x=0 \text{ and } x=l_x,\ t>0 \\ -\lambda_{y_2}\dfrac{\partial T_2}{\partial y} & = 0 \text{ for } y=0 \text{ and } y=l_y,\ t>0 \\ -\lambda_{z_2}\dfrac{\partial T_2}{\partial z} & = -h_b(T_2-T_\infty) \text{ for } z=l_{z_1}+l_{z_2},\ t>0 \end{cases} \tag{4.21}$$

$$\text{Initial condition: } T_1(x,y,z)=0,\ T_2(x,y,z)=0 \text{ for } t=0 \tag{4.22}$$

In the considered case, the thermal resistance at the interface between both layers is neglected. After getting the harmonics by projection of the physical temperature evolution into Fourier space domains (4.6) and into Laplace time domain (4.7), the three dimensional analytical resolution can be conducted using the thermal quadrupoles formalism as follows :

$$\begin{pmatrix} \theta_{m,n}(z=0,p) \\ \phi^{ex}_{m,n}(p)-h_f\theta_{m,n}(z=0,p) \end{pmatrix} = \begin{pmatrix} A_{m,n}(p) & B_{m,n}(p) \\ C_{m,n}(p) & D_{m,n}(p) \end{pmatrix} \times \begin{pmatrix} \theta_{m,n}(z=l_{z_2},p) \\ h_b\theta_{m,n}(z=l_{z_2},p) \end{pmatrix} \tag{4.23}$$

with

$$\begin{pmatrix} A_{m,n}(p) & B_{m,n}(p) \\ C_{m,n}(p) & D_{m,n}(p) \end{pmatrix} = \begin{pmatrix} a_{m,n,1} & b_{m,n,1} \\ c_{m,n,1} & d_{m,n,1} \end{pmatrix} \times \begin{pmatrix} a_{m,n,2} & b_{m,n,2} \\ c_{m,n,2} & d_{m,n,2} \end{pmatrix} \tag{4.24}$$

The resulting analytical expressions of the rear and front face normalized harmonics are respectively:

$$\xi_{m,n}(z=l_{z_1}+l_{z_2},p)) = \frac{\dfrac{Q\cdot F_{m,n}\cdot u(p)}{l_x\cdot l_y}}{C_{m,n}(p)+D_{m,n}(p)\cdot h_b+A_{m,n}(p)\cdot h_f+B_{m,n}(p)\cdot h_f\cdot h_b} \tag{4.25}$$

$$\xi_{m,n}(z=0,p)=\xi_{m,n}(z=l_{z_1}+l_{z_2},p)\cdot(A_{m,n}(p)+B_{m,n}(p)\cdot h_b)= \frac{\dfrac{Q\cdot F_{m,n}\cdot u(p)}{l_x\cdot l_y}\cdot(A_{m,n}(p)+B_{m,n}(p)\cdot h_b)}{C_{m,n}(p)+D_{m,n}(p)\cdot h_b+A_{m,n}(p)\cdot h_f+B_{m,n}(p)\cdot h_f\cdot h_b} \tag{4.26}$$

These normalized harmonics are then projected into the real time domain using De-Hoog inversion technique (as shown in previous chapter), and $\xi^{mod}_{m,n}(\beta,z=0 \text{ or } z=l_{z_1}+l_{z_2},t)$ will represent the model outputs involved in the inverse problem technique and estimation strategy.

4.5.1.2 Sensitivity analysis and discussion

A sensitivity analysis is conducted in order to prioritize the experimental configurations. To recall, the sensibility analysis requires the values of the parameters to estimate. The properties of the liners (Aluminum or polyamide) and CFRP presented in Table 4.3 are chosen based on the literature and previous estimation of a composite stand-alone sample thermal diffusivities specifically prepared for this use. Other parameters, as the in-plane dimension of the sample or the parameters relative to the excitation, are chosen to be respectively $l_x = l_y = 0.1\ m$, $Q = 3.1 \cdot 10^4\ J \cdot m^{-2}$ and $r = \frac{l_x}{7}$. The thicknesses of each layer has been chosen consistently with manufactured samples. In this study, the shape function associated with the laser beam, $F_{x,y}$, is assumed to follow a cosine function already proved in 3.6.1 to be coherent with experimental observations.

Parameters	CFRP	Liner - Aluminum	Liner - polyamide
$\overline{\overline{a}}\ [mm^2 \cdot s^{-1}]$	[0.4; 2.6; 0.4]	[66.6; 66.6; 66.6]	[0.157; 0.157; 0.157]
$\rho C\ [KJ \cdot m^{-3} \cdot K^{-1}]$	1285	2461	1904
$l_z\ [mm]$	50	5	5

Table 4.3 – Model parameters values used to perform the sensitivity analysis.

The present analysis is based on a comparison of temperature measurements sensitivities relative to the composite diffusivities, according to the possible experimental configurations. Both excitation and measurement may being performed on the front or the rear face, it allows 4 distinct excitation/measurement combination, as shown in Fig. 4.8.

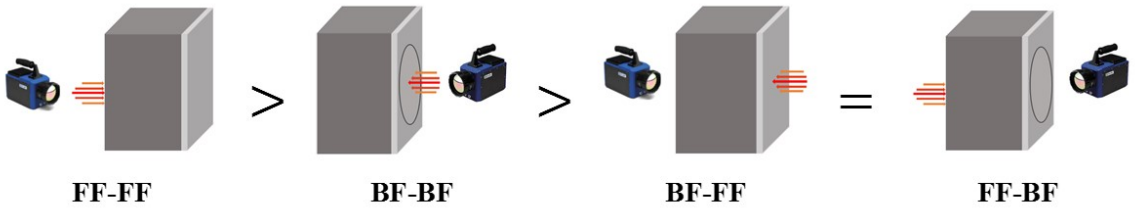

Figure 4.8 – The four possible configurations investigated for the search of the optimal estimation setup of the CFRP diffusivities. FF stands for “Front Face” and BF for “Back Face”. The first acronym corresponds to the excitation location, the second to the measurement.

A typical result is plotted in Fig. 4.9 that shows the sensitivity evolution of the most representative harmonic $\xi_{2,2}(t)$ relative to the in-depth diffusivity a_z of the CFRP, for each configuration and in association with the isotropic polyamide liner.

The analysis of the entire set of results, in terms of sensitivities magnitude, allows a clear prioritization of the configuration. Unsurprisingly, excitation and measurement both performed

on the face of the material to identify has to be preferred. However, it may not always be possible for such experimental protocol to be performed. In some cases, the face of interest may not be accessible, thus it is recommended to perform both, the excitation and the measurement, on the other side of the sample (BF-BF configuration) as the sensitivities magnitudes are still exploitable.

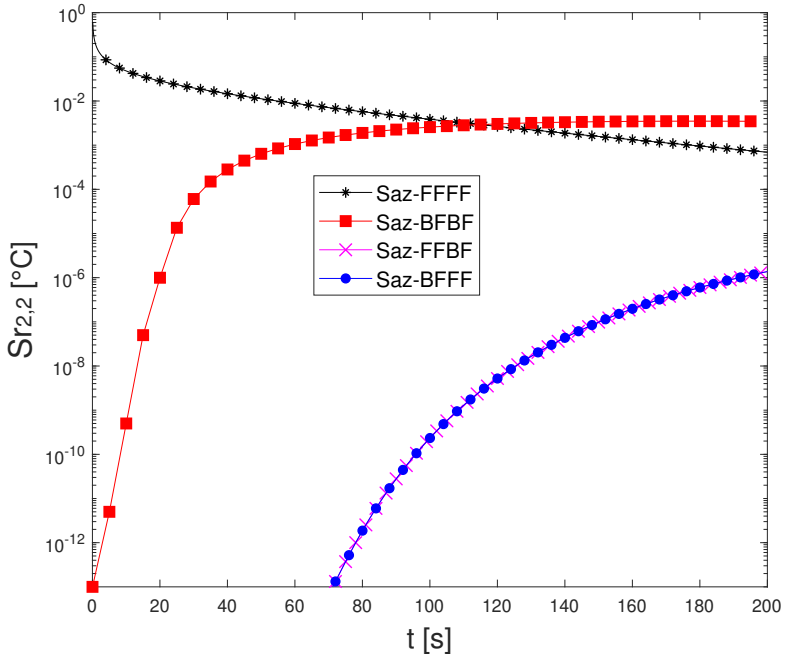

Figure 4.9 – Sensitivity evolution of the harmonic $\xi_{2,2}(t)$ to the CFRP in-depth diffusivity, associated with the polyamide liner, for the four possible configurations.

One should notice that same classification order is observed, regardless the type of the liner (Aluminum or Polyamide), the composite diffusivity (a_x, a_y or a_z), and the harmonic for which the sensitivity is studied. The influence of the overall heat transfer coefficient on both faces is also found to be negligible at the considered short time.

4.5.1.3 Estimation method and results

The estimation method is applied on the best configuration (FF-FF), according to the sensitivity analysis. A two-layer material with front face excitation and measurements is considered for the identification in order to test the feasibility. Both types of liners are considered, and synthetic data are generated using the model over which a certain level of noise is added. Then, the estimation results are compared in terms of accuracy and robustness, with respect to actual experimental constraints.

Model outputs, Front face harmonics

Based on the sensitivity analysis, the most appropriate configuration corresponds to a thermal excitation and measurement both performed on the CFRP side of the sample, whatever the

nature of the liner (whether aluminum or polyamide). Thus $\xi_{m,n}^{mod}(\beta, z=0, t)$ will represent the model outputs.

Cost function and the set of parameters β

Adding to the three dimensional thermal diffusivity tensor of the CFRP composite material, the parameters related to the excitation, assumed to follow the cosine function space shape, the total amount of heat absorbed by the material Q and the sport radius r, are also estimated simultaneously. Therefore the set of parameters will be $\beta = [a_{x,1}, a_{y,1}, a_{z,1}, Q, r]$.

The admitted harmonics, found to be sufficient for such estimation cases, have the maximum modes $M = 6$ and $N = 6$, therefore the objective function is, as previously described:

$$f = \sqrt{\sum_{m=0}^{6}\sum_{n=0}^{6}[\ \xi_{m,n}^{mod}(\beta, z=0, t) - \xi_{m,n}^{exp}(z=0, t)\ ]^2},\ [m \otimes n] = \{0,2,4,6\} \otimes \{0,2,4,6\} \tag{4.27}$$

Minimization algorithm

Estimation is performed using the optimization algorithm investigated in this work (hybrid optimization algorithm described in 2.5.4.3), and minimizing the least-squares criterion between the 3D analytical two-layer model outputs and synthetic noisy data.

Simulated measurements

An inverse crime strategy is performed in order to evaluate the feasibility of the estimation. The experiment is mimicked by means of the direct model, $\xi_{m,n}^{exp}(z=0, t)$, and a random noise is added to the signal to reproduce more or less severe experimental conditions. This exercise tests the potential of the estimation procedure and allows to evaluate its accuracy and its robustness.

Estimation Results

Model outputs data $Y(\beta) = \xi_{m,n}^{mod}(z=0, t)$ are generated by the direct model that predict the temperature evolution under a laser-like excitation, both on the CFRP side of the sample. The exploited signal correspond to both, the excitation and the cooling phases. The numerical experiment is realized by means of the same direct model with an additional noise ranging from 0 to 10% of the initial signal $\xi_{m,n}^{exp}(z=0, t)$. The relative difference between the estimated and the original values, $\frac{\Delta a}{a}$, are compared in Table 4.4 for different values of noise intensity.

The good agreement between the estimated and the actual values of the diffusivities, even for relatively important levels of noise, verify the feasibility and the accuracy of the estimation. The algorithm robustness is in turn verified by running the code several times. The variability of the resulting estimation are very, i.e. it produces similar results each time. The performance of the optimization algorithm applied for the identification of such complex material is clearly highlighted, as the deviation between the actual and the estimated values does not exceed 2.5% and 4.8% when the noise intensity is 5% and 10%, respectively.

Liner	**polyamide**				**Aluminum**			
noise	0%	1%	5%	10%	0%	1%	5%	10%
$\frac{\lvert\Delta a_x\rvert}{a_x}$	$3\cdot10^{-3}$%	10^{-2}%	0.2%	0.5%	$3\cdot10^{-4}$%	$6\cdot10^{-2}$%	0.1%	0.7%
$\frac{\lvert\Delta a_y\rvert}{a_y}$	10^{-4}%	$7\cdot10^{-2}$%	0.2%	0.3%	10^{-4}%	$5\cdot10^{-2}$%	$3\cdot10^{-2}$%	0.1%
$\frac{\lvert\Delta a_z\rvert}{a_z}$	$2\cdot10^{-3}$%	0.8%	2.5%	5.6%	10^{-3}%	0.3%	1.3%	4.8%

Table 4.4 – Relative deviation between the estimated and the actual values of the CFRP diffusivities $\overline{\overline{a}} = [0.4; 2.6; 0.4]\ mm^2 \cdot s^{-1}$.

4.5.2 Characterization of two-layer material: Experimental application on a CFRP-liner composite material

In this section, an actual two-layer plane and opaque material is studied, as shown in Fig.4.10. It is constituted by an isotropic polyamide polymer layer laminated on an orthotropic layer of CFRP.

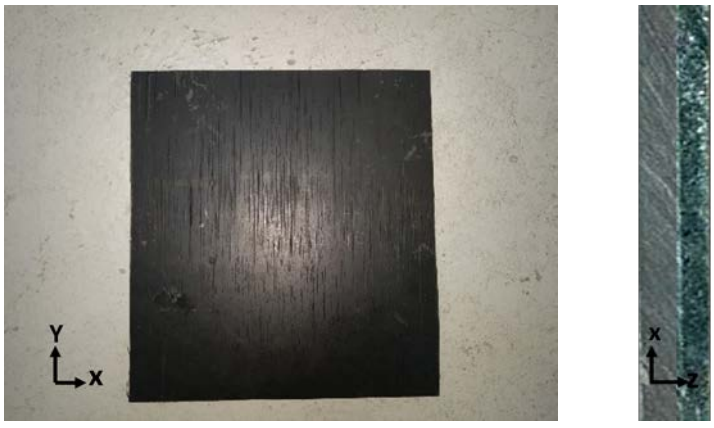

(a) front-face

(b) lateral-face

Figure 4.10 – Front(a) and lateral(b) views of the investigated two-layer material sample.

The properties measured for both layers are tabulated in Table 4.5. The values of the densities ρ and the heat capacities C are found to be very close of the monolayers materials investigated in the previous chapter (i.e. polyamide and the CFRP materials, see 3.4 and 4.3).

Adding to these physical properties, the dimension of the exploitation window, namely the size of the frames, $l_x \times l_y$, is chosen according to the thermal boundary conditions discussed in Sec 4.3.2. As shown in Fig. 4.11, the exploitation window is chosen such as $l_x \times l_y = 50\ mm \times 51\ mm$.

Properties	Values
ρ_1	$1286 \pm 18\ kg \cdot m^{-3}$
ρ_2	$1140 \pm 17\ kg \cdot m^{-3}$
C_1	$1001 \pm 30\ J \cdot kg^{-1} \cdot K^{-1}$
C_2	$1670 \pm 50\ J \cdot kg^{-1} \cdot K^{-1}$
l_{z_1}	$3.2 \pm 0.05\ mm$
l_{z_2}	$2.4 \pm 0.05\ mm$

Table 4.5 – Measured thermophysical properties of both layers include in the bi-layered material [i = 1 corresponds to the layer of Composite, and i = 2 to the layer of polyamide].

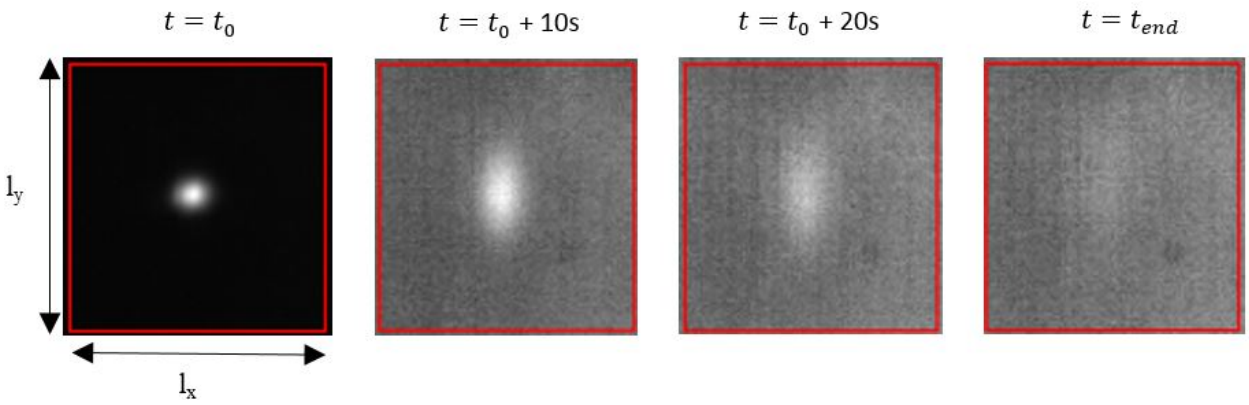

Figure 4.11 – Frames of the raw pictures given by IR camera at different times, following the laser beam excitation at t_0.

For the two-layer material, the sensitivities evolution of the harmonics $\xi_{2,2}(t)$ are presented in Figs. 4.12 according to the CFRP in-depth diffusivity, and the polyamide liner diffusivity, and for the four possible configurations. One can deduce that the classification of the experimental configurations based on sensitivity analysis is not the same as that retrieved in 4.8 and shown in Fig. 4.9.

In this work, two experimental configurations are evaluated and compared for the most sensitive configuration for each case found in Figs. 4.12. The specifications of each configuration are illustrated in Fig. 4.13. The first configuration corresponds to an excitation and IR measurements both performed on the front face of the sample (FF-FF), i.e. on the composite layer side. The second configuration corresponds to an excitation and IR measurements both performed on back face of the sample (BF-BF), i.e. on the polyamide layer side.

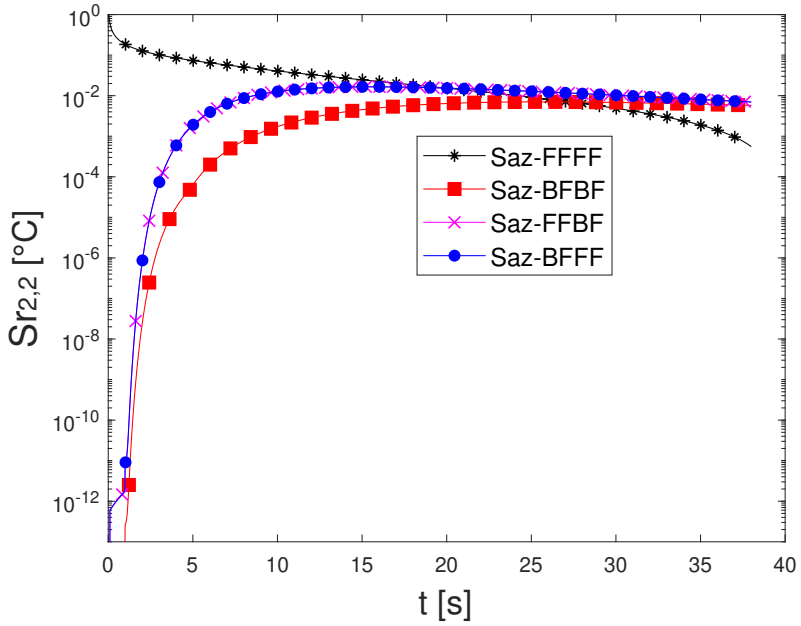

(a) CFRP in-depth diffusivity

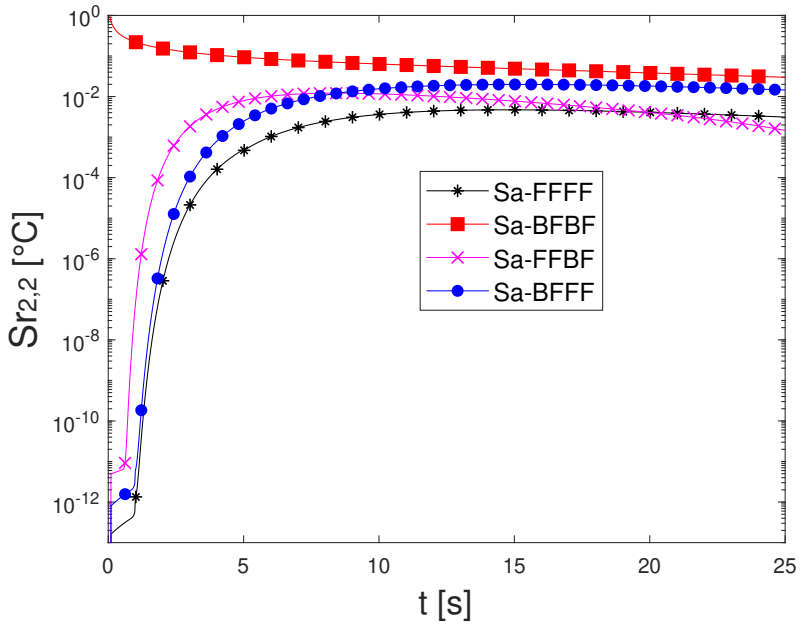

(b) polyamide liner in-depth diffusivity

Figure 4.12 – Sensitivity evolution of the harmonic $\xi_{2,2}(t)$ to the CFRP in-depth diffusivity, and the polyamide liner diffusivity, for the four possible configurations.

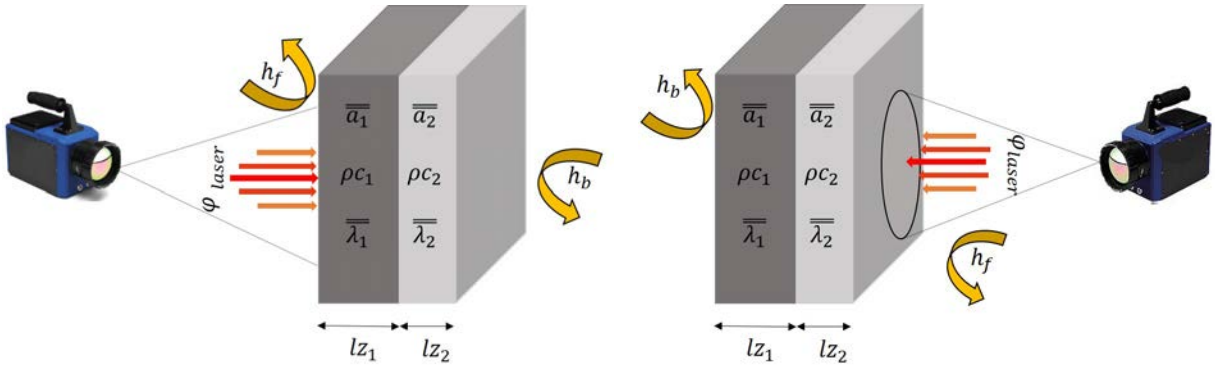

(a) FF-FF (b) BF-BF

Figure 4.13 – The two possible configurations and boundary conditions corresponding to CFRP-PA two-layer case.

4.5.2.1 Method calibration

In order to calibrate the identification method, as well as to estimate the feasibility, the performance and the robustness of the method, synthetic data are produced by means of the direct model to mimic the measurements. As previously done, some noise is added to those synthetic data, whose distribution is uniform and whose modulus ranges from 5% to 10% of the original signal. The results of this theoretical exercise, applied for both configurations shown in Fig. 4.13, allows to found the optimal settings of the PSO algorithm. In addition to the general parameters presented in 2.5.4.3, the PSO algorithm specifications and conditions as well as the stopping criteria, are tabulated in the Table 4.6. The unique difference between the present setting and the setting in Table 3.1 concerns the number of PSO particles.

The measurement acquisition time should be carefully chosen in such a way to ensure that the heat will reach the second layer. This criterion is essential as it ensures that the measurement of the temperature evolution at the surface of the first layer contains information related to the second layer. The thermal response of the sample, in both configurations, are then recorded during 60 s using an IR camera working at 50 Hz frequency.

Since in both configurations the excitation and measurements are conducted at the same sample side, the cost function can be always defined by the Eq. 4.27. The values of the overall heat transfer coefficients are assumed to be equal on both sides, with $h_f = h_b = h = 10\ W.m^{-2}.K^{-1}$. The thermal resistance Rc at the interface between the two layers, is neglected ($Rc = 0\ m^2 \cdot K \cdot W^{-1}$). Two cases will be treated and discussed in the following three sections:

- A case where 4 diffusivities are simultaneously estimated: one diffusivity for the isotropic polymer and three diffusivities for the composite. In this section, hereinafter referred to **4D identification**, the size of β is 20.

- A case where 6 diffusivities are simultaneously estimated, i.e. three for each layer. Here, the polyamide is considered as an orthotropic material. In this section, hereinafter referred to **6D identification**, the size of β is 22.

Conditions	Values
Bounds of $\overline{\overline{a_1}}$ and $\overline{\overline{a_2}}$	$[10^{-9}; 10^{-4}]\ m^2 \cdot s^{-1}$
Bounds of $R_{m,n}$	$[-100; +100]\ J$
Number of PSO particles	50
Maximum iterations	$500\times$ size of β
Maximum stop (stall) iterations	20
Tolerance value	10^{-8}
Maximum time	$+\infty$
Maximum stall time	$+\infty$
Minimum objective value	$-\infty$

Table 4.6 – PSO specifications, and stopping criteria selected for the estimation procedure.

In both cases, two possible experimental configurations (config.(a) and (b), as shown in Fig. 4.13) are tested in order to check and compare the accuracy of the method. The robustness of the algorithm is once again tested while retrieving the same estimation values when running the code several times.

4.5.2.2 Experimental identification results

4.5.2.2.1 4D estimation results

In this section, the composite diffusivity tensor is simultaneously estimated with the single diffusivity value of the isotropic polymer material. The results of the direct and simultaneous estimations for both configurations are represented in Table 4.7. In this case, $\overline{\overline{a_2}} = a_2$ as the same diffusivity value is considered in all directions. Based on Eq. 2.29, the variance covariance matrix of the estimated parameters are calculated and the standard deviations of the results are presented in brackets in Table 4.7.

As expected, the y-component of the composite thermal diffusivity (a_{y_1}) has the highest value. In fact, this direction (y-axis) is the most diffusive due to the presence of the carbon fibers. The most sensitive estimation (i.e. a_{y_1}) varies from about 15% between the two configurations. On the contrary, the in-depth diffusivity a_{z_1} is the less sensitive as the results differ from less than 1%. Adding to that, in both cases, the estimation of the first layer thermal diffusivities shows a good agreement with the values obtained when using a monolayer estimator

Estimated parameter	**Values** [$mm^2.s^{-1}$]	
	Config.(a)	Config.(b)
a_{x_1}	0.416 ($\sigma = 1.38 \cdot 10^{-3}, 0.330\%$)	0.463 ($\sigma = 0.019, 4.190\%$)
a_{y_1}	2.861 ($\sigma = 3.90 \cdot 10^{-3}, 0.140\%$)	2.423 ($\sigma = 0.041, 1.670\%$)
a_{z_1}	0.350 ($\sigma = 1.4 \cdot 10^{-4}, 0.041\%$)	0.349 ($\sigma = 3.74 \cdot 10^{-3}, 1.070\%$)
a_2	0.151 ($\sigma = 1.36 \cdot 10^{-3}, 0.9\%$)	0.161 ($\sigma = 7.62 \cdot 10^{-5}, 0.047\%$)

Table 4.7 – Values of thermal diffusivities resulting from the 4D estimation strategy for both configurations.

that will be discussed later on (see section 4.5.2.4), or when comparing with literature values and previous direct estimations applied on monolayer sample of PA.

The indirect estimated amount of heat absorbed by the material surface, Q, is shown to be equal to 0.446 J in config.(a) and 0.401 J in config.(b). Those values correspond respectively to 34.3% and 30.8% of the maximum laser capacity, which is also consistent with the experimental specification adopted for the present series of tests.

In order to evaluate the effects due to the uncertainty in the layers thickness measurements, the same estimation is performed for two other possible combinations of (l_{z_1} and $l_{z_2} mm$). Estimation results and the percentage of absolute relative deviation from the original estimation are presented in brackets in Table 4.8.

Results	**Config.(a)**		**Config.(b)**	
	3.1 mm ‖ 2.5 mm	3.3 mm ‖ 2.3 mm	3.1 mm ‖ 2.5 mm	3.3 mm ‖ 2.3 mm
a_{x_1} [$mm^2.s^{-1}$]	0.418 (0.5%)	0.416 (0.0%)	0.472 (1.9%)	0.482 (4.1%)
a_{y_1} [$mm^2.s^{-1}$]	2.867 (0.2%)	2.853 (0.3%)	2.615 (7.9%)	2.251 (7.1%)
a_{z_1} [$mm^2.s^{-1}$]	0.348 (0.6%)	0.349 (0.3%)	0.351 (0.6%)	0.340 (2.6%)
a_2 [$mm^2.s^{-1}$]	0.151 (0.0%)	0.150 (0.6%)	0.163 (1.2%)	0.156 (3.1%)

Table 4.8 – Estimated values of thermal diffusivities resulting from the 4D estimation strategy with different values of layers thicknesses for both configurations.

As the relative errors do not exceed 8% when the layers thicknesses vary from ±3.1% and ±4.2%, respectively, the method can be considered robust in terms of a priori knowledge of the geometrical properties.

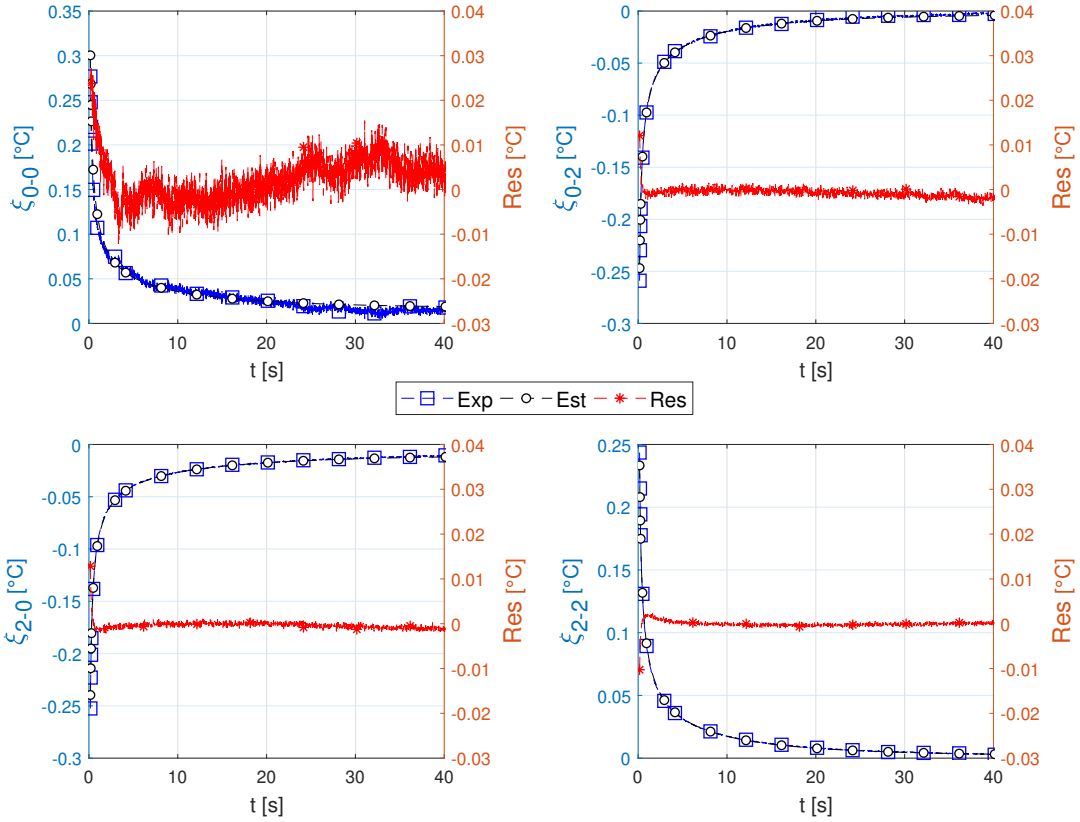

Figure 4.14 – Temporal evolution of the first four normalized harmonics concerning experimental (Exp.) and simulated data (Est.) using 4D estimation applied in config.(a). The absolute residue (Res) between both signals is plotted.

Figs. 4.14 and 4.15 illustrate the evolution of the first four experimental harmonics compared with the estimated harmonics, for both configurations (a) and (b) respectively. The discrepancy between both signals are represented by residual lines that illustrate the great fit between the experimental and the estimated data. One should notice that the highest deviation is always observed in the mean field normalized harmonic $\xi_{0,0}$ which is highly affected by the environmental changes.

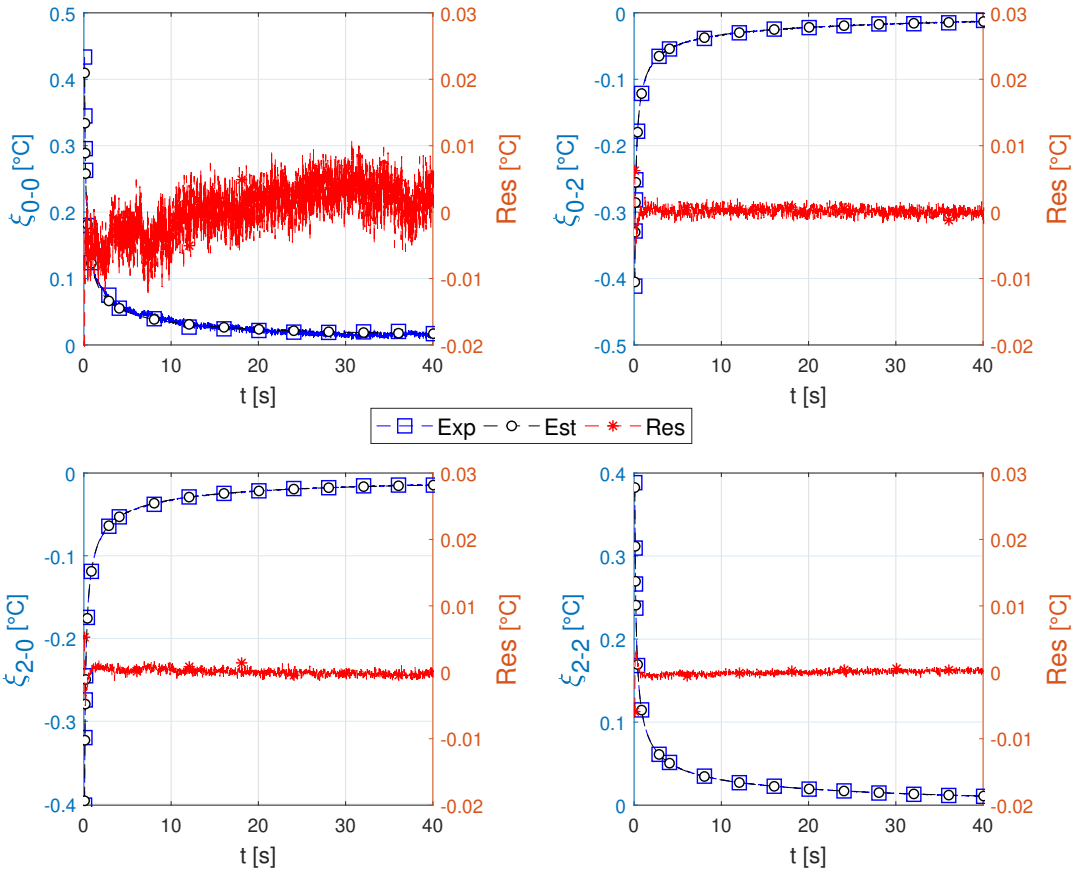

Figure 4.15 – Temporal evolution of the first four normalized harmonics concerning experimental (Exp.) and simulated data (Est.) using 4D estimation applied in config.(b). The absolute residue (Res) between both signals is plotted.

4.5.2.2.2 6D estimation results

In order to evaluate the possibility of considering more complex cases, this part presents the results obtained when considering the polyamide as an orthotropic material. In this case, the composite diffusivity tensor is simultaneously estimated with the polyamide diffusivity tensor. The results of the direct and simultaneous estimations for both configurations are represented in Table 4.9.

Estimated parameter	**Values** [$mm^2.s^{-1}$]	
	Config.(a)	Config.(b)
a_{x_1}	0.413 ($\sigma = 1.73 \cdot 10^{-3}, 0.420\%$)	0.489 ($\sigma = 0.028, 5.810\%$)
a_{y_1}	2.821 ($\sigma = 4.47 \cdot 10^{-3}, 0.160\%$)	2.318 ($\sigma = 0.049, 2.110\%$)
a_{z_1}	0.344 ($\sigma = 1.40 \cdot 10^{-4}, 0.039\%$)	0.371 ($\sigma = 3.74 \cdot 10^{-3}, 1.090\%$)
a_{x_2}	0.388 ($\sigma = 0.024, 6.26\%$)	0.158 ($\sigma = 2.00 \cdot 10^{-3}, 1.270\%$)
a_{y_2}	2.000 ($\sigma = 0.105, 5.28\%$)	0.155 ($\sigma = 1.41 \cdot 10^{-3}, 0.910\%$)
a_{z_2}	0.156 ($\sigma = 1.49 \cdot 10^{-3}, 0.960\%$)	0.157 ($\sigma = 7.827 \cdot 10^{-4}, 0.049\%$)

Table 4.9 – Values of thermal diffusivities resulting from the 6D estimation strategy, for both configurations.

In config.(a), the CFRP diffusivity tensor estimation is consistent as the average relative deviation is less than 3% when compared to previous results (Table 4.7). The maximum relative deviation occurs for the in-depth diffusivity, a_{z_1}, with a value of 6% compared to the 4D estimation in the same configuration. However, the polyamide diffusivity tensor estimation does not capture its isotropic nature with a consequent dispersion in the diffusivity estimation along the 3 directions. Noting that, the in-depth diffusivity estimation, a_{z_2}, is consistent with all the previous estimations, i.e. 6D Config.(b) and 4D Config.(a) and (b).

On the other side, in config.(b), the isotropic nature of the polyamide diffusivity is well captured, as the estimations of the diffusities along the 3 directions differ from less than 1% from the average value $\overline{a_2} = 0.157\ mm^2.s^{-1}$. Moreover, results are in good agreement with those of the 4D identification section, 0.161 and 0.151 $mm^2.s^{-1}$, respectively. The CFRP diffusivity tensor estimation is once again consistent as the average relative deviation is less than 4% when compared to previous results (Table 4.7).

Now for this 6D case, Figs. 4.16 and 4.17 illustrate the evolution of the first four experimental harmonics compared with the estimated ones, for both configurations (a) and (b) respectively, with the same observations as for Figs. 4.14 and 4.15 in the 4D case.

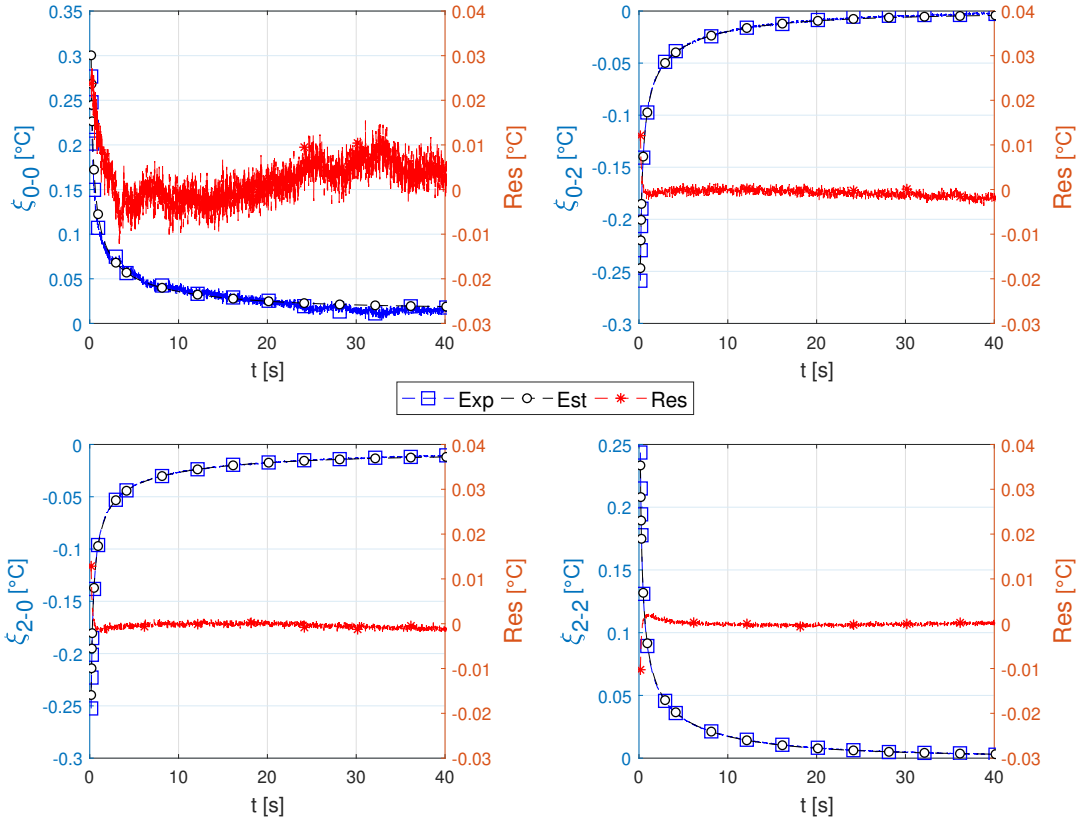

Figure 4.16 – Temporal evolution of the first four normalized harmonics concerning experimental (Exp.) and simulated data (Est.) using 6D estimation applied in config.(a). The absolute residue (Res) between both signals is plotted.

The present analysis is supplemented by a sensitivity study that investigates the influence in changes of model parameters on the model outputs, in this case the harmonics $\xi_{m,n}$.

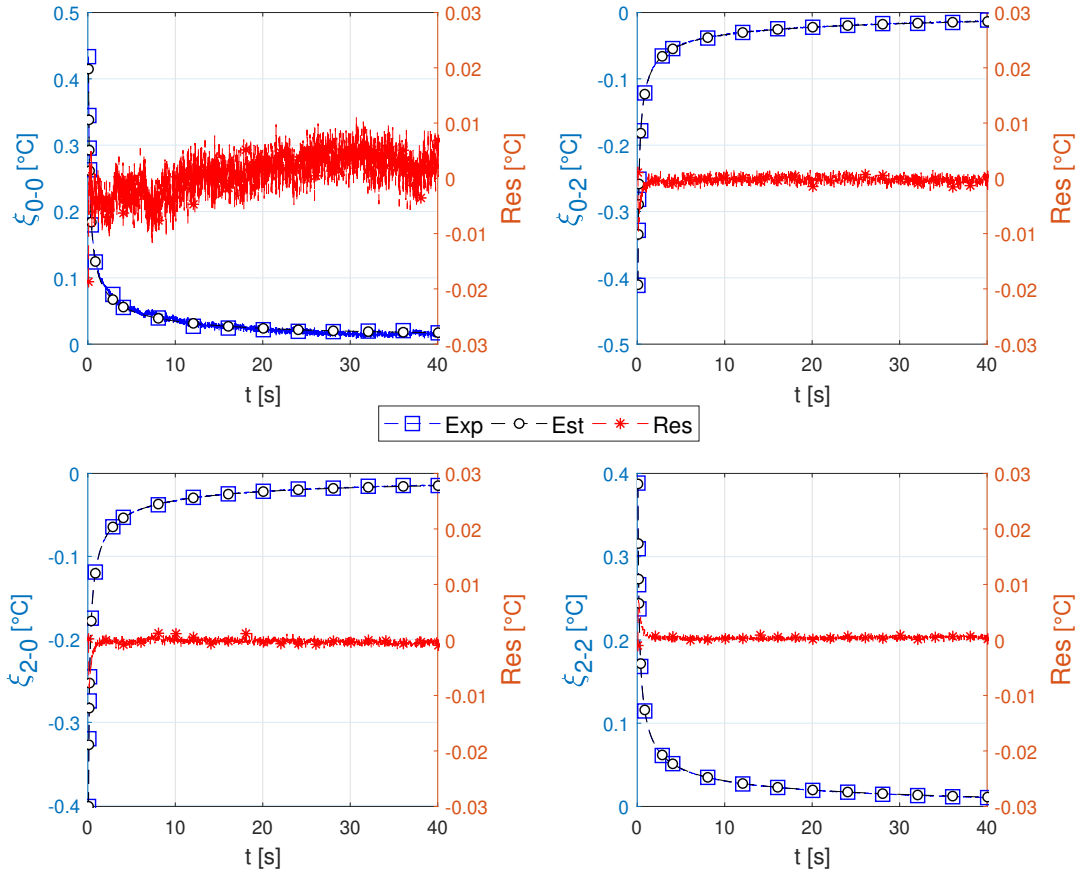

Figure 4.17 – Temporal evolution of the first four normalized harmonics concerning experimental (Exp.) and simulated data (Est.) using 6D estimation applied in config.(b). The absolute residue (Res) between both signals is plotted.

4.5.2.3 Sensitivity analysis

The evolution of the reduced sensitivities of the model outputs $\xi_{m,n}(z=0,t)$ with respect to the parameters of the vector β, is analyzed in this section. The general definition of the reduced sensitivity is recalled in Eq. 4.28.

$$Sr_{m,n}(\beta_j,t) = \frac{\partial \xi_{m,n}(\beta,t)}{\partial \beta_j} \times \beta_j \Big|_{\beta_{k\neq j}} \tag{4.28}$$

The comparison of the reduced sensitivities evolution is performed for the parameters of interest, i.e. the thermal diffusivity tensor of both layers, by means of Figs. 4.25 to 4.21.

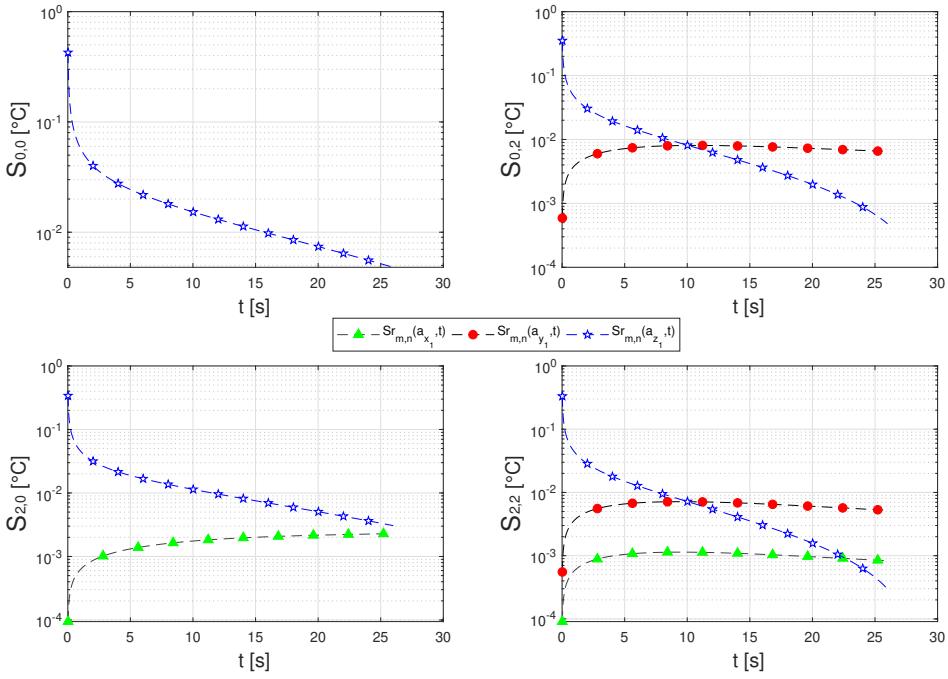

Figure 4.18 – Reduced sensitivities of the first 4 normalized harmonics to the composite diffusivities in config.(a).

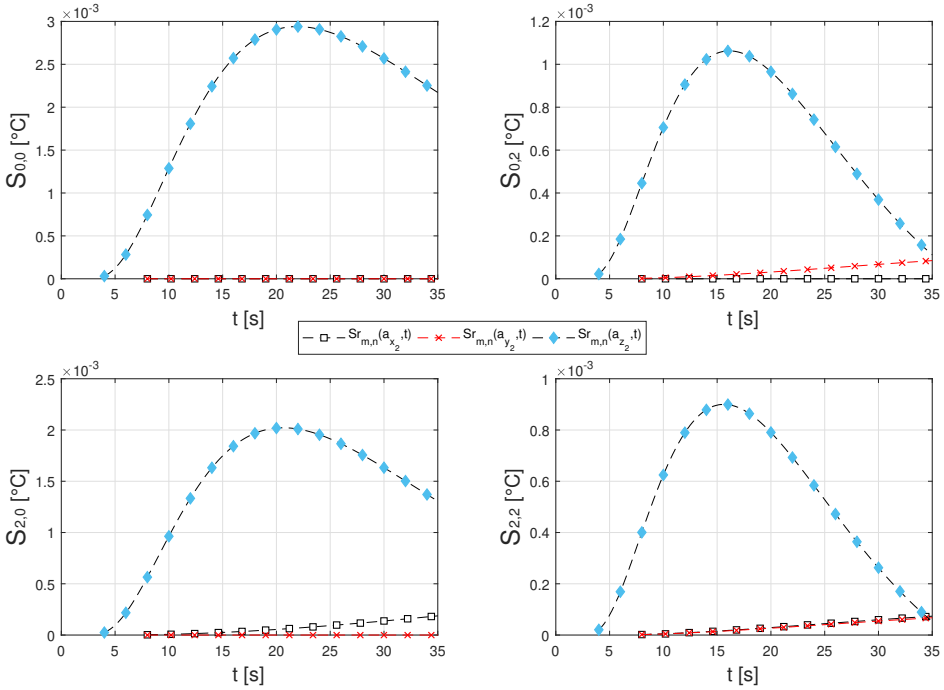

Figure 4.19 – Reduced sensitivities of the first 4 normalized harmonics to the polyamide diffusivities in config.(a).

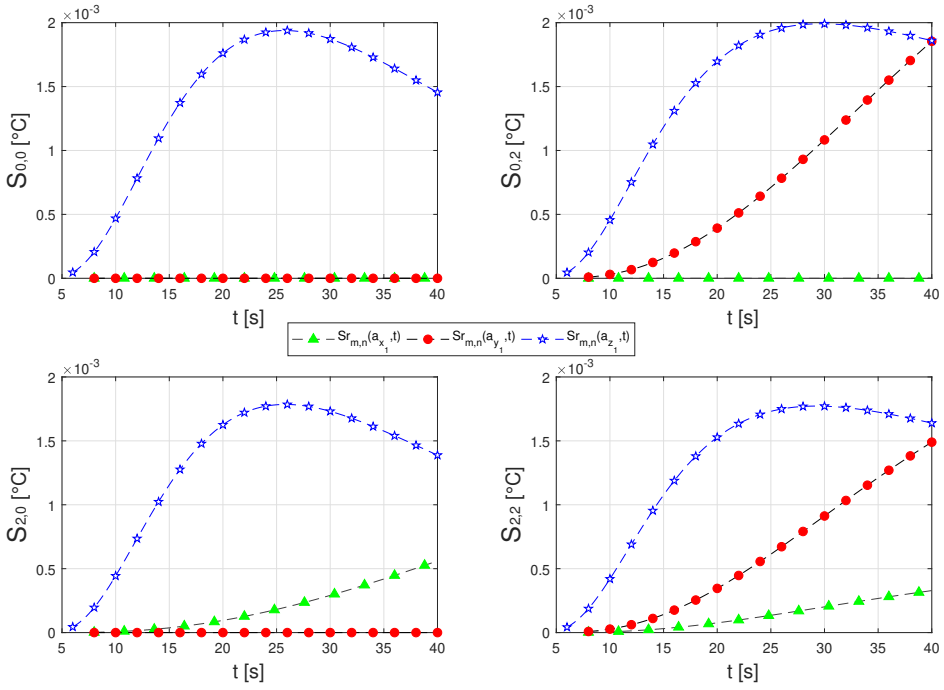

Figure 4.20 – Reduced sensitivities of the first 4 normalized harmonics to the composite diffusivities in config.(b).

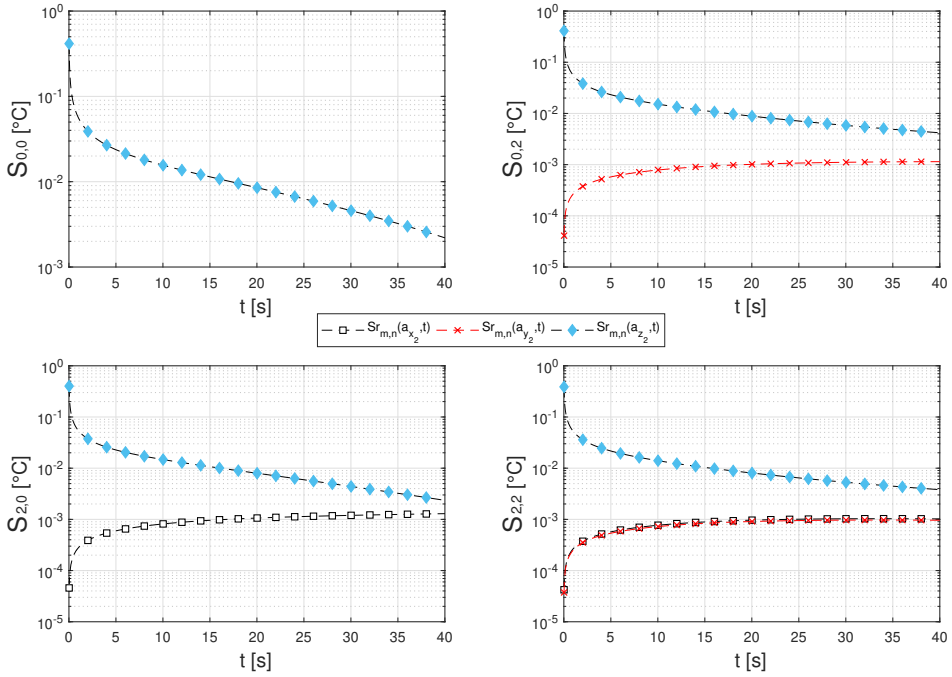

Figure 4.21 – Reduced sensitivities of the first 4 normalized harmonics to the polyamide diffusivities in config.(b).

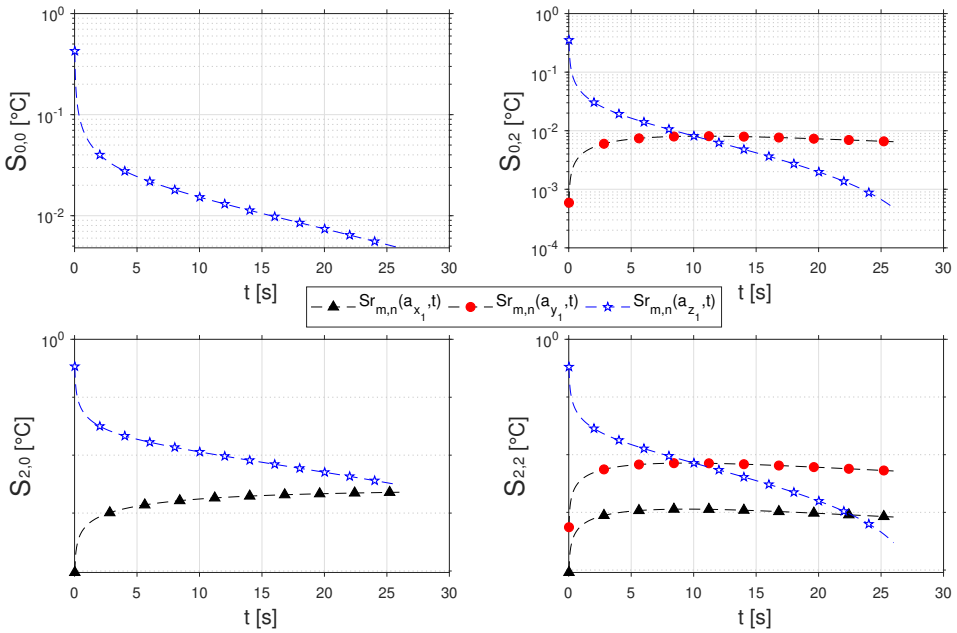

Figure 4.22 – Reduced sensitivities of the first 4 normalized harmonics to the composite diffusivities in config.(a).

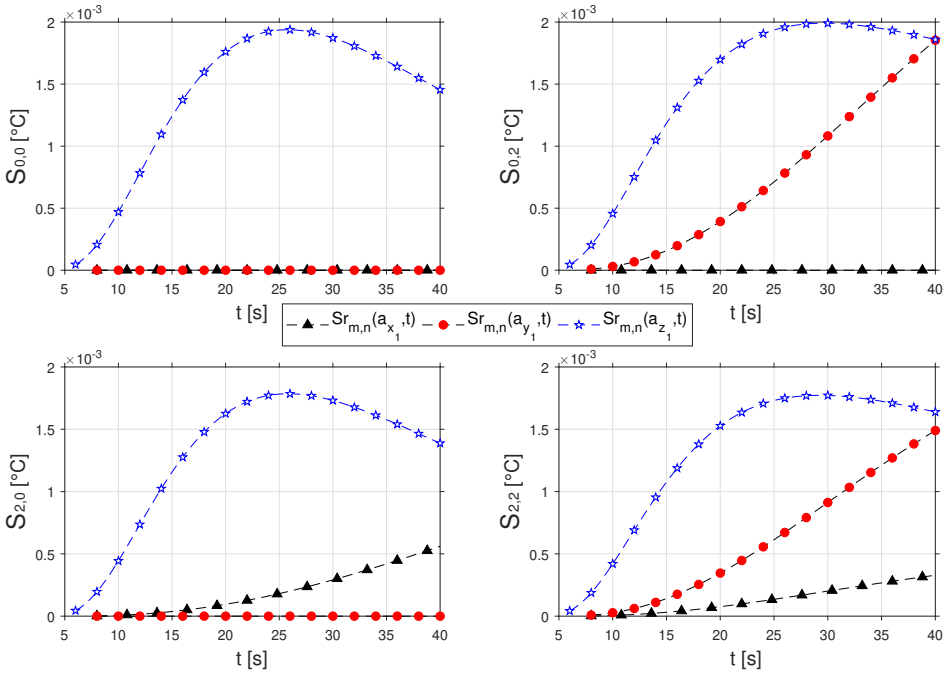

Figure 4.23 – Reduced sensitivities of the first 4 normalized harmonics to the composite diffusivities in config.(a).

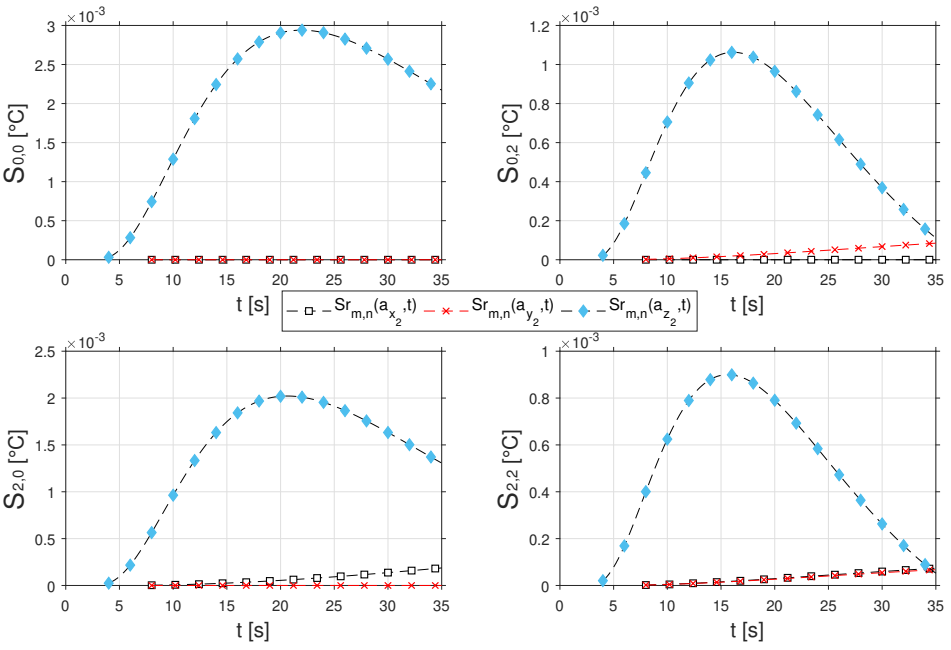

Figure 4.24 – Reduced sensitivities of the first 4 normalized harmonics to the composite diffusivities in config.(a).

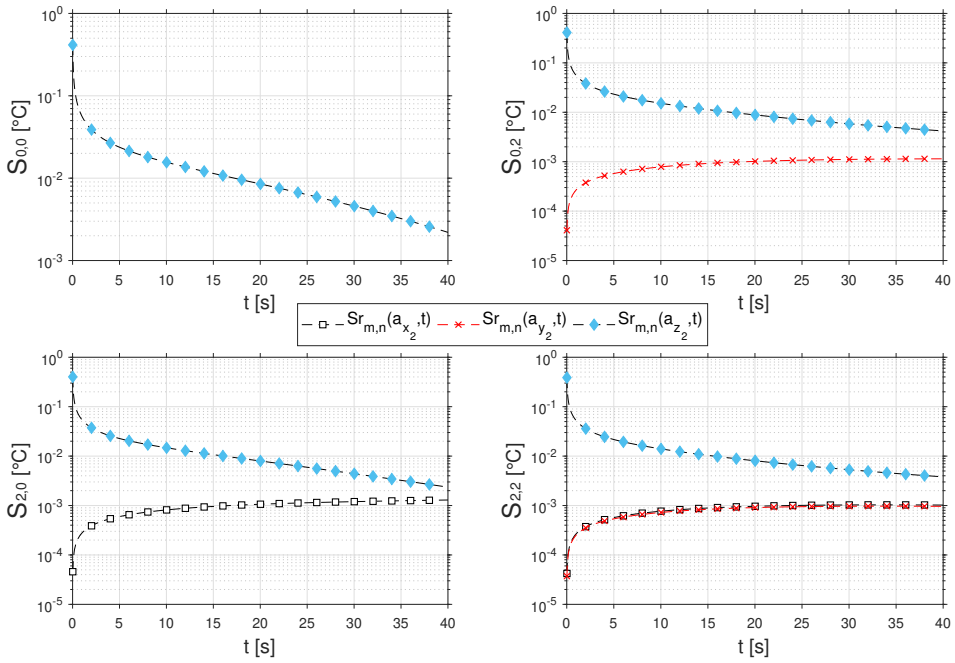

Figure 4.25 – Reduced sensitivities of the first 4 normalized harmonics to the composite diffusivities in config.(a).

As previously interpreted in 3.4.3.1, a key strength of the present method relies on the usage of multiple modes that allow to separate the contribution of the directional diffusivities. For example, the modes with non-zero values of m are dedicated to diffusivities along the x axis, while the modes with non-zero values of n are dedicated to diffusivities along the y axis. Thus, even with a strong coupling between $Sr_{2,2}(a_{x_1}, t)$ and $Sr_{2,2}(a_{y_1}, t)$ in Fig. 4.25, the method is able to independently determine a_{x_1} and a_{y_1} by means of $Sr_{2,0}(a_{x_1}, t)$ and $Sr_{0,2}(a_{y_1}, t)$. It is worth mentioning that the in-depth diffusivity a_z is usually involved in every mode, and the average mode relative to the mean field $Sr_{0,0}$ is exclusively dedicated to this.

From a temporal point of view, the first layer has the greatest values of sensitivities. In Config.(a) the order of sensitivities magnitude for the CFRP diffusivities (Fig. 4.25) is higher then for the polyamide diffusivities (Fig. 4.19). In parallel, in Config.(b), the order of sensitivities magnitude for the polyamide diffusivities (Fig. 4.21) is higher than those for the Composite diffusivities (Fig. 4.20). In config.(a), and due to the anisotropic diffusion in the first layer, the sensitivities to the polyamide in-plane diffusivities are relatively low compared to that of the in-depth direction. This observation explain the relatively poor estimation results of a_{x_2} and a_{y_2} (Table 4.9, Config.(a)).

Another benefit of such study is the analysis, as a preliminary study, of the overall heat transfer coefficient sensitivity. This latter was found to be negligible at the considered data exploitation time.

4.5.2.4 Comparison with ENH at short time

As a preliminary comparative tool, the ENH estimator [78, 81, 270] dedicated to monolayer sample, is conducted for both configurations. To recall, this estimator can only give the in-plane diffusivities of the first layer (the layer having its surface subjected to the thermal excitation). Moreover, the estimation must be performed at very short time in order to imply only the first layer, as shown in Fig. 4.26. Therefore a small comparison between previous results and those obtained with ENH at short time, concerning the first layer in-plane diffusivities in both cases, is performed in Table 4.10. At short time, one can see from the graphs the differences in behavior of one mono-layer and bi-layer models. Both curves superimpose at short time when ENH can estimate the thermal properties of the first layer. Then, the estimation of ENH can be use as a comparative tool for the method proposed in this work. In this study, all resulting values agree with ENH results and with the values found in the literature or from the separated monolayers estimated with the monolayer model before.

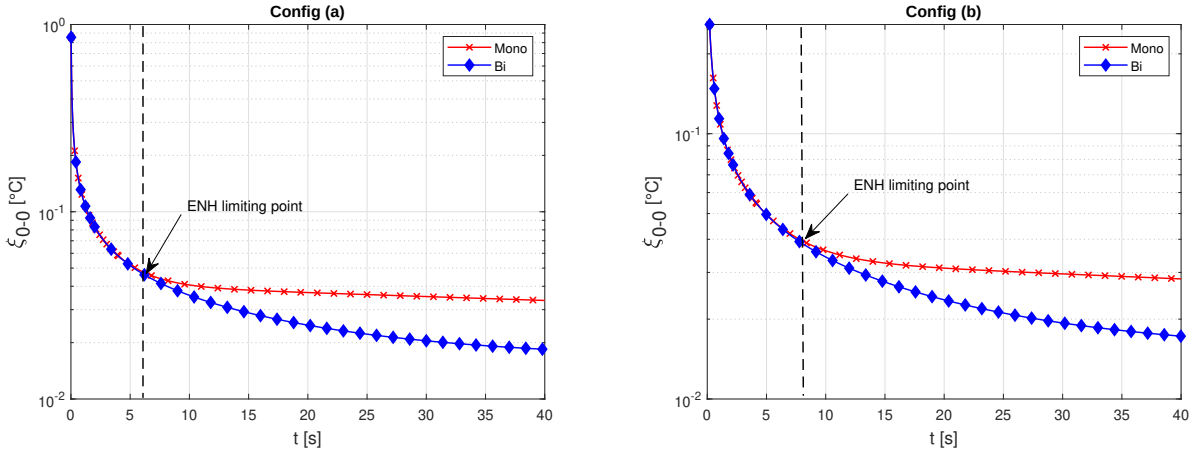

(a) FF-FF (b) BF-BF

Figure 4.26 – The difference in the main field $\xi_{0,0}$ obtained using monolayer (Mono) model and that obtained using bilayer (Bi) model , with an illustration of ENH limitation, applied for both configurations.

Estimated parameter	Monolayer ENH estimation		**4D estimation**				**6D estimation**			
(in $mm^2.s^{-1}$)	Config.(a)	Config.(b)	Config.(a)		Config (b)		Config.(a)		Config.(b)	
a_x	0.408^1	0.176^2	0.416^1	0.151^2	0.463^1	0.161^2	0.4130^1	0.3882^2	0.4891^1	0.1579^2
a_y	2.676^1	0.176^2	2.861^1	0.151^2	2.423^1	0.161^2	2.8210^1	2.1998^2	2.3178^1	0.1554^2

Table 4.10 – Values of in-plane thermal diffusivities resulting from the ENH estimator for both configurations, compared to the results obtained by the 4D and 6D estimation methods, superscript 1 refers to the composite layer and superscript 2 refers to the polyamide layer.

Estimated values of the thermal diffusivities for both layers are consistent with the results obtained previously considering both layers as free-standing samples (i.e. monolayers).

4.5.3 Degenerated case: coating on substrate characterization

This part presents an application of the two-layers model with the overall identification technique developed in this work. In this part, the two-layer material is degenerated in a thin layer, also called coating, deposited on a substrate [271].

4.5.3.1 Context and applications

As already presented in 1.2, coatings are used in many domains, they can serve as thermal (e.g. overheating or fire protection), chemical (i.e. erosion, corrosion or oxidation prevention), mechanical protection (e.g. ablation protection), or even as an improvement of some optical properties (i.e. black coating to have a surface emissivity of a black body). It can be also used for temperature measurement techniques, with the two most important techniques: "IR thermograhy" and "phosphorescence thermometry". The latter is based on the phosphorescent properties of some materials used to determine the surface temperature, deduced from the measurement of the emitted radiation intensity.

Some special applications for the coating handled and thermally characterized in this chapter, is already presented in 1.2. It consists in a thin layer, designated hereinafter by "TPT" coating for "Thermographic Phosphor Thermometry". The thermal characterization (in particular the thermal diffusivity) of such phosphorous layer is crucial in order to accurately predict the intensity of heat transferred through this thin layer and the temperature evolution profile at the surface of the covered material (e.g. piston, valves, etc).

However, due to the impossibility of separating the coating from its substrate, the currently investigated method implementing a direct and simultaneous thermal characterization of both layers constituting the sample, seems inevitable.

4.5.3.2 Problem description

The main aim of this part concerns the thermal characterization of a specific two-layers material constituted of a thin layer or coating deposited on an isotropic or orthotropic material. The coating considered in this study is the a phosphorescent material generally applied in the combustion chambers for thermal measurements. In order to reproduce, as well as possible, the experimental deposition of the TPT coating, the coating should be deposited on a metallic sample, such as copper or aluminum. However, these materials are highly diffusive and due to some experimental limitations related to the achievable acquisition frequency of the handled IR camera, these substrates necessitating a very high acquisition frequency (typically $> 1000 Hz$) are replaced by a substrate having a low thermal diffusion (e.g. HDPE = High Density Polyethylene or polyamide) that requires a moderate acquisition frequency ($\simeq$ 50 Hz).

4.5.3.3 Direct model

The two layers model is already developed in the previous sections 4.5.1.1, and all subsets involved in the inverse heat conduction problem are the same as the two-layers material applica-

tions (see 4.5.2).

The process under which the coating layer is deposited on the surface of the substrate encourage the consideration of a negligible contact resistance Rc at the interface between both layers.

The TPT coating is considered isotropic, i.e. $a_x = a_y = a_z = a_{TPT}$, thus the parameters vector that should be estimated in this case is $\beta = [a_{x,1}, a_{y,1}, a_{z,1}, a_{TPT}, R_{0,0}, R_{0,2}, R_{2,2}, \ldots, R_{m,n}, \ldots, R_{6,6}]$. It corresponds to 20 parameters to estimate for the case where the substrate is considered orthotropic and 18 for the case where it is considered isotropic, $\beta = [a_{HDPE}, a_{TPT}, R_{0,0}, R_{0,2}, R_{2,2}, \ldots, R_{m,n}, \ldots, R_{6,6}]$.

4.5.3.4 Sensitivity analysis

The same study of sensitivities analysis than conducted in 4.5.1.2, is repeated here in order to prioritize the most appropriate configurations for the estimation of the coating properties, with or without the simultaneous estimation of the substrate properties. The classification is shown in 4.27a, and the sensitivity of the harmonic $\xi_{2,2}(t)$ to the coating in-depth thermal diffusivity, for the four possible configurations is presented in Fig. 4.27b.

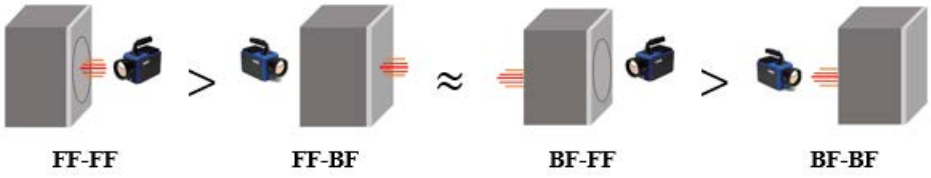

(a)

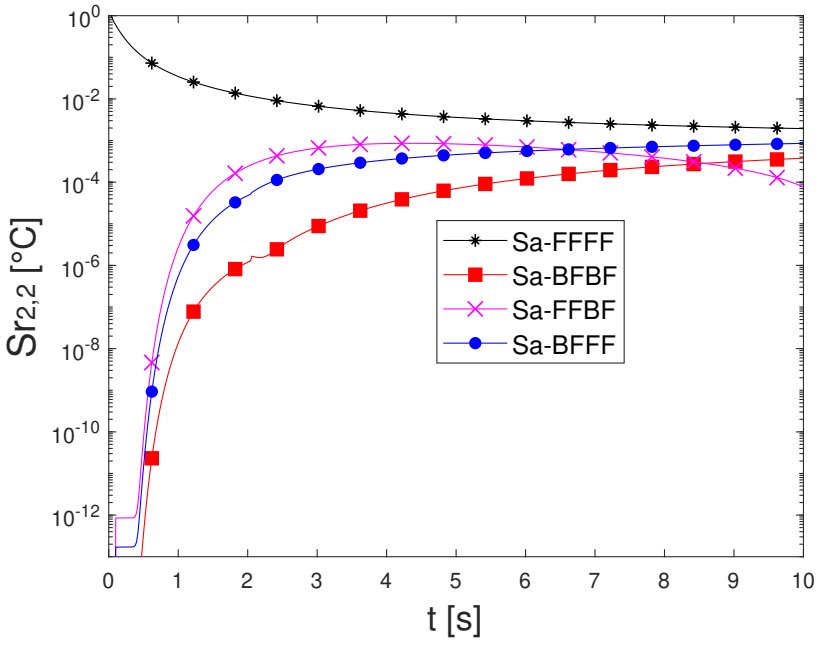

(b)

Figure 4.27 – Sensitivity evolution of the harmonic $\xi_{2,2}(t)$ to the coating in depth thermal diffusivity, for the four possible configurations.

It is important to note that the sensitivity analysis that allows to compare different possible experimental configurations, and the numerical applications represented in 4.5.3.5 require the values of the parameters β or an approximative value in order to simulate data via the direct model. These values are inspired from the litterature [272] and from a study [273] that considered the case of a High-speed thermographic phosphor thermometry used to control the temperature increase and the time and position of flame impingement at the piston surface.

An exploitation window with $l_x = l_y = 50\ mm$ has been proved, through a preliminary study, to be convenient for such application, since it can give a good accuracy/time ratio. The parameters involved in the thermal excitation definition correspond to the total amount of energy deposited on the material, $Q = 0.56\ J$, and to the laser radius $r = \frac{l_x}{9.55} (\approx 5\ mm)$.

While remaining consistent in terms of radius value that can be experimentally generated, this set of parameters can guarantee a temperature evolution at the surface of the material: i) sufficient to be accurately measured and ii) tolerable to avoid any risk of properties modification (i.e. temperature dependence of parameters) that can occur at high temperature (typically $> 10\ ^\circ C$).

The spatial distribution of the thermal excitation is parameterized by a cubic polynomial shape, which is consistent with experimental observations and already tested in previous monolayers applications 3.6.1. This form allows us to calculate the form factors $F_{m,n}$.

Parameters	**TPT coating** [273]	**HDPE** [272]
$a\ [mm^2 \cdot s^{-1}]$	[0.30 - 1.00]	2.77
$\rho C\ [kJ \cdot m^{-3} \cdot K^{-1}]$	1316	1805
$l_z\ [mm]$	[0.05 - 0.30]	[2.0 - 3.0]

Table 4.11 – Model parameters values used to generate synthetic measures signals.

Experimental configurations

Two possible experimental configurations are considered for numerical validation in order to test the feasibility and the accuracy of the identification method for both cases. The FF-FF configuration is the most sensitive, as shown in Fig. 4.27b. The other configuration BF-BF corresponds to the simplest one, in terms of experimental conditions and limitations. Their respective experimental protocols are illustrated in Fig. 4.28. The first configuration (a) or FF-FF as shown in Fig. 4.27a, consists in subjecting the heat flux (laser beam) on the surface of the coating and measuring the resulting temperature evolution profile at the same side. On the contrary, the configuration (b) or BF-BF as shown in Fig. 4.27a, considers the case where the excitation and the temperature profiles measurements are conducted at the substrate surface side.

The excitation of the thin coating surface taking place in the configurations FF-FF and FF-BF is not advisable for degradation and poor control of penetration depth reasons. The same observations can be made for the measurement at this surface, taking place in the configurations FF-FF and BF-FF which is also not advisable, due to the ill-knowledge of the TPT surface emissivity.

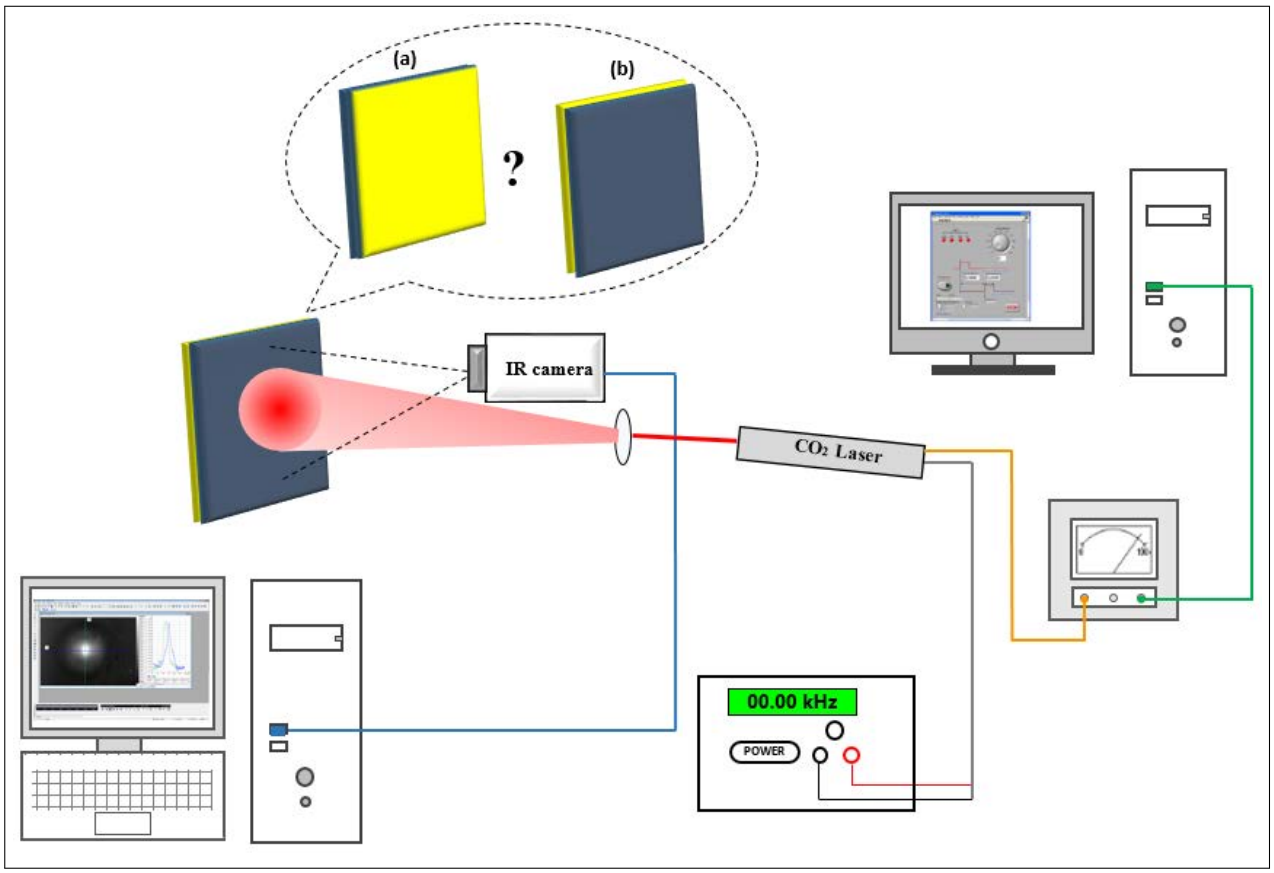

Figure 4.28 – The both numerically tested and compared experimental configurations, dedicated to the thermal characterization of the TPT coating.

4.5.3.5 Numerical validation

The numerical application currently conducted in order to validate the identification feasibility and evaluate the robustness and the accuracy of the estimation method, relies on "synthetic measurements" for both configurations (a) and (b). These data are generated from the direct model for which a certain level of random noise with a Gaussian distribution is added, in order to be close to experimental conditions.

Numerical results

The numerical results for both experimental configurations (a) and (b) and for both cases with isotropic or orthotropic substrate, and with or without random noise added, are presented in Table 4.12 for a 2 mm HDPE covered by a 50 μm TPT coating. These calculations are repeated

Configuration			Config.(a)		Config.(b)	
Case		noise level / Rel. deviation %	0%	5%	0%	5%
1	isotropic substrate	$\frac{\lvert\Delta a\rvert}{a}$	$5.37\cdot10^{-4}$%	0.50%	$1.39\cdot10^{-3}$%	0.51%
	isotropic coating	$\frac{\lvert\Delta a\rvert}{a}$	$2.06\cdot10^{-3}$%	1.81%	$6.18\cdot10^{-2}$%	1.33%
2	orthotropic substrate	$\frac{\lvert\Delta a_x\rvert}{a_x}$	$2.56\cdot10^{-4}$%	1.40%	$1.69\cdot10^{-3}$%	1.02%
		$\frac{\lvert\Delta a_y\rvert}{a_y}$	$2.84\cdot10^{-4}$%	0.66%	$1.64\cdot10^{-3}$%	0.45%
		$\frac{\lvert\Delta a_z\rvert}{a_z}$	$1.77\cdot10^{-4}$%	0.16%	$2.83\cdot10^{-4}$%	0.33%
	isotropic coating	$\frac{\lvert\Delta a\rvert}{a}$	$5.61\cdot10^{-4}$%	0.45%	$2.74\cdot10^{-2}$%	0.42%

Table 4.12 – Estimation results in function of the presupposed nature of the substrate (isotropic or orthotropic) for a 2 mm HDPE covered by a 50 μm TPT coating with a_{HDPE} = 2.77 $mm^2\cdot s^{-1}$ and a_{TPT} = 1 $mm^2\cdot s^{-1}$.

for 3 mm HDPE covered by a 300 μm TPT coating (see Table 4.13) in order to be coherent with experimental applications, that follows this section. Results are presented in terms of relative deviation or error between the parameters values used to generate the synthetic data and those estimated using the current identification investigated in thin study.

One can obviously notice the small relative deviation between the original values and the estimated ones for all treated cases, with and without random noise added. The comparison validate therefore the robustness and accuracy of the current method. Not surprisingly, the configuration (a) gives theoretically better results compared to the configuration (b) and notably without adding noise to the original signal generated by the direct model (with an error $< 2.1\cdot10^{-3}$ without noise and < 2% with 5% noise for the 2 mm HDPE covered by 50 μm of TPT, and an error $< 1.0\cdot10^{-3}$ without noise and < 2% with 5% noise for the 3 mm HDPE covered by 300 μm of TPT).

Despite this, results obtained with (b) are also convincing and promising, specially when adding a certain level of noise (with an error $< 6.2\cdot10^{-2}$ without noise and < 1.4% with 5% noise for the 2 mm HDPE covered by 50 μm of TPT, and an error $< 1.0\cdot10^{-2}$ without noise and < 2% with 5% noise for the 3 mm HDPE covered by 300 μm of TPT). In fact, this latter is preferable from the experimental points of view. It limits the risk of coating degradation that can be important within the first configuration.

Adding to that, impulse model is difficult to realize for the configuration (a), due to the ill-knowledge of the coating thermal characterization time and the necessity of a high acquisition frequency to detect the dynamic of heat transfer through this thin layer. Nevertheless, the acquisition time required for the configuration (a) is quite lower than that required with the con-

Configuration			**Config.(a)**		**Config.(b)**	
Case		noise level / Rel. deviation %	0%	5%	0%	5%
1	isotropic substrate	$\frac{\lvert\Delta a\rvert}{a}$	$1.22\cdot10^{-4}$%	1.88%	$8.16\cdot10^{-4}$%	0.84%
	isotropic coating	$\frac{\lvert\Delta a\rvert}{a}$	$3.01\cdot10^{-4}$%	1.24%	$2.83\cdot10^{-3}$%	1.22%
2	orthotropic substrate	$\frac{\lvert\Delta a_x\rvert}{a_x}$	$3.71\cdot10^{-4}$%	0.68%	$6.13\cdot10^{-4}$%	0.95%
		$\frac{\lvert\Delta a_y\rvert}{a_y}$	$3.15\cdot10^{-4}$%	0.69%	$6.19\cdot10^{-4}$%	0.85%
		$\frac{\lvert\Delta a_z\rvert}{a_z}$	$6.96\cdot10^{-4}$%	1.21%	$1.51\cdot10^{-3}$%	0.85%
	isotropic coating	$\frac{\lvert\Delta a\rvert}{a}$	$9.20\cdot10^{-4}$%	1.86%	$9.01\cdot10^{-3}$%	1.88%

Table 4.13 – Estimation results in function of the presupposed nature of the substrate (isotropic or orthotropic) for a 3 mm HDPE covered by a 300 μm of TPT coating with $a_{HDPE} = 2.77\ mm^2\cdot s^{-1}$ and $a_{TPT} = 1\ mm^2\cdot s^{-1}$.

figuration (b). This intuitive observation is confronted by sensitivity study for the observables to the diffusivities of both layers. The reduced sensitivities for the mode $(2,2)$, generally considered as the reference one, are plotted in Figs. 4.29 for both configurations and for the case 1 where both layers are considered isotropic.

This study proved that the identification of thermal diffusivities is possible at short time for the case (a), whereas the case (b) requires a longer duration time, due to the substrate properties and thickness. Lastly, giving the good accuracy level achieved by the estimation results when implementing the configuration (b), the latter can be envisaged for experimental applications, when taking into account all restrictions and risks that could be faced with configuration (a).

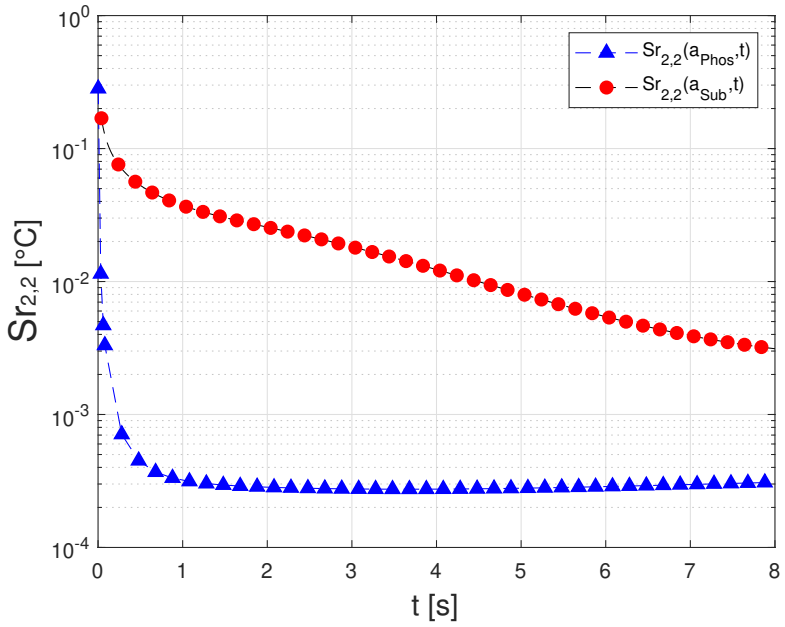

(a) Configuration (a)

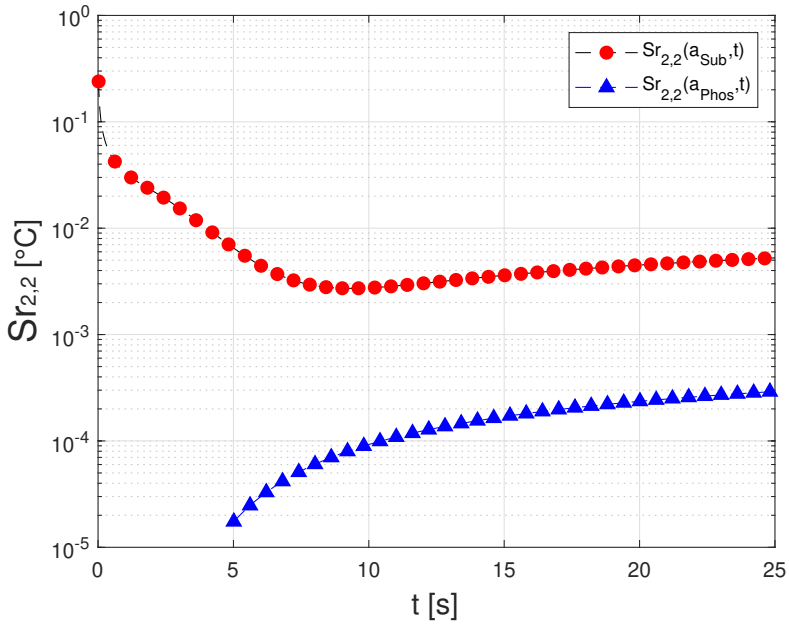

(b) Configuration (b)

Figure 4.29 – The evolution of normalized harmonics $\xi_{2,2}$ reduced sensitivities to the in-depth thermal diffusivities of both layers, and for both configurations (a) and (b).

4.5.3.6 Experimental application and results

At this stage, experimental applications have been carried out within the framework of a collaboration with a team from the "Institut Français du Pétrole et Energies Nouvelles" (IFPEN). The overall identification method is conducted on some of their samples constituted of a HDPE layer of 3 mm thichness covered by a thermal phosphorescent coating whose thicknesses is measured between 300 and 350 μm. The photo of one of these samples is shown in Fig. 4.30.

Figure 4.30 – TPT-coating over HDPE.

First of all, the identification technique was conducted on these sample using the density ρ and heat capacity C values found in the literature (Table 4.16). The results corresponding to the sample 1 constituted of a 3 mm HDPE covered by a 300 μm of TPT coating and sample 2 constituted of a 3 mm HDPE covered by a 350 μm TPT coating are tabulated in Table 4.14.

Estimated parameters	**Sample 1**	**Sample 2**
$a_{xHDPE}\ [mm^2 \cdot s^{-1}]$	0.274 ($\sigma = 1.41 \cdot 10^{-3}, 0.52\%$)	0.265 ($\sigma = 9.50 \cdot 10^{-4}, 0.36\%$)
$a_{yHDPE}\ [mm^2 \cdot s^{-1}]$	0.259 ($\sigma = 1.41 \cdot 10^{-3}, 0.55\%$)	0.265 ($\sigma = 9.50 \cdot 10^{-4}, 0.36\%$)
$a_{zHDPE}\ [mm^2 \cdot s^{-1}]$	0.278 ($\sigma = 1.9 \cdot 10^{-4}, 0.069\%$)	0.279 ($\sigma = 1.4 \cdot 10^{-4}, 0.049\%$)
$a_{TPT}\ [mm^2 \cdot s^{-1}]$	0.399 ($\sigma = 0.035, 8.85\%$)	0.411 ($\sigma = 0.025, 6.20\%$)

Table 4.14 – Experimental results for sample 1 constituted of a 3 mm HDPE covered by a 300 μm TPT coating and sample 2 constituted of a 3 mm HDPE covered by a 350 μm TPT coating.

Regarding the substrate layer, relatively thick compared to the coating layer, and typically isotropic, its estimated thermal diffusivities have been compared with ENH method and results are also reported in Table 4.15.

The thermal conductivity of the TPT coating in both samples can be deduced with $\lambda_{TPT} = 0.525\ W \cdot m^{-1} \cdot K^{-1}$ for sample 1 and $0.540\ W \cdot m^{-1} \cdot K^{-1}$ for sample 2.

The estimations are repeated using the density ρ and heat capacity C values measured using a calorimeter, a digital balance and a digital micrometer. The measured values and the level of

Estimated parameter (in $mm^2.s^{-1}$)	**Sample 1**		**Sample 2**	
	DSEH	ENH	DSEH	ENH
$a_{x\,HDPE}$	0.274	0.277 ($\sigma = 6.73 \cdot 10^{-3}$, 2.43%)	0.265	0.263 ($\sigma = 3.92 \cdot 10^{-3}$, 1.49%)
$a_{y\,HDPE}$	0.259	0.257 ($\sigma = 9.78 \cdot 10^{-3}$, 3.80%)	0.265	0.267 ($\sigma = 6.34 \cdot 10^{-3}$, 2.37%)

Table 4.15 – Thermal diffusivities of HDPE layer using both methods.

uncertainties are indicated in Table 4.16.

The estimation results obtained for the sample 1 are summarized in Table 4.17.

Parameters	**Values from literature** [273][272]	**Measured values**
$\rho_{HDPE}\ [kg \cdot m^{-3}]$	950	897 ± 16
$C_{HDPE}\ [J \cdot kg^{-1} \cdot K^{-1}]$	1900	1950 ± 58
$\rho_{TPT}\ [kg \cdot m^{-3}]$	2800	3131 ± 110
$C_{TPT}\ [J \cdot kg^{-1} \cdot K^{-1}]$	470	400 ± 12

Table 4.16 – Values required for the experimental identification.

Estimated parameters	**Using literature values**	**Using measured values**
$a_{x\,HDPE}\ [mm^2 \cdot s^{-1}]$	0.274 ($\sigma = 1.41 \cdot 10^{-3}$, 0.52%)	0.273 ($\sigma = 1.41 \cdot 10^{-3}$, 0.52%)
$a_{y\,HDPE}\ [mm^2 \cdot s^{-1}]$	0.259 ($\sigma = 1.41 \cdot 10^{-3}$, 0.55%)	0.259 ($\sigma = 1.41 \cdot 10^{-3}$, 0.55%)
$a_{z\,HDPE}\ [mm^2 \cdot s^{-1}]$	0.278 ($\sigma = 1.9 \cdot 10^{-4}$, 0.069%)	0.278 ($\sigma = 1.9 \cdot 10^{-4}$, 0.069%)
$a_{TPT}\ [mm^2 \cdot s^{-1}]$	0.399 ($\sigma = 0.035$, 8.85%)	0.407 ($\sigma = 0.035$, 8.69%)

Table 4.17 – Experimental identification results using the measured values, compared to previous results using literature values of some parameters.

Results discussion

First of all, Table 4.14 shows that the thermal diffusivities identified for both samples are close to each other, which can be considered as a promising results. From Table 4.14 it can

be also observed that the isotropic character (i.e. $a_x \approx a_y \approx a_z$) of HDPE is verified for both samples. For sample 1 $[0.274, 0.259, 0.278]\ mm^2 \cdot s^{-1}$ and for sample 2 $[0.265, 0.265, 0.279]\ mm^2 \cdot s^{-1}$. Furthermore, these values are coherent with those found in the literature [272], and are in a very good agreement with results obtained using ENH method (see Table 4.15) for the substrate.

Regarding the TPT coating, its estimated diffusivities values are found to be in good agreement with that retrieved by Benoit Fond team from Magdeburg: $\lambda_{TPT} = 0.47 \pm 0.07\ W \cdot m^{-1} \cdot K^{-1}$ who conducted a contact thermal characterization method, the "hot disk" method [274]. Adding to that, the estimated values are in the same order of magnitude than those presented in [273]. It should be notice that the composition (i.e. solvent used) and the mixing ratio may vary according to the process and the operator.

Finally a small difference in the results can be observed when repeating the estimation procedure with the measured values of $\rho \cdot C$, as shown in Table 4.17.

Exposing the phosphorescent material to the laser beam is not experimentally recommended as well as measuring its surface (of unknown emissivity). The present study proved that the approach that consists in both applying the excitation and measuring the temperature evolution on the substrate surface, is appropriate and suitable for such identification exercise.

4.6 Conclusion

The principal features of a non-intrusive one step technique dedicated to the thermal characterization of opaque multilayers material is presented in this chapter. The method proposed is of great importance for the multi-layer materials that may not be easily separated. Each element of the method, which allows the simultaneous estimation of the thermal diffusivity tensors of each constituting layers, is described and discussed. Among these elements, the pseudo-analytic model and the hypothesis on which it is based as well as the estimation method used to minimize the discrepancy between the outputs of the model and the measurement, are presented.

After a numerical validation of the direct model, the overall estimation strategy is validated using the experimental measurements conducted on an isotropic monolayer sample of well known properties. Furthermore, thermal characterization of an orthotropic CFRP layer combined to a metallic or polymer liner, frequently used in hydrogen storage and transportation sectors, is investigated. Four possible experimental configurations, in terms of excitation and measurements faces, are compared based on sensitivity analysis of the model outputs (front or rear face normalized harmonics) to the CFRP thermal diffusivity. The most sensitive case, corresponding to a front face (i.e. composite face) excitation and measurement, has been considered for both types of liners, and has given accurate results.

The proposed identification method is then applied on a two-layer material constituted of a CFRP layer combined to polyamide liner, by considering two different configurations found to be the most sensitive for the estimation of CFRP and/or polyamide thermal diffusivities. The estimation is performed in parallel for two version of the identification method : the "4D estimation", i.e. the liner is considered isotropic and the "6D estimation" i.e. the liner is considered

othotropic. The results obtained with the 4D case are shown to be in a good agreement with literature values, with values obtained by means of other methods such as ENH, and with values obtained separately. However in the 6D case, one experimental configuration (i.e. both excitation and measurement are performed on the polyamide side) is found to be more adequate for the estimation.

In a such highly dimensional identification parameter problem, the study of the sensitivities evolution during the present thermal diffusion problem is essential as it allows to check for potential correlations between parameters sensitivities that may affect the whole identification procedure. In non-linear and highly coupled system as the present one, the poor estimation quality of one parameter may affect the estimation of the entire set of parameters. Therefore, a strong emphasis is put on the sensitivity analysis in order to check the feasibility of the simultaneous estimation of the entire set of parameters. A comparative study is then performed between the sensitivity evolution of the main parameters (i.e. the 3 components of the thermal diffusion coefficient for the two layers) in both configurations. The analysis is used to retrospectively explain the difference in estimation between the configurations and identification dimensions (4D and 6D).

Finally, a degenerated case considering the thermal characterization of a special two-layer material constituted of a thin coating deposited on an isotropic or orthotropic substrate, is also considered. Numerical applications considering a TPT coating involved in phosphorescence thermometry and deposited on an HDPE layer, are firstly conducted using noisy synthetic data. After performing a sensitivity study and comparing the feasibility and the estimation accuracy for two experimental configurations, the one considering an excitation and measurement on the substrate surface side has been proved to be more appropriate and suitable for the identification, in terms of compromise between mathematical and experimental limitations. The experimental application of this latter case on two similar samples, has given promising results. Thermal diffusivities of the substrate are close to those found in the literature or obtained using reference methods. Moreover, the isotropic nature of the substrate has been retrieve. The values of the coating thermal diffusivity are in a good agreement with those existing in the literature or obtained by other researchers using different identification methods.

The minimization procedure invoked in 2.5.4.3 has once again proven to be convenient for such complex problems that deal with a non-linearity and a large number of unknown parameters, including those related to the excitation.

4.7 Résumé substantiel du chapitre 4

Introduction

Le présent chapitre présente l'extension d'une technique d'identification expérimentale dédiée à la caractérisation thermique des matériaux multicouches opaques. En effet, certains matériaux orthotropes ne pouvant être utilisés qu'en association avec d'autres matériaux, le développement de techniques adaptées est indispensable de disposer de techniques d'identification permettant de mesurer de manière simultanée les propriétés du matériau orthotrope et celles de son substrat. La section suivante est consacrée à la caractérisation d'un matériau composite PRFC associé à un liner isotrope, constituant ainsi un matériau bicouches couramment utilisé dans de nombreuses industries.

En plus de l'introduction et la conclusion, ce chapitre comporte 4 autres parties, présentées brièvement ci-dessous.

Partie 1. Etat de l'art sur les méthodes existantes de caractérisation thermique des matériaux bicouches et multicouches

Pour mettre en oeuvre l'originalité de la méthode développée dans ce chapitre, un état de l'art sur les méthodes présentes dans la littérature dédiées à la caractérisation des diffusivitées thermiques des matériaux bicouches ou multicouches, est présenté dans 4.2.

Parmi ces travaux de recherche, certains ont tenté d'estimer la diffusivité thermique unidimensionnelle d'une couche isotrope présente dans un système à deux ou trois couches composé de couches isotropes. Dans la plupart des travaux cités précédemment, l'identification des propriétés thermiques d'une couche nécessite la connaissance de toutes ses autres propriétés thermiques et des propriétés de la ou des autres couches. Ainsi, toute erreur dans la connaissance de ces propriétés sera propagée à travers le modèle et entraînera une imprécision de l'estimation.

La plupart des auteurs se sont intéressés à la caractérisation de la diffusivité ou de la conductivité thermique 1D des films minces ou des revêtements déposés sur des substrats. Dans ces travaux, une connaissance a priori des propriétés du substrat ou une détermination de ces propriétés à travers une expérience antérieure est souvent requise.

D'autres auteurs ont tenté de surmonter cette limitation en identifiant les diffusivités thermiques du revêtement sans aucune connaissance des propriétés du substrat. Cependant, leur méthode repose sur une technique d'identification en deux étapes qui plus est au temps très court, limitant ainsi cette méthode à des revêtements relativement épais. En outre, des chercheurs ont développé des stratégies d'estimation pour ce type de matériaux impliquant plus d'une étape. Ces stratégies sont ainsi susceptibles de cumuler et propager des erreurs tout au long de ce processus d'identification multi-étapes.

La présente étude consiste à estimer simultanément, c'est-à-dire en utilisant une étape unique, via une expérience de type flash non intrusive, les diffusivités thermiques de l'ensemble

des couches constituants ce matériau multi-couche. La méthode est ensuite appliquée au cas particulier d'un revêtement mince déposé sur un substrat.

Partie 2. Résolution du problème inverse en conduction thermique

Comme précédemment, le problème traité consiste en un problème inverse de conduction thermique dont l'objectif est d'estimer le tenseur des diffusivités thermiques par la minimisation de l'écart entre la sortie d'un modèle mathématique et les mesures expérimentales. Cet ajustement est obtenu au moyen d'un algorithme d'optimisation qui minimise une fonction coût exprimant l'écart entre les deux signaux, en l'occurrence l'erreur quadratique entre les sorties du modèle et les observables expérimentaux. Les différentes étapes de la stratégie d'estimation sont détaillées et discutées dans 4.3.

Tout d'abord, le processus développé pour identifier la diffusivité thermique 3D de chaque couche est présenté. Le modèle pseudo-analytique, reposant sur le formalisme des quadripôles thermiques et prédisant la conduction thermique transitoire dans un système multicouche et dans un contexte de méthode flash, est décrit.

La méthode de minimisation invoquée dans 2.5.4.3 s'est à nouveau révélée efficace pour la résolution de problèmes aussi complexes, i.e. présentant des non-linéarités, un grand nombre de paramètres inconnus et des paramètres à identifier relatifs à l'excitation.

Partie 3. Validation de la méthode

Dans cette section (voir 4.4), plusieurs cas de validation sont présentés, en commençant par la validation numérique du modèle multicouche direct utilisant le principe de subdivision (cf. 4.4.1). La seconde étape de validation consiste en une comparaison entre les résultats de simulations obtenues via le présent modèle et ceux obtenus via un code basé sur la méthode des éléments finis (FlexPDE) dans 4.4.2. Par la suite, la méthode globale d'identification est évaluée par confrontation avec des données expérimentales dans 4.4.3. Les données utilisées correspondent aux données expérimentales précédemment obtenues sur un matériau monocouche opaque isotrope de polyamide, déjà caractérisé au chapitre précédent (voir 3.4.1).

Partie 4. Applications numériques et expérimentales

Dans cette section 4.5, plusieurs applications sont présentées, en commençant par la caractérisation thermique d'une couche orthotrope de PRFC recouvert d'un revêtement métallique ou de polymère dans 4.5.1, suivie par la caractérisation du PRFC et du revêtement de polymère constituant un bicouche (voir 4.5.2). La dernière application concerne la caractérisation d'un matériau bicouche particulier compte tenu de la relative faible épaisseur du revêtement phosphorescent mince déposé sur son substrat de polyamide (voir 4.5.3).

Tout d'abord, une étude est menée sur deux échantillons fictifs à deux couches, inspirés des technologies de stockage et de transport d'hydrogène. Les échantillons sont constitués d'une couche de PRFC combinée à une couche de métal isotrope (réservoir de type III) ou à une

couche de polymère (réservoir de type IV). Les combinaisons possibles des faces d'excitation et de mesures conduisent à quatre configurations expérimentales possibles, l'objectif principal étant de hiérarchiser, via une étude de sensibilités des sorties du modèle à la diffusivité thermique du PRFC, ces protocoles expérimentaux en fonction du type de revêtement (métal ou polymère). Le cas le plus sensible, correspondant à une excitation et à une mesure en face avant (c'est-à-dire face correspondant au matériau composite), a été pris en compte pour les deux types de revêtement et a permis de retrouver les paramètres de manière précise.

La méthode d'identification proposée est ensuite appliquée sur un matériau bicouche constitué d'une couche de PRFC combinée à un liner polyamide, en considérant deux configurations expérimentales différentes qui se sont révélées les plus sensibles pour l'estimation des diffusivités thermiques du PRFC et/ou du polyamide. L'estimation est effectuée en parallèle pour deux versions d'identification: "l'estimation 4D", pour laquelle le liner est considéré isotrope et "l'estimation 6D", pour laquelle les deux couches sont considérées orthotropes. Les résultats obtenus avec le cas 4D sont en très bon accord avec les valeurs de la littérature, et celles obtenues au moyen d'autre méthode (e.g. ENH) ou précédemment pour les monocouches caractérisées au chapitre 3. Cependant, dans le cas "6D", une configuration expérimentale (l'excitation et les mesures sont effectuées côté polyamide) s'avère plus adéquate pour l'estimation. L'accent est mis sur l'analyse de sensibilités afin d'évaluer la faisabilité de l'identification pour les deux configurations expérimentales et les deux dimensions d'identification (4D et 6D), et pour expliquer de manière rétrospective les différences de résultats d'estimation observées entre les différentes stratégies.

Enfin, un cas dégénéré prenant en compte la caractérisation thermique d'un matériau bicouche spécial constitué d'un revêtement mince déposé sur un substrat isotrope ou orthotrope, est également envisagé. La motivation de cette étude concerne une méthode de mesure non intrusive de la température: la « thermométrie par phosphorescence », qui connait un certain succès chez les manufactures de moteur à combustion interne. Les propriétés d'un revêtement TPT (thermographic phosphor thermometry) utilisé en thermométrie par phosphorescence et déposé sur une couche de polyéthylène haute densité, sont tout d'abord caractérisées à l'aide de données synthétiques bruitées. Après avoir réalisé une étude de sensibilités et comparé la faisabilité et la précision de l'estimation pour deux configurations expérimentales, il s'est avéré que celle qui envisage l'excitation et la mesure du côté de la surface du substrat, était plus appropriée et plus adaptée à l'identification, en termes de compromis entre précision et limitations expérimentales. L'application expérimentale de ce dernier cas sur deux échantillons similaires a donné des résultats prometteurs. Les diffusivités thermiques du substrat sont proches de celles trouvées dans la littérature ou obtenues à l'aide d'une autre méthode de référence. De plus, la nature isotrope du substrat a été vérifiée. Les valeurs de la diffusivité thermique du revêtement sont en bon accord avec celles existantes dans la littérature ou obtenues par d'autres équipes de chercheurs utilisant différentes méthodes d'identification (e.g. technique de type disque chaud).

Conlusion

Ce chapitre présente les principales caractéristiques d'une technique non intrusive et à une seule étape, dédiée à la caractérisation thermique des matériaux multicouches opaques. La méthode proposée revêt une grande importance pour les matériaux multicouches difficilement séparables. Chaque élément du processus, qui permet l'estimation simultanée des tenseurs de diffusivités thermiques de chacune des couches constitutives, est décrit et discuté. Parmi ces éléments, le modèle pseudo-analytique et l'hypothèse sur laquelle il est basé, ainsi que la méthode d'estimation utilisée pour minimiser l'écart entre les sorties du modèle et les mesures, sont présentés. Ce travail néglige la résistance thermique de contact susceptible d'être présente à l'interface entre les couches. L'ajout de ce paramètre au jeu de paramètres actuellement estimé constitue une des perspectives de ce travail.

General Conclusion and Perspectives

***

General Conclusion

This work sets out and develops overall thermal characterization method that is based on the resolution of an inverse heat conduction problem, and could be applied for any isotropic or orthotropic materials or further generalized to mutilayers materials. Such exercises are significantly important for several industrial sectors, for the modeling and control of the heat transferred inside the structures before and during the processes, and to ensure accurate inputs for complex numerical simulations that mimic real applications, in additions to many other benefits.

The studies developed in the frame of this thesis project are summarized here below:

- From the outcomes of the literature review, numerous existing thermal characterization methods can be classified according to many criterion. Some of these latter are relative to the excitation, other dependent on the measurement, the model or the estimation method itself, and many other minor specifications that can differentiate between them.

  The well known flash technique is one of the most frequently conducted methods for thermal diffusivities estimation. During the past decades, this class of methods was improved in terms of estimation possibilities (1D, 2D then 3D flash methods) or measurement technique with the parallel development of the infrared thermography. The advantageous of such methods are numerous, for instance it can be considered as a rapid and simple method, with minimum requirement of special equipment, and with the possibility to non-intrusively characterize the material diffusivity and/or conductivities using only one experiment. After a literature survey, this method has been chosen as a stating point of the following method development.

- Flash based method was investigated in this work as a non intrusive experiment, in terms of excitation and temperature measurements. The present version of method consists in subjecting a short (in most studied cases), non uniform and local laser beam on the surface of the material that should be thermally characterized. This version of method can be qualified as a three dimensional flash experiment due to the non uniformity of the thermal excitation that generate a three dimensional heat transfer inside the structure allowing therefore the estimation of the material three dimensional thermal diffusivity

tensor. This estimation relies on the resolution of an inverse heat conduction problem that consists in fitting the experimental or synthetic measurements into the appropriate representing model outputs, in order to identify the required parameters (especially the thermal diffusivties). The direct model of the problem is obtained by the resolution of the unsteady state heat equation in the considered domain, while reproducing all the experimental boundary and initial conditions. The thermal quadrupoles formalism allows to analytically express the temperature evolution at material front and/or rear faces in the form of normalized harmonics in Laplace domain, resulting from the projection into Fourier Cosine domain for both directions (x and y) by integral transformations. A Laplace inversion is then applied in order to get temporal normalized harmonics which are functions of the parameters to estimate β. Such types of functions that was found to be convenient for such exercise, is then compared into the temperature measurement fields that must be, in their turn, projected twice into the Fourier cosine domain, in order to get the experimental "observables".

Due to the complexity, the non linearity of the cost function that represents the quadratic deviation between the model outputs and the transformed, and the large number of parameters to estimate, including those related to the excitation, the minimization is performed by a hybrid optimization algorithm coupling a stochastic algorithm of PSO and a deterministic one of gradient type. Such type of minimization allows to benefit from both approaches advantages at two different stages, starting by global searching and ending by local minimization, and guarantees a best estimation accuracy.

– The flash method was firstly applied on the front face of monolayer materials. For validation purposes, the first application concerns an isotropic material of polyamide of well-known thermal properties. Due to the additional estimation of the excitation parameters, a total amount of 19 parameters have been estimated.

  The resulting values of the three dimensional thermal diffusivity tensor, ($a_x \approx a_y \approx a_z$) verified the isotropic character of the material and were found to be in a very good agreement with the values found in the literature and obtained using other existing identification methods, 2D ENH estimation method and multi-step MSEH estimation method. After validation, the overall identification method is applied on a CFRP material, frequently used in different sectors (aerospace, automotive, energy production, and others), with similarly convincing results coherent with physical structure, i.e. with highest diffusivity in the carbon fibers direction. Sensitivity analysis has been conducted in order to verify the feasibility of the estimation method by verifying the decorrelations between the parameters that should be identified, and the acquisition time range that allow this estimation. The modal re-partition of the signal, involving some null spatial modes [($m = 0, n = 0$), ($m = 0, n \neq 0$) and ($m \neq 0, n = 0$)] have conveniently ensure a decorrelation between a_x, a_y and a_z estimations. During the measurement/acquisition time, the signal sensitivity to the overall heat exchange coefficient is found to be negligible.

  Furthermore, some alternative methods are proposed for the improvement of the CFRP

thermal characterization method:

  - In terms of time reduction, with successful application of some of these strategies, for instance: imposing the shape of the thermal laser perturbation, or reducing the number of harmonics, giving acceptable and convincing results.
  - In terms of optimization of the experiment design considering rear or front face temperature evolution measurements and an impulse or pulse excitation with different possible time duration τ_{ex} and intensity Q. In this section, a numerical application was conducted using the finite element code FlexPDE that generated pseudo-experimental data for which additional noise, close to experimental observation, was added. The present numerical study, in parallel with the sensitivity analysis, have enabled to identify the rear face to be the most effective in order to successfully estimate the thermal diffusivities of such materials, especially the in-depth thermal diffusivity. For this configuration, excitation having an intensity of 10 J with relatively long duration time (in the order of 10-second), has been proved to be more convenient for such identification problems, compared to the impulse or very short pulse types.

- Other strategies consisting in an additional simultaneous estimation of volumetric heat capacity, when knowing the amount of heat absorbed by the material, or allowing the estimation of thermal diffusivities without any pre-knowledge about this parameter, is developed. In some of these cases, volumetric heat capacity is embedded in a new parameter that should be also identified. These alternative approaches have been verified using noisy synthetic measurements generated by the model, flexPDE numerical signals and experimental measurements, and have given promising results.

- The overall identification method is then generalized to multilayers materials applications, with a special consideration of interface conditions (continuity equations taking into account any possible contact resistance). The proposed method is of great importance, specifically for the multilayers structures that may not be separable or when the layer of interest is not available as a free-standing sample. In those cases, a larger number of parameters should be estimated, i.e. all layers thermal diffusivites in addition to the excitation parameters. In this work, a perfect thermal contact is assumed at the interface between layers, thus the thermal contact resistances are neglected. The overall method is validated using the subdivision principle applied on a monolayer isotropic sample previously characterized using the monolayer model. The proposed identification method is then applied on a two-layers material constituted of a CFRP layer combined to a metallic or polymer liner, and generally used in the hydrogen storage and transportation vessels. Four possible experimental configurations (in terms of excitation and measurement sides) are numerically tested and compared using a sensitivity analysis, in order to define the best strategy to simultaneously estimate the thermal diffusivity tensor of the CFRP material present in the layers structure, for both types of liners.

Experimental application on actual two-layers material of same type as previously investigated (constituted of a CFRP layer combined to a PA liner) but with different thicknesses for both layers, is conducted. Two experimental configurations, both with front face temperature measurements, i.e. the excitation and measurements are both conducted on the same face, are compared. Two possible estimation strategies have been conducted, one qualified as 4D since it considers the polymer liner as isotopic one and the second is 6D and considers the liner as orthotropic. The results of the 4D strategy have been shown to be in a good agreement with the literature and the values obtained with ENH method, which validate the consistency and the accuracy of the method. Regarding the 6D strategy, one experimental configuration has been found to be more convenient than the other one and explained by means of sensitivity analysis.

Finally, a special case of the two-layers material which corresponds to a thin coating deposited on the substrate, has been investigated. This application was a part of a collaborative work conducted with an IFPEN team which uses a TPT coating for temperature measurements using phosphorescence thermometry principle, in their engines internal combustion chambers. For some technical limitations, this coating was deposited on a HDPE polymer substrate layer. In order to verify the feasibility of the simultaneous estimation of the coating diffusivities simultaneously with the substrate, a numerical application by means of noisy synthetic measurements, was first conducted for two possible experimental configurations. One of these latter consists in excitating and measuring the temperature evolution at the coating side and the other considers the case where excitation and measurements are conducted at the substrate surface side. Based on convincing estimation results, sensitivity analysis, and experimental limitations, the last configuration has been proved more convenient for such exercise. The identification has been experimentally conducted on two different samples and has given promising results. The values of the polymer diffusivites verifying the isotropic character of the latter, are in good agreements with the literature and with the ENH estimation results. Regarding the coating, estimated values are in the same order of magnitudes with those found in the literature, and in good agreements with other research team results obtained using a contact characterization method.

As a summary, a direct, simultaneous and three dimensional identification method, allowing the estimation of the thermal diffusivities of a monolayer or each layer in multilayers material, using a unique and non intrusive (perturbation + measurements) 3D flash technique, and one step estimation technique, is developed in this thesis. The proposed method consists in retrieving the parameters to estimate by comparing, via a cost function, the outputs of the direct model analytically solved using the thermal quadrupoles formalism, and the integrally transformed measurements. The minimization of the deviation criterion between the model and the experiments signals, is performed by a global stochastic algorithm coupled to deterministic one to have a better estimation accuracy and robustness. Adding to all listed features and characteristics, the current identification method does not require any pre-knowledge about

the excitation shape and intensity, that represent some additional simultaneously estimated parameters.

Perspectives

The results of the identification methods developed in this work and applied on different types of materials, were very promising and convincing. However, several possible perspectives that may improve and complete the current approaches, can be drawn:

- To be more accurate, the more realistic or concrete shape and intensity level of noise, inspired from real physical measurements of the 3D flash based experiment and that have been evaluated in the experimental design optimization section 3.6.3, should be also applied for all synthetic measurement generations used in the numerical applications that was already conducted in this thesis (inverse crime, finite element numerical data using flexPDE).

- As a future work, the improvement section applied for the monolayer material estimation method and presented in chapter 3, shall be reconducted for two-layers materials of chapter 4.

- This study always considers the opaque materials, nonetheless the problem can propose a coupled conduction-radiation heat transfer when treating the transparent or semi-transparent ones, with the possibility to estimate the absorption coefficient.

- One of the perspectives is to apply the current method on non plane geometries with non Cartesian coordinates. Cylindrical or spherical coordinates require the application of other integral transformations, such as Hankel transform and Bessel functions.

- Experimental application of the rear face flash based methods using a mirror in order to detect the excitation initial time at the front face and simultaneously measure the resulting temperature evolution at the rear face, as represented in the chapters 3 and 4, can be also envisaged.

- Trying to consider other boundary conditions type, for instance non isolated lateral faces, or other initial conditions such as higher initial temperature of the material that can previously heated.

- One of the envisaged works is to experimentally apply the flash experiment under vacuum (i.e. convection and radiation losses are negligible) in order to validate the alternative approach that allows to estimate the thermal diffusivities without any pre-knowldge about the material volumetric heat capacity as discussed in 3.7.2 and 3.7.3.

- As already mentioned, the quadrupoles formalism can involve the contact resistance present at the layers interfaces as an additional parameter Rc_i that may be also estimated.

However this technique considers a global and homogeneous resistance at the overall layers separative surfaces, which is not the real case, since the contact resistance is usually a local parameter that can be represented by $Rc_i(x,y)$. An alternative approach considering this contact between layers and trying to estimate this space dependent parameters, knowing all other parameters (including thermal diffusivities of all layers), can be also envisaged.

- The proposed thermal identification methods are eventually limited for some types of samples and layers diffusivities/thicknesses combinations. These limitation point must be more deeply evaluated according to several criteria, for instance as a function of the dimensionless Fourier number of the present layers (e.g. Fourier number).

Résumé substantiel de la conclusion générale

L'objectif principal de cette thèse concerne le développement d'une méthode de caractérisation thermique de matériaux à structure complexe. Cette méthode, qui repose sur la résolution d'un problème inverse de conduction thermique, a été appliquée avec succès à différentes configurations comme i) la caractérisation de matériaux monocouches orthotropes, ii) la caractérisation simultanées de matériaux bicouches présentant une couche orthtrope et iii) la caractérisation simultanées de matériaux bicouches présentant une couche mince. La connaissance de ces propriétés revêt un enjeu majeur dans plusieurs secteurs industriels, notamment pour la modélisation et le contrôle des transferts de chaleur au sein de systèmes de propulsion ou de production d'énergie. Ces propriétés servant de données d'entrée à des logiciels de simulation de type CAO et CFD.

Le résumé des études menées dans le cadre de cette thèse, ainsi les conclusions qui peuvent être tirées, sont résumés ci-dessous:

- L'étude bibliographique des nombreuses méthodes de caractérisation thermique existantes révèle que celles-ci peuvent être classées selon plusieurs critères. La méthode Flash, considérée comme une classe générique de méthodes radiométriques, est l'une des méthodes fréquemment utilisées pour l'estimation des diffusivités thermiques, si ce n'est la méthode de référence. Au cours des années, cette classe de méthodes qui présente de nombreux avantages, a bénéficié d'améliorations continues, que ce soit au niveau expérimental que des méthodes d'identification à proprement parler.

- La méthode Flash, reposant sur une expérience non intrusive en termes de mesures et d'excitation, est utilisé dans ce travail. La version dont il est question ici est qualifiée de Flash 3D en raison de la non uniformité de l'excitation thermique qui est à l'origine du transfert de chaleur tridimensionnel à l'intérieur du matériau. Cette particularité permet d'envisager l'estimation de l'ensemble des composantes du tenseur tridimensionnel de diffusivité thermique. Cette estimation consiste à ajuster les mesures issues d'une expérience, éventuellement issues d'un modèle (i.e. données synthétiques), aux sorties du modèle direct, afin d'identifier les paramètres requis, en particulier les diffusivités thermiques. Le modèle direct correspond à l'équation de la chaleur en régime instationnaire soumis à un flux de chaleur localisé en espace et en temps et à un refroidissement convectif sur l'ensemble de ces faces. Pour envisager une résolution semi-analytique rapide en comparaison d'une résolution basée sur une approche numérique, les champs de température sont projetés dans une base de Fourier (cosinus) selon les directions dans le plan de l'excitation (i.e. axes x et y). Le formalisme des quadripôles thermiques est ensuite utilisé afin d'exprimer de manière analytique l'évolution de la température sur les faces avant et/ou arrière des échantillons. La transformée de Laplace appliquée permet d'exprimer la solution sous la forme d'harmoniques normalisées dans le domaine des fréquences. Une série de tests menée sur différentes définitions de la fonction coût à minimiser, a révélé la nécessité d'appliquer une inversion de Laplace pour réaliser

l'estimation à partir des harmoniques normalisées temporelles. Ainsi, les prédictions du modèle sont comparées aux champs de températures mesurées, lesquels sont projetés deux fois dans le domaine de "Fourier cosinus".

– En raison de la complexité du problème, qui se traduit par la non linéarité de la fonction coût représentant ici l'écart quadratique entre les sorties du modèle et les observables, et du grand nombre de paramètres à estimer, la minimisation est effectuée par un algorithme d'optimisation hybride couplant un algorithme stochastique de type PSO et un algorithme déterministe de type gradient. Ce type de minimisation permet de bénéficier des avantages des deux approches en commençant par la recherche globale via un algorithme de type évolutionnaire et en terminant par une minimisation locale, garantissant ainsi une précision d'estimation optimale.

– La méthode Flash dans sa version "face avant" a tout d'abord été appliquée sur des matériaux monocouches. Pour la validation, la première application concernait un matériau isotrope de polyamide aux propriétés thermiques bien connues. Les valeurs identifiées du tenseur de diffusivités thermiques ont vérifié le caractère isotrope du matériau et se sont révélées être en très bon avec les valeurs trouvées dans la littérature ainsi que les valeurs identifiées à l'aide de méthodes d'identification existantes, en particulier la méthode d'estimation 2D ENH et la méthode MSEH à plusieurs étapes. Après validation, la méthode d'identification globale est appliquée sur un matériau de PRFC (polymère renforcé de fibres de carbone). Les résultats trouvés sont en accord avec ceux obtenus au moyen d'autres méthodes, et cohérents avec la structure physique, la diffusivité la plus élevée correspondant à la direction des fibres de carbone. Lors de chaque exercice d'estimation, une analyse de sensibilités est effectuée afin d'étudier sa faisabilité en cherchant les éventuels corrélations entre les paramètres à identifier et en identifiant la plage temporelle optimum d'exploitation.

  En outre, plusieurs stratégies ont été investiguées dans le but d'améliorer la méthode de caractérisation thermique, notamment en termes:

  – de réduction du temps de calcul. Notamment, la paramétrisation de la distribution spatiale du flux imposé par le laser a permis de réduire le nombre de paramètres associés à l'excitation. Les résultats, obtenus dans un délai environ 10 fois plus rapide, présentent des niveaux de précision légèrement inférieur à la méthode originale. Selon le niveau de précision requit, les résultats peuvent être utilisés comme tels, ou peuvent servir à initialiser et borner les domaines de recherche associés aux paramètres dans le cadre d'une recherche avec la méthode originale.

  – d'optimisation de l'expérience. Les réglages liés à l'acquisition, comme la durée ou la face de l'échantillon mesuré, ou à l'excitation, comme la face de l'échantillon exposé ainsi que la durée et la quantité d'énergie déposée, ont donné lieu à une étude qui a permis d'identifier les conditions expérimentales les plus adaptée à ce type de matériaux.

– D'autres stratégies permettant d'estimer simultanément la capacité calorifique volumétrique, connaissant a priori la quantité de chaleur absorbée par le matériau, ou encore permettant d'estimer les diffusivités thermiques sans aucune connaissance préalable de ce paramètre, sont développées. Ces approches alternatives ont donné des résultats prometteurs.

– La méthode globale d'identification est ensuite généralisée à des applications destinées à la caractérisation de matériaux multicouches. La méthode d'identification est appliquée à des matériaux bicouches constitués d'une couche de PRFC combinée à un revêtement métallique ou en polymère. Les quatre configurations expérimentales possibles, en termes de faces d'excitation et de mesures, sont testées numériquement et comparées à l'aide d'une analyse de sensibilités, afin de définir la meilleure stratégie pour estimer simultanément le tenseur de diffusivité thermique du PRFC.

  L'application expérimentale est réalisée sur un matériau bicouche de même type que celui étudié précédemment. Les configurations correspondant au cas où l'excitation et les mesures sont toutes deux effectuées du même côté, sont jugées les plus pertinentes et sont comparées. Pour ces 2 configurations, 2 stratégies d'estimation ont été conduites, l'une qualifiée de 4D considère le liner polymère comme étant isotopique, et la seconde qualifiée de 6D considère le liner comme étant orthotrope. Les résultats de la stratégie 4D se sont révélés être en bon accord avec la littérature et avec les valeurs obtenues en appliquant la méthode ENH, et ils ont vérifié la cohérence et la précision de la méthode. En ce qui concerne la stratégie 6D, une des deux configurations expérimentales s'est révélée plus pertinente que l'autre ce qui s'est expliqué au moyen d'une analyse de sensibilités.

– Enfin, un cas particulier de matériau bicouche correspondant à un revêtement mince déposé sur un substrat, a été étudié. Afin de vérifier la faisabilité de l'estimation simultanée des diffusivités du revêtement et du substrat, une application numérique réalisée au moyen de mesures synthétiques bruitées a tout d'abord été réalisée pour deux configurations expérimentales possibles. La première configuration consiste à exciter et à mesurer l'évolution de la température du côté du revêtement et l'autre consiste à exciter et à mesurer du côté du substrat. Les 2 configurations ayant donné des résultats d'estimation convaincants, l'analyse des sensibilités et les limitations expérimentales ont permis d'identifier la dernière configuration comme plus adaptée et donc à préférer pour ce type d'exercice. Cette dernière a été mise en oeuvre expérimentalement sur deux échantillons et a donné des résultats prometteurs. Les valeurs identifiées des diffusivités des substrats polymères ont permis d'une part de vérifier le caractère isotrope de ces dernières et d'autre part se trouvent être en bon accord avec les valeurs issues de la littérature ainsi qu'avec les résultats trouvées par une autre méthode d'estimation (ENH). En ce qui concerne le revêtement phosphorescent, les valeurs estimées sont du même ordre de grandeur que celles trouvées dans la littérature et sont en bon accord avec les résultats obtenus par d'autres équipes de recherche appliquant des méthodes de caractérisation différentes (e.g. disque chaud).

Suite aux différents résultats obtenus dans cette thèse, un certain nombre de perspectives peut être envisagé :

- Cette étude considère des matériaux opaques. L'application de cette méthode a des matériaux semi-transparent nécessiterait la résolution du couplage entre les transferts par conduction et par rayonnement. Ce travail permettrait d'envisager l'estimation simultanée de la conductivité thermique et du coefficient d'absorption.

- Cette étude considère des matériaux à géométrie plane. Modifier le modèle direct de sorte à traiter l'équation de la chaleur en coordonnées cylindrique, en remplaçant les projections dans l'espace de Fourier par des projections dans l'espace de Fourier-Bessel (nommé également projection de Hankel), permettrait de traiter le cas d'échantillons cylindriques.

- Expérimentalement, le cas où l'excitation et les mesures sont réalisées sur la même face de l'échantillon a été traité. L'application expérimentale de la méthode flash arrière nécessiterait d'une part, de positionner la camera thermique derrière l'échantillon et d'autre part, d'utiliser un miroir permettant de détecter le temps initial d'excitation sur la face avant.

- Les travaux ont été menés pour des niveaux de température initiale correspondant à la température ambiante. Afin d'étudier la thermodépendance des diffusivités thermiques, il pourrait être envisagé de réaliser les expériences dans des conditions de température contrôlées. Pour cela, un four muni d'un hublot de visualisation transparent au rayonnement infra rouge est nécessaire. Pour un certain niveau de température, se pose également le problème des conditions aux limites radiatives, qu'il faut alors traité au niveau du modèle direct.

- Les travaux ont été menés pour des échantillons soumis au refroidissement convectif avec l'air ambiant. Bien que l'influence du paramètre de refroidissement convectif soit faible sur le type de matériaux étudiés ici (allant de peu à moyennement diffusifs), il pourrait être intéressant de s'affranchir de ce phénomène afin de mieux caractériser les propriétés de matériaux fortement diffusifs. De plus, cette approche alternative permettrait d'estimer les diffusivités thermiques sans connaissance préalable de la capacité calorifique volumétrique du matériau, comme indiqué dans 3.7.2 et 3.7.3.

- Les travaux ont été menés en considérant un contact parfait entre les couches. Cette hypothèse est valable tant que les matériaux sont relativement isolants, comme c'est le cas dans ce travail. Pour traiter le cas de matériaux plus diffusifs, il conviendrait d'identifier la résistance thermique simultanément aux diffusivités. Se pose alors la question de l'homogénéité de la résistance thermique sur l'ensemble de la surface de contact.

- Les travaux ont été menés en supposant que l'on connaisse parfaitement le temps de référence, i.e. le temps où le laser excite l'échantillon. Compte tenu de la fréquence

d'acquisition de la camera thermique, ce temps n'est connu qu'à une image d'acquisition prêt. Compte tenu des matériaux modérément diffusifs étudiés ici, cette hypothèse n'a que peu d'influence. Pour envisager l'étude de materiaux plus diffusifs, il conviendrait de travailler avec des fréquences d'acquisition plus élevées et d'envisager une correction de l'origine des temps de mesure. Cela reviendrait à estimer, au même titre que les paramètres tels que les diffusivités, le temps de latence entre l'excitation réelle et l'excitation considérée.

References

***

[1] D. Maillet, S. André, J. C. Batsale, A. Degiovanni, and C. Moyne, *Thermal quadrupoles: solving the heat equation through integral transforms*. Wiley, 2000. 1, 5, 59, 87, 92

[2] W. J. Parker, R. J. Jenkins, C. P. Butler, and G. L. Abbott, "Flash Method of Determining Thermal Diffusivity, Heat Capacity, and Thermal Conductivity," *Journal of Applied Physics*, vol. 32, pp. 1679–1684, Sept. 1961. 2, 5, 25, 26, 27, 29, 30, 31, 32, 56, 88, 98, 121

[3] H. Qi, C.-Y. Niu, S. Gong, Y.-T. Ren, and L.-M. Ruan, "Application of the hybrid particle swarm optimization algorithms for simultaneous estimation of multi-parameters in a transient conduction–radiation problem," *International Journal of Heat and Mass Transfer*, vol. 83, pp. 428 – 440, 2015. 2, 5, 67

[4] E. Ruffio, D. Saury, and D. Petit, "Robust experiment design for the estimation of thermophysical parameters using stochastic algorithms," *International Journal of Heat and Mass Transfer*, vol. 55, no. 11, pp. 2901 – 2915, 2012.

[5] R. Rao and V. Patel, "Thermodynamic optimization of cross flow plate-fin heat exchanger using a particle swarm optimization algorithm," *International Journal of Thermal Sciences*, vol. 49, no. 9, pp. 1712 – 1721, 2010. 67

[6] R. Das, K. Singh, B. Akay, and T. Gogoi, "Application of artificial bee colony algorithm for maximizing heat transfer in a perforated fin," *Proceedings of the Institution of Mechanical Engineers, Part E: Journal of Process Mechanical Engineering*, vol. 232, pp. 38–48, Feb. 2018.

[7] B. Zhang, H. Qi, Y.-T. Ren, S.-C. Sun, and L.-M. Ruan, "Application of homogenous continuous Ant Colony Optimization algorithm to inverse problem of one-dimensional coupled radiation and conduction heat transfer," *International Journal of Heat and Mass Transfer*, vol. 66, pp. 507–516, Nov. 2013.

[8] S. Chanda, C. Balaji, S. P. Venkateshan, and G. R. Yenni, "Estimation of principal thermal conductivities of layered honeycomb composites using ANN–GA based inverse technique," *International Journal of Thermal Sciences*, vol. 111, pp. 423–436, Jan. 2017.

[9] S. Orain, Y. Scudeller, S. Garcia, and T. Brousse, "Use of genetic algorithms for the simultaneous estimation of thin films thermal conductivity and contact resistances," *International Journal of Heat and Mass Transfer*, vol. 44, pp. 3973–3984, Oct. 2001.

[10] Y. Billaud, N. Zekri, A. Kaiss, M. Drissi, Y. Pizzo, Z. Acem, A. Collin, P.-A. Santoni, F. Bosseur, P. Boulet, and B. Porterie, "A hybrid small-world network/semi-physical model for predicting wildfire spread in heterogeneous landscapes," *Journal of Physics: Conference Series*, vol. 395, no. 1, p. 012008, 2012. 2, 5

[11] "Aircraft and Aerospace Fields." 12, 237

[12] H. Barthelemy, M. Weber, and F. Barbier, "Hydrogen storage: Recent improvements and industrial perspectives," *International Journal of Hydrogen Energy*, vol. 42, no. 11, pp. 7254–7262, 2017. 13

[13] H. Barthélémy, "Hydrogen storage–industrial prospectives," *International journal of hydrogen energy*, vol. 37, no. 22, pp. 17364–17372, 2012. 13, 237

[14] S. Allison and G. Gillies, "Remote thermometry with thermographic phosphors: Instrumentation and applications," *Review of Scientific Instruments*, vol. 68, no. 7, pp. 2615–2650, 1997. 14

[15] J. T. Kashdan and G. Bruneaux, "Laser-induced phosphorescence measurements of combustion chamber surface temperature on a single-cylinder diesel engine," tech. rep., SAE Technical Paper, 2011. 14

[16] "Heat Losses During Diesel Combustion." 14, 237

[17] A. Omrane, G. Juhlin, M. Aldén, G. Josefsson, J. Engström, and T. Benham, "Demonstration of two-dimensional temperature characterization of valves and transparent piston in a gdi optical engine," *SAE transactions*, pp. 449–457, 2004. 15

[18] N. Fuhrmann, M. Schild, D. Bensing, S. Kaiser, C. Schulz, J. Brübach, and A. Dreizler, "Two-dimensional cycle-resolved exhaust valve temperature measurements in an optically accessible internal combustion engine using thermographic phosphors," *Applied Physics B*, vol. 106, no. 4, pp. 945–951, 2012. 15

[19] A. Degiovanni, *Conductivite et diffusivite thermique des solides*. Ed. Techniques Ingénieur, Jan. 1994. 17, 18, 19, 23, 24, 26, 237

[20] C. Rodiet, *Temperature Measurement by Multi-Spectral Methods and Thermal Characterization of Anisotropic Materials by Integral Transforms: Theoretical and experimental aspects*. Theses, Université de Lorraine ; Institut National Polytechnique de Lorraine (INPL), July 2014. 17, 19, 26, 34, 35, 237

[21] X. Zhang and A. Degiovanni, “Mesure de l’effusivité thermique de matériaux solides et homogènes par une méthode de “sonde” plane,” *Journal de Physique III*, vol. 3, no. 6, pp. 1243–1265, 1993. 17, 26

[22] D. Zhao, X. Qian, X. Gu, S. A. Jajja, and R. Yang, “Measurement techniques for thermal conductivity and interfacial thermal conductance of bulk and thin film materials,” *Journal of Electronic Packaging*, vol. 138, no. 4, p. 040802, 2016. 17, 24, 26, 29

[23] J.-C. Krapez, “Mesure de l’effusivité thermique - méthodes par contact,” *Techniques de l’ingenieur*, vol. TIB544DUO, no. r29582, 2007. 17, 20, 26, 28, 53

[24] B. Djelloul and A. Salim, *Radiométrie photothermique sous excitation aléatoire: application à la mesure de propriétés thermophysiques.* PhD thesis, Reims, 2008. 17, 21, 25, 26, 27, 29

[25] F. de Ponte, *Conductivité thermique des isolants.* Ed. Techniques Ingénieur, 2002. 17, 23, 26

[26] S. E. Gustafsson, E. Karawacki, and M. N. Khan, “Transient hot-strip method for simultaneously measuring thermal conductivity and thermal diffusivity of solids and fluids,” *Journal of Physics D: Applied Physics*, vol. 12, no. 9, p. 1411, 1979. 17, 29

[27] S. E. Gustafsson and E. Karawacki, “Transient hot-strip probe for measuring thermal properties of insulating solids and liquids,” *Review of Scientific Instruments*, vol. 54, no. 6, pp. 744–747, 1983. 17

[28] M. Bamford, “Méthode flash et thermographie infrarouge pour la cartographie de propriétés thermophysiques: Application à la caractérisation en thermomécanique,” *Flash method and infrared thermography for the mapping of thermophysical properties: applications for the thermomechanical characterization-Doctorate Thesis, Université de Bordeauzx*, vol. 1, 2007. 17

[29] V. Schick, *Caractérisation d’une mémoire à changement de phase: mesure de propriétés thermiques de couches minces à haute température.* PhD thesis, Bordeaux 1, 2011. 20, 22, 24, 25, 26

[30] L. Clerjaud, *Méthode d’hétérodynage pour la caractérisation de propriétés thermophysiques par thermographie infrarouge dans une large gamme spatiale et temporelle.* PhD thesis, Bordeaux 1, 2010. 20, 22

[31] F. Lepoutre, “Thermal measurements by photothermal methods,” *REVUE GENERALE DE THERMIQUE*, vol. 26, no. 301, pp. 8–14, 1987. 20

[32] G. Rousset and F. Lepoutre, “Mesures de diffusivités thermiques par la méthode photoacoustique et par l’effet mirage,” *Revue de Physique Appliquée*, vol. 17, no. 4, pp. 201–207, 1982.

[33] D. Balageas, "Le contrôle non destructif par méthodes thermiques," *Revue générale de thermique*, vol. 30, no. 356-57, pp. 483–498, 1991.

[34] B. Rémy, *Mesure de propriétés thermophysiques de matériaux minces et de dépôts par méthode Flash: application aux films polycristallins de diamant.* PhD thesis, Institut National Polytechnique de Lorraine, 1998. 20, 21

[35] D. Balageas, D. Boscher, A. Déom, and F. Enguehard, "Panorama des méthodes thermiques de cnd à l'onera," *Tiré à part- Office national d'études et de recherches aerospatiales*. 20

[36] J.-C. Krapez, "Mesure de l'effusivité thermique-méthodes photothermiques," 2007. 20, 25, 28

[37] Y. Souhar, *Caractérisation thermique de matériaux anisotropes à hautes températures*. PhD thesis, Institut National Polytechnique de Lorraine, 2011. 20, 25, 26, 29, 32, 33, 34, 35

[38] Y. Jannot and P. Meukam, "Simplified estimation method for the determination of the thermal effusivity and thermal conductivity using a low cost hot strip," *Measurement Science and Technology*, vol. 15, no. 9, p. 1932, 2004. 20, 25

[39] I. Blonskij, V. Tkhoryk, and M. Shendeleva, "Thermal diffusivity of solids determination by photoacoustic piezoelectric technique," *Journal of applied physics*, vol. 79, no. 7, pp. 3512–3516, 1996. 20

[40] B. Zhao, Y. Wang, C. Gao, and Q. Sun, "Thermal diffusivity determination of solids by time-domain photoacoustic piezoelectric technique," *Chinese science bulletin*, vol. 59, no. 26, pp. 3348–3351, 2014. 20, 25

[41] F. Lepoutre and J. Roger, "Mesures thermiques par l'effet mirage," *Techniques de l'ingénieur*, p. 30, 1986. 21, 22, 25

[42] D. Balageas, D. Boscher, A. Déom, and F. Enguehard, "Photoacoustic microscopy by photodeformation applied to thermal diffusivity determination," *High Temperatures-High Pressures*, vol. 23, no. 5, pp. 517–528, 1991. 21, 25

[43] J. M. Jewell, C. Askins, and I. D. Aggarwal, "Interferometric method for concurrent measurement of thermo-optic and thermal expansion coefficients," *Applied optics*, vol. 30, no. 25, pp. 3656–3660, 1991. 21

[44] F. Cernuschi, A. Figari, and L. Fabbri, "Thermal wave interferometry for measuring the thermal diffusivity of thin slabs," *Journal of materials science*, vol. 35, no. 23, pp. 5891–5897, 2000. 21

[45] A. Skumanich, H. Dersch, M. Fathallah, and N. Amer, "A contactless method for investigating the thermal properties of thin films," *Applied Physics A*, vol. 43, no. 4, pp. 297–300, 1987. 22

[46] A. Boccara, D. Fournier, and J. Badoz, "Thermo-optical spectroscopy: Detection by the"mirage effect"," *Applied Physics Letters*, vol. 36, no. 2, pp. 130–132, 1980. 22, 25

[47] D. Fournier, C. Boccara, A. Skumanich, and N. M. Amer, "Photothermal investigation of transport in semiconductors: theory and experiment," *Journal of applied physics*, vol. 59, no. 3, pp. 787–795, 1986.

[48] H. Machlab, W. A. McGahan, J. A. Woollam, and K. Cole, "Thermal characterization of thin films by photothermally induced laser beam deflection," *Thin Solid Films*, vol. 224, no. 1, pp. 22–27, 1993.

[49] G. Suber, M. Bertolotti, C. Sibilia, and A. Ferrari, "Test measurements of the photothermal deflection method to determine the thermal diffusivity of solids," *Applied optics*, vol. 27, no. 9, pp. 1807–1810, 1988.

[50] G. Suber, M. Bertolotti, C. Sibilia, A. Ferrari, and F. G. Ricciardiello, "Transverse photothermal deflection spectroscopy (pds) applied to thermal diffusiyity measurements," *Journal of Thermal Analysis and Calorimetry*, vol. 32, no. 4, pp. 1039–1050, 1987. 22

[51] P. Peretti, G. Louis, and B. Mangeot, "Comparative influence of thermal and acoustic methods in the photoacoustic analysis of liquid-crystals," *Revue générale de thermique*, vol. 26, no. 301, pp. 59–62, 1987. 22

[52] Y. Jannot, B. Remy, and A. Degiovanni, "Measurement of thermal conductivity and thermal resistance with a tiny hot plate," *High Temperatures-High Pressures*, vol. 39, no. 1, pp. 1–21, 2009. 23

[53] Y. Jannot, V. Felix, and A. Degiovanni, "A centered hot plate method for measurement of thermal properties of thin insulating materials," *Measurement Science and technology*, vol. 21, no. 3, p. 035106, 2010.

[54] O. Burheim, P. Vie, J. Pharoah, and S. Kjelstrup, "Ex situ measurements of through-plane thermal conductivities in a polymer electrolyte fuel cell," *Journal of Power Sources*, vol. 195, no. 1, pp. 249–256, 2010. 23

[55] C. S. Sanjaya, T.-H. Wee, and T. Tamilselvan, "Regression analysis estimation of thermal conductivity using guarded-hot-plate apparatus," *Applied Thermal Engineering*, vol. 31, no. 10, pp. 1566–1575, 2011. 23, 26

[56] F. Jones and F. Pascal, "Numerical simulation of divided-bar thermal conductivity measurements," *Studia geophysica et geodaetica*, vol. 37, no. 3, pp. 234–257, 1993. 23

[57] A. Beck, "A steady state method for the rapid measurement of the thermal conductivity of rocks," *Journal of Scientific Instruments*, vol. 34, no. 5, p. 186, 1957.

[58] A. E. Beck and J. M. Beck, "On the measurement of the thermal conductivities of rocks by observations on a divided bar apparatus," *EOS, Transactions American Geophysical Union*, vol. 39, no. 6, pp. 1111–1123, 1958.

[59] D. Galson, N. Wilson, U. Schärli, and L. Rybach, "A comparison of the divided-bar and qtm methods of measuring thermal conductivity," *Geothermics*, vol. 16, no. 3, pp. 215–226, 1987. 23

[60] N. Daouas, A. Fguiri, and M.-S. Radhouani, "Solution of a coupled inverse heat conduction–radiation problem for the study of radiation effects on the transient hot wire measurements," *Experimental Thermal and Fluid Science*, vol. 32, no. 8, pp. 1766–1778, 2008. 24

[61] E. Yamasue, M. Susa, H. Fukuyama, and K. Nagata, "Thermal conductivities of silicon and germanium in solid and liquid states measured by non-stationary hot wire method with silica coated probe," *Journal of crystal growth*, vol. 234, no. 1, pp. 121–131, 2002. 24

[62] T. Borca-Tasciuc, A. Kumar, and G. Chen, "Data reduction in 3ω method for thin-film thermal conductivity determination," *Review of scientific instruments*, vol. 72, no. 4, pp. 2139–2147, 2001. 24, 29

[63] T. Tian and K. D. Cole, "Anisotropic thermal conductivity measurement of carbon-fiber/epoxy composite materials," *International Journal of Heat and Mass Transfer*, vol. 55, pp. 6530–6537, Nov. 2012. 29, 89

[64] V. Mishra, C. L. Hardin, J. E. Garay, and C. Dames, "A 3 omega method to measure an arbitrary anisotropic thermal conductivity tensor," *Review of Scientific Instruments*, vol. 86, p. 054902, May 2015. 24, 29

[65] A. Degiovanni and M. Laurent, "Une nouvelle technique d'identification de la diffusivité thermique pour la méthode «flash»," *Revue de physique Appliquée*, vol. 21, no. 3, pp. 229–237, 1986. 25, 26, 29, 32, 35

[66] R. Taylor and J. Cape, "Finite pulse-time effects in the flash diffusivity technique," *Applied Physics Letters*, vol. 5, no. 10, pp. 212–213, 1964. 26, 27, 29, 35, 121

[67] V. Ayvazyan, *Etude de champs de température séparables avec une double décomposition en valeurs singulières : quelques applications à la caractérisation des propriétés thermophysiques des matérieux et au contrôle non destructif*. PhD thesis, Dec. 2012. 26, 27, 32, 34, 35

[68] D. Balageas, "Nouvelle méthode d'interprétation des thermogrammes pour la détermination de la diffusivité thermique par la méthode impulsionnelle (méthode «flash»)," *Revue de Physique Appliquée*, vol. 17, no. 4, pp. 227–237, 1982. 27, 29, 35

[69] Y. Takahashi, K. Yamamoto, T. Ohsato, and T. Terai, "Usefulness of logarithmic method in laser-flash technique for thermal diffusivity measurement," in *Proceedings of the 9th Japanese Symposium on Thermophysical Properties*, pp. 175–178, 1988. 26

[70] M.-A. Thermitus and M. Laurent, "New logarithmic technique in the flash method," *International journal of heat and mass transfer*, vol. 40, no. 17, pp. 4183–4190, 1997. 26, 29, 32, 121

[71] A. Degiovanni, J. C. Batsale, and D. Maillet, "Mesure de la diffusivité longitudinale de matériaux anisotropes," *Revue Générale de Thermique*, vol. 35, pp. 141–147, Feb. 1996. 26, 27, 29, 31, 88

[72] D. Demange, P. Beauchêne, M. Bejet, and R. Casulleras, "Mesure simultanée de la diffusivité thermique selon les deux directions principales d'un matériau," *Revue Générale de Thermique*, vol. 36, pp. 755–770, Nov. 1997. 27, 29, 31, 88

[73] I. Philippi, J. C. Batsale, D. Maillet, and A. Degiovanni, "Measurement of thermal diffusivities through processing of infrared images," *Review of Scientific Instruments*, vol. 66, pp. 182–192, Jan. 1995. 29, 31, 32, 33, 62, 89, 113, 121

[74] Y. Souhar, B. Remy, and A. Degiovanni, "High Temperature Facility Under Vacuum for the Thermal Characterization of Anisotropic Materials," *In Proceedings of the Int. Heat Transfer Conference - IHTC14,*, pp. 381–386, Jan. 2010. 26, 29, 31, 33, 62, 87, 89, 102, 114

[75] Y. Souhar, B. Rémy, and A. Degiovanni, "Thermal Characterization of Anisotropic Materials at High Temperature Through Integral Methods and Localized Pulsed Technique," *International Journal of Thermophysics*, vol. 34, pp. 322–340, Feb. 2013. 26, 32, 121, 161

[76] B. Remy, A. Degiovanni, and D. Maillet, "Mesure de la diffusivité thermique de matériaux anisotropes de petites dimensions par thermographie infrarouge et transformations intégrales," *in SFT*, 2007. 26, 32, 33, 62, 89, 113

[77] J.-C. Krapez, "Simultaneous measurement of in-plane and out-of-plane diffusivity by using a grid-like mask," in *International Workshop on Advanced Infrared Technology and Applications, 5 th, Venice, Italy, Sept. 28-30, 1999, ONERA, TP*, no. 2000-44, 2000. 26, 32, 33

[78] J.-C. Krapez, L. Spagnolo, M. Frieß, H.-P. Maier, and G. Neuer, "Measurement of in-plane diffusivity in non-homogeneous slabs by applying flash thermography," *International Journal of Thermal Sciences*, vol. 43, pp. 967–977, Oct. 2004. 31, 32, 62, 87, 89, 102, 121, 161, 184

[79] L. Spagnolo, J.-C. Krapez, M. Friess, H.-P. Maier, and G. Neuer, "Flash thermography with a periodic mask: profile evaluation of the principal diffusivities for the control of composite materials," in *Thermosense XXV*, vol. 5073, pp. 392–401, International Society for Optics and Photonics, Apr. 2003. 26, 29, 32, 33, 121

[80] V. Vavilov, D. Burleigh, and V. Shiryaev, "IR thermographic evaluation of thermal diffusivity anisotropy: comparative analysis of some algorithms," *Quantitative InfraRed Thermography Journal*, vol. 4, pp. 187–200, Dec. 2007. 26, 32, 62, 89

[81] P. Bison, F. Cernuschi, and E. Grinzato, "In-depth and In-plane Thermal Diffusivity Measurements of Thermal Barrier Coatings by IR Camera: Evaluation of Ageing," *International Journal of Thermophysics*, vol. 29, pp. 2149–2161, Dec. 2008. 26, 27, 29, 32, 62, 87, 89, 102, 121, 150, 184

[82] E. Ruffio, D. Saury, and D. Petit, "Improvement and comparison of some estimators dedicated to thermal diffusivity estimation of orthotropic materials with the 3d-flash method," *International Journal of Heat and Mass Transfer*, vol. 64, pp. 1064–1081, Sept. 2013. 25, 79, 89, 94, 102, 113, 114, 116, 121, 143, 161

[83] Y. Jannot and A. Degiovanni, "Thermal properties measurement of dry bulk materials with a cylindrical three layers device," *Review of Scientific Instruments*, vol. 84, no. 9, p. 094901, 2013. 25, 29

[84] V. Plana, *Caractérisation par méthode inverse et modélisation des propriétés thermophysiques orthotropes des matériaux composites*. Theses, Toulouse, ENSAE, Jan. 2003. 25, 26, 27

[85] J. M. Laskar, S. Bagavathiappan, M. Sardar, T. Jayakumar, J. Philip, and B. Raj, "Measurement of thermal diffusivity of solids using infrared thermography," *Materials Letters*, vol. 62, pp. 2740–2742, June 2008. 25, 29, 31, 121

[86] L. Fabbri and P. Fenici, "Three-dimensional photothermal radiometry for the determination of the thermal diffusivity of solids," *Review of scientific instruments*, vol. 66, no. 6, pp. 3593–3600, 1995. 25

[87] C. Gervaise, *Caracterisation thermique multi-echelles de revetements refractaires. Comportement sous excitation periodique et identification par methodes inverses*. PhD thesis, Toulouse 3, 1999. 25

[88] C. Gervaise, C. Nouals, and J. J. Serra, "Estimation des propriétés thermiques à l'échelle millimétrique par méthodes périodiques: Résolution du problème direct et du problème inverse," *International journal of thermal sciences*, vol. 39, no. 3, pp. 422–432, 2000. 25

[89] A. Mandelis and M. M. Zver, "Theory of photopyroelectric spectroscopy of solids," *Journal of applied physics*, vol. 57, no. 9, pp. 4421–4430, 1985. 25

[90] M. Chirtoc and G. Mihilescu, "Theory of the photopyroelectric method for investigation of optical and thermal materials properties," *Physical Review B*, vol. 40, no. 14, p. 9606, 1989. 25

[91] A. Sánchez-Lavega and A. Salazar, "Thermal diffusivity measurements in opaque solids by the mirage technique in the temperature range from 300 to 1000 k," *Journal of applied physics*, vol. 76, no. 3, pp. 1462–1468, 1994. 25

[92] S. Matteï and E. T. Kwor, "A new periodic technique for thermal conductivity measurement," *High Temperatures–High Pressures(UK)*, vol. 32, no. 1, pp. 3–8, 2000. 25, 27

[93] A. Boudenne, L. Ibos, E. Gehin, and Y. Candau, "A simultaneous characterization of thermal conductivity and diffusivity of polymer materials by a periodic method," *Journal of Physics D: Applied Physics*, vol. 37, no. 1, p. 132, 2003. 25, 26

[94] D. Tang and N. Araki, "An inverse analysis to estimate relaxation parameters and thermal diffusivity with a universal heat conduction equation," *International Journal of Thermophysics*, vol. 21, no. 2, pp. 553–561, 2000. 25

[95] S. Brahim, P. Grossel, *et al.*, "Thermal diffusivity measurement by photothermal radiometry under random excitation and parametric analysis," in *Journal of Physics: Conference Series*, vol. 214, p. 012065, IOP Publishing, 2010. 25

[96] K. Kato, S. Ishino, and Y. Sugitani, "Correlation photoacoustics," *Chemistry Letters*, vol. 9, no. 7, pp. 783–786, 1980. 25

[97] Y. Sugitani and A. Uejima, "Effect of m-series prbs modulation on the time resolution in correlation photoacoustics," *Bulletin of the Chemical Society of Japan*, vol. 57, no. 7, pp. 2023–2024, 1984. 25

[98] E. Merienne, K. Hakem, and M. Egge, "Dispositif d'évaluation non destructive de matériaux par radiométrie photothermique sous excition aléatoire," *Revue générale de thermique*, vol. 30, no. 360, 1991. 26

[99] M. E. K.Hakem, "Contribution à la mesure de la diffusivité thermique par radiométrie photothermique aléatoire," *Actes du congrès de la Société Française de Thermique*, 2005. 26

[100] A. Kavianipour and J. Beck, "Thermal property estimation utilizing the laplace transform with application to asphaltic pavement," *International Journal of Heat and Mass Transfer*, vol. 20, no. 3, pp. 259–267, 1977. 26, 31

[101] D. Hadisaroyo, J. Batsale, and A. Degiovanni, "Un appareillage simple pour la mesure de la diffusivité thermique de plaques minces," *Journal de Physique III*, vol. 2, no. 1, pp. 111–128, 1992. 26, 31, 35

[102] Y. Jannot, "Théorie et pratique de la métrologie thermique," *Laboratoire d'Energétique et de Mécanique Théorique et Appliquée (LEMTA)*, 2011. 26, 29

[103] B. Hay, *Mesure de la diffusivité thermique par la méthode flash*. Ed. Techniques Ingénieur, 2004. 26, 27, 32, 35, 78

[104] M. Akoshima and T. Baba, "Study on a thermal-diffusivity standard for laser flash method measurements," *International journal of thermophysics*, vol. 27, no. 4, pp. 1189–1203, 2006. 26, 35

[105] N. D. Milošević and M. Raynaud, "A parameter estimation procedure in thermal diffusivity measurements using the laser flash method," 26, 29, 121

[106] M. Bamford, J. C. Batsale, and O. Fudym, "Nodal and modal strategies for longitudinal thermal diffusivity profile estimation: Application to the non destructive evaluation of sic/sic composites under uniaxial tensile tests," *Infrared Physics & Technology*, vol. 52, no. 1, pp. 1–13, 2009. 26, 121

[107] T. Kruczek, W. P. Adamczyk, and R. A. Bialecki, "In Situ Measurement of Thermal Diffusivity in Anisotropic Media," *International Journal of Thermophysics*, vol. 34, pp. 467–485, Mar. 2013. 26, 27, 121

[108] P. G. Bison, E. Grinzato, and S. Marinetti, "Local thermal diffusivity measurement," *Quantitative InfraRed Thermography Journal*, vol. 1, no. 2, pp. 241–250, 2004. 26, 27, 29, 121

[109] N. W. Pech-May, A. Mendioroz, and A. Salazar, "Simultaneous measurement of the in-plane and in-depth thermal diffusivity of solids using pulsed infrared thermography with focused illumination," *NDT & E International*, vol. 77, pp. 28–34, 2016. 26

[110] E. Ruffio, *Estimation de paramètres et de conditions limites thermiques en conduction instationnaire pour des matériaux anisotropes*. Chasseneuil-du-Poitou, Ecole nationale supérieure de mécanique et d'aérotechnique, Jan. 2011. 26, 29, 33, 35, 51, 57, 59, 60, 61, 62, 63, 75, 77, 78, 94

[111] E. El Rassy, Y. Billaud, and D. Saury, "Simultaneous and direct identification of thermophysical properties for orthotropic materials," *Measurement*, vol. 135, pp. 199 – 212, 2019. 26, 29, 62, 89, 121

[112] J.-C. Batsale, J.-L. Battaglia, and O. Fudym, "Autoregressive algorithms and spatially random flash excitation for 2d non destructive evaluation with infrared cameras," *Quantitative InfraRed Thermography Journal*, vol. 1, no. 1, pp. 5–20, 2004. 26, 27, 29, 32, 33, 121

[113] A. B. Donaldson and R. E. Taylor, "Thermal diffusivity measurement by a radial heat flow method," *Journal of Applied Physics*, vol. 46, pp. 4584–4589, Oct. 1975. 26, 31, 88, 121

[114] M. Amazouz, Moyne, and A. Degiovanni, "Measurement of the thermal diffusivity of anisotropic materials," *High Temperatures. High Pressures*, pp. 37–41, 1987. 31, 88, 121

[115] M. Lachi and A. Degiovanni, "Détermination des diffusivités thermiques des matériaux anisotropes par méthode flash bidirectionnelle," *Journal de Physique III*, vol. 1, no. 12, pp. 2027–2046, 1991. 26, 31, 88

[116] S. W. Kim, J. C. Kim, and S. H. Lee, "Analysis of thermal diffusivity by parameter estimation in converging thermal-wave technique," *International journal of heat and mass transfer*, vol. 49, no. 3-4, pp. 611–616, 2006. 27

[117] J. C. Kim, D. J. Kim, D. S. Kim, S. W. Kim, and O. Y. Troitsky, "One-Level, Two-Point Method for Estimation of Thermal Diffusivity by the Converging Thermal-Wave Technique," *International Journal of Thermophysics*, vol. 22, pp. 933–942, May 2001. 27

[118] W. Adamczyk, R. A.Białecki, and T. Kruczek, "Measuring thermal conductivity tensor of orthotropic solid bodies - ScienceDirect," *Measurement*, pp. 93–102, Apr. 2017. 27, 88, 89

[119] T. Baba, M. Kobayashi, A. Ono, J. Hong, and M. Suliyanti, "Experimental investigation of the nonuniform heating effect in laser flash thermal diffusivity measurements," *Thermochimica acta*, vol. 218, pp. 329–339, 1993. 29, 35, 121

[120] T. Baba and A. Ono, "Improvement of the laser flash method to reduce uncertainty in thermal diffusivity measurements," *Measurement Science and Technology*, vol. 12, no. 12, p. 2046, 2001. 27, 29, 121

[121] J. Gembarovic and R. E. Taylor, "A method for thermal diffusivity determination of thermal insulators," *International Journal of Thermophysics*, vol. 28, no. 6, p. 2164, 2007. 27

[122] J. Beňačka, L. Vozár, and I. Štubňa, "Design of Experiment for Thermal Diffusivity Measurements of Composite Material with Orthogonal Anisotropy," *International Journal of Thermophysics*, vol. 29, pp. 2088–2101, Dec. 2008. 29, 31, 33, 88, 89, 121

[123] S. K. Kim, B. S. Jung, H. J. Kim, and W. I. Lee, "Inverse estimation of thermophysical properties for anisotropic composite," *Experimental Thermal and Fluid Science*, vol. 27, no. 6, pp. 697–704, 2003. 27

[124] J.-C. Krapez, *Mesure de l'effusivité thermique.* Ed. Techniques Ingénieur, 2007. 28

[125] M. Diot, *Capacités thermiques.* Ed. Techniques Ingénieur, 1993. 28

[126] J. Grenet and B. Legendre, "Analyse calorimétrique différentielle à balayage (dsc)," 2010. 28

[127] K. B. Larson and K. Koyama, "Measurement by the Flash Method of Thermal Diffusivity, Heart Capacity, and Thermal Conductivity in Two-Layer Composite Samples," *Journal of Applied Physics*, vol. 39, pp. 4408–4416, Aug. 1968. 28, 150

[128] N. Araki, A. Makino, and J. Mihara, "Measurement and evaluation of the thermal diffusivity of two-layered materials," *International Journal of Thermophysics*, vol. 13, pp. 331–349, Mar. 1992. 150

[129] P. Emeric and W. Winfree, "Thermal Characterization of Multilayer Structures from Transient Thermal Response," *Review of Progress in Quantitative Nondestructive Evaluation*, Jan. 1995.

[130] R. Derbal, D. Defer, A. Chauchois, and E. Antczak, "A simple method for building materials thermophysical properties estimation," *Construction and Building Materials*, vol. 63, pp. 197–205, July 2014. 150

[131] G. Wei, X. Zhang, F. Yu, and K. Chen, "Thermal Diffusivity Measurements on Insulation Materials with the Laser Flash Method," *International Journal of Thermophysics*, vol. 27, pp. 235–243, Jan. 2006. 150

[132] G. H. He, J. D. Guo, Y. Y. Zhang, B. Q. Wang, and B. L. Zhou, "Measurement of Thermal Diffusivity of Thermal Control Coatings by the Flash Method Using Two-Layer Composite Sample," *International Journal of Thermophysics*, vol. 21, pp. 535–542, Mar. 2000. 28, 150

[133] N. D. Milošević, M. Raynaud, and K. D. Maglić, "Simultaneous Estimation of the Thermal Diffusivity and Thermal Contact Resistance of Thin Solid Films and Coatings Using the Two-Dimensional Flash Method," *International Journal of Thermophysics*, vol. 24, pp. 799–819, May 2003. 28, 150

[134] O. Faugeroux, B. Claudet, S. Bénet, J. J. Serra, and D. Boisson, "Caractérisation thermophysique de revêtements par méthode photothermique impulsionnelle en face avant," *International Journal of Thermal Sciences*, vol. 43, pp. 383–401, Apr. 2004. 150

[135] L. Chen, A. M. Limarga, and D. R. Clarke, "A new data reduction method for pulse diffusivity measurements on coated samples," *Computational Materials Science*, vol. 50, pp. 77–82, Nov. 2010. 28, 32, 150

[136] W. Nunes dos Santos, P. Mummery, and A. Wallwork, "Thermal diffusivity of polymers by the laser flash technique," *Polymer Testing*, vol. 24, pp. 628–634, Aug. 2005. 29, 102

[137] P. H. A. Nóbrega, H. R. Orlande, and J.-L. Battaglia, "Bayesian estimation of thermophysical parameters of thin metal films heated by fast laser pulses," *International Communications in Heat and Mass Transfer*, vol. 38, no. 9, pp. 1172–1177, 2011.

[138] B. Hay, S. Barré, J.-R. Filtz, M. Jurion, D. Rochais, and P. Sollet, "New Apparatus for Thermal Diffusivity and Specific Heat Measurements at Very High Temperature," *International Journal of Thermophysics*, vol. 27, pp. 1803–1815, Nov. 2006. 32

[139] T. Baba and A. Cezairliyan, "Thermal diffusivity of POCO AXM-5q1 graphite in the range 1500 to 2500 K measured by a laser-pulse technique," *International Journal of Thermophysics*, vol. 15, pp. 343–364, Mar. 1994. 32

[140] L. Vozár, G. Labudová, and W. Hohenauer, "The Laser Flash Method with Repeated Pulses—Optimal Experimental Design Analysis," *International Journal of Thermophysics*, vol. 23, pp. 1157–1170, Sept. 2002. 29, 31, 121

[141] P. Andersson and G. Bäckström, "Thermal conductivity of solids under pressure by the transient hot wire method," *Review of Scientific Instruments*, vol. 47, no. 2, pp. 205–209, 1976. 29

[142] S. E. Gustafsson, "Transient hot strip techniques for measuring thermal conductivity and thermal diffusivity," *The Rigaku Journal*, vol. 4, no. 1/2, pp. 16–28, 1987. 29

[143] S. E. Gustafsson, E. Karawacki, and M. N. Khan, "Determination of the thermal-conductivity tensor and the heat capacity of insulating solids with the transient hot-strip method," *Journal of Applied Physics*, vol. 52, no. 4, pp. 2596–2600, 1981. 29

[144] M. Bamford, M. Florian, G. L. Vignoles, J.-C. Batsale, C. A. A. Cairo, and L. Maillé, "Global and local characterization of the thermal diffusivities of sicf/sic composites with infrared thermography and flash method," *Composites Science and Technology*, vol. 69, no. 7-8, pp. 1131–1141, 2009. 29, 121

[145] S. Graham, D. L. McDowell, and R. B. Dinwiddie, "Multidimensional Flash Diffusivity Measurements of Orthotropic Materials," *International Journal of Thermophysics*, vol. 20, pp. 691–707, Mar. 1999. 31, 88

[146] T. Harmathy, "Variable-state methods of measuring the thermal properties of solids," *Journal of Applied Physics*, vol. 35, no. 4, pp. 1190–1200, 1964. 31

[147] R. C. Steere, "Thermal properties of thin-film polymers by transient heating," *Journal of Applied Physics*, vol. 37, no. 9, pp. 3338–3344, 1966. 31

[148] K. Katayama, K. Ohuchi, and S. Kotake, "A transient method of simultaneous measurement of thermal properties using a plane heat source," *Bulletin of JSME*, vol. 12, no. 52, pp. 865–872, 1969. 31

[149] B. Remy, A. Degiovanni, and D. Maillet, "Measurement of the In-plane Thermal Diffusivity of Materials by Infrared Thermography," *International Journal of Thermophysics*, vol. 26, pp. 493–505, Mar. 2005. 31, 32, 33, 62, 89, 113

[150] A. Degiovanni, "Diffusivité et méthode flash," *Revue générale de thermique*, vol. 185, pp. 420–442, 1977. 32, 35

[151] D. Maillet, S. André, and A. Degiovanni, "Les erreurs sur la diffusivité thermique mesurée par méthode flash: confrontation théorie-expérience," *Journal de Physique III*, vol. 3, no. 4, pp. 883–809, 1993. 32, 35

[152] B. Hay, J. Filtz, J. Hameury, and L. Rongione, "Uncertainty of thermal diffusivity measurements by laser flash method," *International journal of thermophysics*, vol. 26, no. 6, pp. 1883–1898, 2005. 32, 35

[153] R. Pujolà and D. Balageas, "Derniers développements de la méthode flash adaptée aux matériaux composites à renforcement orienté," *High Temperatures. High Pressures*, vol. 17, no. 6, pp. 623–632, 1986. 32

[154] D. Balageas and A. Luc, "Transient thermal behavior of directional reinforced composites-applicability limits of homogeneous property model," *AIAA journal*, vol. 24, no. 1, pp. 109–114, 1986. 32

[155] S. André and A. Degiovanni, *A theoretical study of the transient coupled conduction and radiation heat transfer in glass: phonic diffusivity measurements by the flash technique - ScienceDirect*. 32

[156] A. Degiovanni, B. Remy, and S. Andre, "Transient radiation-conductive heat transfer problems: "The quadrupole method"," *Journal of Thermal Science*, vol. 11, pp. 359–371, Nov. 2002.

[157] M. Lazard, S. André, and D. Maillet, "Diffusivity measurement of semi-transparent media: model of the coupled transient heat transfer and experiments on glass, silica glass and zinc selenide," *International Journal of Heat and Mass Transfer*, vol. 47, pp. 477–487, Jan. 2004. 32

[158] P. Bison, F. Cernuschi, E. Grinzato, S. Marinetti, and D. Robba, "Ageing evaluation of thermal barrier coatings by thermal diffusivity," *Infrared Physics & Technology*, vol. 49, no. 3, pp. 286–291, 2007. 32

[159] O. Fudym, J.C. Batsale, and J.L. Battaglia, "Thermophysical properties mapping in semi-infinite longitudinally cracked plates by temperature image processing: Inverse Problems in Science and Engineering: Vol 15, No 2," *Inverse Problem in Science and Engineering*, pp. 163–176, 2007. 32

[160] R. Taylor, "Construction of apparatus for heat pulse thermal diffusivity measurements from 300-3000k," *Journal of Physics E: Scientific Instruments*, vol. 13, no. 11, p. 1193, 1980. 32

[161] J. Gounot and J. L. Battaglia, "Thermal diffusivity identification and measurement noise," *High Temperatures. High Pressures*, vol. 26, no. 2, pp. 177–182, 1994. 32

[162] C. Gru, "Theoretical and experimental applications of the flying spot camera.," 1992. 33

[163] C. Gruss, F. Lepoutre, and D. Balageas, "Nondestructive evaluation using a flying-spot camera," *ONERA TP*, vol. 1, 1993. 33

[164] B. Hay, J.-R. Filtz, J. Hameury, and L. Rongione, "Estimation de l'incertitude de mesure de la diffusivité thermique par méthode flash-application à cinq matériaux homogènes uncertainty assessment of thermal diffusivity measurements by flash method," 2008. 35

[165] L. Vozár and W. Hohenauer, "Flash method of measuring the thermal diffusivity. A review," *High temperatures-High pressures*, vol. 36, no. 3, pp. 253–264, 2004. 35

[166] L. Vozár and W. Hohenauer, "Uncertainty of thermal diffusivity measurements using the laser flash method," *International journal of thermophysics*, vol. 26, no. 6, pp. 1899–1915, 2005. 35

[167] J. Cape and G. Lehman, "Temperature and finite pulse-time effects in the flash method for measuring thermal diffusivity," *Journal of applied physics*, vol. 34, no. 7, pp. 1909–1913, 1963. 35

[168] K. Larson and K. Koyama, "Correction for finite-pulse-time effects in very thin samples using the flash method of measuring thermal diffusivity," *Journal of Applied Physics*, vol. 38, no. 2, pp. 465–474, 1967.

[169] R. Heckman, "Finite pulse-time and heat-loss effects in pulse thermal diffusivity measurements," *Journal of Applied Physics*, vol. 44, no. 4, pp. 1455–1460, 1973.

[170] T. Azumi and Y. Takahashi, "Novel finite pulse-width correction in flash thermal diffusivity measurement," *Review of scientific instruments*, vol. 52, no. 9, pp. 1411–1413, 1981.

[171] A. Degiovanni, "Correction de longueur d'impulsion pour la mesure de la diffusivité thermique par méthode flash," *International journal of heat and mass transfer*, vol. 30, no. 10, pp. 2199–2200, 1987.

[172] T. Lechner and E. Hahne, "Finite pulse time effects in flash diffusivity measurements," *Thermochimica acta*, vol. 218, pp. 341–350, 1993.

[173] A. P. F. Albers, T. A. Restivo, L. Pagano, and J. B. Baldo, "Effect of testing conditions on the laser flash thermal diffusivity measurements of ceramics," *Thermochimica acta*, vol. 370, no. 1-2, pp. 111–118, 2001. 35

[174] J. Blumm and S. Lemarchand, "Influence of test conditions on the accuracy of laser flash measurements," *High Temperatures. High Pressures*, vol. 34, no. 5, pp. 523–528, 2002. 35

[175] Z. Soilihi and A. Degiovanni, "Influence de la non-linéarité dans la mesure de la diffusivité thermique par la méthode flash," *Revue générale de thermique*, vol. 22, no. 262, pp. 649–661, 1983. 35

[176] M. Lachi and A. Degiovanni, "Influence de l'erreur de mesure de température de surface par thermocouples de contact sur la détermination de la diffusivité thermique par méthode "flash"," *Journal de Physique III*, vol. 2, no. 11, pp. 2247–2265, 1992. 35

[177] K.-H. Lim, S.-K. Kim, and M.-K. Chung, "Improvement of the thermal diffusivity measurement of thin samples by the flash method," *Thermochimica Acta*, vol. 494, no. 1-2, pp. 71–79, 2009. 35, 121

[178] D. I. Hadisaroyo, *Mesure de diffusivité thermique de plaques minces, conductrices ou isolantes*. PhD thesis, Institut National Polytechnique de Lorraine, 1993. 35

[179] H. R. B. Orlande, O. Fudym, D. Maillet, and R. M. Cotta, *Thermal Measurements and Inverse Techniques*. CRC Press, May 2011. 43, 66, 76

[180] O. M. Alifanov, *Inverse Heat Transfer Problems*. Springer Science & Business Media, Dec. 2012. 43

[181] D. Maillet, Y. Jarny, and D. Petit, "Problèmes inverses en diffusion thermique - Modèles diffusifs, mesures, sensibilités," p. 32, 2018. 43

[182] J. Kaipio and E. Somersalo, *Statistical and Computational Inverse Problems*. Springer Science & Business Media, Mar. 2006. 45

[183] "C80 Calorimeter - Setaram - PDF Catalogs | Technical Documentation | Brochure." 52, 53, 237

[184] "TCi Thermal Conductivity Analyzer - C-Therm - Thermal Conductivity Instruments." 53, 54, 237

[185] H. Hassanzadeh and M. Pooladi-Darvish, "Comparison of different numerical Laplace inversion methods for engineering applications," *Applied Mathematics and Computation*, vol. 189, pp. 1966–1981, June 2007. 59

[186] H. Stehfest, "Algorithm 368: Numerical Inversion of Laplace Transforms [D5]," *Commun. ACM*, vol. 13, pp. 47–49, Jan. 1970. 59, 107

[187] D. J. Halsted and D. E. Brown, "Zakian's technique for inverting Laplace transforms," *The Chemical Engineering Journal*, vol. 3, pp. 312–313, Jan. 1972. 59

[188] P. Den Iseger, "Numerical Transform Inversion Using Gaussian Quadrature," *Probab. Eng. Inf. Sci.*, vol. 20, pp. 1–44, Jan. 2006. 59

[189] F. de Hoog, J. Knight, and A. Stokes, "An Improved Method for Numerical Inversion of Laplace Transforms," *SIAM Journal on Scientific and Statistical Computing*, vol. 3, pp. 357–366, Sept. 1982. 60, 93, 107

[190] K. Kurpisz and A. Nowak, *Inverse thermal problems*. Computational mechanics, 1995. 61

[191] J.-C. Trigeassou, "Recherche de modèles expérimentaux," 1988. 61

[192] C. T. Kelley, *Solving nonlinear equations with Newton's method*, vol. 1. Siam, 2003. 64

[193] P. Wolfe, "The secant method for simultaneous nonlinear equations," *Communications of the ACM*, vol. 2, no. 12, pp. 12–13, 1959. 64

[194] M. Minoux, *Programmation mathématique: théorie et algorithmes*. Dunod, 1983. 64

[195] D. P. Bertsekas, "Nonlinear programming," *Journal of the Operational Research Society*, vol. 48, no. 3, pp. 334–334, 1997. 64

[196] P. E. Gill, W. Murray, and M. H. Wright, "Practical optimization," 1981. 64, 65

[197] C. Porte, *Méthodes directes d'optimisation*. Ed. Techniques Ingénieur, 2002. 64

[198] A. Antoniou and W.-S. Lu, *Practical Optimization: Algorithms and Engineering Applications*. Springer Science & Business Media, Dec. 2007. 64

[199] G. Laurent, "Optimisation sans contrainte de fonctions continues non linéaires," p. 27. 65, 69, 70

[200] D. Maillet, Y. Jarny, and D. Petit, "Problèmes inverses en diffusion thermique: Formulation et résolution du problème des moindres carrés," *Techniques de l'ingénieur-Transferts thermiques*, 2011. 65, 77

[201] D. P. Bertsekas, "Linear network optimization," 1991. 65

[202] J. Dréo, A. Pétrowski, P. Siarry, and E. Taillard, *Metaheuristics for Hard Optimization: Methods and Case Studies*. Springer Science & Business Media, Jan. 2006. 65

[203] H.-G. Beyer, *The Theory of Evolution Strategies*. Natural Computing Series, Berlin Heidelberg: Springer-Verlag, 2001. 65

[204] R. Storn and K. Price, "Differential Evolution – A Simple and Efficient Heuristic for global Optimization over Continuous Spaces," *Journal of Global Optimization*, vol. 11, pp. 341–359, Dec. 1997. 65

[205] E. Ruffio, D. Saury, D. Petit, and M. Girault, "Tutorial 2: Zero-Order optimization algorithms," p. 25. 65

[206] M. Gambardella, M. B. A. Martinoli, and R. P. T. Stützle, "Ant colony optimization and swarm intelligence," in *5th international workshop, Springer*, Springer, 2006. 65

[207] D. Karaboga, "AN IDEA BASED ON HONEY BEE SWARM FOR NUMERICAL OPTIMIZATION," 2005. 65

[208] C. Blum, "Metaheuristics in Combinatorial Optimization: Overview and Conceptual Comparison," *ACM Computing Surveys*, vol. 35, no. 3, p. 41. 65

[209] J. Pearl, *Heuristics: Intelligent Search Strategies for Computer Problem Solving*. Addison-Wesley, 1984. 65

[210] S. Surjanovic and D. Bingham, "Virtual Library of Simulation Experiments: Test Functions and Datasets." 65

[211] D. G. E. Elbeltagi, T. Hegazy, "Comparison among five evolutionary-based optimization algorithms - ScienceDirect."

[212] M. A. Panduro, C. A. Brizuela, L. I. Balderas, and D. A. Acosta, "A Comparison of Genetic Algorithms, Particle Swarm Optimization and the Differential Evolution Method for the Design of Scannable Circular Antenna Arrays," *Progress In Electromagnetics Research*, vol. 13, pp. 171–186, 2009. 65

[213] A. Khare and S. Rangnekar, "A review of particle swarm optimization and its applications in Solar Photovoltaic system," *Applied Soft Computing*, vol. 13, pp. 2997–3006, May 2013. 67

[214] Z.-L. Gaing, "A Particle Swarm Optimization Approach for Optimum Design of PID Controller in AVR System," *IEEE Transactions on Energy Conversion*, vol. 19, pp. 384–391, June 2004.

[215] M. Y. Hassan, M. N. Suharto, M. P. Abdullah, M. S. Majid, and F. Hussin, "Application of Particle Swarm Optimization for Solving Optimal Generation Plant Location Problem," p. 10, 2012.

[216] B. Mohammadi-Ivatloo, M. Moradi-Dalvand, and A. Rabiee, "Combined heat and power economic dispatch problem solution using particle swarm optimization with time varying acceleration coefficients," *Electric Power Systems Research*, vol. 95, pp. 9–18, Feb. 2013.

[217] M. R. AlRashidi and M. E. El-Hawary, "A Survey of Particle Swarm Optimization Applications in Electric Power Systems," *IEEE Transactions on Evolutionary Computation*, vol. 13, pp. 913–918, Aug. 2009.

[218] N. Jin and Y. Rahmat-Samii, "Particle Swarm Optimization for Antenna Designs in Engineering Electromagnetics," *J. Artif. Evol. App.*, vol. 2008, pp. 9:1–9:10, Jan. 2008.

[219] Eberhart and Y. Shi, "Particle swarm optimization: developments, applications and resources," in *Proceedings of the 2001 Congress on Evolutionary Computation (IEEE Cat. No.01TH8546)*, vol. 1, pp. 81–86 vol. 1, May 2001.

[220] Y. d. Valle, G. K. Venayagamoorthy, S. Mohagheghi, J. Hernandez, and R. G. Harley, "Particle Swarm Optimization: Basic Concepts, Variants and Applications in Power Systems," *IEEE Transactions on Evolutionary Computation*, vol. 12, pp. 171–195, Apr. 2008. 67

[221] B. Zhang, H. Qi, S.-C. Sun, L.-M. Ruan, and H.-P. Tan, "Solving inverse problems of radiative heat transfer and phase change in semitransparent medium by using Improved Quantum Particle Swarm Optimization," *International Journal of Heat and Mass Transfer*, vol. 85, pp. 300–310, June 2015. 67

[222] S. Soleimani, D. D. Ganji, M. Gorji, H. Bararnia, and E. Ghasemi, "Optimal location of a pair heat source-sink in an enclosed square cavity with natural convection through PSO algorithm," *International Communications in Heat and Mass Transfer*, vol. 38, pp. 652–658, May 2011.

[223] V. K. Patel and R. V. Rao, "Design optimization of shell-and-tube heat exchanger using particle swarm optimization technique," *Applied Thermal Engineering*, vol. 30, pp. 1417–1425, Aug. 2010.

[224] K. H. Lee, S. W. Baek, and K. W. Kim, "Inverse radiation analysis using repulsive particle swarm optimization algorithm," *International Journal of Heat and Mass Transfer*, vol. 51, pp. 2772–2783, June 2008. 67

[225] J. Kennedy, "Swarm Intelligence," in *Handbook of Nature-Inspired and Innovative Computing*, pp. 187–219, Springer, Boston, MA, 2006. 67

[226] Q. Bai, "Analysis of Particle Swarm Optimization Algorithm," *Computer and Information Science*, vol. 3, p. 180, Jan. 2010.

[227] I. C. Trelea, "The particle swarm optimization algorithm: convergence analysis and parameter selection," *Information Processing Letters*, vol. 85, pp. 317–325, Mar. 2003. 67

[228] R. Waltz, J.L. Morales, J. Nocedal, and D. Orban, "An interior algorithm for nonlinear optimization that combines line search and trust region steps," 2006. 69

[229] M. Avriel, *Nonlinear programming: analysis and methods*. Courier Corporation, 2003. 70

[230] D. Petit and D. Maillet, "Techniques inverses et estimation de paramètres. Partie 1," Jan. 2008. 72

[231] D. Petit and D. Maillet, "Techniques inverses et estimation de paramètres. Partie 2," Jan. 2008. 72, 73, 74, 77, 238

[232] H. W. Engl, M. Hanke, and A. Neubauer, *Regularization of Inverse Problems*. Springer Science & Business Media, July 1996. 72, 74, 75

[233] J. Hadamard, *Lectures on Cauchy's Problem in Linear Partial Differential Equations*. Courier Corporation, Aug. 2014. 75

[234] R. C. Aster, B. Borchers, and C. H. Thurber, *Parameter Estimation and Inverse Problems*. Elsevier, Oct. 2018. 74

[235] Y. Jarny and D. Maillet, "Problèmes inverses et estimation de grandeurs en thermique," *Ecole d'hiver METTI*, vol. 99, pp. 1–51, 1999. 75

[236] G. Chouteau, "Bruit dans les mesures électriques," Mar. 1997. 77

[237] D. Maillet, M. Lachi, and A. Degiovanni, "Simultaneous measurements of axial and radial thermal diffusivities of an anisotropic solid in thin plate: Application to multi-layered materials," *Thermal Conductivity*, vol. 21, pp. 91–107, 1990. 88

[238] B. Sawaf and M. N. Özisik, "Determining the constant thermal conductivities of orthotropic materials by inverse analysis," *International Communications in Heat and Mass Transfer*, vol. 22, pp. 201–211, Mar. 1995. 88

[239] S. Chanda, C. Balaji, S. P. Venkateshan, A. Ambirajan, and V. Ramakrishnan, "Simultaneous Estimation of Principal Thermal Conductivities of an Anisotropic Composite Medium: An Inverse Analysis," *Journal of Heat Transfer*, vol. 135, Jan. 2013. 88, 89

[240] V. Plana, P. Reulet, and P. Millan, "Experimental Characterization of the Thermophysical Properties of Composite Materials by an Inverse Heat Conduction Method," *Journal of Composite Materials*, vol. 40, pp. 1247–1258, July 2006. 88

[241] M. Thomas, N. Boyard, N. Lefèvre, Y. Jarny, and D. Delaunay, "An experimental device for the simultaneous estimation of the thermal conductivity 3-D tensor and the specific heat of orthotropic composite materials," *International Journal of Heat and Mass Transfer*, vol. 53, pp. 5487–5498, Nov. 2010. 88, 89

[242] W. P. Adamczyk, R. A. Białecki, and T. Kruczek, "Retrieving thermal conductivities of isotropic and orthotropic materials," *Applied Mathematical Modelling*, vol. 40, pp. 3410–3421, Feb. 2016. 88, 89

[243] N. S. Mera, L. Elliott, D. B. Ingham, and D. Lesnic, "Use of the boundary element method to determine the thermal conductivity tensor of an anisotropic medium," *International Journal of Heat and Mass Transfer*, vol. 44, pp. 4157–4167, Nov. 2001. 88

[244] M. R. Hematiyan, A. Khosravifard, and Y. C. Shiah, "A novel inverse method for identification of 3d thermal conductivity coefficients of anisotropic media by the boundary element analysis," *International Journal of Heat and Mass Transfer*, vol. 89, pp. 685–693, Oct. 2015. 88

[245] B. Chen, W. Chen, A. H.-D.Cheng, L.-L. Sun, X. Wei, and H. Peng, "Identification of the thermal conductivity coefficients of 3d anisotropic media by the singular boundary method," pp. 24–33, Sept. 2016. 88

[246] C. Rodiet, B. Remy, and A. Degiovanni, "Thermal characterization of anisotropic materials by integral transforms taking into account the thermal coupling with the sample-holder," *International Journal of Thermal Sciences*, vol. 79, pp. 67–75, May 2014. 89, 121

[247] L. Perez and L. Autrique, "Robust determination of thermal diffusivity values from periodic heating data," *Inverse problems*, vol. 25, no. 4, p. 045011, 2009. 89

[248] M. Thomas, L. Perez, N. Boyard, Y. Jarny, and D. Delaunay, "A new measurement method to characterize thermal properties of composite materials used in aeronautics," in *19th National and 8th ISHMT-ASME, Heat and Mass Transfer Conference*, 01 2008. 89

[249] E. El Rassy, Y. Billaud, and D. Saury, "Estimation directe de propriétés thermophysiques de matériaux orthotropes," *in SFT*, 2018. 89, 121

[250] M. Sheikh, S. Taylor, D. Hayhurst, and R. Taylor, "Measurement of thermal diffusivity of isotropic materials using a laser flash method and its validation by finite element analysis," *Journal of Physics D: Applied Physics*, vol. 33, no. 12, p. 1536, 2000. 121

[251] E. J. Carr, "Rear-surface integral method for calculating thermal diffusivity from laser flash experiments," *Chemical Engineering Science*, vol. 199, pp. 546–551, 2019. 121

[252] J. Luo, K. Ying, and J. Bai, "Savitzky–golay smoothing and differentiation filter for even number data," *Signal Processing*, vol. 85, no. 7, pp. 1429–1434, 2005. 132

[253] W. Hohenauer and L. Vozar, "An estimation of thermophysical properties of layered materials by the laser-flash method," *High Temperatures-High Pressures*, vol. 33, pp. 17–25, Jan. 2001. 150

[254] M. Akabori, Y. Nagasaka, and A. Nagashima, "Measurement of the thermal diffusivity of thin films on substrate by the photoacoustic method," *International Journal of Thermophysics*, vol. 13, pp. 499–514, May 1992. 150

[255] S. W. Kim and R. E. Taylor, "Estimation of thermophysical properties of a film coated on a substrate using pulsed transient analysis," *International Journal of Thermophysics*, vol. 14, pp. 135–147, Jan. 1993.

[256] S. Orain, Y. Scudeller, S. Garcia, and T. Brousse, "Use of genetic algorithms for the simultaneous estimation of thin films thermal conductivity and contact resistances," *International Journal of Heat and Mass Transfer*, vol. 44, no. 20, pp. 3973 – 3984, 2001. 150

[257] F. Rigollet, F. Papini, and D. Boisson, "Identification optimale des propriétés thermophysiques d'un revêtement," *Comptes Rendus de l'Académie des Sciences - Series IV - Physics*, vol. 1, pp. 111–117, Mar. 2000. 150

[258] I. Perry, B. Remy, and D. Maillet, "Thermal Characterization of a Multilayer Material Through the Flash Method," *Journal of Thermophysics and Heat Transfer*, vol. 20, no. 2, pp. 231–237, 2006. 150

[259] M. Akoshima, T. Baba, M. Ogawa, T. Tanaka, Y. Harada, A. Kawasaki, and F. Ono, "Thermal Diffusivity Measurements of the Layered Materials by the Laser Flash Method," *Materials Science Forum*, vol. 631-632, pp. 103–108, 2010.

[260] M. Akoshima, T. Tanaka, S. Endo, T. Baba, Y. Harada, Y. Kojima, A. Kawasaki, and F. Ono, "Thermal Diffusivity Measurement for Thermal Spray Coating Attached to Substrate Using Laser Flash Method," *Japanese Journal of Applied Physics*, vol. 50, Nov. 2011.

[261] B. Hay, J.-R. Filtz, J. Hameury, G. Davée, L. Rongione, and O. Enouf, "Thermal-Diffusivity Measurement of Ceramic Coatings at High Temperature using "Front-Face" and "Rear-Face" Laser Flash Methods," *International Journal of Thermophysics*, vol. 30, pp. 1270–1282, Aug. 2009. 150

[262] J.-L. Battaglia, A. Kusiak, M. Bamford, and J.-C. Batsale, "Photothermal radiometric characterization of a thin deposit using a linear swept-frequency heat flux waveform," *International Journal of Thermal Sciences*, vol. 45, no. 11, pp. 1035 – 1044, 2006. 150

[263] L. Perez, L. Autrique, and M. Gillet, "Implementation of a conjugate gradient algorithm for thermal diffusivity identification in a moving boundaries system," in *Journal of Physics: Conference Series*, vol. 135, p. 012082, IOP Publishing, 2008. 150

[264] N. Milošević, *Mesure de la diffusivité thermique et de la résistance de contact thermique des couches minces sur des substrats par la méthode impulsionnelle*. Lyon, INSA, Jan. 2008. 150

[265] J.-L. Battaglia, A. Kusiak, M. Bamford, and J.-C. Batsale, "Photothermal radiometric characterization of a thin deposit using a linear swept-frequency heat flux waveform," *International Journal of Thermal Sciences*, vol. 45, no. 11, pp. 1035 – 1044, 2006.

[266] W. P. Adamczyk, T. Kruczek, G. Moskal, and R. A. Białecki, "Nondestructive technique of measuring heat conductivity of thermal barrier coatings," *International Journal of Heat and Mass Transfer*, vol. 111, pp. 442–450, Aug. 2017. 150

[267] C. Gobbé, S. Iserna, and B. Ladevie, "Hot strip method: application to thermal characterisation of orthotropic media," *International Journal of Thermal Sciences*, vol. 43, pp. 951–958, Oct. 2004. 150

[268] B. Li, L. Pottier, J. P. Roger, D. Fournier, and E. Welsch, "Thermal characterization of film-on-substrate systems with modulated thermoreflectance microscopy," *Review of Scientific Instruments*, vol. 71, pp. 2154–2160, May 2000. 150

[269] E. El Rassy, Y. Billaud, and D. Saury, "Best startegy to simultaneously estimate the thermal diffusivities of orthotropic composite medium embedded in two-layer materials," *In Proceedings of the Int 4th Thermal and Fluids Engineering Conference -TFEC*, 2019. 162

[270] V. Vavilov, D. Burleigh, and V. Shiryaev, "Ir thermographic evaluation of thermal diffusivity anisotropy: comparative analysis of some algorithms," *Quantitative InfraRed Thermography Journal*, vol. 4, no. 2, pp. 187–200, 2007. 184

[271] E. El Rassy, Y. Billaud, and D. Saury, "Etude de faisabilité de la caractérisation thermique d'un matériau bicouche constitué d'un revêtement ou d'un film mince déposé sur un substrat," *in SFT*, 2019. 185

[272] “Polyethylene - High density - online catalog source - supplier of research materials in small quantities - Goodfellow.” 187, 193, 194

[273] C.-P. Ding, R. Honza, B. Böhm, and A. Dreizler, “Simultaneous measurement of flame impingement and piston surface temperatures in an optically accessible spark ignition engine,” *Applied Physics B*, vol. 123, no. 4, p. 110, 2017. 187, 193, 194

[274] M. Gustavsson, E. Karawacki, and S. E. Gustafsson, “Thermal conductivity, thermal diffusivity, and specific heat of thin samples from transient measurements with hot disk sensors,” *Review of Scientific Instruments*, vol. 65, no. 12, pp. 3856–3859, 1994. 194

List of Figures

***

List of Tables

***

List of Publications

***

International Journals

E. El Rassy, Y. Billaud, and D. Saury, Simultaneous and direct identification of thermophysical properties for orthotropic materials, Measurement, vol. 135, pp. 199–212, Mar. 2019.

(Under-review) **E. El Rassy**, Y. Billaud, and D. Saury, Simultaneous identification method of multilayers thermal diffusivity tensors using unconventional flash technique: application to a two-layer material.

(Under-review) **E. El Rassy**, Y. Billaud, and D. Saury, Flash method experimental design for the thermal characterization of an orthotropic material.

Peer-Reviewed Conference Papers

E. El Rassy, Y. Billaud, and D. Saury, Estimation directe de propriétés thermophysiques de matériaux orthotropes, SFT Congress, Pau, 05/29 - 06/01/2018

E. El Rassy, Y. Billaud, and D. Saury, Best strategy to simultaneously estimate the thermal diffusivities of orthotropic composite medium embedded in two-layer materials, TFEC2019, Las Vegas, Nevada, USA, 04/14 - 04/17/2019.

E. El Rassy, Y. Billaud, and D. Saury, Etude de faisabilité de la caractérisation thermique d'un matériau bicouche constitué d'un revêtement ou d'un film mince déposé sur un substrat, SFT Congress 2019, Nantes, 06/03 - 06/06/2019.

Résumé

***

Développement de méthodes pour la caractérisation de propriétés thermophysiques de matériaux à structure complexe

Résumé

Les matériaux à structures complexes (anisotropes, multicouches et hétérogènes comme poreux) sont de plus en plus utilisés dans de nombreuses applications (ex. automobile, aéronautique, industrie chimique, génie civil et biomédical), notamment en raison de leur amélioration des propriétés mécaniques et physiques. L'identification des propriétés thermophysiques de ces matériaux devient un enjeu incontournable dans plusieurs applications afin de prédire correctement l'évolution de la température au sein de ces structures et d'assurer le contrôle et la modélisation des transferts de chaleur au cours des processus. Dans ce contexte, l'identification des propriétés thermophysiques de tels matériaux, suscitent depuis de nombreuses années une préoccupation importante et croissante. La principale caractéristique de cette thèse concerne la mise en œuvre d'une méthode d'identification directe et simultanée des diffusivités thermiques de matériaux monocouches ou multicouches à l'aide d'un modèle 3D transitoire analytique et d'une expérience unique et non intrusive. La méthode proposée est d'abord validée sur un matériau monocouche opaque et isotrope, puis appliquée et vérifiée sur un matériau orthotrope. La méthode d'identification est basée sur l'expérience bien connue de la méthode flash, qui utilise l'évolution de la température sur la face avant ou arrière de l'échantillon, enregistrée via une caméra infrarouge, pour identifier les paramètres inconnus. Compte tenu de la complexité et de la non-linéarité du problème inverse, un algorithme d'optimisation hybride couplant un algorithme stochastique (Optimisation par essaims particulaires) et un déterministe (de type gradient), a été choisi. L'estimation repose sur la minimisation de l'écart entre les mesures et la réponse d'un modèle semi-analytique inspiré de l'approche des quadripôles thermiques qui prédit l'évolution de la température sur la face avant ou la face arrière. L'excitation thermique, générée par un laser CO_2, est représentée par un flux de chaleur localisé imposé qui peut être de type Dirac ou créneau. Les estimations sont comparées aux valeurs trouvées dans la littérature et aux résultats obtenus en utilisant d'autres méthodes bien établies. Enfin, quelques améliorations de la méthode sont étudiées, en termes de temps de calcul et de précision, avec une optimisation des conditions expérimentales

(durée et intensité des créneaux, face de mesure...). La méthode est ensuite généralisée aux matériaux multicouches, puis appliquée expérimentalement à un matériau bicouche. Cette stratégie, qui peut être considérée comme une tâche difficile, est motivée par l'impossibilité, dans certains cas, de séparer les 2 couches, en particulier pour les revêtements déposés sur des substrats, qui sera la dernière application investiguée dans ce travail. Une analyse de sensibilité est souvent effectuée afin de tester la faisabilité de l'estimation et de la comparaison, pour les matériaux à deux couches et multicouches, de plusieurs configurations possibles en termes de faces d'excitation/de mesures. La pré-évaluation des méthodes d'identification et les études paramétriques sont effectuées à l'aide de données synthétiques bruitées et obtenues à l'aide du modèle ou d'un code numérique d'éléments finis (pseudo-expérience) afin de vérifier la faisabilité et la robustesse des approches. L'une des caractéristiques les plus distinctes de cette approche est que l'estimation peut être réalisée, et avec succès, sans aucune connaissance préalable de la forme ou de l'intensité de l'excitation. En effet, outre l'estimation simultanée des diffusivités thermiques, la méthode peut prédire la quantité de chaleur absorbée par le matériau ainsi que la distribution spatiale de l'excitation thermique.

Mots clés: Diffusivité thermique, Matériaux–Propriétés thermiques, Problème inverse de diffusion, Revêtements, Modélisation tridimensionnelle, Quadripôles thermiques, Transformations intégrales, Analyse de sensibilités, Méthode flash, Thermographie infrarouge, Estimation de paramètres, Optimisation par essaims particulaires, Isotropie, Matériaux orthotropes, matériaux multicouches.

Development of methods to identify thermophyscial properties of complex media

Abstract

Advanced materials with complex structures (anisotropic, multilayers and heterogeneous like porous) are increasingly used in many applications, (e.g. automotive, aeronautics, chemical industry, civil and biomedical engineering) due to their advantages, in terms of mechanical and physical properties enhancements. Estimating thermophysical properties of such materials becomes a crucial issue in several applications in order to correctly predict temperature evolution inside these structures and to ensure the control and the modelling of heat transfers through the processes. In this context, the identification of such materials thermophysical properties, has taken from many years, a significant and increasing concern. The main feature of this thesis relies on the devolvement of a direct and simultaneous identification method of the thermal diffusivities of monolayer or multilayer materials using an analytical 3D transient model and a unique and non-intrusive experiment. The proposed method is firstly validated on an isotropic opaque monolayer material, then applied and verified on an orthotropic one. The identification method is based on the well-known flash-method experiment whose temperature evolution on the front or rear face on the sample, recorded via an IR camera, is used to identify the unknown parameters. Considering the complexity, and the non-linearity of the inverse problem, a hybrid optimization algorithm combining a stochastic algorithm (Particles Swarm Optimization) and a deterministic one (gradient based), has been chosen. This minimization procedure is applied to fit the observation to the output of a pseudo- analytical model inspired from the thermal quadrupoles approach that predicts the temperature evolution on the front or rear face. The thermal excitation, generated by a CO_2 laser, is mimicked by an imposed localized heat flux that may be of Dirac or pulse type. The estimations are compared with values from literature and results obtain from well-established methods. Finally, some improvement of the method are investigated, in terms of time consumption and accuracy, with an optimization of the experiment design (pulse time and intensity, measurement face). The method is then generalised to multi-layer materials, then applied experimentally to a two-layer material. This strategy, which can be considered as a challenging task, is motivated by the impossibility, in some cases, to separate the 2 layers, especially for coatings deposited on substrates which is the last application investigated in this work. A sensitivity analysis is often conducted in order to test the feasibility of the estimation and compare, for two-layer and multilayers materials, several possible configurations in terms of excitation/measurements faces. Pre-evaluation of the overall identification methods and parametric studies are performed using synthetic noisy data generated using the model or a numerical finite element code (pseudo-experiment) to verify the approaches feasibility and robustness. One of the most distinctive features of our approach is that the estimation may be successfully achieved without any a priori knowledge about the shape or the intensity of the excitation. Indeed, besides the simultaneous estimation of the thermal diffusivities, the method predicts the total amount of heat absorbed by the material as well as the space shape of the thermal excitation.

Key words: Thermal diffusivity, Materials–Thermal properties, Inverse scattering transform, Coatings, Three-dimensional modeling, Thermal quadrupoles, Integral transformations, Sensitivity analysis, Flash method, Infrared thermography, Parameters estimation, Particles swarm optimization, Isotropy, Orthotropic materials, Multilayers.